ZfK-410

PROCEEDINGS OF THE IXth INTERNATIONAL SYMPOSIUM ON THE INTERACTION OF FAST NEUTRONS WITH NUCLEI

November 26–30, 1979 in Gaussig (GDR)

Organized by
the Technical University of Dresden

Edited by
D. Seeliger and S. Unholzer

January 1980

Postanschrift: Akademie der Wissenschaften der DDR
Zentralinstitut für Kernforschung Rossendorf
8051 Dresden
Postfach 19 Deutsche Demokratische Republik

Diese Publikation wurde in der Abteilung Literatur und Information des Zentralinstitutes für Kernforschung hergestellt

III-12-12 J 720 00

AKADEMIE DER WISSENSCHAFTEN DER DDR

Z E N T R A L I N S T I T U T F Ü R K E R N F O R S C H U N G

R O S S E N D O R F B E I D R E S D E N

ZfK - 410

Proceedings
of the IXth International Symposium on the Interaction of Fast Neutrons with Nuclei

organized by

the Technical University of Dresden

November 26-30, 1979 in Gaussig (GDR)

edited by

D. Seeliger and S. Unholzer

January 1980

Organizing Committee

H. Helfer
U. Kaiser
D. Seeliger

Technical University Dresden
Section of Physics, Nuclear Physics Group

Materials of the previous symposia have been published in:

1971: Wiss. Zeitschrift TU Dresden 21 (1972) 691
1972: ZfK - 261 (1973)
1973: ZfK - 271 (1974)
1974: Wiss. Zeitschrift TU Dresden 24 (1975) 1351
1975: ZfK - 324 (1976)
1976: not published
1977: ZfK - 376 (1978)
1978: ZfK - 382 (1979)

ACKNOWLEDGEMENTS

At the IXth International Symposium on the Interaction of Fast Neutrons with Nuclei, organized by the Nuclear Physics Group of the Technical University Dresden, participated scientists from eight countries and three international scientific organizations, which presented results obtained in more than twenty institutes.
We wish to thank all participants for their effort and active discussions during the meeting in Gaussig.
Thanks are directed to all person at the TU Dresden, who actively supported or contributed to the organization of this Symposium. We are indepted to the Central Institute of Nuclear Research for publication of the proceedings as a ZfK - report.
For technical assistance thanks are directed to U. Kaiser, B. Krause, R. Krause, R. Prengel and R. Richter.

Organizing Committee

CONTRIBUTIONS

LIST OF PARTICIPANTS

Arlt, R.	TU Dresden, GDR
Barit, I.J.	NRI Moscow, CCP
Blumentritt, G.	ZfK Rossendorf, GDR
Eckstein, P.	JINR Dubna, CCP
Enghardt, W.	ZfK Rossendorf, GDR
Fawzy, A.	Univ. Cairo, EGYPT
Förtsch, H.	TU Dresden, GDR
Gareev, A.	JINR Dubna, CCP
Gleisberg, F.	TU Dresden, GDR
Grimm, W.	TU Dresden, GDR
Gueth, S.	Univ. Budapest, HUN
Guratzsch, H.	ZfK Rossendorf, GDR
Helfer, H.	TU Dresden, GDR
Hermsdorf, D.	TU Dresden, GDR
Hlavac, I.	SAW Bratislava, CSSR
Hofmann,	IHS Dresden, GDR
Jankowski	ZfI Leipzig, GDR
Josch, M.	TU Dresden, GDR
Kleinwächter	ZfK Rossendorf, GDR
Kloß, G.	TU Dresden, GDR
Konshin, V.A.	Inst. of Heat and Mass Minsk, CCP
Kusminov, B.D.	PEI Obnfnsk, CCP
Lasarenko B.A.	Sibir. AdW Novosibirsk, CCP
Lang	ZfK Rossendorf, GDR
Letz	ZfI Leipzig, GDR
Liskien, H.	CBNM (CEC) Geel, Belgium
Lovchikova, G.	PEI Obninsk, CCP
Märten, H.	TU Dresden, GDR
Meiling, W.	TU Dresden, GDR
Meister, A.	VIK Dubna, CCP
Mostovaja	IAE Moscow, CCP
Netzband, D.	ZfK Rossendorf, GDR
Ortlepp, G.	TU Dresden, GDR
Pöthig, J.	TU Dresden, GDR
Przytula, M.	Univ. Lodz, Poland
Qaim, S.M.	KFA Juelich, Austria
Raics, P.	Kossuth Univ. Debrecen, HUN
Rondio, J.	KFI Warsaw, Poland
Rotter, I.	ZfK Rossendorf, GDR
Schmidt, D.	TU Dresden, GDR
Schmidt, J.J.	NDS, IAEA Vienna, Austria
Schweitzer, T.	TU Dresden, GDR
Seeliger, D.	TU Dresden, GDR
Seidel, K.	TU Dresden, GDR
Shuravlov, B.V.	PEI Obninsk, CCP

Streil, T.	TU Dresden, GDR
Teichner, R.	TU Dresden, GDR
Truvancv, A.	PEI Obninsk, CCP
Tschammer, H.	LNP (VIK) Dubna, CCP
Tschammer, R.	LNP (VIK) Dubna, CCP
Turkiewicz, I.	PPI Warsaw, Poland
Unholzer, S.	TU Dresden, GDR
Vitenko	Radiuminst. Leningrad, CCP
Vonach, H.	Radiuminst. Vienna, Austria
Wagner, W.	TU Dresden, GDR
Weißbach, B.	TU Dresden, GDR
Wolf, R.	TU Dresden, GDR

RECENT DEVELOPMENT OF SPECIAL DETECTION SYSTEMS AT THE VAN DE GRAAFF LABORATORY OF CBNM

H. Liskien, C. Budtz-Jørgensen, H.-H. Knitter, A. Paulsen
Commission of the European Communities, Joint Research Centre
Central Bureau for Nuclear Measurements, B-2440 Geel, Belgium

Abstract

A measuring programme has been set up by the CBNM Van de Graaff laboratory to determine (a) gas production cross sections for fast reactor structural materials and (b) fission cross sections of rare actinide isotopes. In both cases special detection systems had to be developed which will be described together with examples of results obtained so far.

1. Introduction

The main tasks of the CBNM are the development of nuclear reference materials and methods, and the determination of nuclear data in fulfillment of high priority requests. For the latter task a 120 MeV electron linear accelerator is available which (via bremsstrahlung and the (γ,n)-process) produces high intense neutron bursts with widths down to 5 ns. This pulsed neutron source is mainly exploited by time-of-flight experiments in the resolved and unresolved resonance region using flight paths up to 400 m. Fast neutrons are produced (via reactions like ^{7}Li(p,n), T(p,n), D(d,n), T(d,n)) using a 7 MV single stage Van de Graaff accelerator in its pulsed (~ 1 ns) or unpulsed mode. Presently this accelerator is used to determine gas production cross sections for fast reactor structural materials and fission cross sections of rare actinide isotopes.
Especially helium is contributing to the embrittlement of material via the stabilization of micro-voids. As the (n,α)-reactions on most of the involved main isotopes lead to stable nuclei, activation techniques are not applicable. Gas extraction combined with mass spectrometry fails due to the limited fluences of mono-energetic neutrons available. Therefore we designed a reaction chamber for direct particle detection [1].
Fission cross sections for rare actinide isotopes are needed for fuel cycle strategy and estimation of properties of burned fuel elements. Half-lives of such isotopes are very often rather short, such that the neutron-induced fission fragment rate is many orders of magnitude smaller than the α-activity of the sample used. Normally designed fission ionization chambers therefore can not be used in such experiments due to pile-up problems. Approaches of CBNM Geel to overcome this problem will be presented further below [2].

2. The Multi-Angle Reaction Chamber

A cross section view of this chamber is shown in Fig. 1. Five charged particle detector telescopes, each consisting of two energy loss detectors (proportional counters) and one total energy detector (surface barrier counters) in a triple-coincidence arrangement, are registering the charged particles emitted from thin metallic foils in the centre of the chamber. All the energy loss detectors are combined in two pairs of proportional counters, one pair on each side of the sample. For this sample we are using a tantalum backing and two metallic foils (~ 3 mg/cm^2) on each side to avoid prompt coincidences from particles created in one half of the chamber but passing through a single sample foil into the other half. This sandwiched sample is mounted on a movable slide which permits to insert different samples: the sample to be studied, a reference sample, a background position and an α-source. The mean observation angles relative to the incoming neutron beam are 14, 51, 79, 109 and 141°. The aperture functions for the five detectors

are given in Fig. 2. Monoenergetic neutrons in the 5 to 10 MeV range are produced using the D(d,n)-reaction and the 0° direction. A neutron collimator is used to keep random coincidences at an acceptable level and to suppress charged-particle productions in the surface barrier detectors. This collimator is a fixed mechanical part of the chamber to ease alignment. Its length varies with neutron energy. The neutron flux is deduced from a measurement of the recoil proton scattering rate from a polyethylene foil into detector 1 (14° observation angle). At each neutron energy eight runs are performed: with the metallic sample, with its backing only, with the hydrogen radiator, with the backing of the hydrogen radiator only, all these four runs with and without gas in the target. Since the deuterium gas pressure in the target is very stable with time, the beam charge integrator serves as a neutron monitor linking these runs. The obtained differential cross sections depend on the assumed differential n-p scattering cross section [3] and on the ratios of the detector solid angles. These ratios of solid angles are determined with an ^{241}Am source which at the same time allows a calibration of the α-particle energy scale.

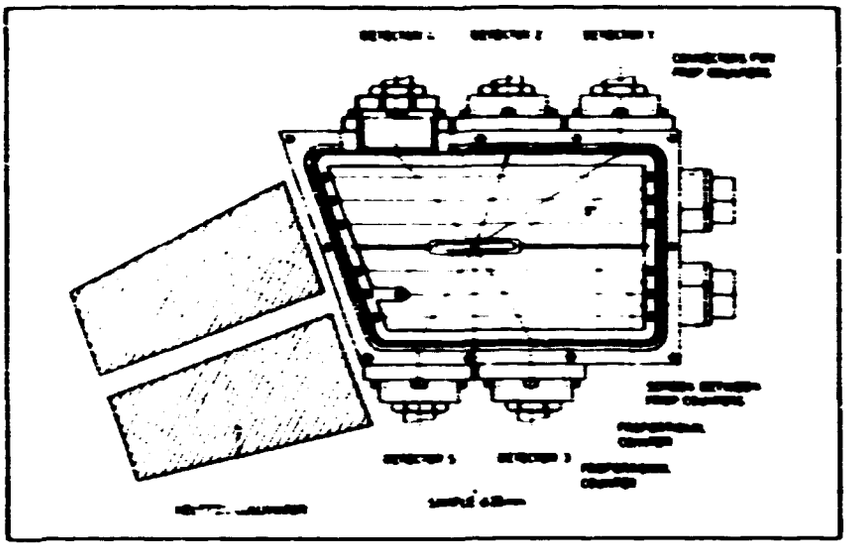

Fig.1 : Cross section view of the multi-angle reaction chamber together with the neutron collimator.

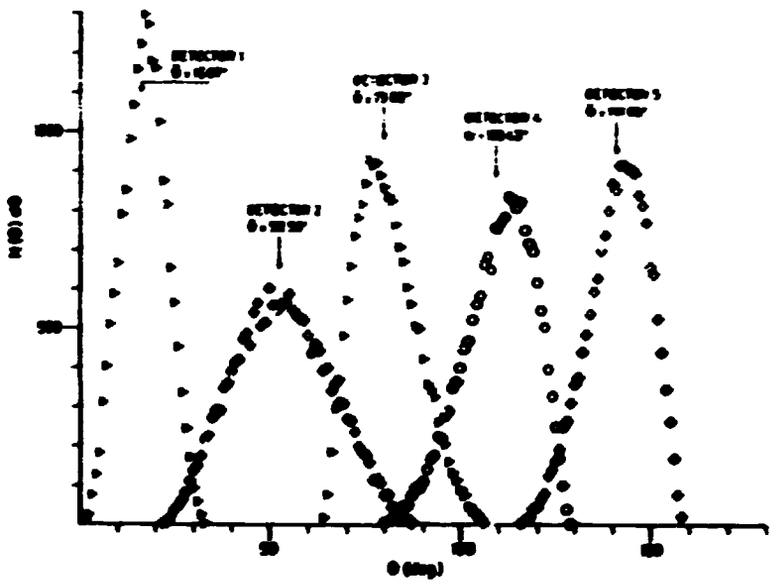

Fig.2 : The aperture function of the five detectors.

The electronics of this chamber is sketched in Fig. 3. Evidently the timing characteristics of the chamber determines the forground/background ratio. Best time resolution of about 150 ns has been obtained with pure methane, fixed standard resolution is 250 ns. After extraction of the timing information by the indicated threshold discriminators the analogue signals from each pair of proportional counters are summed. These two signals together with the five total energy signals are fed into a multiparameter data acquisition system, MD 6660, which serves in this

case as a fivefold biparametric analyzer. The dynamic range of the electronics used is insufficient to record simultaneously all kind of particles. At present we are concentrating on α-particles. For the detection of the proton recoils for flux determination the setting of the electronic has to be changed. As an example, results on natural iron after integration over the α-particle energy and the emission direction are given in Fig. 4. Up to now experimental information was only available around 14.8 MeV [4-6] where due to the T(d,n)-resonance much stronger neutron sources are available. For the references 5 and 6 even the world's most intense 14 MeV source RTNS at Livermore was employed using a magnetic spectrometer [5] in one case, and gas extraction combined with mass spectrometry [6] in the other case.

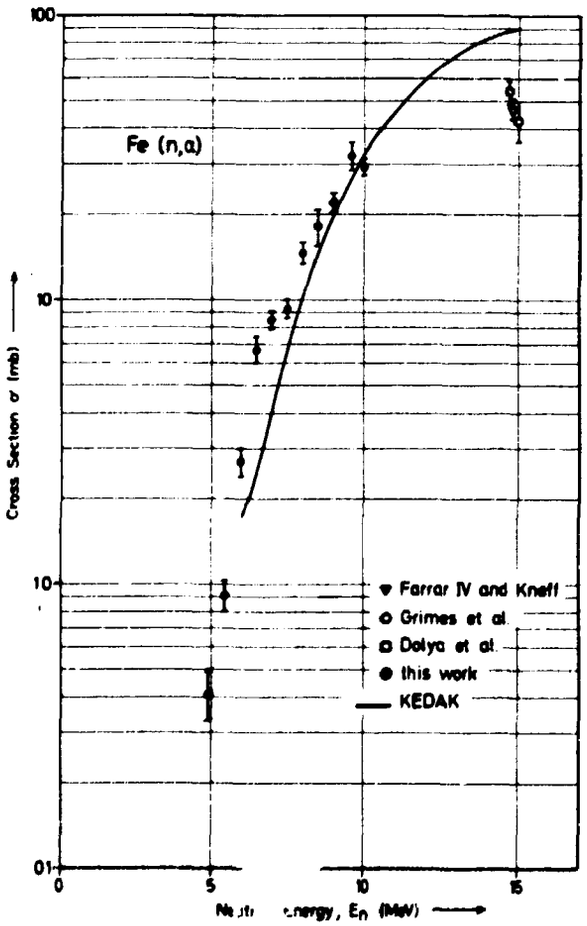

Fig.4 : Obtained energy- and angle-integrated Fe(n,α) cross sections together with existing data.

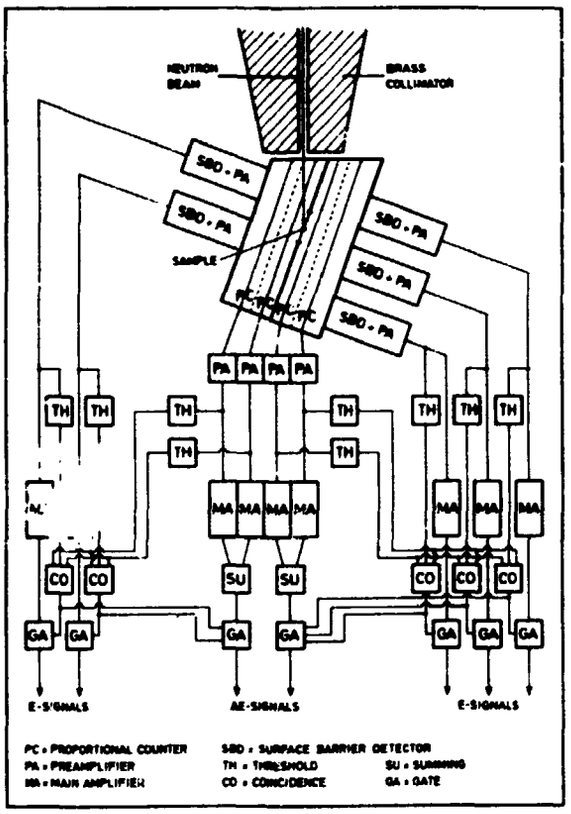

Fig.3 : The electronics used for the multi-angle reaction chamber.

3. A Parallel Plate Ionization Chamber with Special Characteristics

Normally used parallel plate fission ionization chamber have an electrode distance much smaller than the fission fragment range. As will be demonstrated below, such devices can be considerably improved by using an electrode distance longer than the fission fragment range R and appropriate double differentiation of the charge signal.

Part a of Fig. 5 shows the electrodes of the chamber and an ionization track forming an angle ϑ with respect to the normal of the electrode. The time dependence of the induced charge q(t) from the ionization electrons is shown in Fig.5b. As long as all electrons move under the action of the electric field towards the collector plate with the same

speed, a signal with constant rise is induced. This rise becomes smaller when the first electrons reach the collector (t_1) and it becomes zero when all electrons have reached the plate (t_2). The times t_1 and t_2 are given by

$$t_1 = (d - R\cos\vartheta)/v\ , \quad t_2 = d/v$$

with v being the electron drift velocity. The pulse height at time t_2 is given by

$$q(t_2) = E\left(1 - \frac{\bar{x}}{d}\cos\vartheta\right) \qquad \text{with}$$

$$\bar{x} = \frac{\int_0^R x \cdot \rho(x)dx}{\int_0^R \rho(x)dx}$$

where $\rho(x)$ is the ionization density of the track and E the particle energy. The direction dependence can be used to investigate fission fragment angular distributions as explained in the last section of this paper. The sharp rise of the current pulse shown in Fig.5c depends in principle only on the time it takes the fission fragment to stop in the gas; its height is proportional to E. A differentiation of the current pulse results in the extremely sharp pulse shown in Fig. 5d which has an area proportional to the particle energy E. The short width of the obtained pulses ensures that the chamber can operate with a high α-background. The ratio of pulseheights from FF to α-particles is larger than 12, considerably higher than with a normally used ionization chamber. In fact the power of this type of desing can not be fully exploited because the best rise time of commercially available preamplifiers is ~ 10 ns. Using delay line clipping we obtained pulses of 30 ns width. Although this is one order of magnitude more than is ideally obtainable, the chamber has proved to operate satisfactorily with a sample of 1.6 mg ^{240}Pu which produces an α-background of 1.5 10^7 s^{-1}. As an example Fig.6 shows a part of the cross section results obtained [8].

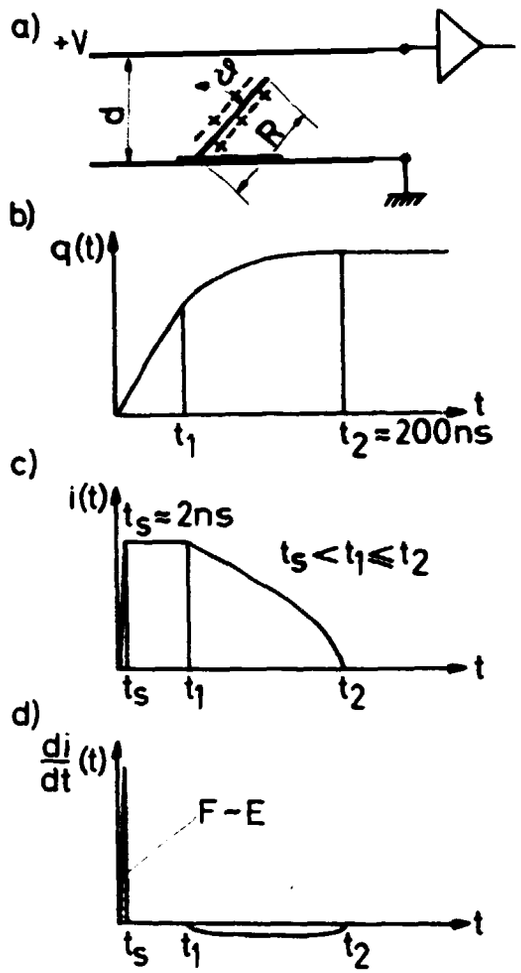

Fig.5 : Part a shows schematically the parallel plate chamber with an ion track. R is the range of the ionization particle, ϑ the emission angle formed by the track and the normal of the electrodes, d the electrode distance. Parts b, c and d show the charge, the current and the differentiated current signals, respectively.

Moreover, to our knowledge, this is the first time that a fast pulse is formed from an ionization chamber applicable to fast timing ($\Delta t \leq 1.5$ ns) and carrying the energy information with it.

4. The Compensation Chamber with Intrinsic Suppression of α-Particle Background

Even higher α-accivities can be accepted by a compensation chamber which has been successfully used for ^{241}Am. The underlying idea of this detector is based on the fact that the ranges of 5 to 6 MeV α-particles is much longer than the ranges of fission fragments. Fig. 7 shows the working principle of this detector. Only the upper chamber is of relevance here. It contains a middel electrode (8 μm Al) such that fission fragments moving normal to the sample are just being stopped in this foil, whereas the 5.4 MeV α-particles will pass the foil and are stopped in the outer electrode. Methane at NTP was used as counter gas because of its large electron drift velocity. The distances between the three electrodes have been chosen such that the α-particles create nearly the same charge in the two parts of the chamber. Hence, under the influence of the electric field, no net charge will flow to the middle electrode. That means, in principle, no signal will arise from α-particles. Concerning fission fragments the detector behaves as a normal parallel plate ionization chamber with an electrode distance smaller than the range of the particles. In order to ensure that all α-particles from the sample will pass the middle electrode, a 0.3 mm stainless steel plate with ~ 1500 holes of 0.5 mm diameter, is placed above the sample.

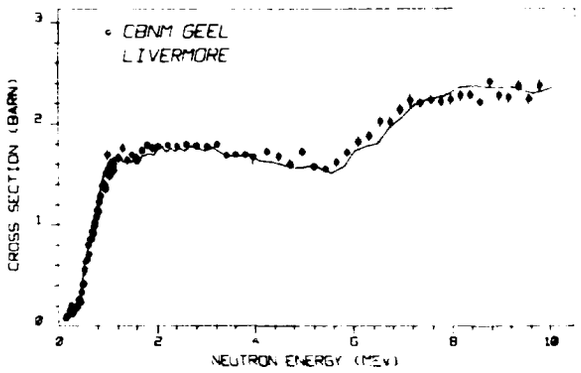

Fig.6 : The high energy part of the obtained fission cross section of ^{240}Pu.

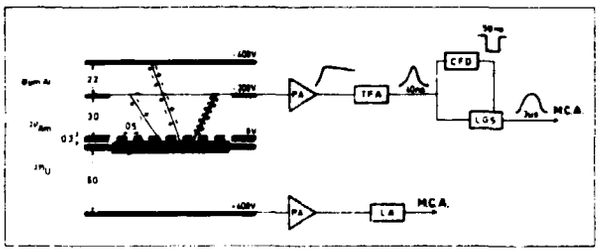

Fig.7 : Schematics of the chamber with intrinsic suppression of α-particle pulses. Distances are in mm. The track of a FF stopping in the thin Al foil is shown as thick line. The tracks of the α-particles, thin lines, pass the Al foil except in the rare cases where the α-particle loses too much energy in the edges of the collimator.

The typical efficiency of such a collimator is about 13 %. Further details on this detector can be found in ref. [9]. Measurements were performed on ^{241}Am using both the Van de Graaff and the linear accelerator. Results are published [10, 11]. Fig. 8 shows the high energy part of the results.

5. Ionization Chamber for the Determination of Fission Fragment Angular Distributions.

Fig. 9 shows the principle of our fission ionization chamber with an inserted Frisch-grid used for fission fragment angular distribution measurements. The charge signal q_{ca} taken from the cathode was given already in section 3:

$$q_{ca} \approx E \left(1 - \frac{\bar{x}}{d} \cos \vartheta\right).$$

Hence, the pulse height distribution of this signal leads directly to the cos ϑ-distribution of

the ion tracks in the case of mono-energetic particles($E,\bar{x}$ = const.). The situation is more difficult when fission fragments are to be detected. The direct dependence on E can easily be removed, as the anode signal q_{an} is proportional to E. To this end the two signals q_{ca} and q_{an} were fed to a multiparameter data acquisition system, ND 6660, where they were digitized and stored event by event. At the same time the quantity

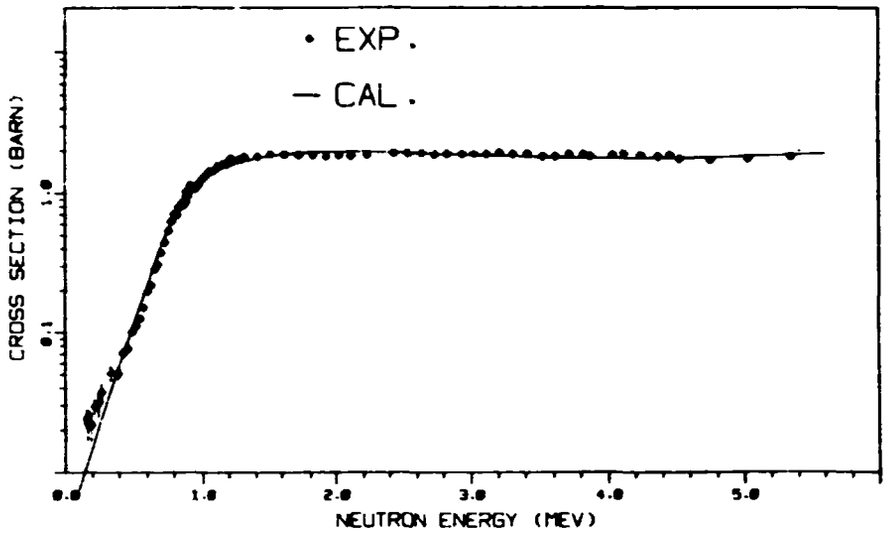

Fig.8 : The obtained fission cross section of ^{241}Am at and above the fission threshold, together with a best theoretical fit [10].

$$v = 1 - \frac{q_{ca}}{q_{an}} \approx \frac{\bar{x}(E,A,Z)}{d} \cdot \cos\vartheta$$

was formed. There remains the dependence of v on $\bar{x}(E,A,Z)$. Keeping $q_{an} \approx E$ fixed, distributions for the v-quantities were determined. These distributions were found to have a sharp fall at the largest values which correspond to $\cos\vartheta = 1$, showing that the dependence on A and Z is smaller than 5 %. The widths of these distributions $\Delta(q_{an}) \approx \bar{x}(E)/d$ were stored, and from the stored events the quantity

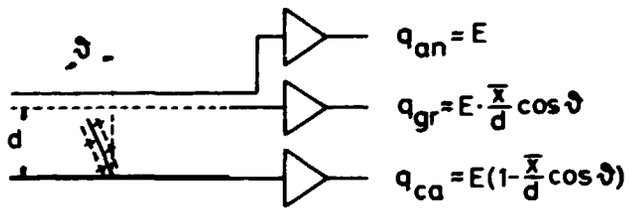

Fig.9 : Schematics of a detector capable for angle determination, energy determination and ns-timing.

$$v' = \frac{v}{\Delta(q_{an})} \approx \frac{\bar{x}(E,A,Z)}{\bar{x}(E)} \cdot \cos\vartheta \approx \cos\vartheta$$

was generated which yields the final fission fragment angular distribution. Up to now the method has been successfully applied for ^{238}U. Results obtained at 1.6 MeV neutron energy are given in Fig. 10.

6. References

[1] A. Paulsen, H. Liskien, F. Arnotte and R. Widera, Proc. Intern. Conf. on Nuclear Cross Sections for Technology, Knoxville (1979) to be published.

[2] H.-H. Knitter and C. Budtz-Jørgensen, Proc. Intern. Conf. on Nuclear Cross Sections for Technology, Knoxville (1979) to be published.

[3] J.C. Hopkins and G. Breit, Nucl. Data Tables A9 (1971) 137

[4] G.P. Dolya, A.P. Klyucharev, V.P. Bozhko, V. Ya. Golovnya, A.S. Kachan and A.I. Tutubalin, Proc. 3rd All-Union Conf. on Neutron Physics Kiev (1975) part 4, p.173

[5] S.M. Grimes, R.C. Haight, K.R. Alvar, H.H. Barshall and R.R. Borchers, Phys. Rev. C19 (1979) 2127

[6] H. Farrar IV and D.W. Kneff, Transact. ANS 28 (1978) 197

[7] Compiled by G. Goel, Report KfK 2386/II (1977) part 1

[8] C. Budtz-Jørgensen and H.-H. Knitter, Report BNL-50991 (1979) 239

[9] C. Budtz-Jørgensen and H.-H. Knitter, NIM 154 (1978) 122

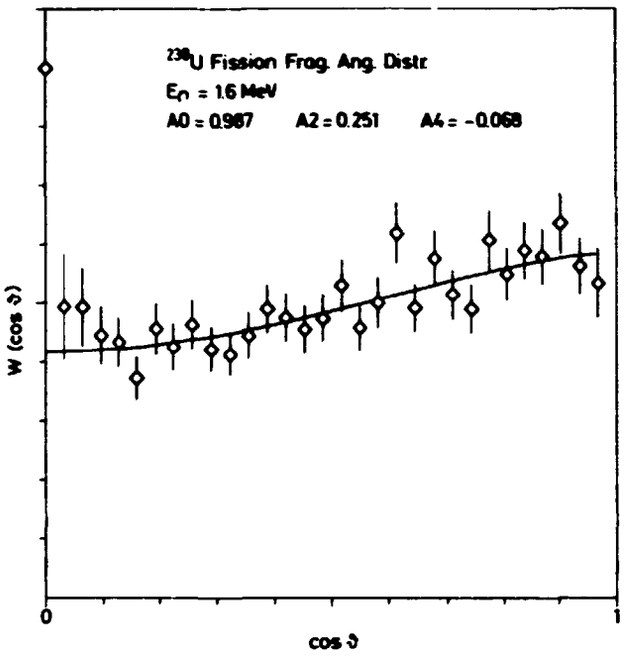

Fig.10 : Angular distribution of ^{238}U fission fragment at 1.60 MeV neutron energy. The full line represents least squares fit with even Legendre polynomials up to A_4.

[10] H.-H. Knitter and C. Budtz-Jørgensen, ATKE 33 (1979) 205

[11] H.-H. Knitter, C. Budtz-Jørgensen and A.S. Jensen, Proc. Intern. Symp. on Physics and Chemistry of Fission, Jülich (1979) to be published.

RECENT DEVELOPMENTS IN THE STUDY OF (n,charged particle) REACTIONS

S.M. Qaim
Institut für Chemie 1 (Nuklearchemie), Kernforschungsanlage Jülich GmbH,
517 Jülich, Federal Republic of Germany

Abstract

Some of the recent advances in the experimental techniques for the study of (n,charged particle) reactions are briefly described and a short survey of the newest results is given. Wherever possible, a short discussion of the reaction mechanism is also included.

1. Introduction

Investigations of (n,charged particle) reactions are of significance for an interpretation of the phenomenon of radiation damage in structural materials of nuclear reactors as well as for enhancing our understanding of basic nuclear theory. The emission of charged particles from excited nuclei is generally favoured in the light mass region; in the medium and heavy mass regions, due to the increasing domination of neutron emission processes, charged particle emission is rather weak and difficult to investigate. Of all the light mass charged particles, i.e. p, d, t, ^{3}He and ^{4}He, the emission of protons and α-particles has been more thoroughly investigated; the available information in the other cases, however, is rather small. The status of (n,charged particle) and other neutron threshold reactions was recently reviewed [1]; the present paper, therefore, gives only a brief account of the newest developments in this field.

2. Experimental techniques

The (n,charged particle) reactions are generally investigated using three major techniques, viz. activation, mass spectrometry and on-line measurement of the emitted charged particles. We discuss the recent developments in the three techniques below.

2.1 Activation method

This relatively simple technique involving an off-line identification and radiometric determination of the radioactive reaction products has been in use for a long time. Because of high sensitivity it has been advantageously applied to the investigation of low-yield reactions, and cross sections on the order of a few microbarns could be measured [2]. In recent years the technique has been applied at Jülich using highly enriched isotopes as target materials, modern radiochemical separations for isolating low-yield transmutation products from strong matrix activities, and specific and high-resolution counting methods, such as soft β^- ray counting in the gas phase, Ge(Li) detector γ-ray spectroscopy, Si(Li) detector X-ray spectroscopy, low-level methods of counting, 4πβγ-coincidence counting, etc. Radiochemical separations not only enhance the sensitivity of detection of the activation products but also facilitate making thin sources for soft X-ray counting, such as in the case of ^{55}Fe and ^{49}V [3].

In the special case of (n,t) reactions the activation technique has been applied in two variations, namely, identification of the activation products (cf. [4]) and estimation of the formed tritium by β^- counting in the gas phase [5-8].

2.2 Mass spectrometry

This method involves an off-line identification of the generally stable reaction products via their masses. As far as the (n,charged particle) reactions are concerned, so far the technique has been applied exclusively to the estimation of light mass gaseous products ^{3}He and ^{4}He, mainly at Atomics International, California [9,10] and Jülich [11]. Whereas at Atomics International the produced ^{4}He was heated out of the irradiated material, spiked with ^{3}He and measured using a high sensitivity mass spectrometer in a static mode, in our Institute relative measurements of ^{3}He and ^{4}He, both produced in fast neutron induced reactions, were carried out in a dynamic mode using a quadrupole mass spectrometer. Though presently limited in application, this technique constitutes a sensitive method for the detection of light mass stable gaseous products and about 10^8 atoms can be detected. The dynamic range of the system is generally $\approx 10^7$, which means that the intensity ratios of $1:10^7$ for neighbouring masses can be well distinguished. The method, however, has the disadvantage of yielding only integral cross-section values so that no information on the reaction mechanism is obtained. In this respect it is similar to the activation technique. Furthermore, no distinction is made between (n,x) and (n,n'x) type reactions. Nonetheless, the technique has proven to be very useful for estimating total gas production in various structural materials (cf. [9,10]).

2.3 On-line measurement of emitted charged particles

The techniques for the on-line detection of emitted charged particles like protons, deuterons, tritons, α-particles are somewhat similar. For studies with 14 MeV neutrons nuclear emulsions, thin scintillators (e.g. CsI(Tl)), small semiconductor detectors and various types of counter telescopes have been in use in several laboratories for quite some time. Recently at Livermore a high resolution magnetic quadrupole spectrometer has been developed (cf. [12,13]) which has been yielding extensive data on p, d and α emitting reactions on structural materials. Charged particles emitted from a thin target are collimated and focussed by a magnetic quadrupole triplet lens onto a detector telescope. The quadrupole transports charged particles of a given momentum from a specific point on the target to a specific point on the detector. By doing measurements at various field gradient settings it is possible to cover the entire charged-particle energy range, i.e. from 1 to 15 MeV, and thus to detect and analyse even low-energy charged particles, such as those emitted in (n,n'x) reactions.

At energies other than 14 MeV, due to the low intensities of available neutron sources, on-line measurement of the emitted charged particles, especially from medium and heavy mass nuclei, has been rather little investigated. Some work has been reported at 18 MeV from Warsaw (cf. [14]). Recently at Geel a reaction chamber has been constructed [15] for the on-line detection of α-particles in the interactions of 5 to 10 MeV neutrons with structural materials. The chamber contains five charged particle detector telescopes, each consisting of two energy loss detectors (proportional counters) and one remaining energy detector (surface

barrier counter) in a triple coincidence arrangement. In this system α-particles with energies above 4 MeV can be easily detected.

3. Recent results

Similar to earlier studies, most of the recent measurements on (n,charged particle) reactions have also concentrated on neutron energies around 14 MeV. The data at other energies are still scanty but the situation is improving. Some of the most recent results on the emission of various types of charged particles are discussed below.

3.1 (n,p), (n,d) and (n,α) reactions

The angle integrated cross sections for the emission of p, d and α-particles in the interactions of 15 MeV neutrons with a few target nuclei in the medium mass region, as reported by the Livermore group [13] are reproduced in Fig. 1. The low-energy components of the emitted charged particles indicate the occurrence of (n,n'x) type reactions. Such investigations are of importance in the context of total hydrogen and helium production in structural materials as well as for an understanding of the phenomenon of sequential emission of neutrons and charged particles.

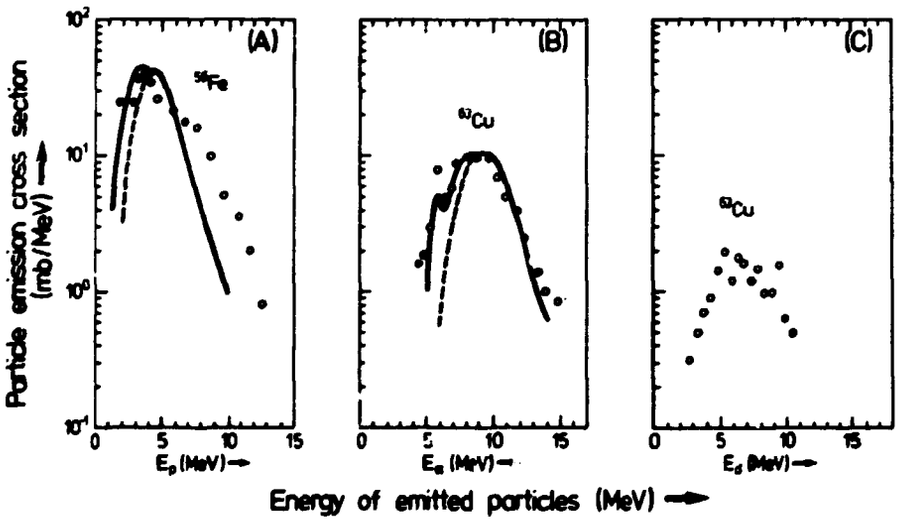

Fig. 1 Angle-integrated cross sections for the emission of various charged particles in reactions induced by 14.8 MeV neutrons on different targets: (A) protons from ^{56}Fe, (B) α-particles from ^{63}Cu and (C) deuterons from ^{63}Cu. The multistage Hauser-Feshbach calculation is represented by a solid line. A dashed line indicates the calculated contribution from protons or α-particles emitted by the first compound nucleus in the region where (n,n'p) or (n,n'α) reactions are also energetically allowed [13].

Using the activation technique we recently carried out extensive studies on 14.7 MeV neutron induced (n,p) reactions [16] in various mass regions and (n,α) reactions in the region of rare-earths where the existing cross-section data showed large discrepancies. Our cross-section data show a strong dependence on (N-Z)/A of the target nucleus.

In recent years a considerable amount of ^{4}He gas production data for fission neutrons as well as for 15 MeV neutrons has been reported from Atomics International using the mass spectrometric technique (cf. [9,10]).

The above mentioned three techniques complement each other and make it possible to estimate the total helium emission from elements of natural isotopic composition. A typical example is provided by the case of nickel. The counter telescopic measurement of the emitted α-particles gave a cross-section value of 129±14 mb [17] and the magnetic quadrupole spectrometric method a value of 97±16 mb [13]. Using the mass spectrometric method a value of 98±6 mb was obtained [10]. Our radiochemical measurements on ^{58}Ni, ^{62}Ni and ^{64}Ni gave (n,α) cross-section values of 125, 20 and 7 mb respectively [18]. From our (N-Z)/A systematics for (n,α) reactions, cross-section values for ^{60}Ni and ^{61}Ni were obtained as 52 and 40 mb, respectively. Taking into account the % isotopic composition of the various stable nickel isotopes, an (n,α) cross-section value of 100±10 mb was obtained for natural nickel. Though the value obtained by the counter telescopic method of detecting charged particles [17] is somewhat higher than the other values, in general the agreement between the various values for nickel is good. Such comparisons emphasize the role of radiochemical measurements and cross-section systematics, especially in those cases where the cross sections are low and thus difficult to measure via mass spectrometry or on-line detection of charged particles.

For neutron energies below 14 MeV, especially in the region of 5 to 10 MeV, recently a comprehensive programme of α-emission cross-section measurements has been initiated at Geel and some data have already been reported [15]. Further measurements should provide a very useful data base for calculations on helium gas production in structural materials.

At neutron energies above 15 MeV, most of the investigations so far have been limited to (n,xn) reactions. Though some measurements on (n,p) and (n,α) reactions have been carried out in the energy range of 15 to 20 MeV, using mainly the activation method (cf. [19]), the available total information is still scanty.

Recently we reported some activation measurements on (n,2α) reactions induced by high energy d/Be break-up neutrons [11]. The results show that in spite of the relatively high excitation energy involved, in the medium mass region the emission of two α-particles is a rather rare process.

Theoretical analyses of the 14-15 MeV data tend to show that the (n,p) reaction is best described by the statistical model incorporating precompound effects. At higher energies the hybrid model has been quite successful in defining the (n,p) cross section. In the case of (n,α) reactions at 14 MeV and higher energies, more direct processes have been postulated than in the case of (n,p) reactions, especially in the region of rare-earths, where the knock-on model seems to give the best fit to the experimental data. The angular distribution data for the (n,d) reactions have been generally fitted by the DWBA-calculations, suggesting thereby the predominant occurrence of direct processes, probably proton pick-up.

3.2 (n,n'p) and (n,n'α) reactions

The sequential emission of two or more nucleons in which one of the emitted nucleons is a charged particle is not well understood. The activation technique gives a sum

of (n,d), (n,n'p) and (n,pn) reaction cross sections. Though the direct detection of emitted charged particles distinguishes between deuterons and protons, the relative contributions of (n,p) and (n,n'p) reactions can be obtained only by a detailed theoretical analysis of the energy and angular distributions of the emitted protons. So far the mass spectrometric technique has not been applied to the study of total proton emission.

The trend in the [(n,d)+(n,n'p)+(n,pn)] cross sections at 14.7 MeV based on data measured at Jülich [18] for about 25 target nuclei is shown in Fig. 2 and compared with that for the (n,p) reaction [16]. It is apparent that for many light mass nuclei the [(n,d)+(n,n'p)+(n,pn)] cross section is comparable to the corresponding (n,p) cross section. For those nuclei, after the emission of a neutron competition between neutron, proton and γ-emission sets in. Since in many of those cases the proton binding energy is smaller than the neutron binding energy, emission of a proton is favoured over that of a neutron. This results in a higher cross section for the (n,n'p) process than that for the (n,2n) process.

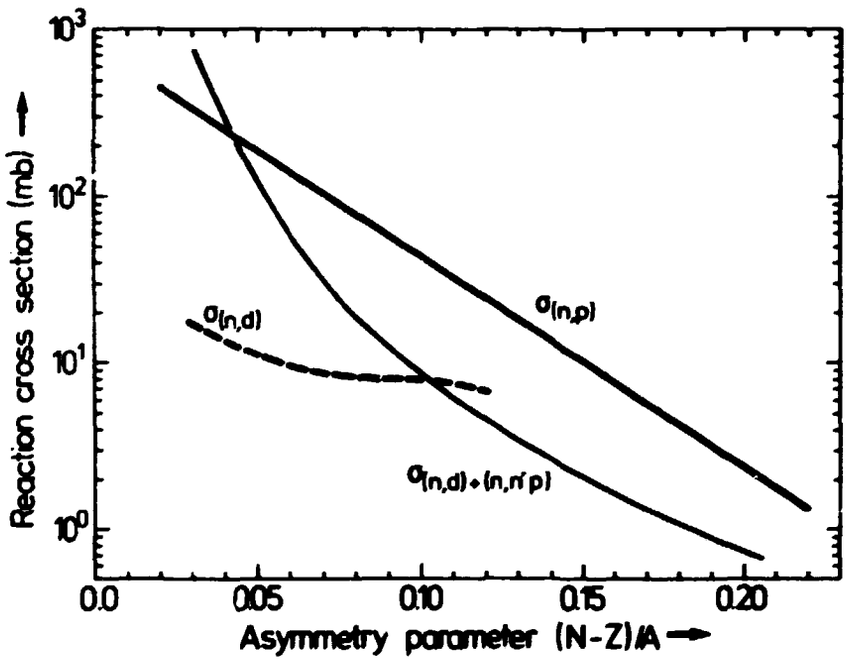

Fig. 2 Systematics of (n,p), (n,d) and [(n,d)+(n,n'p)+(n,pn)] reaction cross sections at 14.7 MeV. The trends in the (n,p) and [(n,d)+(n,n'p)+(n,pn)] reaction cross sections are based on radiochemical measurements done at Jülich, that in the (n,d) cross sections on magnetic quadrupole spectrometric measurements carried out at Livermore.

The trend in the (n,d) cross sections at 15 MeV, based on data reported from Livermore (cf. [12,13]), is also shown in Fig. 2. For nuclei with A≳30 the (n,d) cross section is small compared with the [(n,d)+(n,n'p)+(n,pn)] cross section. The sequential emission of a neutron and a proton is therefore more favoured than the emission of a bound deuteron. In the medium mass region, however, the (n,d) cross section almost approaches the sum of the (n,d), (n,n'p) and (n,pn) cross sections.

This shows that in that mass region the (n,n'p) and (n,pn) processes are much less probable than that involving the emission of a deuteron (probably via proton pick-up).

At energies other than 14-15 MeV very few measurements on (n,n'p) reactions have been carried out; the only recent study deals with fission neutrons for which the [(n,d)+(n,n'p)+(n,pn)] cross sections are very low [3].

As far as the (n,n'α) reaction is concerned, the activation technique has an advantage over the direct charged particle detection and mass spectrometric techniques since the latter two methods yield experimentally a sum of the (n,α) and (n,n'α) cross sections, the individual contributions of which can only be obtained by an analysis of the emitted α-particle spectra. Our activation measurements at 14.7 MeV show [1] that in the medium mass region the contribution of the (n,n'α) cross section amounts to between 10 and 15 % of the (n,α) reaction cross section. At higher excitation energies, however, the (n,α) and (n,n'α) cross sections are comparable [11].

Evidence seems to be growing that in reactions like (n,n'p) and (n,n'α) neutron emission precedes charged particle emission. Though statistical model incorporating precompound effects has been used in some cases to define those processes, due to the paucity of experimental data such calculations have as yet not been put to rigorous tests.

3.3 (n,t) and (n,^{3}He) reactions

Except for the (n,t) reactions on light mass nuclei, the cross sections of these two types of reactions are small and relatively difficult to measure. We carried out extensive studies on (n,t) reactions by the activation technique using both measurement of the residual activity and tritium counting. For 14.6 MeV neutron induced (n,t) reactions we reported (cf. [4]) phenomenological formulae which describe the systematic trend in the cross-section data as well as an observed isotope effect. Recently Sudar and Csikai [8] measured (n,t) cross sections for six odd mass target nuclei. Since those cross-section values are by an order of magnitude higher than the trend suggested by us, the existence of an odd-even effect was postulated. A recent activation measurement of the (n,t) cross section for the odd mass target isotope ^{141}Pr by Csikai and Chouak [20] and our normalized value for the same reaction [4], however, are in agreement. Though the cross-section value for ^{141}Pr is higher than the trend reported by us [4], the occurrence of such a strong even odd effect as suggested by Sudar and Csikai [8] is not definitely proven and further studies in this direction are needed.

We also investigated the (n,^{3}He) reactions at 14.6 MeV using extensive radiochemical methods (cf. [2]). The trend in (n,^{3}He) cross sections is similar to that for (n,t) cross sections; in absolute terms, however, the (n,^{3}He) cross section is by an order of magnitude smaller than the (n,t) cross section.

The (n,t) reaction has been recently investigated at Jülich at high incident neutron energies as well (cf. [5,6]). The results obtained using both tritium counting and γ-ray spectroscopy of the activation products are shown in Fig. 3. It is evident that even at high incident neutron energies the (n,t) cross section is

significant only for very light nuclei; for nuclei with A>40 the (n,t) cross section is small and is relatively independent of the target nucleus. Furthermore, a comparison of the activation and tritium counting data shows that the emission of a bound triton is much less favoured than the emission of three unbound nucleons.

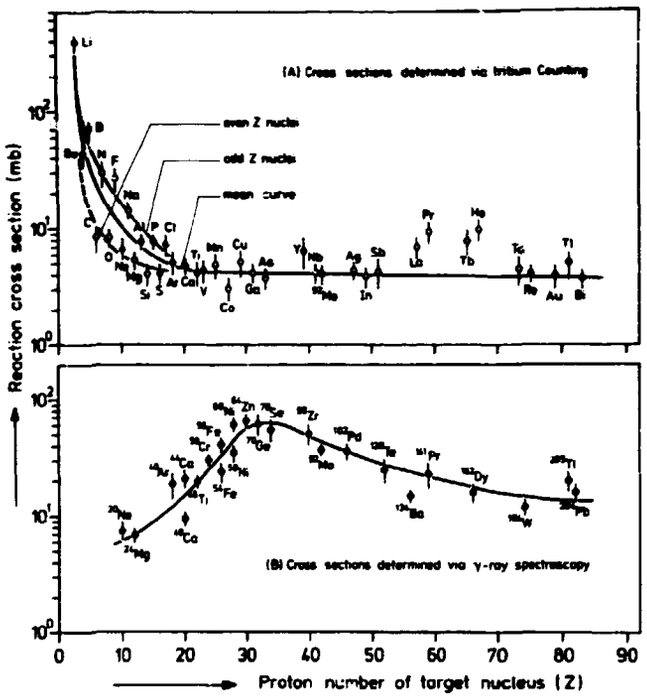

Fig. 3 Cross sections of nuclear reactions induced by fast neutrons (produced via break-up of 53 MeV deuterons on Be) plotted as a function of Z of the target element: (A) $\sigma(n,xt)$ obtained via tritium counting, (B) $\sigma[(n,t)+(n,dn)+(n,n'pn)+(n,2np)]$ obtained via γ-ray spectroscopy of the activation products [5,6].

Our recent measurements on the $(n,{}^3He)$ reaction at high incident neutron energies incorporated both the activation and mass spectrometric techniques [11]. Similar to the (n,t) reaction, even at the relatively high excitation energy, the emission of ${}^3He$ particles constitutes a relatively weak reaction channel. The ratios of ${}^3He$ to ${}^4He$ emission cross sections determined using the two techniques were found to be identical and are shown in Fig. 4 as a function of Z. This observation seems to indicate that the emission of a bound ${}^3He$ particle is favoured over that of three single nucleons. The emission of ${}^3He$ particles relative to ${}^4He$ particles increases with the increasing Z of the target nucleus, presumably due to increasing contributions from direct processes in the case of $(n,{}^3He)$ reactions.

The angular distributions of tritons emitted in the (n,t) reactions on light mass nuclei (cf. several papers from Zagreb) depict that this reaction proceeds via direct interactions, mainly deuteron pick-up. In the medium and heavy mass regions, however, since both (n,t) and $(n,{}^3He)$ reactions have been studied only through integral cross-section measurements, little information is available on the mechanism of those reactions. A Hauser-Feshbach analysis of the two reactions suggests that at 14.6 MeV both statistical and direct processes contribute significantly.

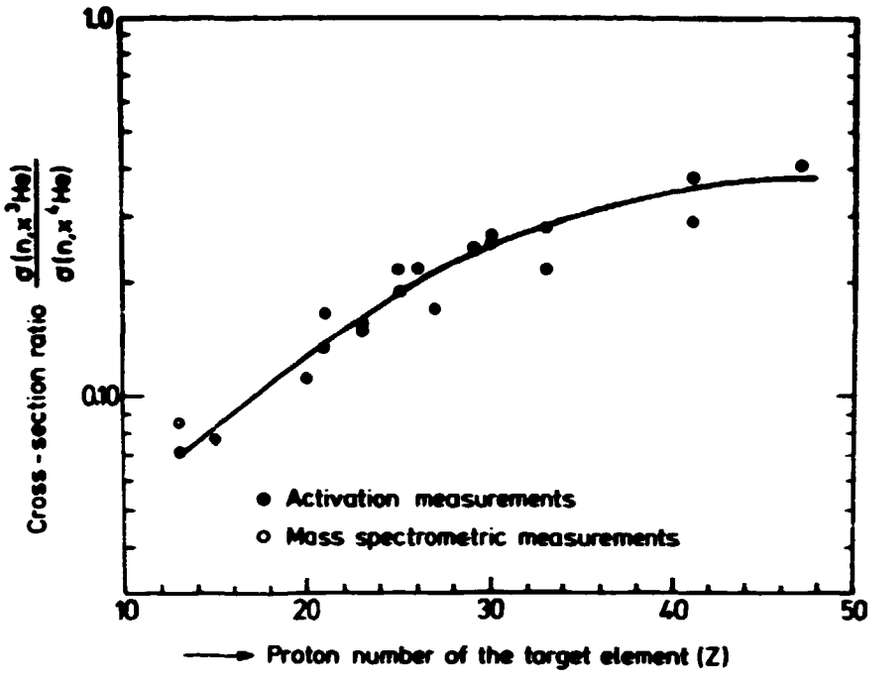

Fig. 4 Fast neutron (produced via break-up of 53 MeV deuterons on Be) induced ^{3}He to ^{4}He emission cross-section ratios as a function of Z of the target element. The activation data describe the ratio of $\sigma(n,{}^3He)$ to $\sigma(n,{}^4He)$ whereas the mass spectrometric data give $\sigma(n,x^3He)/\sigma(n,x^4He)$ [11].

References

[1] S.M. Qaim, Proc.Int.Conf. Neutron Physics and Nuclear Data for Reactors and other Applied Purposes, Harwell, September 1978, OECD-NEA Paris, 1979, 1088
[2] S.M. Qaim, Radiochimica Acta 25 (1978) 13
[3] R. Wölfle and S.M. Qaim, Radiochimica Acta, in press
[4] S.M. Qaim and G. Stöcklin, Nucl.Phys. A257 (1976) 233
[5] S.M. Qaim, R. Wölfle and G. Stöcklin, J.Inorg.Nucl.Chem. 36 (1974) 3639
[6] S.M. Qaim and R. Wölfle, Nucl.Phys. A295 (1978) 150
[7] T. Biro, S. Sudar, Z. Miligy, Z. Dezső and J. Csikai, J.Inorg.Nucl.Chem. 37 (1975) 1583
[8] S. Sudar and J. Csikai, Nucl.Phys. A319 (1979) 157
[9] H. Farrar IV, W.N. McElroy and E.P. Lippincott, Nucl.Tech. 25 (1975) 305
[10] H. Farrar IV and D.W. Kneff, Trans.Am.Nucl.Soc. 28 (1978) 197
[11] C.H. Wu, R. Wölfle and S.M. Qaim, Nucl.Phys. A329 (1979) 63
[12] S.M. Grimes, R.C. Haight and J.D. Anderson, Nucl.Sci.Eng. 62 (1977) 187
[13] S.M. Grimes, R.C. Haight, K.R. Alvar, H.H. Barschall and R.R. Borchers, Phys.Rev. C19 (1979) 2127
[14] L. Glowacka, M. Jaskola, J. Turkiewicz, L. Zemlo and M. Kozlowski, Nucl.Phys. A329 (1979) 215
[15] A. Paulsen, H. Liskien, F. Arnotte and R. Widera, Proc.Conf. Nuclear Cross Sections and Technology, Knoxville, October 1979, in press; H. Liskien, C. Budtz-Jørgensen, H.-H. Knitter and A. Paulsen, these proceedings
[16] N.I. Molla and S.M. Qaim, Nucl.Phys. A283 (1977) 269
[17] G.P. Dolya, A.P. Klyucharev, W.P. Boshko, W.Ya. Golovnya, A.S. Katshan and A.I. Tutubalin, Proc. 3rd All-Union Conference on Neutron Physics, Kiev, June 1975, Part 4, 173
[18] S.M. Qaim and N.I. Molla, Proc. 9th Symposium on Fusion Reactor Technology, Garmisch Partenkirchen, June 1976, Pergamon Press, 1976, 589
[19] A. Paulsen, R. Widera, F. Arnotte and H. Liskien, Nucl.Sci.Eng. 72 (1979) 113
[20] J. Csikai and A.K. Chouak, Radiochimica Acta, in press

STUDY OF $^{24}Mg(n,\alpha)^{21}Ne$ REACTION MECHANISM

W.Trzaska, S.Burzyński, K.Rusek, A.Trzciński, I.M.Turkiewicz, J.Turkiewicz and P.Żupranski

Institute of Nuclear Research, Warsaw, Poland.

Abstract.

Angular distributions of several groups of alpha particles emitted in the ^{24}Mg/n,alpha/^{21}Ne reaction have been measured at a neutron energy of 18.1 MeV. An attempt has been made to describe the $^{24}Mg/n,\alpha_{01}/^{21}Ne$ angular distribution in terms of the DWBA.

Experimental data for /n,alpha/ reactions on target nuclei from the s-d shell are in many cases inconsistent and the conclusions concerning the reaction mechanism are often contradictory. In view of this situation we decided to extend our experimental program for investigation of /n,alpha/ reactions to include target nuclei from the $20 < A < 30$ region. Our choice were the three isotopes of magnesium: $^{24,25,26}Mg$. The first experimental difficulties connected with the use of targets containing some thorium contamination /which must have been introduced in the process of magnesium oxide reduction with Th / were succesfully solved when International Atomic Energy Agency kindly supplied us with magnesium targets manufactured in Oak Ridge. In the course of our measurements the results of the Tübingen group [1] came to our knowledge. From a good quality data on the angular distributions at a reaction energy around 14 MeV these authors concluded that both direct and compound nucleus mechanisms have comparable contributions to /n, α_0/ cross sections on the magnesium isotopes. We have found it desirable to obtain informations on the mechanism of these reactions at higher incident neutron energies.

We present here our first results obtained for ^{24}Mg/n,alpha/^{21}Ne reaction at 18.1 MeV. A self supporting foil of metallic magnesium, 1mg/cm^2, enriched to 99.94% in ^{24}Mg was bombarded by neutrons from T/d,n/^4He reaction induced by 2 MeV deuterons. A single $\Delta E_1, \Delta E_2, E$ counter telescope was used to detect reaction products and three dimentional data were stored event by event in a magnetic tape and then analysed off line by a computer. Angular distributions obtained for the ^{24}Mg/n,alpha/^{21}Ne reaction for several alpha particle groups are shown on fig.1. The solid lines represent fit with Legendre polynomials.

As the first step of the analysis of the reaction we have made an attempt to apply the DWBA method assuming the direct pick-up of ^3He cluster. Here the results of calculations are presented for the angular distribution of the two non resolved alpha particle groups corresponding to the transitions to the ground $3/2^+$ and first excited $5/2^+$ states of final nucleus. The allowed bound states of the ^3He cluster and the ^{21}Ne core forming the ^{24}Mg nucleus are $2D_{3/2}$ and $2D_{5/2}$ resulting in the angular momentum transfer L=2 and J=3/2 or 5/2 respectively. The bound state wave functions were calculated as eigenfunctions of real Saxon-Woods potential with the depth adjusted to reproduce the separation energy of ^3He and geometrical parameters, as commonly used, $R=1.25/A^{1/3}$ $3^{1/3}$ and a=0.65. As no experimental data on the n-^{24}Mg elastic scattering at 18.1MeV are available, the optical model potential in the entrance channel has been taken in the form given by Wilmore and Hodgson [2] .

We have checked that this potential provides a good fit to the 14,6 MeV elastic scattering data of Bjorklund et al. [3] . The excit channel optical potential has been taken with the parameters obtainned by England et al [4] from the analysis of the α-^{20}Ne elastic scattering data at 20.2 MeV.

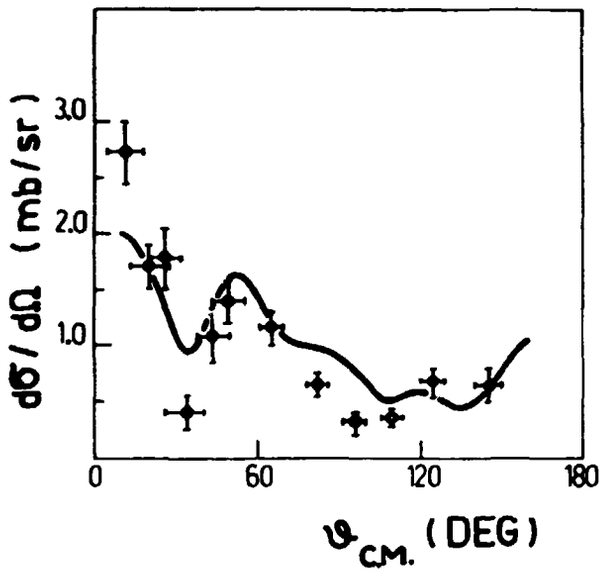

Fig.2. Angular distribution of the transition group ^{24}Mg/n,α_{01}/^{21}Ne at 18.1 MeV. The curve represent the result of a finite - range DWBA calculation.

Table I
Optical model parameters used for the DWBA calculations.

	n	α
V	-47.62	-194.0
r_{OR}	1.31	1.1
a_{OR}	0.66	0.814
$4W_D$	34.25	44.77
r_{OI}	1.26	1.37
a_{OI}	0.48	0.29
r_C		1.3

Energies in MeV
Lengths in fm

The DWBA calculations have been performed using finite - range DWBA code LOLA [5] . The results of calculations are compared with the experimental data in fig 2. The normalisation as shown in fig 2 has given the value for spectroscopic factor of S /^{24}Mg - ^{3}He+^{21}Ne/ equal to 0.22. A rather good agreement of the experimental and calculated distributions may suggest that the ^{24}Mg/n,α_{01}/^{21}Ne reaction direct effects play an important role at E_n=18 MeV.

We are greatly indepted to the International Atomic Energy Agency for supplying us with targets of separated magnesium isotopes.

References.

1 M.Brendle, R.Enge and G.Steigl, Z.Physik A285, 293 /1978/
2 D.Wilmore and P.E.Hodgson, Nucl.Phys. 55, 673 /1964/
3 F.E.Bjorklund, S.Fernbach and N.Sherman, Phys.Rev. 101, 1832 /1956/
4 J.B.A.England, E.Casal, A.Garcia, T.Picazo, J.Aguilar and H.M.Sen Gupta, Nucl.Phys. A284, 29 /1977/
5 R.De Vries, code LOLA, unpublished, The University of Rochester.

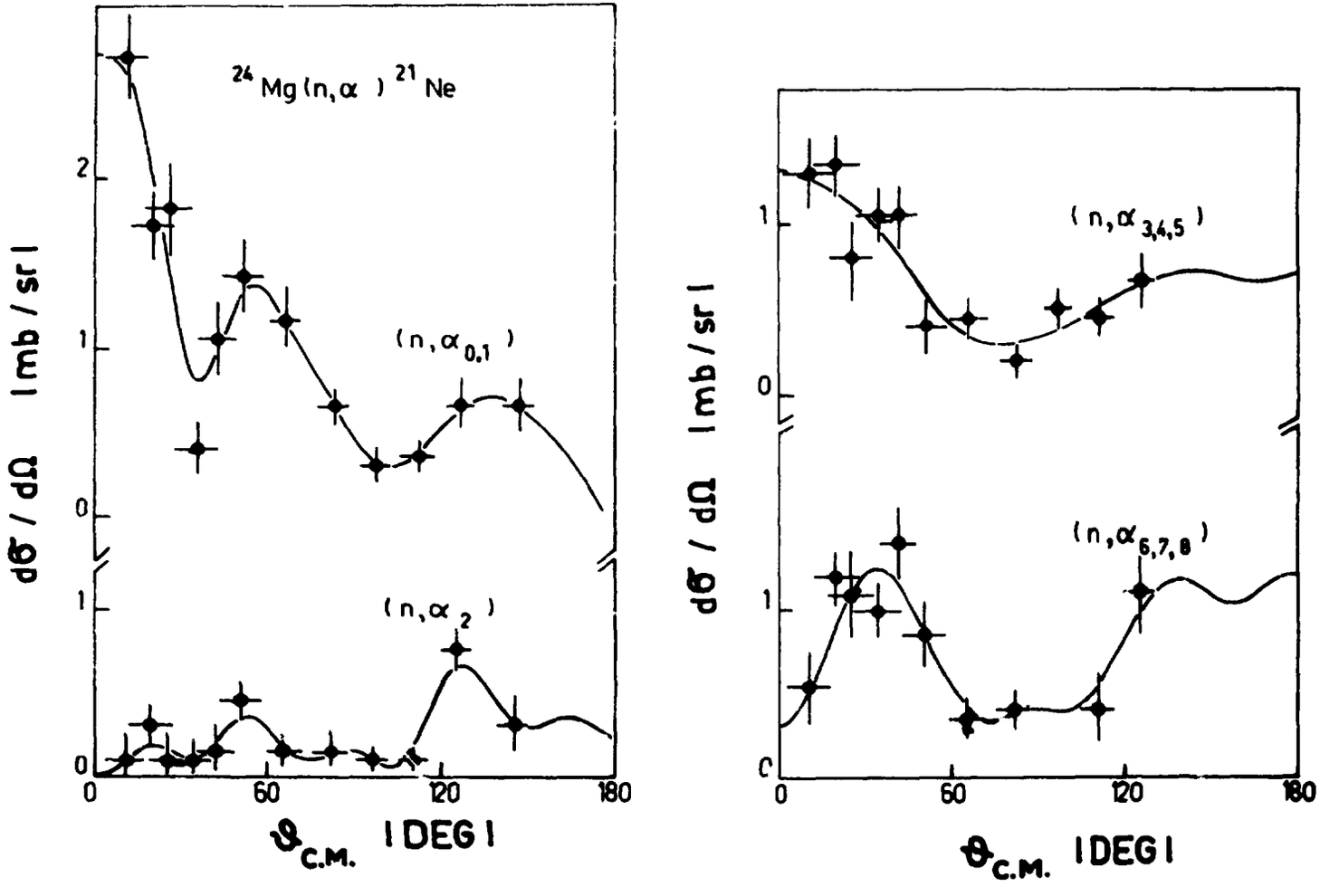

Fig.1.Angular distributions of the alpha particles from ^{24}Mg/n,alpha/^{21}Ne reaction at 18.1 MeV.The curves are Legendre-polynomial fits.

MEASUREMENT OF THE ANGLE-INTEGRATED SECONDARY NEUTRON SPECTRA FROM INTERACTION OF 14 MEV NEUTRONS WITH MEDIUM AND HEAVY NUCLEI

A. Chalupka, G. Staffel, H. Vonach and F. Wenninger
Institut für Radiumforschung und Kernphysik der Österr. Akademie der Wissenschaften, Wien, Österreich.

Abstract

The angle-integrated secondary neutron spectra from interactions of 14.1 MeV neutrons with 17 elements in the range Ti to Bi were measured over the secondary neutron energy range 0.5 - 6 MeV with special emphasis on obtaining reliable and accurate neutron production cross-sections in the low energy region (0.3 - 1 MeV) An overall accuracy of 5 - 7% was obtained over most of the investigated energy ranges. The results are in good agreement with the predictions of statistical model calculations and in the neutron energy range above 1.5 MeV also with other recent measurements; in the low energy range there are still large discrepancies between the results of different measurements.

Secondary neutron spectra from the interactions of 14 MeV neutrons with nuclei have been investigated in a considerable number of experiments (1 - 7) and reasonable agreement on both the form of the spectra and the absolute neutron emission cross-sections has been obtained in the neutron energy range above about 1.5 MeV. The low energy parts of the secondary spectra, however, are rather poorly known in most cases due to experimental difficulties especially with n-γ-discrimination background and multiple scattering at low secondary neutron energies. An excess of low energy neutrons compared with the theoretical predictions has been observed by a number of authors /1-4/ whereas Salnikov and co-workers /6/ found much smaller neutron production cross-sections and also a measurement on iron at our institute /7/ did not show any indication for abnormally high low-energy neutron-production cross-sections. Therefore new measurements have been performed at our institute to determine those spectra for a large number of elements.

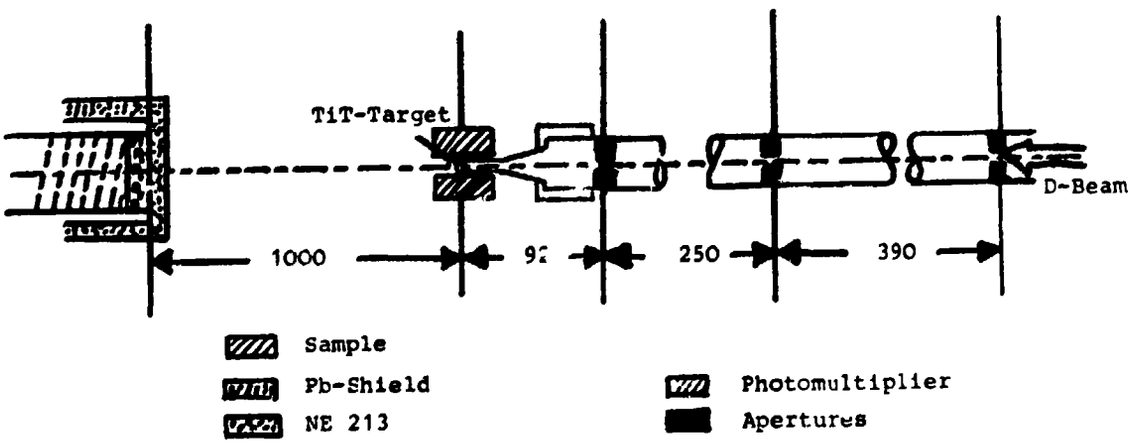

Fig. 1. Experimental set-up for measurement of the angle-integrated low energy parts of the secondary neutron spectra from the interaction of 14 MeV neutrons with nuclei (Tritium target is located in the center of the scattering sample)

Fig. 1 shows the experimental set-up. Pulsed neutrons are produced by means of the 250 keV Cockroft-Walton accelerator of the institute in an extremely small low mass TiT target construction. The scattering samples (hollow cylinders) surrounded the target and the neutron time of flight spectrum is measured at a distance of 1 m by means of a NE213 (1.5 x 0.5") scintillator.The scintillator is operated at a very low threshold (equivalent to about 200 keV proton recoil energy) and a pulse-shape (PSD) method is used to discriminate between neutrons and photons. As reported earlier /8/ the application of the PSD method is possible down to the very low threshold. Time of flight, recoil proton energy and pulse-shape detector output for each event is recorded on disc in order to enable optimal off-line analysis with respect to n-γ-discrimination and background reduction. Both the direct neutrons and the neutrons from inelastic scattering and (n,2n) reaction are detected simultaneously in the NE 213 detector and thus absolute production spectra can be derived directly from the measured time of flight spectra, the target sample geometry and the energy dependence of the detector efficiency. The latter is determined at low energies (0.3 - 6 MeV) by means of a ^{252}Cf calibration measurement, whereby the TiT target is replaced by a fast ionization chamber containing a ^{252}Cf source. The special low mass chamber developped in this way exhibits a time resolution of about 0.5 nsec and an efficiency of about 99% for detection of fission products /9/. For 14 MeV neutrons the scintillator is calibrated by means of the well-known $Al(n,\alpha)^{24}$ activation cross-sections. The raw time of flight spectra were analyzed and transformed into energy differential cross-sections in the following way:

1) Elimination of γ-induced events:
   γ-induced events were eliminated with minimum loss of neutron events by admitting only pulses on appropriate region of the E_{recoil}-PSD plane. All spectra including the ^{252}Cf calibration spectra were treated in exactly the same way. Thus the efficiency determined with the ^{252}Cf measurement takes care of any neutron loss resulting from the γ-rejection procedure. As on the other hand inclusion of γ-induced events constitutes a source of systematic error which is difficult to correct for, considerable loss of neutrons was admitted in the low-energy region in order to get sufficient γ-rejection down to the lowest recoil pulse heights included.
2) Considerable reduction of background due to room scattered neutrons was achieved by admitting only pulses from that region of the E_{recoil}-TOF plane which is physically allowed for neutrons originating from target and scattering sample. Especially in the low neutron energy region a background reduction of about a factor of 2 could be obtained in this way.
3) Background subtraction:
   After execution of step 1 and 2 on all measured (sample-in and sample-out) spectra background subtraction is performed by subtracting from each sample-in spectrum an average of the background spectra measured before and after the respective measurement. In this way the effect of build-up of DD neutrons in the target is essentially eliminated. Background spectra are renormalized relative to the sample-in spectra by means of the intensity in the 14 MeV time of flight peak taking into account the small (1 - 3%) contribution of elastically scattered neutrons to the 14 MeV peaks in the sample-in spectra. The above procedure assumes that the background can be

determined from the sample-out measurements and is not changed by putting the samples around the target. This condition is certainly not strictly full-filled, however, as inspection of the spectra shows that it is a very reasonable approximation. In the time region beyond the time of flight of the slowest neutrons detected, where only background neutrons can contribute also in the sample-in spectra, intensities in the sample-in and sample-out spectra were found equal within about 2%, if normalized to each other as described before. Thus it was considered safe to take care of the uncertainties in the background subtraction by assigning a systematic error of 1.5% to the normalization factors used in the subtractions.

Fig. 2 and 3 show the results of these data reduction procedures for both a sample-in and a background measurement. For technical reasons only every tenth pulse was recorded in the upper parts of the time of flight spectrum (above channel 690) containing the 14 MeV peak thus there is corresponding discontinuity in the time spectra of Fig. 2 and 3 at about channel 690. The broad peaks at the right edge in the spectra of Fig. 2 and 3 are due to DD neutrons originating from one of the apertures (see figure 1).

Fig. 4 shows the resulting background-subtracted in time of flight spectra (difference between Fig. 3b and 2b) and Fig. 5 shows the ^{252}Cf time of flight spectrum used for the detector efficiency calibration.

Finally the reduced background-subtracted time of flight spectra were transformed into energy spectra $\sigma_{nM}(E)$ using the efficiency values derived from the ^{252}Cf experiment for the secondary neutrons and the 14 MeV efficiency value. The results of the evaluation of Grundl and Eisenhower /10/ were used for the ^{252}Cf neutron spectra and the values of Vonach et al. /11/ for the ^{27}Al(n,α) cross-sections. Corrections for attenuation of the primary and secondary neutrons in the sample and for the contribution of doubly inelastic scattered neutrons were applied to all spectra. Neutron emission cross-sections $\sigma_{nM}(E,E')$ calculated by means of the code STAPRE /12/ were used in the double scattering calculations. Finally the cross-sections were averaged over suitable neutron energy bins (either 0.25 or 0.5 MeV) and the errors of these group cross-sections derived by quadratic addition of the statistical error and the estimated contributions from all recognized sources of systematic error. The following error contributions were taken into account: statistical error including the statistical error of the ^{252}Cf measurement for the efficiency determination, error of the normalization factor used in background subtraction, uncertainty in the used form of the ^{252}Cf neutron spectra and in the absolute strength of the source used, uncertainty in the 14 MeV efficiency and uncertainties of the absorption and double scattering corrections.

Secondary neutron spectra were measured in this way for the elements Ti, Cr, Fe, Ni, Cu, Zn, Zr, Nb, Mo, Ag, Sn, Ba, Ta, W, Au, Pb and Bi. Due to lack of space a complete presentation of the result is not possible in this report. Thus only results on 6 elements (which are however typical for the whole data set) are presented in figures 6 - 11. In these figures the results of this work are compared to nuclear reaction calculations and the results of other measurements.

Calculations have been performed using the code STAPRE /12/ based on the exciton model for the precompound part of the reaction and the statistical model including full angular momentum and parity conservation for the equilibrium part of

the reaction. All calculations shown were performed using standard parameter sets with no parameter adjustment to the specific cases.
In detail the following parameters were used:
Optical model parameters: The potentials of Perey-Buck /13/, Becchetti-Greenlees /14/ and Huizenga and Igo /15/ were used for neutrons, protons and α-particles respectively.
Level densities: Back-shifted Fermi-gas Parameters of Dilg et al. /16/
Gamma widths: The energy dependence of the gamma width according to giant resonance to the model of Axel /17/ with absolute values fitted to the measured average γ-width at the neutron binding energy /18/
Precompound matrix elements: Precompound matrix elements were adjusted to result in a transition rate of $5.10^{-21}sec^{-1}$ for the transitions from 3 to 5 exciton states at an excitation energy of 21 MeV.
Numerical data for the results of Hermsdorf et al. /5/ and Salnikov et al. /6/ were taken from the EXFOR file, the data of Schectman and Anderson /1/ were read from the figures in their publication. The results of Mathur /2/ and Kammerdiener /3/ were not included in the comparison as the accuracy of those data is rather poor compared to the other data discussed above.
Although the figures for the different elements do show some differences with respect to the comparison of the various data the following general statements can be made.

1) Above about 1.5 MeV there is reasonable agreement between all measurements.
2) Below 1.5 MeV our data do not confirm the high neutron production cross-sections found in ref. 1 - 4, but show in all cases that the spectra do have the theoretically expected form; in general they are in fair agreement with the results of Salnikov et al. /6/ although for some elements (not shown in fig. 6 - 11) the data of ref. 6 seem to be somewhat too low at the lowest energies.
3) Our data for Fe are in excellent agreement with the results measured previously at our institute /7/ using a quite different experimental set-up and all of our spectra do show a very smooth behaviour as function of A resp. Z, confirming the consistency of our measurements.
4) There is a good overall agreement between our measured neutron production cross-sections and the results of the STAPRE calculations using no free parameters indicating that such calculations may be used to predict unmeasured neutron production cross-sections with an accuracy of better than 20%. Fig. 7 for copper shows an apparent exception. In this case, however, the discrepancy to the calculated values is probably due to the neglect of the (n,pn) contributions to the theoretical spectra which are negligible for all elements shown except for Cu where this cross-section is large for ^{63}Cu and by further calculations this point will be investigated quantitatively.

The authors gratefully acknowledge the help of Dr. G. Stengl in the development of the electronics and of Dr. K. Hansjakob for doing most of the Stapre calculations and the financial support by the Jubiläumsfond der Österr. Nationalbank.

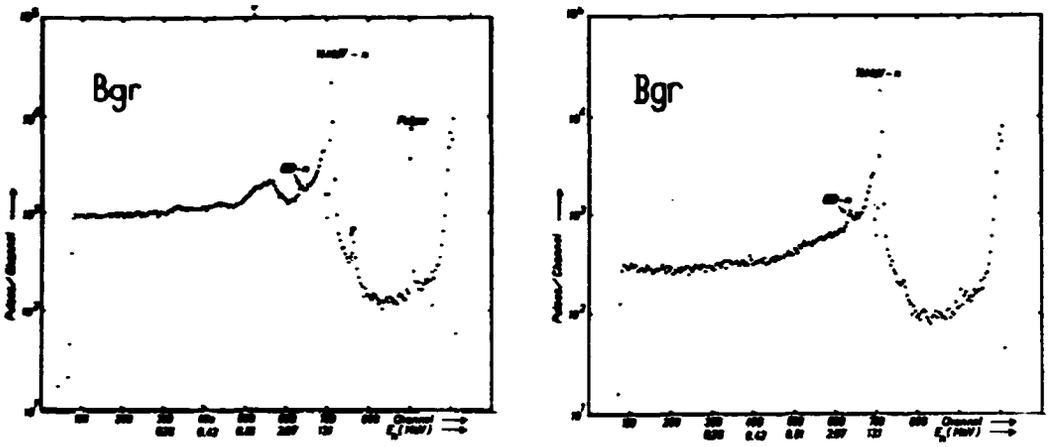

Fig. 2. Background time spectra observed with experimental set-up of Fig. 1.
a) run time of flight spectrum
b) same spectrum after elimination of γ-induced and kinematically forbidden events

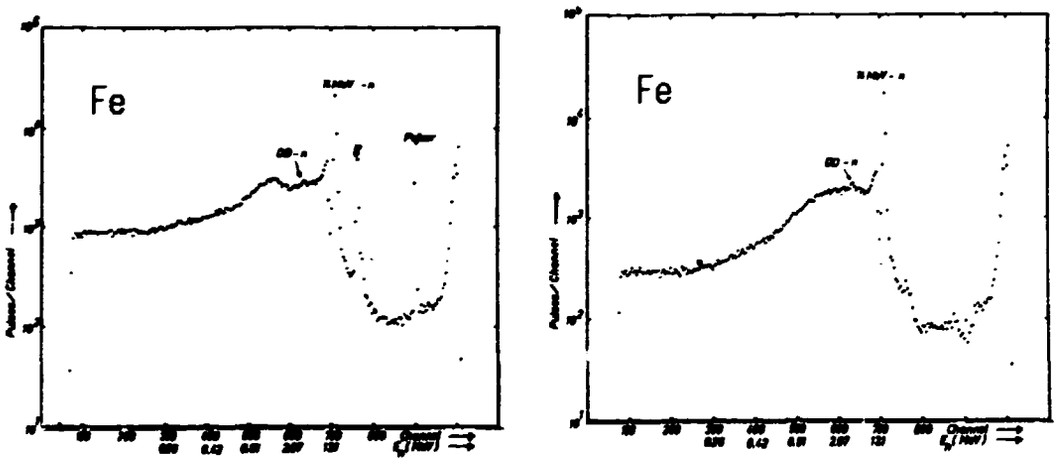

Fig. 3. Time spectra with iron scatterer around TiT target
a) run time spectrum
b) same spectrum after elimination of γ-induced and kinematically forbidden events

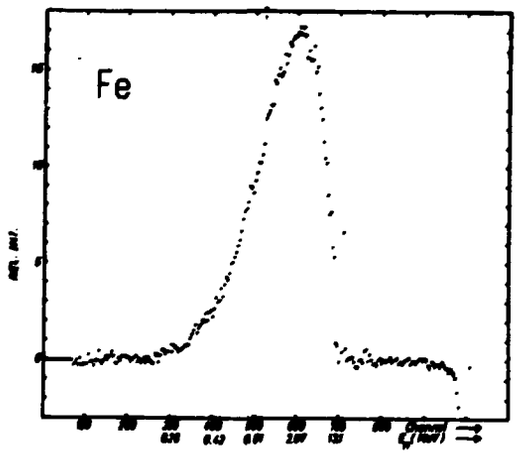

Fig. 4. Background-subtracted neutron time-of-flight spectrum from iron scatterer (difference of spectra 3b and 2b)

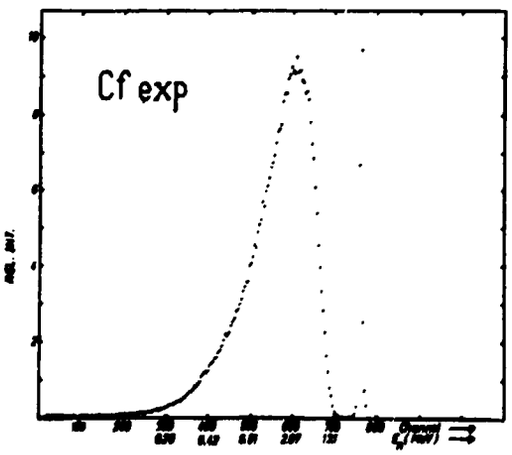

Fig. 5. Neutron time of flight spectrum observed in the 252Cf calibration experiment

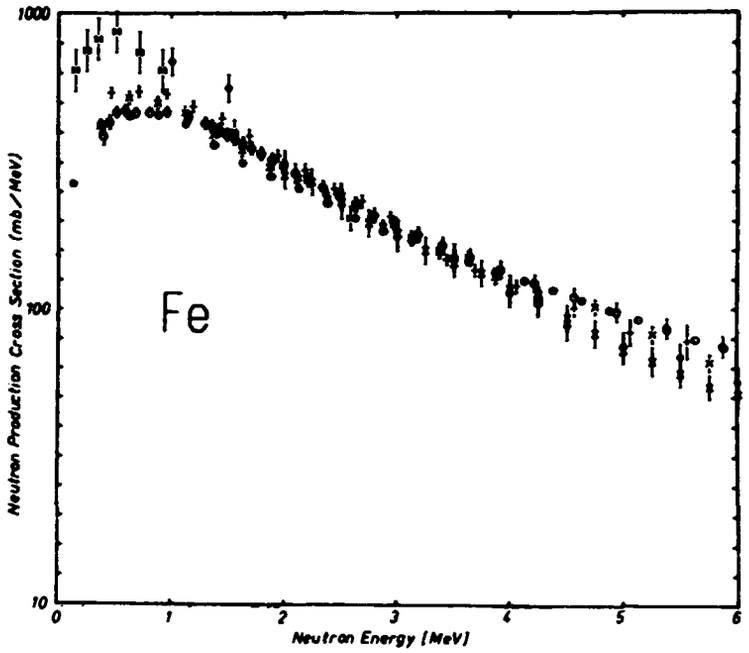

Fig. 6. Angle integrated secondary neutron spectrum from interactions of 14 MeV neutrons with iron; × present result; ▫ Hermsdorf et al. /5/; ⊙ Salnikov et al. /6/; ▪ Clayeux /4/; ◊ Schectman /1/; + Stengl et al. /7/; ⊙ statistical model calculation

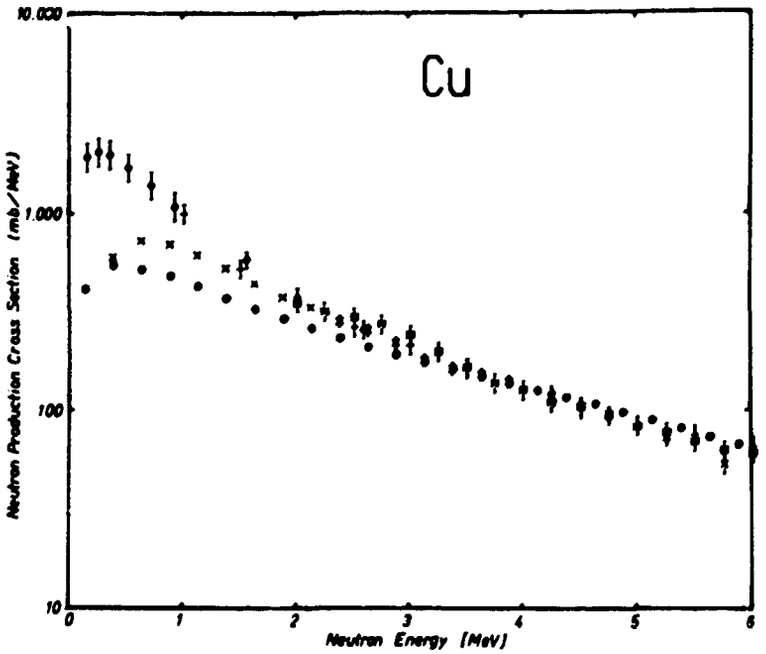

Fig. 7. Angle integrated secondary neutron spectrum from interactions of 14 MeV neutrons with copper; × present reult; + Schectman /1/; ◊ Clayeux /4/; ▪ Hermsdorf et al. /5/; ⊙ statistical model calculation

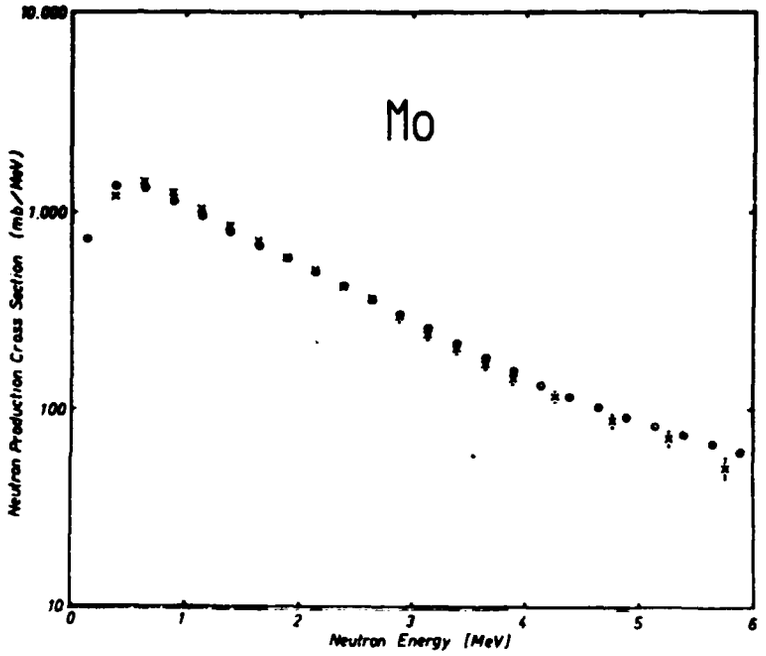

Fig. 8. Angle integrated secondary neutron spectrum from interactions of 14 MeV neutrons with molybdenum; × present result; ⊙ statistical model calculation

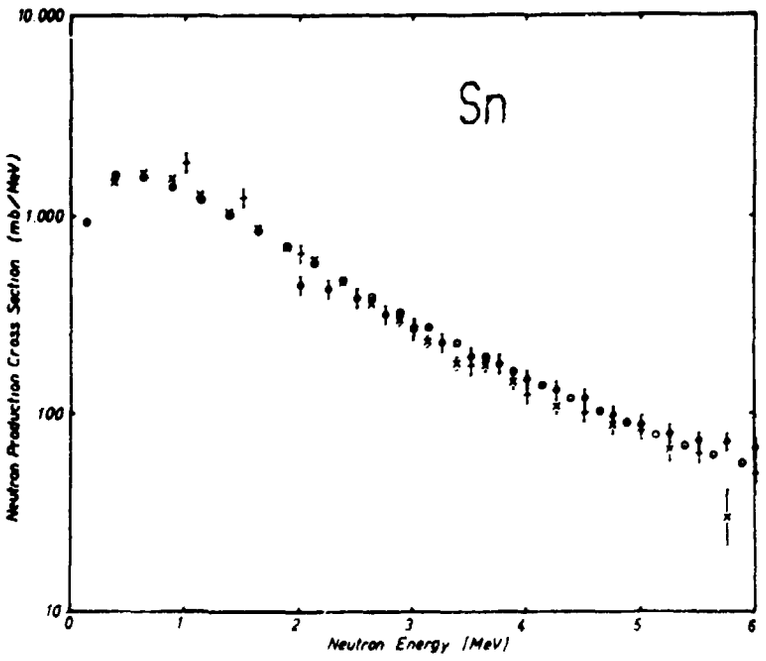

Fig. 9. Angle integrated secondary neutron spectrum from interactions of 14 MeV neutrons with tin; × present result; + Schectman /1/; ◊ Hermsdorf et al. /5/; ⊙ statistical model calculation

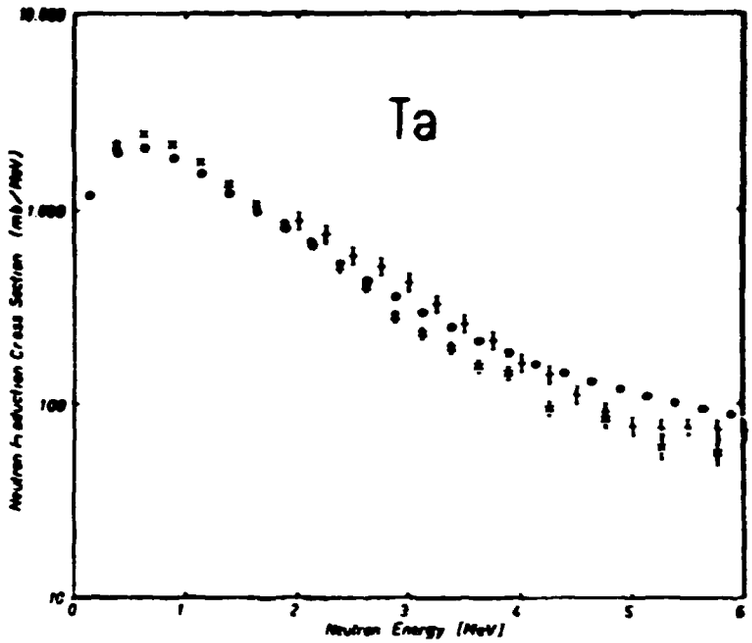

Fig. 10. Angle integrated secondary neutron spectrum from interaction of 14 MeV neutrons with tantalum; × present result; + Hermsdorf et al. /5/; ⊙ statistical model calculation

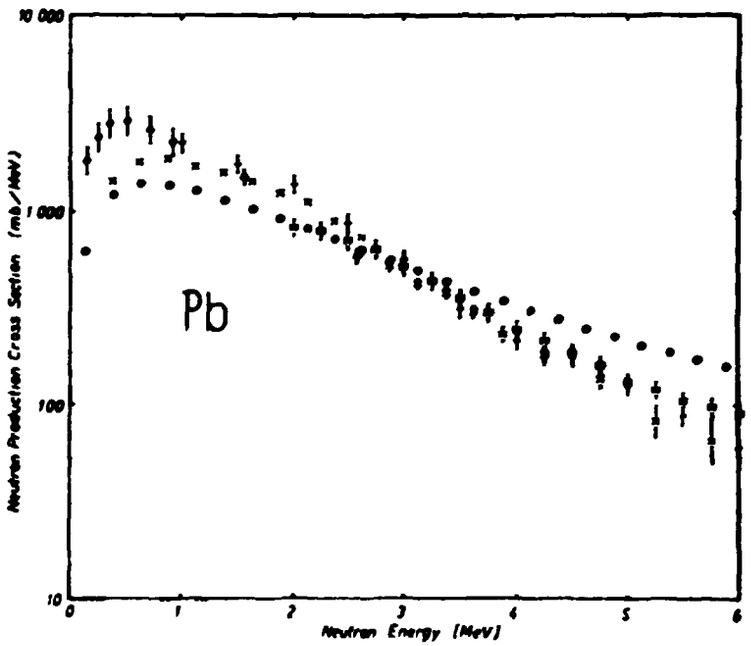

Fig. 11. Angle integrated secondary neutron spectrum from interactions of 14 MeV neutrons with lead; × present result; + Schectman /1/; ⊕ Clayeux /4/; ⊠ Hermsdorf et al. /5/; ⊙ statistical model calculation

Literature

1) R.M. Schectman and J.D. Anderson, Nucl. Phys. 77 (1966) 241
2) C.S. Mathur et a., Phys. Rev. 186 (1969) 1038, NDL-TR 86 (1967)
3) J.L. Kammerdiener, UCRL 51232 (1972)
4) G. Clayeux and J. Voignier, CEA R 4279 (1972)
5) D. Hermsdorf et al., Kernenergie 17 (1974) 76, 17 (1974) 259, 18(1975) 83, 19(1976) 241 and Bericht ZfK 277U(1975)
6) O.A. Salnikov et al., Sov. J. Nucl. Phys. 122(1971)620, YK 7(1972)102
7) G. Stengl et al., Nucl. Phys. A290 (1977) 109
8) A. Chalupka et al., Nucl. Instr. and Meth. 150 (1978) 209
9) A. Chalupka, Nucl. Instr. and Meth. 164 (1979) 105
10) J.M. Grundl and C. Eisenhower, IAEA-208 (1978) Vol. I, p. 64
11) H. Vonach et al., Z. f. Physik 237 (1970) 155
12) B. Strohmaier and M. Uhl, Proc. Winter Course on Nuclear Physics and Reactors, Trieste, 16. Jan. - 10. Feb. 1978
13) F. Perey and B. Buck, Nucl. Phys. 32 (1962) 350
14) F.D. Becchetti jr. and G.W. Greenlees, Phys. Rev. 182 (1968) 1190
15) J.R. Huizenga and G.I. Igo, ANL-6373 (1961)
16) W. Dilg et al., Nucl. Phys. A217 (1973) 269
17) P. Axel, Phys. Rev. 83 (1951) 1073
18) S.F. Mughabghab and D.J. Garber, BNL-325 (1973)

INVESTIGATION OF NUCLEAR REACTION MECHANISM IN 3.4 MEV-NEUTRON SCATTERING ON 2p-1f-SHELL NUCLEI

Mohamed+,A.H.,T.Schweitzer,D.Seeliger and S.Unholzer
Technical University Dresden,GDR

Absolute differential cross sections for elastic and inelastic scattering of 3.4 MeV neutrons are presented for V-51,Mn-55,Fe-56,Co-59.The theoretical analysis of angular distributions in the framework of a simple but absolute reaction model results in good accordance between theory and experiment.Direct reaction contributions are detected in this low energy region and can be attributed to the direct excitation of collective(vibrational) degrees of freedom in the nucleus.For all calculations as DWBA,Coupled Channels,Hauser-Feshbach-theory one set of generalized optical model parameters has been used.

Introduction

This work is part of systematical investigations of nuclear reaction mechanism in 3.4 MeV neutron scattering.Measurements of differential cross section data for elastic and inelastic neutron scattering by TOF-experiments have been carried out in the last years on the pulsed beam(d,d)-neutron generator of the Technical University Dresden/ 1 /.The physical analysis of neutron scattering on 2s-1d-shell nuclei is closed and results have been partially published/ 2 /. What is the aim of such investigations and which problems occur in analysis? One reason is to test statistical and direct reaction theories near the limits of their applicability.Low level densities in the compound nucleus,low energy application of direct reaction theories require a careful analysis,and there must be strong restrictions in the number of free parameters to get physical results.Behind that, such tests can be also of practical importance,because they give instructions for nuclear data evaluations.

Further are the quest of direct reaction parts in this low energy region and the investigation of nuclear reaction mechanism of fundamental physical interest.We remember, that the inherent physical interest to understand the nuclear reaction mechanism from a more general point of view/3-6/ was emphatically stimulated in the last ten years by experimental evidences for direct reaction contributions in neutron scattering experiments below 7MeV.

In spite of progress this problem is not closed today,so that we have not any general reaction model to solve our problems.Limited models,based on direct and statistical reaction parts,must be applied in this matter.Coherence effects can not be excluded,and we must minimize the number of free parameters in this theory, and take care for physical reliability.

An additional point-not unessentially-is the production of more exact nuclear data for Fast Breeder and Fusion Reactors.The energy region is of interest,and the nuclei of investigations are components of structure,cooling and shielding materials for such reactors.We believe,that systematic experiments enable us to reduce experimental errors in the most simple way.Some systematic errors for example as in neutron source strength or detection efficiency are the same for all measurements in such experiments and can be separated.

Physical results

The analysis of angular distributions of neutron scattering on nuclei with low lying discrete levels gives possibilities to test the common idea of reaction mechanism in the two extreme cases of either statistical or direct nuclear

+now Kairo-University,Egypt

reaction.In simplification we expect a pure statistical reaction to be symmetric around 90 degrees in CM-system contraray to the direct angular distribution,which shows a more diffractional structure.

With this experience and with the exspectation that direct excitation of low lying collective states gives measurable contributions,we have absolutely measured the angular distributions of elastically and inelastically scattered neutrons from a number of 2p-1f-shell nuclei.This shell is a region of vibrational structure of low lying excited nuclear states,what is easy to see from the equidistant level spacing for the first excited 2^+ and 4^+ levels.

We have used in our calculations the Hauser-Feshbach Compound Reaction Model (HFC)/7,8/with Moldauer-Corrections for level width fluctuations and for the direct reaction part DWBA-theory and the Coupled Channels Method(CCC)/9/. Applications within the bounds of these models are standard techniques and yield a description of experimental data,which is succesfully.In our intermediate situation,where not only compound but also direct reaction parts are exspected,a simple reaction model was used of incoherent superposition of direct and statistical reaction parts.

$$\frac{d\sigma}{d\Omega} = \frac{d\sigma}{d\Omega}\Big|_{HFC} + \frac{d\sigma}{d\Omega}\Big|_{DIRECT}$$

We have made the following assumptions for physical consistency:

only one set of generalized optical model parameters for all nuclei and for all used reaction models,

β-deformation parameters from reliable literature values

We do not fit theory to experimental data.With that assumptions we have not any free parameter in our theory.We compare our absolute data with an absolute reaction model.

Afew examples are given in the following figures to show the quality of analysis and the usefullness of the reaction model.

In fig.1a,b we give the low energy nuclear structure of Fe-56 and Co-59 for argument of the coupling modes.The 2^+-one quadrupole-phonon-state(qp-state) and 4^+two qp-state are the first members of the quasi ground state band in Fe-56.We explain the Co-59 structure to be caused by weak coupling of a $f_{7/2^-}$ proton-hole to the first vibrational 2^+one qp-state of the neighbouring even-even Ni-60.With an equidistant level spacing(2^+one qp-state at 1.33 MeV,4^+two qp-state at 2.62 MeV)the Ni-60 - stucture is markedly vibrational (fig.1c).Second $0^+$and 2^+-states are the other members of the two qp-triplet and heads for β- or γ-vibrational bands.Coupling of $f_{7/2^-}$ o 2^+gives J -values:$3/2^-$, $5/2^-$,$7/2^-$,$9/2^-$and $11/2^-$ for excited states in Co-59,whereat the mean energy value of the first 2^+-state in Ni-60 will be reached in the frame of weak coupling model. That can roughly be seen also from fig.1b,c.The direct excitation of

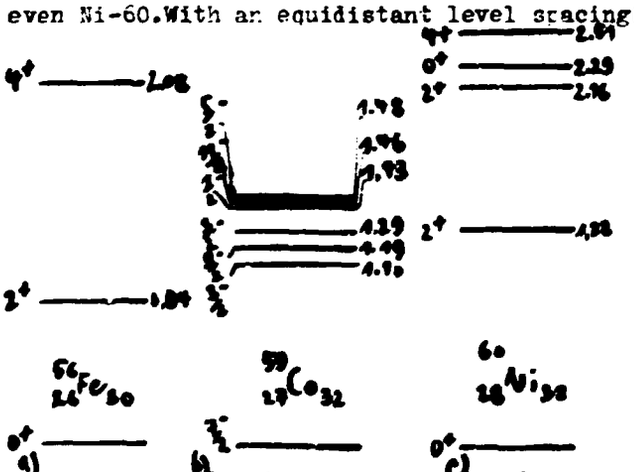

fig.1 Nuclear level sequence of low lying excited states for Fe-56 a),Co-59 b) and Ni-60 c).J^π-values,excit.energies are given

the quasi ground state band is the most strongest,and directly coupled states can differ in only one quadrupole phonon number.This are the main suppositions of our coupling modes.

For calculations we have used the following computer codes:

HFC-code ELISA/10/,CCC-code CHUCK/11/,DWBA-code DWUCK/11/.

Our optical potential is a local potential with imaginary surface part,spin-orbit part and Wood-Saxon formfactors.For all calculations we used a generalized optical parameter set(GOMP) /12/.

Experimental and calculated angulardistributions are shown for Fe-56 and Co-59 in fig.2 and fig.3

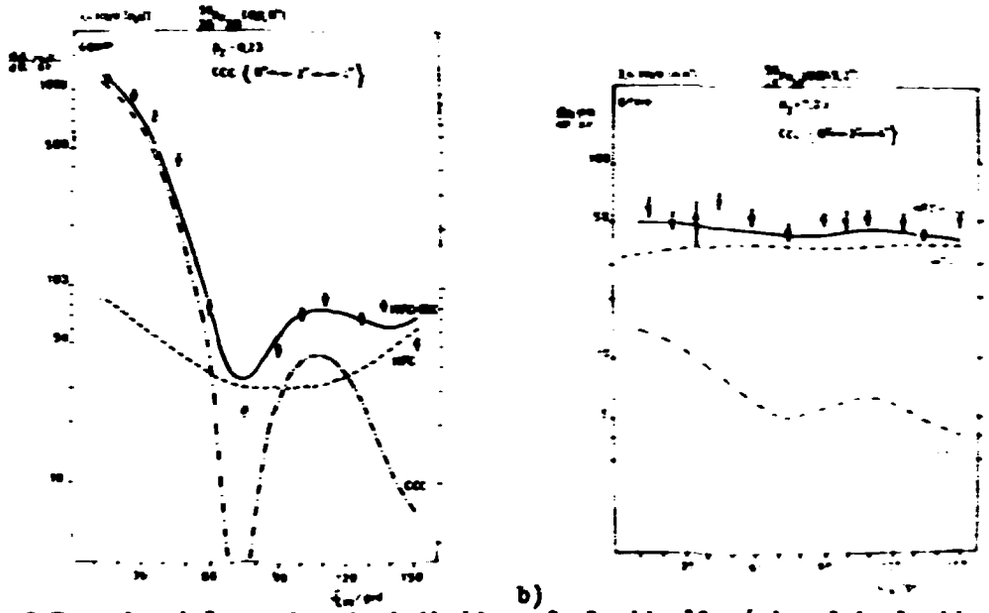

a) b)

Fig.2 Experimental angular distribution of elastically (a) and inelastically(b) scattered 3.4 MeV neutrons on Fe-56 and theoretical analysis by incoherent superposition of HFC-reaction part and CCC-reaction part

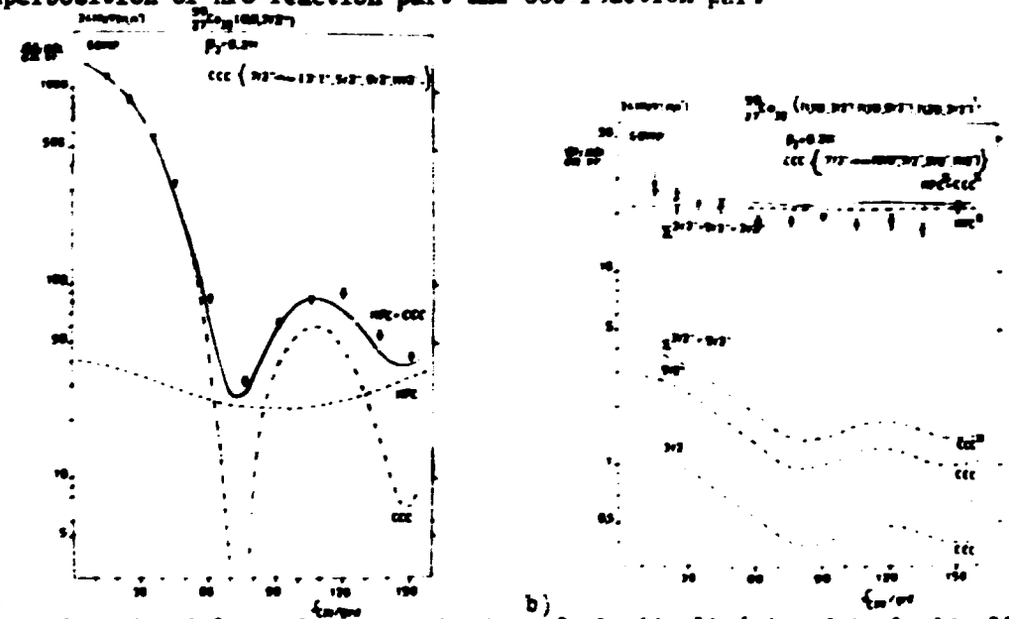

a) b)

Fig.3 Experimental angular distribution of elastically(a) and inelastically(b) and c) scattered neutrons on Co-59 and theoretical analysis by incoherent

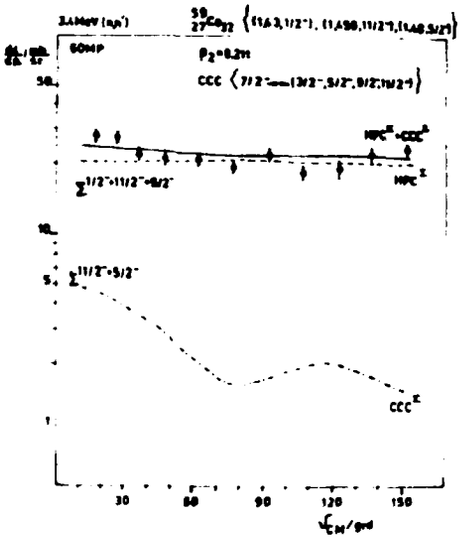

c)
superposition of HFC-reaction part and coupled channel (CCC)-reaction part. Unresolved levels are given in braces on top of figures. Single HFC-and CCC-parts are then summarized indicated by ,where the upper index characterizes the contributing levels.

A systematic error of 8% in normalization, which is the same for all measuring points, is not marked. Excitation energy in MeV and J -values of nuclear levels are given in parentheses on top of figures. Coupling modes and ß-deformation parameters can also be found here.

The general accordance between theory and experiment is very well with regard to the very hard demands and the simplicity of the reaction model.

References

/1/ Schweitzer, T., Unholzer, S., Thesis, 1978, Technical Univ. Dresden
Schweitzer, T. et.al., Kernenergie, 6 (1977), 174
Schweitzer, T. et.al., Jadern.Constant, 22 (1976), 15

/2/ Schweitzer, T. et.al., Report ZfK 376 (1978), ZfK 382 (1979)

/3/ Feshbach, H., Ann.Phys. 5 (1958), 257 and 19 (1962), 287

/4/ Mahaux, C., Nucl.Phys. 68 (1965), 481

/5/ Weidenmüller, H.A., Nucl.Phys. 75 (1966), 19

/6/ Rotter, I. et.al., Particles and Nucleus 6 (1975), 435

/7/ Hauser, H. and Feshbach H., Phys.Rev. 87 (1952), 366

/8/ Moldauer, P.A., Phys. Rev. 135 (1964), 642

/9/ Tamura, T., Rev.Mod.Phys. 37 (1965), 678

/10/ Kießig, G., Thesis, 1974, Technical University Dresden

/11/ Kunz, P.D., code unpubl., Univ. of Colorado

/12/ Holmquist, B. and Wiedling, T., Journ.Nucl.En. 27 (1973), 543

ИССЛЕДОВАНИЯ ВЗАИМОДЕЙСТВИЯ БЫСТРЫХ НЕЙТРОНОВ СО СРЕДНИМИ И ТЯЖЕЛЫМИ ЯДРАМИ В ИНСТИТУТЕ ЯДЕРНЫХ ИССЛЕДОВАНИЙ.

И.Я.Барит
Институт ядерных исследований АН СССР, Москва.

Аннотация

Обсуждаются экспериментальные данные о сечениях возбуждения первых уровней 2^+ у четно-четных ядер при неупругом рассеянии нейтронов низкой энергии, а также о взаимодействии нейтронов с энергиями около 17 МэВ с изотопами свинца ^{206}Pb и ^{207}Pb. Показано, что особенности поведения сечений могут быть объяснены эффектами промежуточных резонансов.

С целью поиска нестатистических эффектов при взаимодействии нейтронов с ядрами было предпринято экспериментальное исследование неупругого рассеяния нейтронов мегаэлектронвольтной энергии на сферических ядрах. Кроме того, был также предпринят поиск промежуточной структуры типа изобар-аналоговых состояний (ИАС) в нейтронных сечениях для тяжелых ядер вблизи замкнутых оболочек (изотопы свинца).

В.И.Попов и др.[1] измеряли энергетическую зависимость сечений возбуждения первых уровней 2^+ и некоторых более высоких уровней четно-четных ядер от порога возбуждения уровня до нескольких сотен кэВ над ним с разрешением порядка 10-15 кэВ в области массовых чисел 40-200. Сечение неупругого рассеяния измерялось по выходу γ-излучения, сопровождающего неупругое рассеяние нейтронов. Экспериментальные данные для функций возбуждения сравнивались с расчетами по статистической теории Хаузера - Фешбаха с учетом поправки на флуктуацию ширин ((независимые каналы)(рис.1). Проведенное сравнение (рис.2) показывает, что различие между расчетными и экспериментальными сечениями для всей исследованной области ядер в большинстве случаев не выходит за пределы 30%, если в расчете используется оптический потенциал с едиными параметрами. Исключение представляли данные для изотопов Ge и Se, экспериментальные сечения для которых значительно (до 2 раз) превышали расчетные величины и в меньшей степени для изотопов Ru и Pd (рис.3). Никаким выбором потенциала и его параметров нельзя описать экспериментальные данные для изотопов Ge, Se, Ru и Pd, сохраняя возможность такого описания для остальных ядер.С точки зрения статистической теории этот результат свидетельствует о корреляции ширин входных и выходных каналов.

Учет связи входных и выходных каналов может быть решен в рамках обобщенной оптической модели. В.И.Поповым и др. были выполнены расчеты прямого сечения методом связанных каналов для вибрационной модели, а также флуктуационного сечения для изотопов Ge и Se. Для вычисления флуктуационного сечения в этом случае использовалась методика Хофмана и др.[2], позволяющая его рассчитать в присутствии прямого процесса. Сравнение результатов расчета с экспериментальными данными показывает (рис.1), что учет связи каналов в однофононном приближении незначительно влияет на величины сечения неупругого рассеяния. Двухфононное приближение приводит к хорошему описанию экспериментальных сечений. Силовые функции в обоих приближениях описываются удовлетворительно. Вклад в сечение процессов, вызываемых связью каналов, уменьшается как с уменьшением, так и с увеличением A. Малые значения W указывают на то, что в рассматриваемом случае

поглощение идет в основном через возбуждение сильно связанных коллективных состояний. Вклад прямой реакции в сечение неупругого рассеяния составляет 30%.

Характер зависимости расчетных парциальных сечений для отдельных каналов реакций от энергии и их высокая чувствительность к величине действительной части потенциала свидетельствует о том, что в данном случае для входных каналов с орбитальным моментом ℓ =I и 2 возникает промежуточная структура сечений. Полная ширина этой структуры ~ I МэВ.

Аналогичные расчеты были выполнены для четно-четных ядер с A = I00–I20 (рис.3). Наряду с исследованием сферических ядер были начаты измерения для деформированных ядер. Получены функции возбуждения для неупругого рассеяния нейтронов с возбуждением первых 4^+ уровней изотопов $^{152,154}Sm$ и $^{158,160}Gd$ вблизи порога реакций. Расчеты были выполнены по той же схеме как для сферических ядер, с той разницей, что использовался потенциал связи для ротационной модели. Учитывалась связь состояний $0^+, 2^+, 4^+$. Наблюдается удовлетворительное согласие расчета с экспериментальными данными. Вклад прямого сечения при энергии ~ 800 кэВ составляет 5–I0%.

Поиск промежуточной структуры нейтронных сечений для изотопов свинца и нейтронов с энергиями I4–I8 МэВ был выполнен в работах Б.А.Бенецкого и др.[3] и Г.Е.Беловицкого и др.[4].

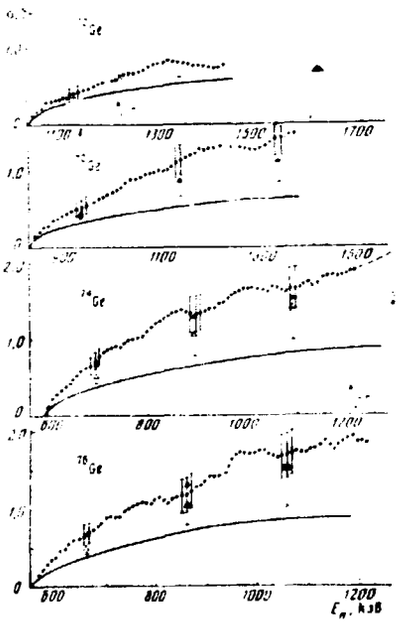

Рис.I. Экспериментальные сечения реакции $(n,n'\gamma)$ для изотопов Ge, усредненные по интервалу энергии I00 кэВ и расчетные: — в приближении независимых каналов, + – в однофононном приближении с W= 5 МэВ, ▲ – в двухфононном приближении с V_0 = 52 МэВ и W = I МэВ, Δ – в двухфононном приближении с V_0 = 5I МэВ и W = I МэВ.

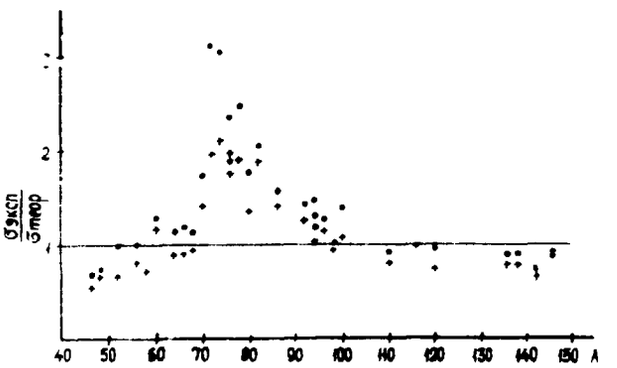

Рис.2. Отношение экспериментальных сечений для первых уровней 2^+ к рассчитанным в приближении независимых каналов. + – отношения сечений при энергии рассеянных нейтронов I00 кэВ; • – то же при энергии 300 кэВ.

Б.А.Бенецкий и др. измерили энергетическую зависимость полного сечения для изотопов свинца ^{206}Pb и ^{207}Pb (рис.5) и дифференциального сечения упругого рассеяния для естественного свинца на углы 45^0, 55^0, 60^0 и 70^0 в интервале энергий от I6 МэВ до I8 МэВ.

В энергетической зависимости полных сечений для ^{207}Pb наблюдаются для нейтронов с энергиями I6,8 и I7,2 МэВ особенности резонансного характера. Для изотопа ^{206}Pb такие особенности отсутствуют. В энергетических зависимостях дифференциальных сечений рассеяния для свинца

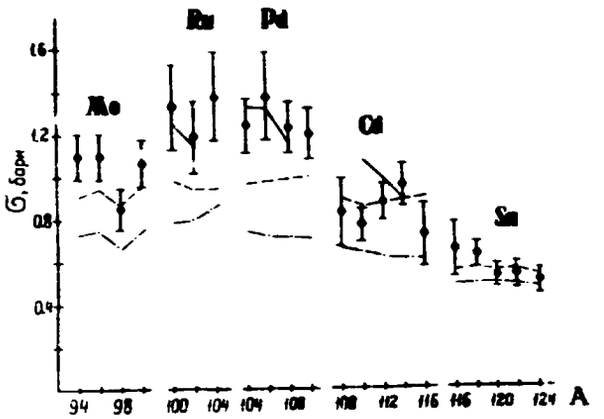

Рис.3. Экспериментальные и расчетные сечения для первых уровней 2^+:
-·-·- расчет в приближении независимых каналов;
– – – расчет в однофононном приближении V_0= 51 МэВ, W_1= 1 МэВ, W_2= 6 МэВ;
——— расчет в двухфононном приближении V_0 = 49 МэВ, W = 1 МэВ.

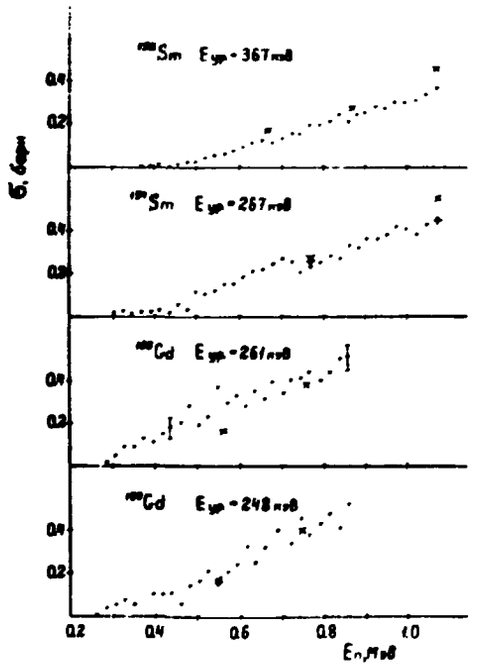

Рис.4. Экспериментальные и расчетные сечения для ротационных уровней 4^+ Sm и Gd
× - расчет со схемой связи 0^+-2^+-4^+. При V_0 = 53 МэВ, W = 2 МэВ;
+ - расчет со схемой связи 0^+-2^+-4^+ при V_0 = 51 МэВ, W= 2 МэВ.

также проявляются нерегулярности, положение которых коррелировано с резонансными особенностями в полном сечении. Значимость гипотезы о том, что эти нерегулярности обусловлены статистическим разбросом экспериментальных данных в соответствии с критерием Стьюдента не превышает 10^{-3} для каждого случая.

Наличие резонансов в полном сечении для ^{207}Pb находит свое подтверждение при сопоставлении экспериментальных данных с расчетами по оптической модели. Параметры, описывающие энергетическую зависимость полного сечения ^{207}Pb во всем исследованном интервале, существенно отличаются от общепринятых аномально большой глубиной мнимой части потенциала (19,1 МэВ вместо 8,6 МэВ). Аномально большая величина W для ^{207}Pb может быть естественно объяснена влиянием сильных неусредненных резонансов.

Ширины наблюденных резонансов составляют 190±40 кэВ, а отношение упругой нейтронной ширины Γ_{n0} к полной, оцененное по максимуму резонансной части сечения, равно $g\Gamma_{n0}/\Gamma \sim 0{,}6$.

В связи с этими результатами Г.Е.Беловицким и др. [4] были предприняты эксперименты по поиску резонансов промежуточной структуры в реакции (n,p) на изотопах свинца ^{206}Pb и ^{207}Pb для той же области энергии нейтронов [4]. Реакции (n,p) идентифицировались по наведенной

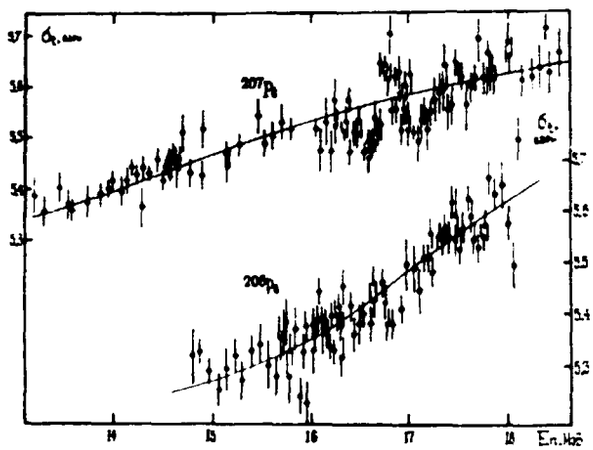

Рис.5. Энергетическая зависимость полного нейтронного сечения для ^{206}Pb и ^{207}Pb . Кривые - расчет по оптической модели.

β-активности. В функции возбуждения для ^{207}Pb не наблюдается никаких нерегулярностей, которые выходили бы за пределы экспериментальных ошибок (рис.6). Из этих данных следует, что резонансная часть сечения реакции (n,p), если таковая имеется, меньше $0,1\,\sigma_{n,p} = 0,5$ мбн. Если учесть, что резонансная часть полного сечения порядка 100 мбн., то можно заключить, что для резонансов, наблюдаемых в полном сечении, $\Gamma_p/\Gamma \leqslant 0,005$.

В аналогичных измерениях для ^{206}Pb и интервала энергий нейтронов 13,4-15,0 МэВ наблюдено отклонение от регулярного хода при E_n = 13,9-14,9 МэВ. Положение по энергии и ширины аномалий согласуются с предположением о том, что они обязаны возбуждению ИАС. Превышение экспериментального сечения над монотонным ходом составляет 0,12 мбн., а ширина резонанса 150 кэВ. Сопоставим эти характеристики с теоретическими предсказаниями. Для ядер в области свинца из опытом по возбуждению ИАС протонами следует, что $0,1 \leqslant \Gamma_p \leqslant 0,7$. Согласно теоретическому расчету работы [5] упругая нейтронная ширина для прямого распада ИАС равна 0,08 кэВ. Если теперь в резонансную формулу Брайт - Вигнера подставить значения ширин, то получим $0,03 \leqslant \sigma^{res}_{n,p} \leqslant 0,21$ мбн., что согласуется с результатами эксперимента.

Возможной причиной наблюденных в полном сечении для ^{207}Pb резонансов является возбуждение ИАС нейтронами. Ширины наблюденных резонансов той же величины, что ширины ИАС для ядер в этой области массовых чисел, а энергия возбуждения (24,5±0,2 МэВ) в пределах ошибок, совпадает с энергиями уровней, обнаруженными в реакциях (γ,p), (γ,np) и $(e,e'p)$ (24,9-25,0 МэВ) и интерпретированными как ИАС [6]. Против того, чтобы интерпретировать рассматриваемые резонансы

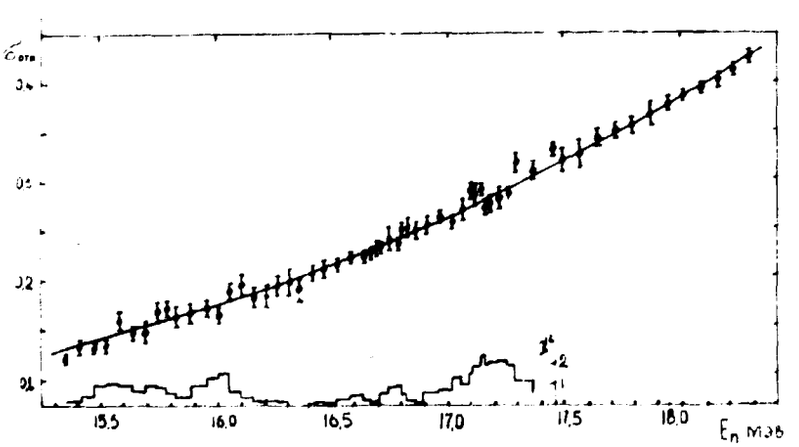

Рис.6. Энергетическая зависимость сечений реакции (n,p) для ^{207}Pb и гистограмма χ^2_i

как возбуждение ИАС, говорит большая величина отношения Γ_n/Γ и малая величина Γ_p/Γ. Большая величина Γ_n/Γ противоречит запрету по изоспину и в 10^3 раз больше теоретических расчетов [5]. Малая величина Γ_p/Γ противоречит экспериментальным данным для ИАС. Кроме того, малая величина Γ_p/Γ противоречит тому, что резонанс при энергии 25 МэВ не наблюдается для реакции (γ, n), несмотря на то, что $\Gamma_n/\Gamma_p \sim 10^2$. Следовательно, резонансы, наблюдаемые для нейтронов и γ-лучей, должны соответствовать разным состояниям ядра ^{208}Pb.

Таблица

Возбуждение ИАС нейтронами и прямой нейтронный распад ИАС

Процесс	J^π	E, МэВ	Γ_{n^0}, кэВ	Γ, кэВ	Γ_{n^0}/Γ	Γ_p/Γ	Ссылка
$^{24}_{12}Mg + n$	$3/2^+$	0,555	0,009	0,014	0,63		[7]
$\sigma_t(E_n)$	$1/2^+$	1,567	4,2	5	0,85		
$^{28}_{14}Si + n$ $\sigma_t(E_n)$; $\frac{d\sigma_{el}}{d\Omega}(E_n)$	$1/2^+$	1,254	9,0	9,0	1,0		[8]
$^{90}_{40}Zr + n$, $\sigma_t(E_n)$	$5/2^-$	6,15	3	45	0,06		[9]
$^{90}_{40}Zr(n,p)$	$5/2^-$	6,15		45		0,01	[9]
$^{117}_{50}Sn(p,n)$	0^+	4,49	$\gtrsim$4,66	32	$\gtrsim$0,15		[10]
$^{93}_{41}Nb(p,n)$	7^+	4,00	$\gtrsim$0,26	22	$\gtrsim$0,012		[11]
$^{207}_{82}Pb + n$, $\sigma_t(E_n)$	1^-	16,6	160	190	0,8		
$^{207}_{82}Pb(n,p)$	1^-	16,6		190		$\lesssim$0,005	

В таблице суммированы имеющиеся литературные данные по наблюдению промежуточной структуры нейтронного сечения, которые интерпретировались авторами как возбуждение ИАС нейтронами. Таблица включает все исследованные реакции, но в целях экономии не все наблюденные резонансы. В таблицу включены также данные по ширинам прямого нейтронного распада, полученные Б.Н.Гуковским [10,11]. Из таблицы видно, что во всех случаях, когда наблюдается большая упругая нейтронная ширина и большая величина ее отношения к полной ширине, мишенью является магическое ядро. Исключение составляет ^{24}Mg и ^{28}Si. В двух случаях, когда для исследованных резонансов измерена протонная ширина, она оказывается значительно меньше наблюдаемых обычно для ИАС. Для тех резонансов, для которых имеются теоретические расчеты [5] экспериментальные данные больше их от двух до двадцати раз. Исключение составляет ядро ^{207}Pb. По-видимому природа состояний ^{208}Pb другая чем ИАС.

Литература

I. Е.С.Конобеевский, Р.М.Мусаелян, В.И.Попов и И.В.Суркова, Известия АН СССР, сер.физ. 40, 803(1976).
В.П.Ефросинин, Р.М.Мусаелян, В.И.Попов, Ядерная физика, 29, 631(1979).
2. H.M. Hofman J. Richert, J.W. Tepel, H.A. Weidenmuller Ann. of Phys. 90,403 (1975)
3. Б.А.Бенецкий, А.В.Клячко, В.В.Нефедов, И.М.Франк, И.В.Штраних. Нейтронная физика. ЦНИИатоминформ, М., 1977, ч.2, стр.44,47.
Б.А.Бенецкий, А.В.Клячко. В.В.Нефедов, И.М.Франк, И.В.Штраних. Краткие сообщения по физике. ФИАН, № 4, стр.23,27 (1978).
4. Г.Е.Беловицкий, О.С.Пресняк. Письма в ЖЭТФ, 29, 791(1979).
5. В.Г.Губа, Д.Ф.Зарецкий, И.Г.Урин. Письма в ЖЭТФ, 21, 386(1975).
6. K. Shoda, S. Oikawa, T. Saito, H. Miyase and A. Suzuki Nucl. Phys. A246,365(1975)
7. H. Weigmann, R.L.Macklin, J.A. Harvey, Phys. Rev. C14,1328(1976).
8. S. Cierjacks, S.K. Gupta, I.Schouky, Phys. Rev. C17,12(1978)
9. G. C. Hicks, C.J.F. Legge, J.Phys.,A7,132(1974).
10. Б.А.Гуковский. Письма в ЖЭТФ, 26, 408(1977).
11. Б.А.Гуковский. Ядерная физика, 28, 957(1978).

АНАЛИЗ ЖЕСТКОЙ КОМПОНЕНТЫ СПЕКТРОВ РЕАКЦИИ $^{113}In(n,n')$

А.В. Игнатюк, Г.Н. Ловчикова, В.П. Лунев, О.А. Сальников, С.П. Симаков
Физико-энергетический институт, Обнинск, СССР

Аннотация
В рамках борновского приближения искаженных волн проанализирован интегральный вклад прямых переходов в жесткую часть спектров неупругого рассеяния нейтронов с энергией 5,34 МэВ.

В последние годы исследования жесткой компоненты спектров неупругого рассеяния нуклонов средних энергий вызывают особый интерес в связи с развитием представлений о предравновесном механизме распада составного ядра. Модель предравновесного распада интенсивно развивалась не только для процессов неупругого рассеяния, но и для реакций обмена или передач нуклонов, и во многих случаях с ее помощью удавалось достичь сравнительно хорошего описания высокоэнергетической составляющей наблюдаемых спектров или соответствующих участков функций возбуждения [I]. Однако, при обсуждении полученных результатов остается в значительной степени неясным вопрос, в какой мере достигнутое описание свидетельствует о новом механизме ядерных реакций, отличающемся по своим свойствам как от традиционного статистического механизма распада составного ядра, так и от хорошо известных прямых процессов. Чтобы ответить на этот вопрос необходимо определить характерные признаки каждого из механизмов и проанализировать их проявление в рассматриваемых реакциях. Для изучения интегрального вклада прямых процессов ряд благоприятных возможностей представляет сравнительный анализ спектров (n,n') и (p,n) - реакций. Если энергии налетающих частиц и ядра-мишени в этих реакциях подобраны таким образом, что испарительная компонента спектров соответствует одному и тому же остаточному ядру, то проявляющиеся различия спектров естественно связать с прямыми переходами. Нейтронные спектры реакций $^{113}In(n,n')$ и $^{113}Cd(p,n)$ были исследованы в работе [2] при энергиях налетающих частиц 5,34 МэВ и 6,0 МэВ. Необходимое систематическое превышение жесткой компоненты спектров неупругорассеянных нейтронов над аналогичными спектрами реакции (p,n) соответствует интегральному сечению прямых процессов ~200 мбарн, и отчетливо выраженная асимметрия углового распределения нейтронов, связанных с этой компонентой, может служить дополнительным аргументом в пользу предложенной идентификации природы данной части спектров. Так как прямые переходы при неупругом рассеянии возбуждают в первую очередь коллективные степени свободы ядер, то для интерпретации полученного результата важно понять, как согласуется найденная величина сечения прямых процессов с имеющимися данными о спектральной интенсивности вибрационных возбуждений ядер. Используя традиционные соотношения борновского приближения искаженных волн и модель слабой связи нечетной частицы с фононными возбуждениями остова [3], мы провели расчеты ожидаемых для указанной выше энергии налетающих нейтронов сечений прямых переходов. Результаты этих представлены в таблице.

Мультиплет состояний	Средняя энергия мультиплета, МэВ	L^{π}	β_L	σ мбарн
$(2^+ \otimes 9/2^+)$	I,4	2^+	0,I8	I80
$(3^- \otimes 9/2^+)$	2,6	3^-	0,I7	43
$(2^+ \otimes 2^+ \otimes 9/2^+)$	2,4	$0^+, 2^+, 4^+$		36
$(4^+ \otimes 9/2^+)$	3,2	4^+	0,09	25

Параметры динамической деформации β_L для рассматриваемых переходов были получены из систематики данных по возбуждению заряженными частицами низколежащих фононных состояний соседних четно-четных ядер [4], и использовавшиеся в расчетах параметры оптического потенциала были взяты в соответствии с рекомендациями работ [5]. Полученная в расчетах оценка интегрального сечения прямых переходов ~ 280 мбарн не сильно отличается от приведенной выше экспериментальной этого сечения. Таким образом, вывод о доминирующей роли прямых процессов в формировании наблюдаемых "нестатистических" компонент спектров неупругого рассеяния, сделанный в работе [2] на основе феноменологического анализа спектров (n,n') и (p,n) реакций, получает подтверждение и при теоретическом анализе сечений прямых переходов. Но прямым следствием этого вывода является заключение о роли предравновесного механизма распада. Если такой механизм и существует, то его вклад в спектры неупругого рассеяния должен быть значительно ниже, чем это следует из оценок, полученных в работах [I]. Механизм предравновесного распада должен проявляться не в асимметрии угловых распределений, а скорее в увеличении по сравнению с равновесным распадом составного ядра анизотропии углового распределения продуктов реакции [6]. Поиски такого увеличения представляли бы значительный интерес для развития представлений о различных механизмах ядерных реакций. Особенно интересными в этом отношении могли бы быть эксперименты по рассеянию нейтронов с более высоким разрешением, с помощью которых можно было бы более детально локализовать прямые переходы и изучить не связанные с ними компоненты распада составного ядра.

Литература

[I] J.J. Griffin, Phys. Rev.Lett., 17, 478, 1966.
C. Kolbach, Acta Phys. Slov., 25, 100, 1975.
D. Seeliger, III School on Neutron Physics, JINR, Dubna, 1978, p, 486.

[2] О.А. Сальников и др., Доклад на данной симпозиум,

[3] N. Austern, The Direct Nuclear Reaction Theories, Wiley Interscience, N.Y., 1960.

[4] M. Koike, Nucl.Phys., A 98, 209, 1967.
W. Makofske et al. Phys. Rev., 174, 1429, 1968.

[5] G. Haouat, Proc.Sec. Int. Symposium on Neutron Induced Reactions (Smolenice, 1979).

[6] А.В. Игнатюк и др., Изв. АН СССР, сер. физ., 39, 2I44, I975,

МЕХАНИЗМЫ РЕАКЦИЙ $^{113}In(n,n')^{113}In$ и $^{113}Cd(p,n)^{113}In$ ПРИ ЭНЕРГИИ ВОЗБУЖДЕНИЯ СОСТАВНОГО ЯДРА ~ 12,65 МЭВ

О.А. Сальников, Г.Н. Ловчикова, С.П. Симаков, А.М. Труфанов, Н.И. Фетисов, Г.Е. Котельникова
Физико-энергетический институт, Обнинск, СССР

Аннотация

В работе исследованы дважды дифференциальные сечения $^{113}In(n,n')^{113}In$ и $^{113}Cd(p,n)^{113}In$ и на основе анализа их показано отличие в механизме этих реакций. Реакция (n,n') обусловлена прямыми и равновесными процессами. В обеих реакциях при рассматриваемых энергиях отсутствует заметный вклад предравновесных процессов.

1. Введение

Неупругое рассеяние нейтронов может протекать трояко: при взаимодействии налетающего нейтрона с отдельным нуклоном ядра или с возбуждением коллективного состояния (прямой процесс), испускание нейтрона ядром в процессе установления статистического равновесия (модель предравновесного распада) и, наконец, испускание нейтрона ядром, находящимся в статистическом равновесии. Соотношение между вкладами от этих механизмов реакции меняется с энергией. В наших работах [1 ÷ 3] было показано, что вплоть до энергии нейтронов 14 МэВ всё сечение неупругого рассеяния обусловлено только двумя механизмами: прямым и равновесным. Между тем модель предравновесного распада [4] нашла широкое применение для описания спектров неупругорассеянных нейтронов. Нам это представляется необоснованным. Кроме внутренних противоречий самой модели, ее неполноты (она ничего не говорит об угловых распределениях), особенно видны ее недостатки, когда она используется для сравнительного описания нейтронных спектров из реакций (p,n) и (n,n'). В ряде работ [5, 6] отмечалось существенное различие жесткой части спектров и угловых распределений как по форме, так и по величине из реакций (p,n) и (n,n'), и наблюдаемое различие ~ в 20 раз больше, чем это предсказывается моделью предравновесного распада.

Однако не существовало экспериментов, где бы исследуемые реакции давали одно и то же составное ядро. (Подобные работы проведены с α-частицами и нуклонами, нотам сильное отличие может быть за счет большой разницы вносимых угловых моментов). Важно было получить сведения о нейтронных спектрах из разных реакций при одном и том же промежуточном и конечном ядре. Для этого было проведено совместное исследование спектров нейтронов из реакций $^{113}Cd(p,n)^{113}In$ и $^{113}In(n,n')^{113}In$, то есть исследования спектров нейтронов эмиссий из одного и того же составного ядра In^*-114. Начальные энергии протонов и нейтронов были выбраны так, чтобы в обоих случаях энергия возбуждения составного ядра In^*-114 была одинаковой. Исследования были проведены на одной установке а одинаковых экспериментальных условиях, что существенно повышает надежность сравнения.

2. Эксперимент

Исследования спектров нейтронов из реакций $^{113}In(n,n')^{113}In$ и $^{113}Cd(p,n)^{113}In$ проводились на спектрометре нейтронов по времени пролета на базе тандема

ЭГП-10М [7]. Источником нейтронов являлась реакция $T(p,n)He^3$. Использовалась газовая мишень. Начальная энергия нейтронов равнялась $E_0 = 5,34 \pm 0,05$ МэВ. Рассеивателем служил пустотелый цилиндр из металлического индия (87 % In-113 и 13 % In-115). Для оценки вклада от In-115 проводились измерения с таким же образцом из 100 % In-115. Для изучения спектра нейтронов из реакции $^{113}Cd(p,n)^{113}In$ использовалась фольга толщиной 58,6 кэВ из 90 % Cd-113. Энергия протонов была равна $6,0 \pm 0,03$ МэВ. Детектор (стильбен с ФЭУ-30) работал со схемой n-γ разделения. Относительная эффективность измерялась по выходу нейтронов из реакции $T(p,n)^3He$ в диапазоне энергий 0,5 ÷ 8 МэВ и она абсолютизировалась при измерении спектра спонтанного деления Cf-252, (T = 1,42 МэВ и $\bar{\nu}$ = 3,78). Абсолютное значение прямого потока нейтронов определялось по (n,p) рассеянию на полиэтилене [8]. При выделении из общего спектра вклада упругорассеянных нейтронов, форма пика последних определялась по пику упругорассеянных нейтронов на Pb-208, который при нашем разрешении полностью отделялся от пика соответствующего возбуждению первого уровня ($E_{1ур.}$ = 2,6 МэВ для Pb-208). При определении дважды дифференциальных сечений неупругого рассеяния нейтронов вводилась поправка на многократное рассеяние нейтронов и ослабление прямого потока в образце, вычисленная по методу Монте-Карло.

3. Результаты

Непосредственными результатами измерений являлись дважды дифференциальные сечения реакций (p,n) и (n,n') $d^2\sigma(E_0,E,\theta)/dEd\theta$ для (n,n') и $d^2\sigma(E_p,E,\theta)/dEd\theta$ для (p,n).

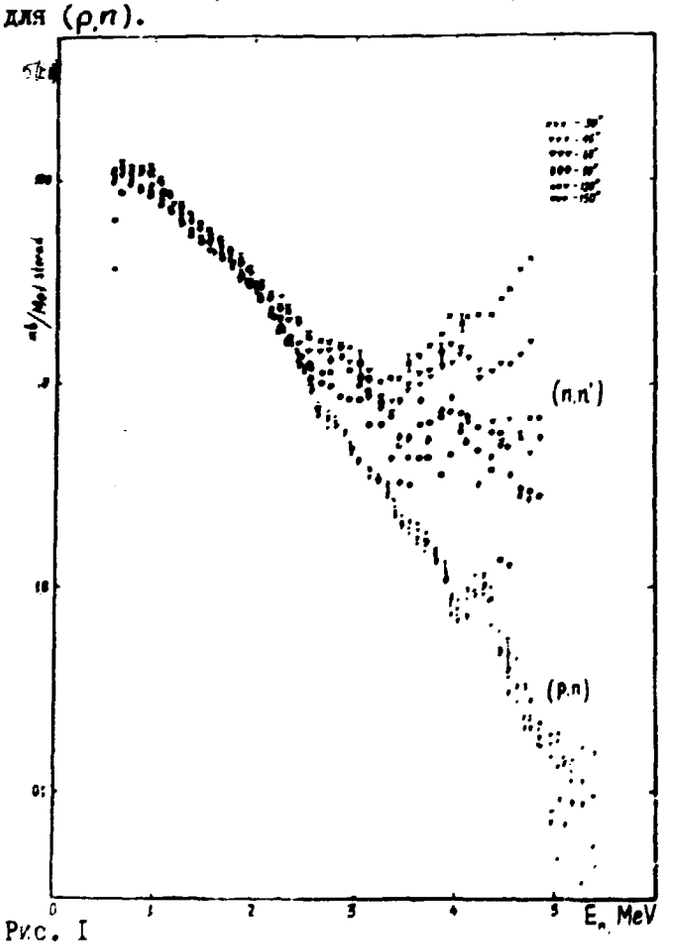

Рис. 1

Выбор начальных энергий протонов и нейтронов обеспечил одинаковую энергию возбуждения ядра In^*-114 обеих реакциях (~12,65 МэВ). Измерения сечений проводились под 6-ью углами в интервале $30^0 \div 150^0$. Ошибки измерений складывались из статистических ошибок и ошибок определения эффективности детектора (~ 3 %). Для реакции (n,n') добавлялась еще ошибка нормировки прямого потока, и, для жесткой части спектра ошибка вычитания пика упругорассеянных нейтронов. Из сравнения рис. 1 видно сильное отличие спектров нейтронов из реакций (n,n') и (p,n). Наблюдается так же сильное отличие в характере угловых распределений испускаемых нейтронов.

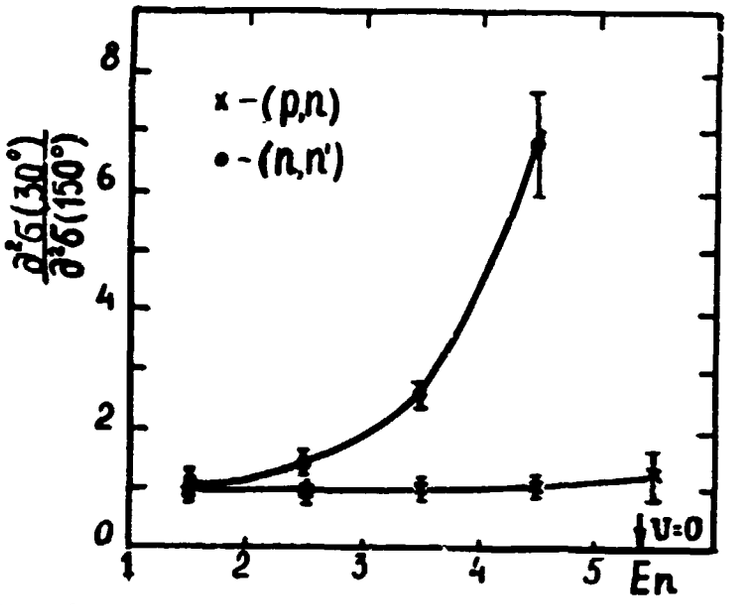

Рис. 2

Для реакции (p,n) оно симметрично относительно 90^0, тогда как для реакций (n,n') асимметрия заметна уже для малых энергий. Для более наглядного сравнения на рис. 2 приведено соотношение

$$\frac{d^2\sigma(E_0,E,30°)}{dE\,d\theta} \Big/ \frac{d^2\sigma(E_0,E,150°)}{dE\,d\theta}$$

для реакций (n,n') и (p,n) как функция энергии вылетающих нейтронов E.

4. Обсуждение результатов

Более жесткий спектр и асимметрия угловых распределений неупругорассеянных нейтронов указывает на вклад прямых процессов в реакцию (n,n'), тогда как для реакции (p,n) этого вклада неблюдается. Поскольку составные и конечные ядра одинаковы для исследуемых реакций и энергия возбуждения составных ядер Jn^*-II4 так же одинакова, то можно предположить, что форма спектров, обусловленных той частью реакции, что идет через составное ядро, так же будет одинаковой для обоих реакций. Тогда, принимая с соответствующей нормировкой спектр нейтронов из реакции (p,n) за часть сечения реакции (n,n'), обусловленную составным ядром, можно по разности полного спектра неупругорассеянных нейтронов и этой части сечения оценить вклад прямых процессов в реакцию (n,n'). Это было сделано как для каждого угла рассеяния (см. таблицу), так и для интегрального сечения. Неопределенность вклада прямых преоцессов не более 20 % т.е. II,3 ± 2 %. Полный вклад прямых процессов оказался равным 200 мб, что составляет II % от полного сечения реакции (n,n'). Таким образом оказалось, что даже для такой, сравнительно низкой энергии налетающих нейтронов (~ 5 МэВ) вклад прямых процессов для реакции (n,n') уже существенен.

Таблица

θ°	30^0	60^0	90^0	120^0	150^0	Интегральное сечение
						I72I,4
Сечения прямой реакции (мб/стер)	35,5	22,5	II,2	I2,4	7,5	I94,I
Вклад прямой реакции в %	I9,7	I4,5	8,3	I0,2	9,6	II,3

Отсутствие подробного вклада для реакции (p,n) показывает неприменимость модели предравновесного распада, так как она должна давать подобные результаты для обеих реакций. Прямое же неупругое рассеяние нейтронов осуществляется преимущественно изменением энергии и направления движения налетающих нейтронов в результате их взаимодействия с отдельными нуклонами ядра, а не в выбивании этих нуклонов (что требует гораздо большего переданного импульса, и, следовательно, происходит с меньшей вероятностью), и в этом случае отсутствие прямых процессов для реакции (p,n) для этой энергии становится понятным.

Литература

[1] О.А. Сальников, Г.Н. Ловчикова, Г.В. Котельникова и др. Препринт ФЭИ-216, (1970),

[2] О.А. Сальников, Е.М. Сапрыкин и др. Ядерная физика, т. 17, (1973), 1001,

[3] А.А. Лукьянов, О.А. Сальников, Е.М. Сапрыкин, Ядерная физика, т. 21, (1975), 67,

[4] I. I. Griffin, Phys.Lett. 17, (1966), 478

[5] Г.Н. Ловчикова, Г.В. Котельникова и др., Препринт ФЭИ-738, (1977),

[6] Н.С. Бирюков, Б.В. Журавлев, и др., Ядерная физика, т. 26, вып. 6, (1977), 1146,

[7] А.М. Труфанов, В.С. Нестеренко и др., ПТЭ, 2, (1979), 50,

[8] Дж. Л. Гаммель, В сб. "Физика быстрых нейтронов" т. 2, Атомиздат, Москва, (1966), 740.

О РАБОТАХ С БЫСТРЫМИ НЕЙТРОНАМИ НА ТАНДЕМ- УСКОРИТЕЛЯХ ЭГП-10

Д. Шмидт
Технический университет Дрезден, Секция физики, Дрезден, ГДР

Представлены работы на тандем-ускорителях, которые проведены в прошлых 10 лет в кооперации между институтами ФЭИ Обнинск и ТУ Дрезден.

1. Введение

Цель представленных здесь работ - исследование механизма ядерных реакции с быстрыми нейтронами в выходном канале. Это-актуальная задача и в настоящее время. При этом важную роль играет и получение ядерных данных для прикладных применений. Эти работы были выполнены в последние десять лет главным образом на нейтронных генераторах при энергиях близко к и четырнадцати МэВ.

Силами ТУ Дрезден в Россендорфе и в ФЭИ Обнинск в последние годы были созданы возможности для того, чтобы расширить эти эксперименты в новые области энергий и для новых типов реакций. При этом кооперация между обеими институтами, в этом году уже через 10 лет, развивалась в областях экспериментальной техники, совместенных измерений и интерпретаций полученных данных.

2. Источники нейтронов

Источники нейтронов - тандем-ускорители ЭГП-10 в обеих институтах. В стационарном режиме они характеризуются следующими параметрами:

E_p макс.	-	10 МэВ
ΔE	-	≤2 КэВ
част.	-	p, d, α и тяж. ионы
I_p	-	3 ... 8 μA

Обе ускорители были оборудованы наносекундной пульсацией и спектрометрами быстрых нейтронов по методу времени пролета. Электронные блоки для пульсации были проектированы и построены в ТУ Дрезден [1]. Надо заметить, что и другие группы используют импульсный режим работы ускорительей в ФЭИ и ЦЯЯК.

3. Техника детектирования

Детектирование нейтронов осуществляется с сцинтилляционными детекторами с помощью рассеяния на водороде. На основании этого был создан в ФЭИ спектрометр с одним детектором, который позволяет измерения под углами от 0^0 до 150^0 с пролётной базой 2 метра.

На тандеме в Россендорфе группа ТУ построила многодетекторную систему с 8 детекторами [2]. Схема этой системы показана на рис. 1. Преимущества этой системы состоят в значительно более высокой эффективности и уменьшении ошибок мониторировании. С другой стороны надо заложить большую затрату при построении, естественно, и при содержании в исправности и при калибровке.

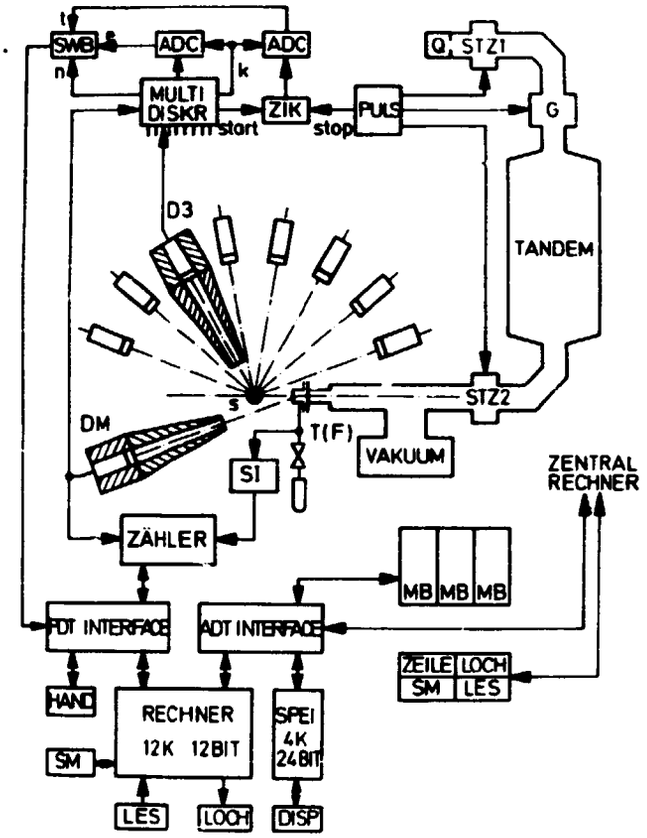

Рис. I Схема многодетекторной системы (значение блоков описались в работе [2])

Обработка измеренных спектров происходит на малой ЭВМ, но для вычисления сечений выработана комплексная программа, которую можно использовать и для дискретных и для сплошных спектров.

Одна из задач, особенно важная при использовании многодетекторной системы состоит в том, что точно контролировать или измерить разницы эффективности между всеми отдельными детекторами. Полезно оказалось в последние годы применение источника, который испускает нейтроны из спонтанного деления, как например ^{252}Cf. Форма спектра нейтронов хорошо известна. С помощью регистрации осколков, как сопуствующих частиц, можно измерить нейтронный спектр по методу времени пролета.

Как пример эффективность детектора представлена на рис. 2 в сравнении с вычислением по методу Монте-Карло.

Для исследований реакций типа (p,n) особенно важно следующие пункты:

а) Такие эксперименты можно проводить с высоким разрешением энергии во входном канале, это значит возможность исследовать структуры в функции возбуждения этой энергетической ширины.

б) Отсутствие упругого рассеяния дает возможность точного экспериментального анализа высоко-энергетической части нейтронных спектров, с другой стороны

эмиссия нейтронов возможно для наивысших энергий возбуждения конечного ядра из-за отсутствия кулоновского барьера.

в) Прямые процессы играют значительно меньшую роль относительно равновесных процессов чем в случае реакций типа (n,n'), за исключением зеркальных ядер.

Связано с этим были исследованы следующие проблемы:

I) Нейтронный распад изобар-аналоговых резонансов (ФЭИ - ^{115}In, ТУ - ^{109}Ag),

2) Исследование энергетического хода плотности состояний для ядер с массовым числом близко 100 (ФЭИ - ^{94}Zr, ^{119}Sn, ^{122}Sn, ТУ - ^{109}Ag),

3) Анализ реакции $^{11}B + p$ (ТУ).

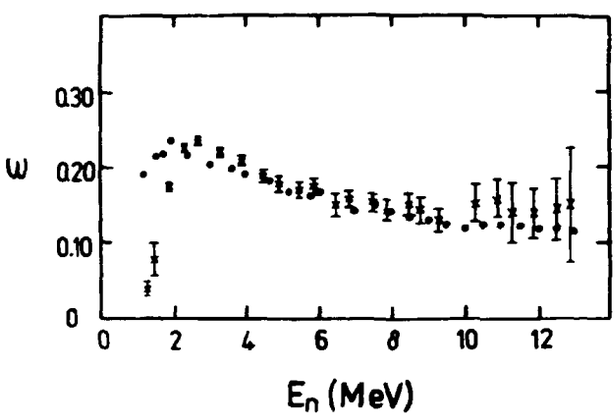

Рис. 2 Измерение эффективности (✱) в сравнении с вычислением программа EFFI (•)

I) В первом комплексе были измерены нейтронные сплошные спектры в резонансах для того, чтобы получить информацию о механизме распада изобар-аналоговых резонансов. В начале были измерены функции возбуждения для реакций типа (p,n) и (p,p_0) на ^{109}Ag[3]. Понятно, что такие эксперименты сопряжены с большими трудностями: сложная техника времени пролета особенно при использовании тонких мишеней (в порядке ≈4 КэВ) и маленькая разница между спектрами в резонансе и вне резонанса, потому что увеличение резонансного сечения только по порядку 30 %. Для двух резонансов измерялись нейтронные спектры под углом 80° и угловые распределения.

Для анализа экспериментального материала дважды-дифференциальное сечение разделяется в два члена:

$$\frac{d^2\sigma}{d\Omega\, dU}(E_p;\, U,\theta) = \left(\frac{d^2\sigma}{d\Omega\, dU}\right)_{изар} + \left(\frac{d^2\sigma}{d\Omega\, dU}\right)_{ср.} .$$

При этом сечение $(d^2\sigma/d\Omega\, dU)_{ср.}$ - средняя величина для энергий протонов $E_p < E_{изар}$ и $E_p > E_{изар}$. Было вычислено соотношение

$$V(U) = \left(\frac{d^2\sigma}{d\Omega\, dU}\right)_{изар} \Big/ \left(\frac{d^2\sigma}{d\Omega\, dU}\right)_{ср.} ,$$

представлено на рис. 3. Как видно, формы спектров значительно отличаются друг от друга для обеих резонансов. Кроме того, в рамках экспериментальных ошибок угловые распределения измерены в резонансах - изотропны, и при наивысших энергиях нейтронов.

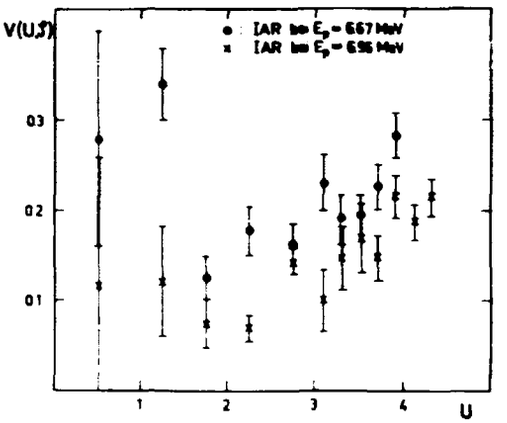

Рис. 3 $V(U)$ в двух изобар-аналоговых резонансах ядра ^{109}Ag

Подобные результаты были найдены в случае ^{115}In. Как следует из измерений, $V(U)$ для 6^+-резонанса почти постоянно, но в случае 5^+-резонанса $V(U)$ сильно повышается с ростом U. Прямой нейтронный распад запрещен по изоспину ($\Delta T = 3/2$). Поэтому предпологалось, что аналоговое состояние ($T = T_3 + 1$) может переходить в состояния компаунд-ядра ($T = T_3$), у которых тот-же спин и та-же четность, что и у аналогового состояния. При этом нередко предпологалось, что нейтронный распад происходит тогда, если возбуждены большое число компаунд-состояний. Тогда можно описать распад изобар-аналоговых состояний в рамках статистической теории, а компаунд-ядро имеет определенные спин и четность.

Такое описание в нашем случае невозможно, так как тогда предпологалось, что средний спин уровней в конечном ядре ^{109}Cd уменьшается с ростом U. Но из других работ известно, что средний спин повышается с ростом U монотон.

Полученные нами результаты показывают, что нестатистические процессы играют существенную роль при нейтронном распаде изобар-аналоговых резонансов. Это может быть и прямой распад и предравновесный распад состояний промежуточного ядра. Последнее подверждается и в других работа о структуре состояний в ^{109}Cd.

2) Измерены нейтронные спектры реакции $^{109}Ag(p,n)$ в области энергий протонов от 5 до 9 МэВ с шагом 500 КэВ. Кроме того были измерены угловые распределения при двух энергиях, которые оказались изотропными [4].

При предположении, что эмиссия нейтронов происходит из статистического равновесия, можно применять формулу Вейскопфа:

$$\frac{d^2\sigma}{d\Omega\, dE} = K \cdot \sigma_{inv} \cdot E_n \cdot P(U)$$

В случае ^{109}Ag было найдено, что нельзя описать ход функции $P(U)$ в рамках модели ферми-газа:

$$P(U) = \frac{\sqrt{\pi}}{12\, a^{1/4}\, (U-\delta)^{5/4}} \exp\left(2\sqrt{a(U-\delta)}\right),$$

то есть нельзя найти параметры a и δ, которые независимо от U и E_p. Из этого следует, что в механизме реакций включены неравновесные компоненты или описание плотности состояний $P(U)$ невозможно в рамках модели ферми-газа. Поэтому форма спектров описалась с суммой равновесного и предравновесного вкладав рамках экситонной модели. Но это не возможно без противоречий.

Делалась попытка сравнивать ход функции $P(U)$ с вычислениями из различных моделей. Для этого функция $P(U)$ была нормирована абсолютно с помощью схемы уровней для энергий возбуждения $U < 0{,}65$ МэВ. На рис. 4 представлены полу-

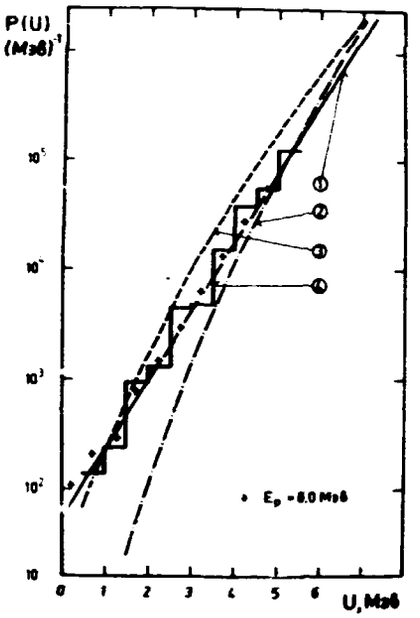

Рис. 4 Плотность состояний в ядре ^{109}
I – *параметризация по формуле*

$$P(U) = R \cdot e^{U/T}\ ;\ R = 54.4\ \text{МэВ}^{-1},\ T = 0.64\ \text{МэВ}$$

2 – модель Ферми-газа с учетом энергии спаривания (*)

$$P(U) = \frac{\sqrt{\pi}}{12\, a^{1/4} (U-\delta)^{5/4}}\, e^{2\sqrt{a(U-\delta)}}$$

3 – модель Ферми-газа с смещением энергии основного состояния (**)

$$P(U) = \frac{\sqrt{\pi}}{12\, a^{1/4} (U-\Delta+t)^{5/4}}\, e^{2\sqrt{a(U-\Delta)}}$$

4 – полумикроскопическая модель

(*) $a = 16\ \text{МэВ}^{-1}$, $\delta = 1.2$ МэВ

(**) $(U-\Delta) = at^2 - t$; $a = 13.4\ \text{МэВ}^{-1}$, $\Delta = -0.42$ МэВ

ченные результаты.

Кривая 4 была вычислена в рамках полумикроскопической модели. При этом учитывали реальные одночастичные состояния, корреляция спаривания и возбуждение коллективных уровней.

Как видно, феноменологичное описание моделью ферми-газа плохо описывает экспериментальную плотность состояний в полной области энергий возбуждения, но полумикроскопическая модель дает хорошее согласие.

Подобные измерения были проведены в ФЭИ на ядрах Zr, Nb и ^{119} и ^{122}Sn. Результаты из Zr-я и Nb-я согласуют с результатами на ^{109}Ag. Но для изотопов оловы было найдено, что в спектрах нейтронов существует значительный вклад неравновесных процессов.

3) При исследовании реакции $^{11}B + p$ ожидают не только компаундные процессы, но и прямые процессы обмена заряда. Но описание компаундных процессов в этом случае в рамках статистической модели делать не возможно. Поэтому использовалась оболочечная модель несвязанных состояний для описания механизма реакции.

Измерения были проведены в области энергий протонов E_p = 5,4 до 7,5 МэВ с шагом 30 КэВ, экспериментальные данные показывают следующие тенденции [5]:

- переходы в основное состояние несколько раз более вероятно чем в возбужденное состояние конечного ядра. Это показывает на прямые процессы, так как ядро-мишень и конечное ядро-зеркальные ядра,
- в функциях возбуждения видно максимумы совместно для различных углов и различных каналов реакции, что показывает на компаундные процессы.

Оболочная модель несвязанных состояний может описывать прямые и компаундные процессы и их интерференции без предложений их относительных вкладов. При этом известная оболочная модель расширяется на состояния, у которых один

нуклон находится в несвязанном состоянии.

Заметим, что уже для описания основного состояния ^{11}C и ^{11}B надо включить конфигурация типа 2p - 3h, но например в случае ^{15}N основное состояние - чистое 1h - состояние. На рис. 5 представлены результаты.

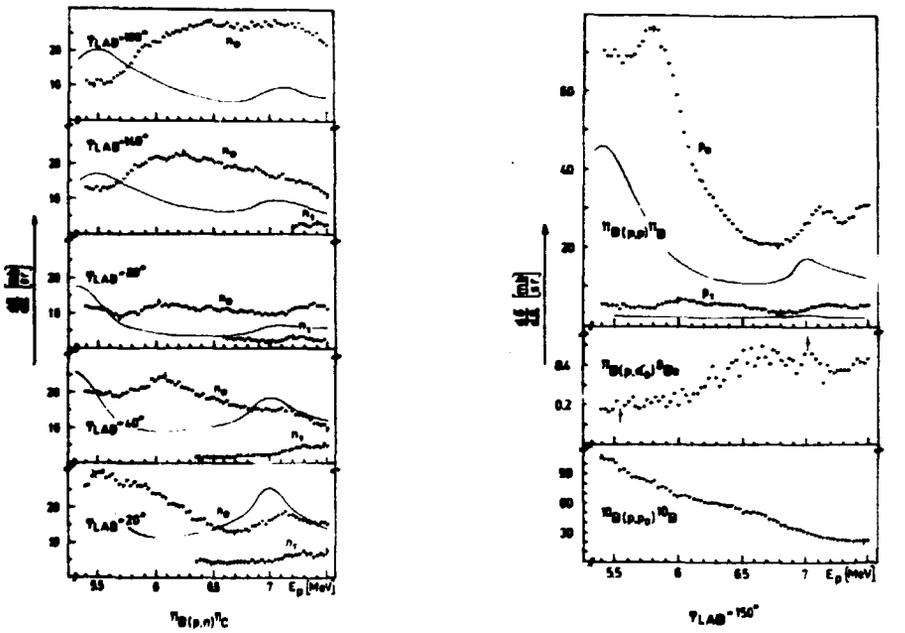

Рис. 5 Сравнение экспериментальных сечений из реакции $^{11}B + p$ с вычислением в рамках оболочной модели несвязанных состояний. (точки - эксперимент, линия - расчет)

Какие успехи этого подхода можно называть:

- Абсольютное вычисление хорошо дает порядок и грубую структуру функции возбуждения.
- Отношение между n_0 - и n_1- группами описывается правильно.
- В случае (p, p_0)-реакции даже форма функции возбуждения хорошо описывается.

Но

- Вычисление не дает тонькую структуру функций возбуждения.

Улучшения можно ожидать с помощью включения других каналов реакции, как протонных, и более комплексных конфигурацией.

Исследование реакций типа (n,n') началось несколько лет тому назад и до сих пор не окончалось. Такие работы важны для получения ядерных данных, например для развития термоядерных реакторов.

Но с другой стороны из таких экспериментов можно получить качественную и количественную информацию о роли равновесных или других процессов.

Для исследования реакций типа (n,n') используют в Россендорфе газовую мишень с помощью DD-реакции. Таким образом можно достигать область энергий нейтронов E_n = 7 ... 12 МэВ. Средний выход нейтронов под углом 0^0 порядка $2 \cdot 10^8$ (сек·стер)$^{-1}$.

Нейтроны, испускаемые из такой газовой мишени не моноэнергетически из-за реакции разрыва дейтона или других причин [6]:

а) нейтроны из реакций (d,n) на углероде и кислороде: при этом эти элементы находятся в виде тонких слоев на поверхностях мишени, особенно на фольгах;

б) нейтроны из разрыва дейтона: сечение этой реакции сильно растет при энергиях DD-нейтронов выше 10 МэВ.

Эти немоноэнергетические нейтроны тоже рассеиваются на образце и представляют собой ошибки в измеренных спектрах, особенно при малых углах. В первом случае их можно удалить из экспериментальных спектров, но континуум разрыва дейтона ограничивает область обработки спектров.

Результаты измерений на ядрах ^{28}Si и ^{32}S представлены в других работах этого симпосиума.

Литература

[1] P. Eckstein et al., Kernenergie 20 (1977) 161
[2] P. Eckstein et al., Nucl. Instr. & Meth., in print
[3] Г.Н.Ловчикова и др., Ядерная Физика т.28,вып.3(9), 605, 1978
[4] J. Kayser et al., TU-Informationen, Sektion Physik 05-22-78 (1978)
[5] J. Höhn et al., TU-Informationen, Sektion Physik 05-24-78 (1978)
[6] S. Mittag et al., Kernenergie 7 (1979) 257

SCATTERING OF 10 MEV NEUTRONS ON SILICON

W. Pilz, D. Schmidt, D. Seeliger and T. Streil
Technische Universität Dresden, Sektion Physik, Dresden, GDR

Angular distributions for several neutron groups of the $^{28}Si(n,n')$ reaction are measured at 10 MeV bombarding energy. The experimental data are analyzed in a combined statistical and direct reaction model. The theoretical description gives informations about excitation modes and strengths.

1. Introduction

All investigations of the $^{28}Si(n,n')$ reaction done until now were restricted to a narrow energy region between the energies 3 and 14 MeV, respectively. This experiments differ from each other in respect of both the measuring technique and the model and parameters of the theoretical analysis used.
The present work has been started with the aim to analyze on an uniform basis the reaction mentioned above in the energy range between 7 and 14 MeV. This reaction is known to be described by incoherent superposition of compound contribution calculated in the Hauser-Feshbach formalism and the direct one /1/. It is well known that a good agreement between experimental points and theoretical curves can be obtained easily for one incident energy by convenient choice of model parameters. But more attractive is the theoretical description of experimental data, obtained at the same conditions, with a consistent set of parameters in a wide energy range, because this allows to get more information about the reaction mechanism. Furthermore, such measurements are important for nuclear data collection and evaluation.
The topic of the present work are the measurements and its theoretical interpretation of the data at 10 MeV bombarding energy only. A more complex description for the mentioned energy range will be reported later.

2. Experimental Procedure

The elastic and inelastic differential neutron scattering cross sections were measured with the tandem facility in the ZfK Rossendorf. A deuterium gas target /2/ using the D(d,n) reaction was employed. The measurements were carried out with a computer-coupled multi-angle TOF-detector system consisting of eight detectors. The experiment is characterized by measuring angles between 15 and 160 degrees, an energy spread of 120 keV, averaged flight pathes of 3 meters and the angle uncertainty of $\pm$ 3 degrees. A more detailed description is given in ref. /3/.
As monitor a ninth TOF-detector was included into the system to reduce the dead time correction. Because the efficiency ratio of monitoring and measuring detector can be measured with sufficient accuracy (error less than 2%) for determination of the absolute cross sections the relative efficiency function is necessary only. The angular distributions were measured in two independent runs at 15, 30, 50...150 and 20, 40, 60...160 degrees. The absolute cross sections for each run were determined independently and are shown in fig.1.
The scattering sample consists of natural silicon with a cylindrical shape

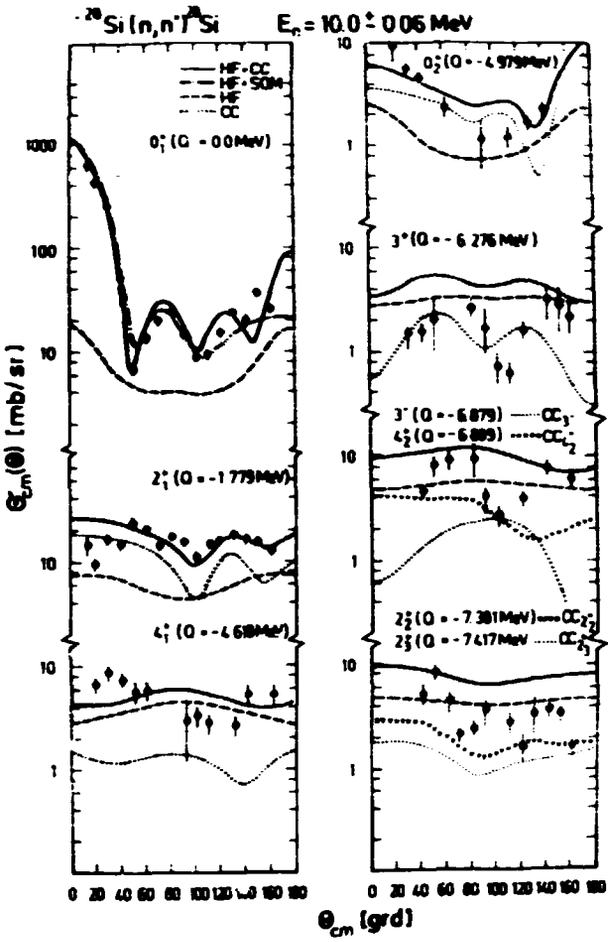

fig.1 Angular distributions of elastic and inelastic scattered 10 MeV neutrons. The experimental cross sections (ϕ) are shown with their absolute errors. (SOM - spherical optical model, CC - collective model in the coupled channels representation, HF - Hauser-Feshbach contribution)

(3 x 3ϕ cm^2) and a weight of 43.53 g. The measured cross sections were corrected for finite geometry and multiple scattering, which are rather low for the chosen sample size. The background from elastically scattered non-monoenergetic neutrons of the source /2/ have been taken into account for the calculation of the cross sections of higher inelastic neutron groups using a special computer code.

3. Analysis of the Experimental Data

The elastic scattering is described as a sum of shape and compound elastic part (fig.2). The calculation of the shape elastic contribution was performed with the spherical optical model (SOM) using parameters from ref. /1/ slightly varying in the spin-orbit term. The choice of the parameters was made with the aim to describe all experimental cross sections in the full energy range. An optical parameter fit of our data at 10 MeV bombarding energy reproduces satisfactory the parameter values of ref./1/.

The calculation of the compound reaction contribution for both the elastic and inelastic scattering are based on the statistical model code ELIESE /4/ including p- and α-channels. In this code transmission coefficients are calculated with the same parameter set as used for the SOM. This code takes into account discrete levels only. For higher energies the normalization with results from statistical model code STAPRE /5/ is necessary. The code STAPRE gives angle-integrated cross sections only, but it takes into account level densities for the unknown higher excited states. The parameters used in the code STAPRE were adjusted to reproduce the total cross sections.

Almost the same parameters were used for calculation of the direct reaction part with the coupled channels method (CC) in the code CHUCK /6/. Table 1 gives the parameters used for the SOM and CC calculations.

Table 1 : Optical parameters

	V_V (MeV)	r_V (fm)	a_V (fm)	W_s (MeV)	r_s (fm)	a_s (fm)	V_{so} (MeV)
SOM	52.0	1.15	0.78	12.1	1.25	0.47	9.0
CC	"	"	"	6.0	"	"	0.0
		$a_{so} = a_s$; $r_{so} = r_s$					

The elastic scattering is described in the CC analysis also. In this case the influence of the channel coupling on the elastic channel is taken into consideration.

In order to describe the inelastic scattering an incoherent superposition was carried out of compound and direct reaction contribution, where the second one is obtained from the collective model with the coupled channels method.

Table 2 gives the excitation modes and their parameters used in the CC-calculation, with notation: β_o - monopole vibration, β_2 - quadrupole vibration etc. These parameters result from the CC-calculation to reproduce shape and absolute magnitude of the angular distributions as seen in fig.1, and they are in good agreement with results from other investigation /7/.

Table 2 : Excitation mode and parameters of the first low lying states in ^{28}Si

level	group	J^π	excit.mode	parameters
g.s.		0^+_1	-	$\beta_2 = -0.48$, $\beta_{2+2} = -0.15$
1		2^+_1	rot	" "
2	I	4^+_1	"	" "
3		3^+	vibr	$\beta_2 = +0.3$
4		0^+_2	"	$\beta_o = +0.25$
5	II	3^-	"	$\beta_3 = +0.3$
6		4^+_2	"	$\beta_4 = +0.6$
7		0^+_3	rot	$\beta_2 = +0.5$
8	III	2^+_2	vibr	$\beta_2 = +0.6$
9		2^+_3	rot	$\beta_2 = +0.5$

(The groups denote that levels, which are coupling to the ground state and/or together in three different calculation runs.)

The Hauser-Feshbach contribution is seen to be to high for the higher excited levels (3^+ and higher). The reason for this overestimation could be fluctuations in the compound level density of ^{29}Si /1/. Some details of this coupled channels calculations are of interest:

(1) The direct excitation of the 4^+_1 state from ground state is rather small (in order of 20%), i.e. multi-step processes must be taken into account.

(2) The excitation of the 3^+ non-normal parity state can be understood as spin-flip process, the $l = 2$ transition contributes mainly to the cross section (in order of 90%).

(3) The contribution of the 2^+_3 state in the second rotational band to the cross section is small, this level is coupled only to its 0^+_3 "ground" state.

In opposite to the ground state rotational band with oblate deformation the second rotational band has a prolate one ("cigar" shape).

Finally it should be noted that by extension of our investigations into the energy range between 7 and 14 MeV on an uniform theoretical basis it can be expected more information about tendencies of the reaction mechanism.

4. References

/1/ A.W.Obst and J.L.Weil, Phys.Rev. C 7 (1973) 1076

/2/ S.Mittag et al., Kernenergie 7 (1979) 237

/3/ P.Eckstein et al., Nucl. Instr.& Meth., to be publ.

/4/ G.Kießig, thesis, Technische Universität Dresden (1974)

/5/ M.Uhl and B.Strohmaier, report IRK 76/01, Vienna (1976)

/6/ P.D.Kunz, University of Colorado, code CHUCK (unpublished)

/7/ H.W.Barz et al., report ZfK-185, Rossendorf (1969)

ANALYSIS OF NEUTRON SCATTERING ON ^{32}S IN THE ENERGY RANGE FROM 7 TO 11 MEV

M. Adel-Fawzy, D. Schmidt, D. Seeliger and T. Streil

Technische Universität Dresden, Sektion Physik, Dresden, GDR

Experimental results from elastic and inelastic scattering on ^{32}S with bombarding energies between 7 and 11 MeV are compared with theoretical description in different models.

1. Introduction

The present work was undertaken as an extension of measurements in order to obtain information on neutron scattering in a wide energy range on some light nuclei.

In this experiments, measurements of neutron differential elastic and inelatic scattering cross sections were made at bombarding energies 7, 8, 9, 10 and 11 MeV on sulphur. Natural sample was used, but it is nearly monoisotopic ^{32}S. All the measurements were interpreted theoretically with convenient models.

2. Experimental Conditions

For measurements of the neutron differential cross sections a time-of-flight multi-angle system consisting of 8 detectors was used /1/. The ZfK Rossendorf tandem accelerator was used to produce fast monoenergetic neutrons in this energy range from the DD-reaction /2/. The neutron detectors have a 5" diameter and 1.5" thick liquid organic scintiliator of the type NE-213. The 8 detectors are placed around the scattering sample with respect to the accelerator beam between 20 and 160 degrees in steps of 20 degrees with averaged flight pathes of 3 meters. The scattering sample has the shape of a hollow cylinder with the dimensions ($3 \times 3 \times 1$ cm^3) and a weight of 36.30 g.

Monitoring of the neutron flux from the source was achieved with a small scintillation detector placed with an angle of 20 degrees relatively to the gas cell at a distance of about 3 m from the target.

All the measured differential cross sections were corrected for finite size, flux attenuation and multiple scattering, which are rather small for the chosen sample size.

3. Results of the Measurements and Interpretation

Theoretical calculations were made by incoherent addition of a compound contribution in the Hauser-Feshbach theory (HF) and a direct reaction contribution calculated in the framework of the spherical optical model (SOM) as well as by the coupled channels method (CC). One set of optical potential parameters in the full energy range was used. This parameters were taken from the work of Brandenberger and coworkers/3/, because this work was a specific measurement of elastic scattering with high accuracy, whereas our aim was to measure and calculate the inelastic scattering cross sections accurately together with the elastic ones. There is no investigations of the elastic and inelastic scattering of neutrons on sulphur in the full energy range which was investigated in the present work.

The sulphur nucleus is known to be a shperical nucleus in the ground state and is considered as a vibrational nucleus in the low lying excited states.

Moreover, all the compound contributions (HF) were corrected due to Moldauer's level width fluctuation correction. Fig.1 shows the effect of this correction, the elastic compound part will be higher by a factor of about 3, while the inelastic part will be smaller by less than 6%.

Fig.2 shows as an example the results of the differential cross sections at 10 MeV bombarding energy in comparison with the theoretical description. It can be seen from the curves, that

(1) an agreement between the experimental and theoretical results is evident,

(2) the theoretical calculation with the optical model or with the coupled channels method give approximately the same structure, but with a remarkable deviation between each other in the minimums of the angular distribution, that is due to the coupling of the first excited state with the ground state.

A comparison between the integrated elastic scattering cross sections from the present work and the results of other authors at the same or near energies shows a good agreement.

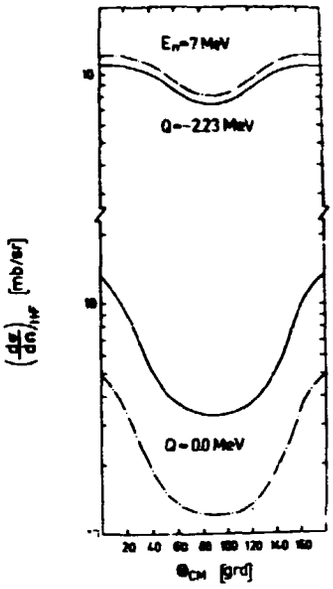

Fig.1 : Influence of Moldauer's width fluctuation correction : ——— with, — · — without correction.

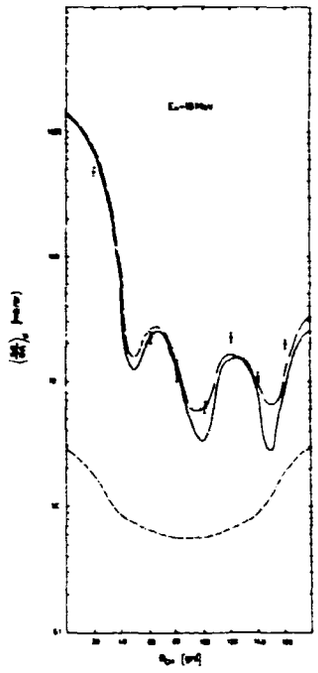

Fig.2 : Angular distribution of elastic scattered 10 MeV neutrons (——— HF and CC calculation, — · — HF and SOM calculation, - - - HF contribution only)

Fig.3 shows the results of inelastic differential cross sections for the first excited state. A significant agreement between the measured and the calculated results is remarkable.
It is clearly seen, that there is a variation in the excitation mechanism of the first inelastic state as a consequence of the decrease of the compound contribution, that is due to increase of the number of open channels for the decay of the compound nucleus, while the direct contribution varies only weakly with respect to the energy.

There are only a few data for the inelastic scattering of neutrons with sulphur in this energy range. Especially, in the present work experimental results were represented firstly for bombarding energies 7 and 11 MeV.

4. References

/1/ P.Eckstein et al., Nucl. Instr. & Meth., in print
/2/ S.Mittag et al., Kernenergie 7 (1979) 237
/3/ J.D.Brandenberger et al., Nucl.Phys. A 196 (1972) 65

(fig.3 on the following page)

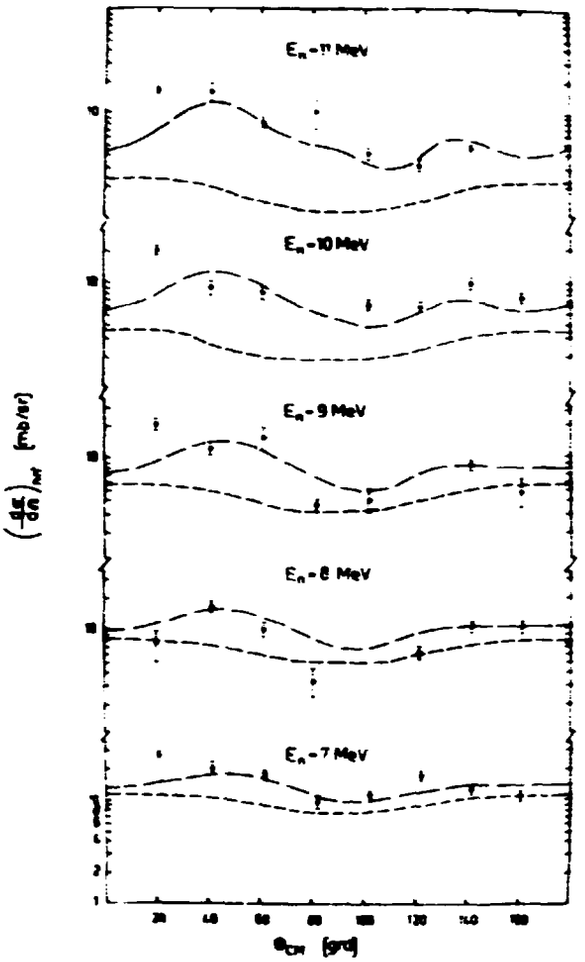

Fig.3 : Angular distributions of the inelastic scattered neutrons (first 2^+ excited state) for several bombarding energies
(– – – – – HF contribution only, – · – · – sum of HF and CC contribution)

DETERMINATION OF THE NEUTRON-NEUTRON EFFECTIVE RANGE PARAMETER BY THE $^2H(n,2n)p$ QUASIFREE SCATTERING AT 25 MeV

H. Guratzsch, B. Kühn, H. Kumpf, J. Mösner, W. Neubert, W. Pilz, G. Schmidt and J. Tesch

Zentralinstitut für Kernforschung, Rossendorf, DDR

1. Introduction

The nucleon-nucleon interaction at low energies is usually expressed in terms of the scattering length and the effective range parameters. In the case of the neutron-neutron interaction the scattering length a_{nn} has been determined in numerous experiments investigating the n-n final state interaction (FSI) in $^2H(n,2n)p$ and $^2H(\pi^-,2n)\gamma$ reactions. An average value $a_{nn} = (-18.8 \pm 0.4)$ fm has been deduced [1]. The value of the effective range parameter r_{nn} however is not so well determined. As proposed by Vranić et al. [2] the investigation of the neutron induced deuteron break-up in the kinematical region of n-n quasi-free scattering (QFS) seems to be suitable for the determination of r_{nn}. We performed a measurement at an incident energy of 25 MeV.

2. Experimental procedure

The incident neutrons were produced via the $^3H(d,n)^4He$ reaction. The experimental arrangement is shown in fig. 1. A heavy water sample was used as deuterium

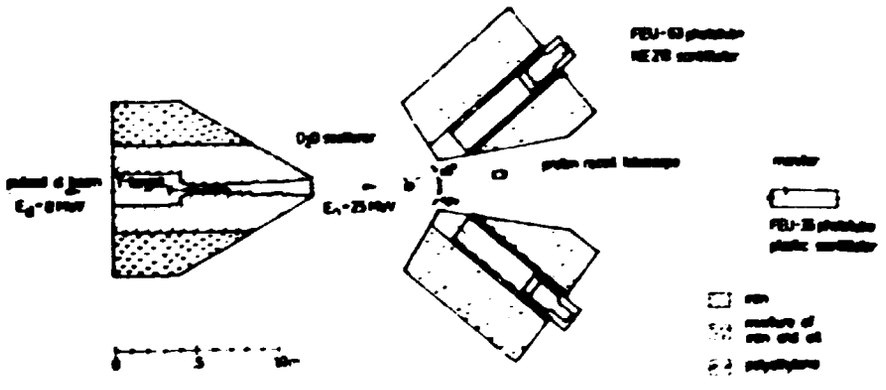

Fig. 1. Experimental set-up.

target. Both secundary neutrons of the $^{2}H(n,2n)p$ reaction were measured in coincidence. The crucial problem was the reduction of the background. Therefore, the neutron source and the detectors were shielded by about 15 tons of steel and oil. In order to suppress γ-ray detection pulse shape discrimination was used [3]. Fig. 2 shows the measured time-of-flight spectrum together with the

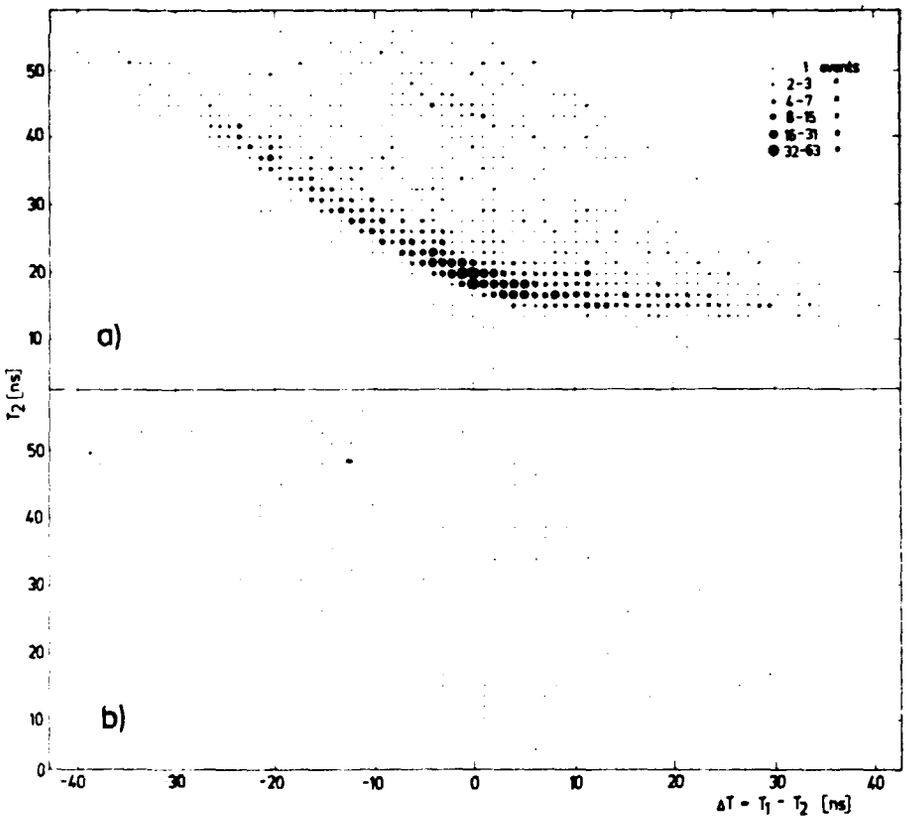

Fig. 2. Map-display of the time-of-flight coincidence spectra from $^{2}H(n,2n)p$ break-up reaction at $\Theta_1 = \Theta_2 = 40^{o}$, $\Delta\varphi = 180^{o}$.
(a) True and random events together.
(b) Random events measured simultanously.

background spectrum of random events which were measured simultaniously. Coincidences occured at a rate of about three events per hour whereas the single rates amounted to $5 \cdot 10^{3}\ s^{-1}$. During several weeks 1825 coincidence events were collected. The absolute flux of the 25 MeV neutons was determined by a ΔE-E semiconductor counter telescope.

3. Data analysis and result

The experimental data are affected by a number of inevitable imperfections such as the finite dimensions of the sample and of the detectors, time resolution, the energy width of the incident neutrons and multiple neutron scattering in the sample. Therefore, the experimental data were compared with Monte Carlo simulated spectra. Break-up cross sections were calculated by using the Ebenhöh-Bruinsma-Stuivenberg code [4] solving the three-particle Faddeev equations for charge-dependent rank-one S-wave nucleon-nucleon interaction. For the comparison between simulated and measured results the contents of the two-dimensional spectra were projected onto the ΔT axis (fig. 3). In this representa-

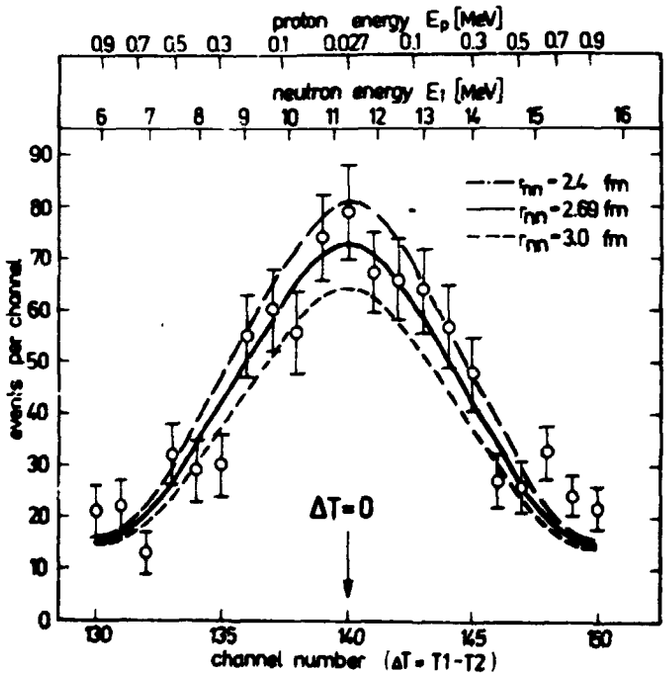

Fig. 3. Events of the kinematical locus of fig. 2a projected onto the ΔT axis after subtracting the random background of fig. 2b. The upper scales indicate the energy of one neutron and the corresponding proton energy valid for point geometry, respectively. The curves represent Monte Carlo simulations.

tion the fit of the simulated curve to the measured distribution yielded a value for the effective range

$$r_{nn} = (2.69 \pm 0.27) \text{ fm.}$$

This result is in fairly good agreement with the value (2.9 ± 0.4) fm which was recently derived from measurements [5] outside the exact QFS condition $\theta_1 = \theta_2$ etween 19° and 35°.

References

1. B. Kühn, Fiz. Ehlem. Chastits At. Yadra 6 (1975) 348
2. D. Vranić et al., Proc. Int. Conf. on Few Body Problems in Nuclear and Particle Physics, Quebec, 1974 (Les Press de l'Université Laval, Quebec, 1975) p. 660
3. H. Guratzsch et al., Exp. Technik Physik 26 (1978) 561
4. J. Bruinsma, J. Ebenhöh, J. H. Stuivenberg and R. van Wageningen, Nucl. Phys. A228 (1974) 52
5. J. Soukup et al., Nucl. Phys. A322 (1979) 109

MEASUREMENT OF CROSS SECTIONS FOR THE $^{238}U(n,2n)$ REACTION FROM 6.5 TO 10.5 MeV

N.V.Kornilov, B.V.Zhuravlev, O.A.Salnikov, Fiziko-Energeticheskij Institut, Obninsk, USSR

P.Raics, S.Nagy, S.Daróczy, K.Sailer, J.Csikai, Institute of Experimental Physics, Kossuth L. University, Debrecen, Hungary

Cross sections of the $^{238}U(n,2n)^{237}U$ reaction have been determined by the activation method for neutron energies of 6.54, 6.78, 7.00, 7.50, 7.99, 8.50, 8.99, 9.49, 10.00 and 10.50 MeV. Neutron flux density was measured by three standard reactions. Corrections for background neutrons and sample counting are discussed. Measured data are compared with results of previously reported experiments.

1. Introduction

Investigations on the excitation function of the $^{238}U(n,2n)$ reaction from threshold up to 10 MeV is important mainly for practical purposes (fast reactors, hybrid systems, fuel cycles), /1/. Till now two systematical investigations were reported only. Knight et al. /2/ measured cross sections from 6 to 10 MeV (and at 16 MeV) by radiochemical methods in 1958. Recently Fréhaut and Mosinski investigated this reaction from 8 to 15 MeV by a Gd-loaded large liquid scintillator system /3/. There is a difference of about 8 % between these results in the overlapping region. Our experiments give results for the $^{238}U(n,2n)$ reaction cross section in the 6.5-10.5 MeV interval measured by the activation technique.

2. Experimental

Samples of uranium oxide of 1.9-2.8 g in the form of 18.5 mm diameter by 1-1.7 mm thick disk were prepared by thermal pression. The chemical composition was determined to be 90.0±0.6 %, isotopic content of ^{238}U was higher than 99.99 %.

Neutrons with energies in the range 6.54-10.50 MeV were produced via the $D(d,n)^3He$ reaction on the EGP-10M tandem generator using a 40 mm long gas target. The cell was filled with deuterium gas up to 106.6 kPa except for irradiations with 6.54 and 6.78 MeV neutrons when the pressure was 66.6 kPa. For input window a 14.3±0.3 mg/cm^2 thick Mo-foil was used causing a 32 keV (1σ, E_d=6 MeV) straggling determined experimentally. The end-wall of the cell had a 0.2 mm Pt cover to reduce the background from (d,n)-neutrons. Details of the target are described in /4/.

The energy distribution of neutrons impinging the sample, its average value and dispersion were calculated from the deuteron stopping and reaction kinematics using data from /5/ and /6/. The mean neutron energy and its estimated total uncertainties are listed in Table 1.

The neutron flux density was measured by the $^{238}U(n,f)$, $^{27}Al(n,\alpha)^{24}Na$ and $^{56}Fe(n,p)^{56}Mn$ reactions. Uranium samples between two Al and Fe foils of 19 mm in diameter were put on a fission detector and placed on the beam line 40.0±0.5 mm from the end of the gas target. The flow-type proportional fission chamber contains a 0.28 mg/cm^2 thick ^{238}U layer of 19 mm in diameter weight of which was determined with a precision of about 2 %. The following counting corrections were taken into account for the fission detector: losses in pulses due to the discrimination threshold, selfabsorption in the layer and laboratory angular distribution of fragments. (Discriminator threshold made it impossible to count events from uranium alphas as well as from charged particles of reactions induced in the chamber.) Total of these

Work supported by the Hungarian Ministry of Education and the Academy of Sciences.

corrections amounts to 2.5±1.0 %. Effect of D(d,np)d neutrons on the fission counts was estimated to be from 1.0±0.5 to 18±4 % for E_n=8.50-10.50 MeV according to data of /7/. Corrections for (d,n)-neutrons from the structural materials of the target were determined by experiments with empty target cell before and after each irradiation and amount to 1.0±0.5 - 11±1 % for E_n=6.54 - 10.50 MeV. Thus the flux determination by the fission chamber has an accuracy of 1-4 % without the uncertainty in the (n,f) cross section. Activity of ^{24}Na and ^{56}Mn was measured by β-γ coincidence method and GeLi-spectrometry with an uncertainty of 1-3 % giving the main source of error in the flux determination. Background effects of (d,n)-neutrons were investigated by a particular irradiation with empty gas target at E_d=8.10 MeV (which would correspond to a neutron energy of 10.50 MeV with deuteron gas in the cell). Contribution to the activity of ^{24}Na, ^{56}Mn and ^{237}U was found to be 3.9, 2.0 and 1.0 %, respectively. These values were then used together with the counting rate of a stilbene spectrometer of 6 MeV threshold and current integrator to estimate background for other neutron energies. Decrease in the neutron flux density along the sample thicknes was measured to be 3 %/mm. Correction due to the flux variation in time reached 12 % for ^{56}Mn.

γ-activity of ^{24}Na, ^{56}Mn, ^{237}U and standard sources were taken by a 42 cm^3 GeLi-detector of type DGDK-70V. Spectra were analysed by a 4096-channel ADC with peak stabilization /8/ and were fed to the physical measurement centre (FIC) of FEI. Pile-up and dead-time corrections measured by a pulse generator did not exceed 10 % for counting rates up to 1000/s. Correction for coincidences of cascade γ-rays was calculated from measured total detection efficiency and recommended decay schemes and had a greatest value of 10 %. Absolute full-energy peak efficiency of the GeLi-spectrometer and its dependence on the detector-sample distance have been determined in the 60-1500 keV region by a combined method of point-like standards and calibrated sources of 19 mm in diameter /9/. Spectrum measurements were carried out at a distance of 15 mm. Accuracy of the efficiency in the 200-1500 keV interval is expected to be 2 %.

Gamma-spectra and decay-curves were evaluated with a MULTI-20 minicomputer.

Activity of ^{237}U of half-life 6.75 days /10/ was determined by its 208.0 keV γ-line having branching intensity of 21.80 % /11/. Peaks of 205.33 keV from ^{235}U and 209.73 keV from ^{239}Np were accounted for as interferences in the 208±3 keV interval (fwhm=2.6 keV) giving contribution up to 6 and 10 %, respectively. Background of the ^{235}U line was determined from spectra taken before irradiation while that of 209.73 keV was estimated from the intensity of the 277.60 keV ^{239}Np peak. Contribution from fission fragment γ-lines may be neglected after a 15 hour cooling time. Duration of irradiations with an average target current of 2 μA ranged from 7 to 30 hours according to the expected (n,2n) cross section. γ-spectra of the activated samples were analyzed in a time period of 20-300 hours. Statistical accuracy in the initial intensity at E_n=6.54 and 6.78 MeV was 3 and 2 %, respectively, while at other neutron energies <1 % was achieved. γ-ray selfabsorption determined experimentally ranged from 0.61 to 0.72 for 208.0 keV depending on the sample thickness.

3. Results and discussion

Neutron flux densities determined by the three standard reactions are listed in Table 1. Cross sections from /12/ were used for ^{238}U(n,f) reaction while data for ^{27}Al(n,α) and ^{56}Fe(n,p) reactions were taken from /13/. Although the quoted preci-

Table 1.

Results of the cross section measurements for the $^{238}U(n,2n)$ reaction

$E_n \pm \Delta E_n$ MeV (ΔE_n:68 %)	Neutron flux density 10^6 $cm^{-2}s^{-1}$ n,α	n,p	n,f	(K)	Averaged flux density	σ(n,2n) mbarn
$6.54^{+0.09}_{-0.07}$	2.01	-	2.28	(2)	2.19 ±0.13	72 ± 5
$6.78^{+0.08}_{-0.06}$	1.66	1.65	1.87	(2)	1.76 ±0.08	251 ±13
$7.00^{+0.10}_{-0.07}$	-	3.32	3.57	(2)	3.49 ±0.12	402 ±18
$7.50^{+0.10}_{-0.07}$	3.48	3.32	3.64	(1)	3.48 ±0.09	830 ±30 } 831 ±30
	4.02	3.69	4.06		3.92 ±0.12	832 ±32
$7.99^{+0.10}_{-0.08}$	3.73	3.57	3.74	(1)	3.68 ±0.06	1077 ±31
$8.50^{+0.10}_{-0.08}$	3.81	3.92	4.09	(1)	3.94 ±0.08	1244 ±41
$8.99^{+0.10}_{-0.08}$	4.14	4.24	4.22	(1)	4.20 ±0.04	1345 ±35 } 1344 ±35
	4.36	4.62	4.62		4.53 ±0.09	1343 ±42
$9.49^{+0.08}_{-0.08}$	2.74	-	2.69	(0.5)	2.72 ±0.03	1371 ±36
10.00 ±0.08	4.07	4.03	4.19	(0.5)	4.08 ±0.0[illegible]	1413 ±37
10.50 ±0.08	4.17	4.39	4.76	(0.5)	4.38 ±0.15	1466 ±63

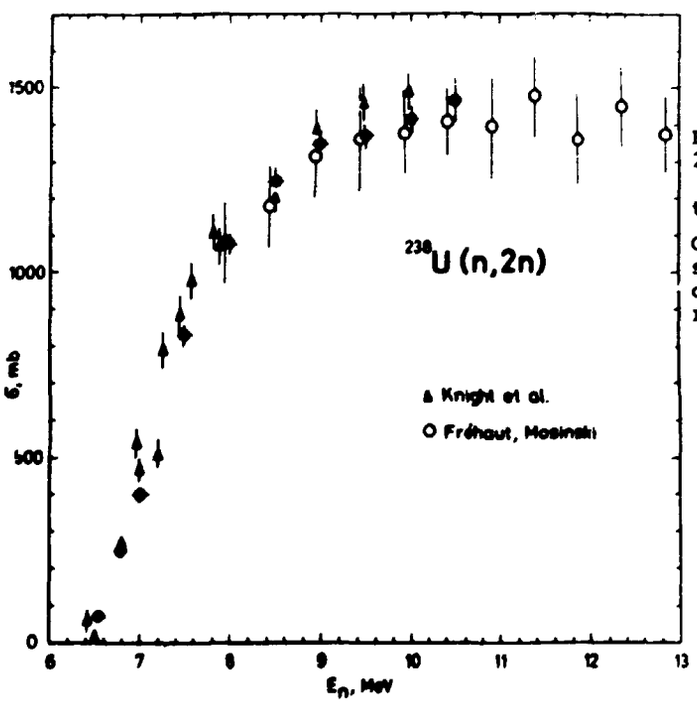

Fig. 1.
Excitation function of the $^{238}U(n,2n)$ reaction from threshold to 13 MeV.
Cross sections of the present work shown by filled circles are compared with results of /2/ and /3/.

sion of the (n,f)-cross section was lower than that of the others we considered the different measurement technique as well as the sensitivity to background neutrons and chose the following averaging procedure for flux densities:

$$\bar{\Phi} = \frac{\Phi(n,\alpha) + \Phi(n,p) + K\cdot\Phi(n,f)}{2 + K}$$

K values are listed in Table 1. The average neutron flux density and its deviation as well as the cross sections of the $^{238}U(n,2n)$ reaction and their estimated error are summarized also in Table 1. Quoted errors contain: standard error of the mean for the averaged flux density as well as error of the determination of the ^{238}U mass (0.6 %),GeLi-detector efficiency (2.0 %), selfabsorption correction (1.5 %) and branching intensity of the 208.0 keV line (1.0 %). Reliability of our experiments was checked by repeating the irradiations at 7.50 and 8.99 MeV neutron energies. Results in Table 1 show an excellent reproducibility.

Cross sections of the present measurement are compared with data of earlier experiments /2/ and /3/ in Fig. 1. A good agreement may be found with results of Fréhaut and Mosinski while Knight's data are systematically higher.

Acknowledgements

The authors would like to thank V.A. Tolstikov for supplying the GeLi detector, G.P. Makhova and S.A. Kremenetzkaya for the chemical analysis of the samples, A.M. Gontchar for help in operating the electronic systems, FIC-group and the accelerator laboratory of FEI for their help in this work. Thanks are also due to L.Vas (IEP, Debrecen) for the fission chamber electronics.

The authors are indebted to the Hungarian Ministry of Education and the Academy of Sciences for the interest and financial support to this work.

References

1 WRENDA 76/77, p. II/63 and III/23-24, INDC/SEC/-55/URPS, IAEA, Vienna, 1976

2 J.D.Knight, R.K.Smith, B.Warren, Phys.Rev. 112 259 (1958)

3 J.Fréhaut, G.Mosinski, CEA-R-4627 CEN-Saclay (1974); Nucl.Cross Sect.Techn. vol.II. 855 (Proc.Conf.3-7 March 1975, Washington)

4 N.S.Biryukov, B.V.Zhuravlev, N.V.Kornilov, Yu.S.Kulabukhov, V.I.Plyaskin, O.A.Salnikov, Prib.Teh.Eksp. 3 66 (1971)

5 H.Liskien, A.Paulsen, Nucl. Data Tabl. A11 569 (1973)

6 C.W.Williamson, J.B.Boujot, J.Picard, CEA-R-3042 CEN-Saclay (1966)

7 D.L.Smith, J.W.Meadows, ANL/10M-9, Argonne Nat. Lab., Aug. 1974.

8 A.I. Gonchar, 1.Vsesoyuznoe sov. po avt. nauchn. issl. v yadernoy fizike, 167. (Oktyabr, Kiev 1976); A.I.Gonchar, S.I.Chubarov, B.V.Nesterov, Prib.Teh.Eksp. 4 69 (1974)

9 Nagy S., Sailer K., Daróczy S., Raics P., Nagy J., Germán E., Magy. Fiz. Foly. 22 323 (1974), in Hungarian

10 Nuclear Data Sheets 6 539 (1971)

11 R.Gunnink, Gamma-library file output Oct. 1. 1975, Lawrence Livermore Laboratory, private communication

12 M.G.Sowerby, B.H.Patrick, D.S.Mather, Ann.Nucl.Sci.Eng. 1 409 (1974)

13 V.Kanda, R.Nakasima, Neutron Cross Sect.Techn. vol. I.193 (Proc.Conf.4-7 March 1968 Washington)

EFFECT OF SCATTERED NEUTRONS ON THE 14 MeV REACTION CROSS SECTIONS DETERMINED BY THE ACTIVATION METHOD

P.Raics, S.Nagy, S.Daróczy, Institute of Experimental Physics, Kossuth L. University, Debrecen, Hungary

Effects of neutrons scattered from a water cooled target assembly of stainless steel on the activation measurements are discussed. Neutron spectra were estimated from elastic and inelastic processes and then absolutized experimentally by foil activation. Activity fractions for the "14 MeV neutron group" were calculated for reactions of different threshold.

1. Introduction

Effects of scattered neutrons on the 14 MeV cross section of (n,γ) reactions measured by the activation technique are well known /1,2/. Such problems are sometimes arise for reactions of higher (>0.1 MeV) threshold, too. Nethaway mentioned the effect of neutrons scattered from the room walls only /3/. Michel and Weigel estimated the distortion of the 14 MeV peak and mean neutron energy for a neutron tube /4/. Ricci calculated the neutron spectrum for a water cooled Al target assembly taking into account elastic scattering only /5/. Spectrum measurements of Graves and Rosen /6/ made by nuclear emulsion, show a pronounced increase of low energy neutrons of evaporation shape when the target is surrounded by iron. The role of the inelastic processes was also confirmed by Shani's experiments on the cross section ratio of the $^{238}U(n,f)$ and $^{238}U(n,2n)$ reactions for iron absorbers /7/. Influence of the source surroundings on the spectrum was also demonstrated by Nagy et al. with activation measurement for neutrons slowing down from 14 MeV in a paraffin moderator /8/.

These problems have some general importance nowadays when high power generators and neutron tubes are in operation with special tritium target systems for efficient cooling and large radiation shielding. The present work is dealing with the estimation of the contribution of the low energy neutrons to the 14 MeV activity.

2. Experimental

The following reactions have been used to measure the neutron flux density: $^{115}In(n,n')^{115m}In$, $^{27}Al(n,p)^{27}Mg$, $^{27}Al(n,\alpha)^{24}Na$, $^{65}Cu(n,2n)^{64}Cu$ and $^{63}Cu(n,2n)^{62}Cu$ having thresholds of 0.339 MeV, 1.895 ("effective"~3) MeV, 3.248 (~5) MeV, 10.058 and 11.023 Mev, respectively.

Neutrons were produced via the D+T reaction with analyzed deuterons of 175 ±5 keV energy. A water cooled robust target holder of stainless steel contained the TiT layer on a Mo-backing. The target surface was directed at 45° to the deuteron beam. Sandwiches from In, Al and Cu foils of 19 mm in diameter arranged in a Cd-box were placed on a thin Al-ring with radius of 70 mm at angles of 0°, ±60°, ±90°, ±120° and -150° to the beam. (The original experiment was devoted to determine the $^{238}U(n,2n)$ reaction cross section therefore the sandwiches contained also U_3O_8 powder of 1.5 g pressed in a thin plexiglass box.) This arrengement is reproduced in the insert of Fig. 1.

Activity of the Al and Cu samples was determined by a flow-type 4πβ-counter while that of In was measured by a GeLi-spectrometer. The following corrections were applied to calculate the reaction rates: time fluctuation of the neutron flux during the irradiations, change of flux due to absorption in the sandwich and the distance between the foils, selfabsorption of β-particles and γ-quanta, dead-time of countings, losses due to pulse pile-up and cascade coincidences of γ-rays, interference from the $^{63}Cu(n,\gamma)^{64}Cu$ reaction. The following references for the cross

sections were accepted: /9/ for the $^{115}In(n,n')$ and $^{27}Al(n,p)$ reactions, /10/ for $^{63}Cu(n,2n)$, /10/ for the $^{27}Al(n,\alpha)$ reaction up to 13.5 MeV while /11/ was used for the 13.5-15 MeV region, /12/ for the $^{65}Cu(n,2n)$ process around 14 MeV and data of /10/ were chosen below it after a normalization to values of /12/ in the 14 MeV region.

3. Results and discussion

Neutron flux densities calculated in the usual way are shown in Fig. 1, which may be a characteristic picture for neutron fields of such a target assembly. Presence of low energy neutrons is well demonstrated mainly by the $^{115}In(n,n')$ reaction. Results of the $^{63}Cu(n,2n)$ reaction contradict to the others which can be explained perhaps by the uncertainty in the cross section therefore it was neglected in the further calculations.

However, inconsistency in the data set of the remaining reactions as well as the relatively low intensity of the scattered neutrons made it impossible to de-

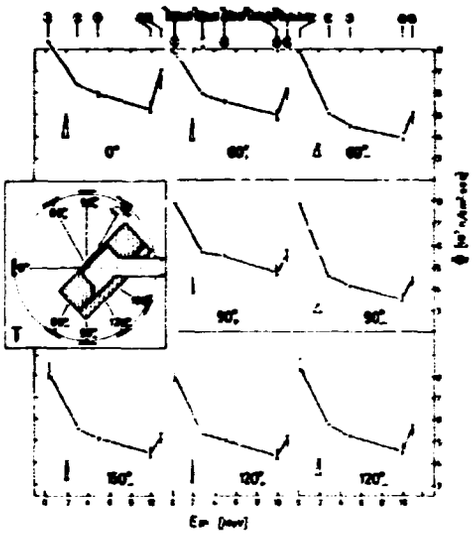

Fig. 1.

Neutron flux density as a function of the reaction threshold

Results for the (n,p) and (n,α) reactions are indicated at their "effective threshold". Error bar shows fluxes calculated with extreme values of literature cross sections. Top of triangles represents corrected flux density while their base indicate the 2σ (95%) width of the estimated energy distribution in the 14 MeV peak. Neutron source - sample arrengement inserted in "T".

termine the complete spectrum directly from the results of foil activation, without any knowledge about its but qualitative structure. A starting distribution shape was estimated on the basis of single elastic and inelastic processes on the structural materials of the target assembly (H,O,C,Fe,Mo). This spectrum can be characterized by main regions as follows: 0-4 MeV, 4-9 MeV, from 9 MeV to the beginning of the 14 MeV peak and this latter itself which has some distortions, too. Absolutization of these intervals was carried out by the experimental reaction rates. Such a procedure has the adventage also to imply effects from all the other sources of background neutrons which are difficult to be considered accurately in the theoretical spectrum calculations, e.g. (d,d)-selftargets in the beam handling system, scattering in the sample itself, room walls, etc. (Cd-cover of the sandwiches increases the intensity appreciably in the 0-4 MeV region.) The following features can be drawn from the spectrum of neutrons impinging the sample at 0° direction: 0-4 MeV represents 11.3%, 4-9 MeV 0.4%, 9-14.2 MeV 12.4% and 14.2-15.1 MeV (with a mean energy of 14.80 MeV) 75.9%. It is interesting to com-

Table 1. Fractions of the activity induced by the "real 14 MeV neutrons", %

ϑ	$\langle E_n \rangle \pm \Delta F_n$ MeV	U-238 n,γ	U-235 n,f	In-115 n,n'	U-238 n,f	Al-27 n,p	Al-27 n,α	U-238 n,2n	Cu-65 n,2n	Cu-63 n,2n
		E_{th}=0	0	0.339	0.8	3.0	5.0	6.17	10.06	11.02
0°	14.80 $^{+0.16}_{-0.18}$	5.63	86.1	59.6	81.1	82.8	85.5	76.1	91.9	94.6
+60°	14.45 ±0.12	6.75	81.9	59.7	85.7	82.1	85.7	76.5	92.8	95.6
-60°	14.40 $^{+0.12}_{-0.20}$	2.01	69.7	46.6	80.6	78.5	82.5	72.7	90.8	93.6
+90°	14.13 ±0.08	8.40	78.8	54.9	81.0	77.1	81.6	71.9	90.4	93.8
-90°	14.10 $^{+0.13}_{-0.25}$	2.26	68.3	42.3	77.2	75.1	80.6	70.9	89.8	94.3
+120°	13.75 ±0.10	6.36	76.7	54.3	77.4	76.3	81.5	73.3	90.6	94.3
-120°	13.76 ±0.10	3.48	70.9	48.8	76.7	74.4	78.9	71.2	87.4	92.3
-150°	13.51 $^{+0.13}_{-0.11}$	5.23	71.2	52.0	77.6	76.7	80.4	73.8	89.2	94.3
45°	14.62 $^{+0.20}_{-0.22}$	12.95	88.6	68.9	90.9	88.0	91.1	83.5	96.2	97.9

pare situations for +90° and -90° positions: 0-4 MeV 7.5%, 4-9 MeV 0.5%, from 9 MeV to peak 17.8%, peak 74.2% and for the same regions 24.9, 0.4, 15.1, 59.6%, respectively. Our results agree qualitatively with those of /6/ although show a pronounced neutron excess between 9 MeV and the peaks. This character also supposed in /7/ is perhaps due to inelastic neutron scattering. More details are given in /13/.

Fractions of the activity induced by neutrons in the 14 MeV peak for different directions were calculated on the basis of the spectra and excitation functions. Results are summarized in Table 1, where cross section for the $^{238}U(n,\gamma)$, $^{238}U(n,f)$ and $^{235}U(n,f)$ reactions were taken from /14/ while that of $^{238}U(n,2n)$ is our compilation /13/. The last line in Table 1 refers to data for 5 mm distance of a sample from the source, surface of which is also directed at -45°. Energy distribution of the peak was estimated from the reaction kinematics for completely stopped deuterons (E_d=175 keV) and irradiation geometries and then distorted by the scattering processes. $\langle E_n \rangle$ is its mean value while ΔE_n is used in the usual 1σ (68%) sense. Uncertainty of the fractions was estimated to be about ±4%, excluding (n,γ) reaction. For comparison, results in /5/ gave fractions of 86 and 92 % for the $^{27}Al(n,\alpha)$ and $^{63}Cu(n,2n)$ reactions, respectively.

It is now clear what an error can be introduced with the neglect of background neutrons when cross section of reactions having significantly different excitation function is compared - as it is usual in the foil activation experiments.

References

1 G.Pető, J.Csikai, Neytronnaya Fizika vol.III. 78 (Obninsk 1974; Proc. 2nd All-Union Conf. 28 May-1 June 1973, Kiev)
2 M.Valkonen, Research Rep. 1/1976, Dep.Phys.Univ. Yväskylä, Finland (1976)
3 D.R.Nethaway, Nucl.Phys. A190 635 (1972)
4 R.Michel, H.Weigel, Radiochim.Acta 22 1 (1975)
5 E.Ricci, J.Inorg.Nucl.Chem. 27 41 (1965)
6 E.E.Graves, L.Rosen, Phys.Rev. 89 343 (1953)
7 G.Shani, Ann.Nucl.En. 3 431 (1976)
8 S.Nagy, J.Csikai, I.Angeli, Nucl.Instr.Meth. 91 345 (1971)
9 ENDF/B-IV Dosimetry File (Ed.B.A.Magurno) BNL-NCS-50446, INDC/US/-70/L, 1975
10 V.Kanda, R.Nakasima, Neutron Cross Sect.Techn., vol.I.193 (Proc.Conf. 4-7 March 1968 Washington)
11 H.Vonach, M.Hille, G.Stengl, W.Breunlich, E.Werner, Z.Phys. 237 155 (1970)
12 W.Mannhart, H.Vonach, Z.Phys. A272 279 (1975)
13 P.Raics, Thesis for Ph.D. Kossuth L. University, Debrecen, 1978
14 M.G.Sowerby, B.H.Patrick, D.S.Mather, Ann.Nucl.Sci.Eng. 1 409 (1974)

ПРЯМЫЕ И РАВНОВЕСНЫЕ ПРОЦЕССЫ В (p,n) РЕАКЦИЯХ ПРИ ЭНЕРГИИ ПРОТОНОВ 22,2 ± 0,2 МЭВ

Н.С.Бирюков, Б.В.Журавлёв, А.П.Руденко, О.А.Сальников, В.И.Трыкова

Физико-энергетический институт, г.Обнинск, СССР

Спектры нейтронов из (p,n) реакций на ядрах ^{27}Al, ^{52}Cr, ^{56}Fe, $^{58,60}Ni$, $^{90,91,94}Zr$, ^{115}In, ^{181}Ta, ^{197}Au измерены при энергии протонов 22,2 ± 0,2 МэВ под углами 30°, 60°, 90°, 120°, 150° Результаты анализа экспериментальных данных показывают, что неравновесная часть спектров практически полностью обусловлена прямыми процессами, ответственными за асимметрию в угловом распределении нейтронов.

Проведенные нами исследования спектров и угловых распределений нейтронов из (p,n) реакций при энергии протонов 11,2 ± 0,1 МэВ [1,2] показали, что выделение вклада прямых процессов, определяемых как асимметричная компонента наблюдаемых угловых распределений, приводит к более согласованным значениям параметров плотности ядерных уровней по сравнению с результатами, получаемыми в рамках модели предравновесного распада ядер или без учета неравновесных процессов вообще. Однако, хотя асимметрия в угловом распределении несомненно указывает на наличие прямых процессов, она позволяет определить лишь нижнюю границу их вклада. Прямые процессы могут приводить и к симметричному или изотропному угловому распределению продуктов реакции, в частности, из-за искажения волновых функций начального и конечного состояний потенциалом ядра, отделить которые от распада через составное ядро экспериментально не представляется возможным и приходится делать оценку вклада этой составляющей в рамках имеющихся моделей [3,4] . При энергии налетающего нуклона около 10 МэВ вклад этой составляющей прямых процессов в интегральный спектр близок к асимметричной компоненте [1,2,3,4] . С увеличением энергии, однако, имеется тенденция к росту асимметричной компоненты и можно надеяться на получение более точной информации об интегральном спектре частиц, испущенных в прямых взаимодействиях, из анализа измеряемых угловых распределений.

В данной работе измерялись спектры нейтронов из (p,n) реакций на ядрах ^{27}Al, ^{52}Cr, ^{56}Fe, $^{58,60}Ni$, $^{90,91,94}Zr$, ^{115}In, ^{181}Ta, ^{197}Au при энергии протонов 22,2 ± 0,2 МэВ под углами 30°, 60°, 90°, 120°, 150°. Измерения проводились на спектрометре нейтронов по времени пролета, созданном на базе 150-см циклотрона ФЭИ [5]. Характерные интегральные спектры и угловые распределения нейтронов приведены на рис. 1,2,3. В виде гистограммы на рисунках представлены спектры нейтронов, имеющих асимметричное угловое распределение. Для получения таких спектров угловые распределения нейтронов по энергетическим интервалам 1 МэВ аппроксимировались разложением по полиномам Лежандра до второго порядка включительно; вклад асимметричной компоненты при таком представлении определяется коэффициентом при первом полиноме [1 ÷ 3]. Для всех исследуемых ядер в высокоэнергетичной части гистограммы совпадают в пределах точности измерения с интегральными спектрами эмиссии нейтронов, указывая тем самым на правильность и полноту определения вклада прямых процессов через асимметрию в угловом распределении, по крайней мере, для этой области энергий.

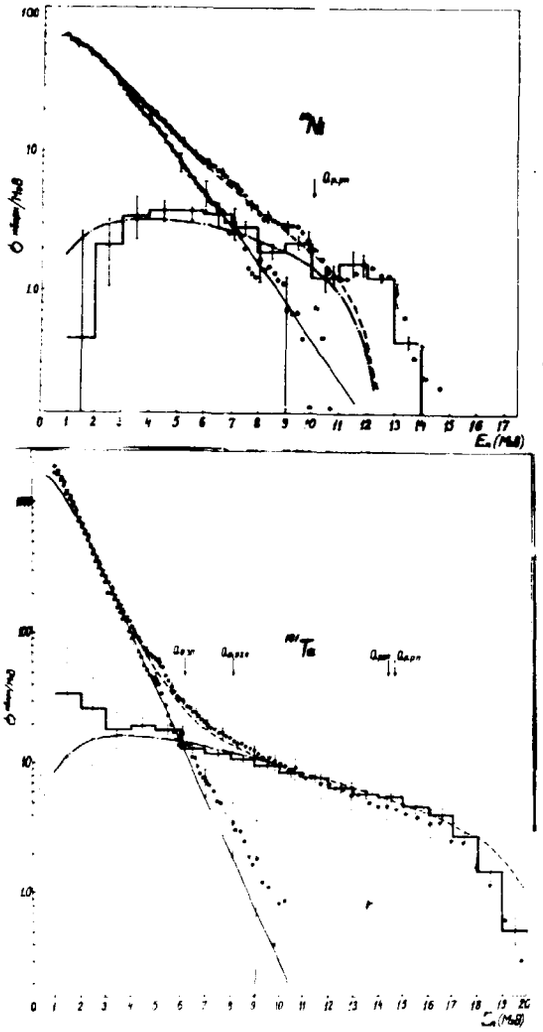

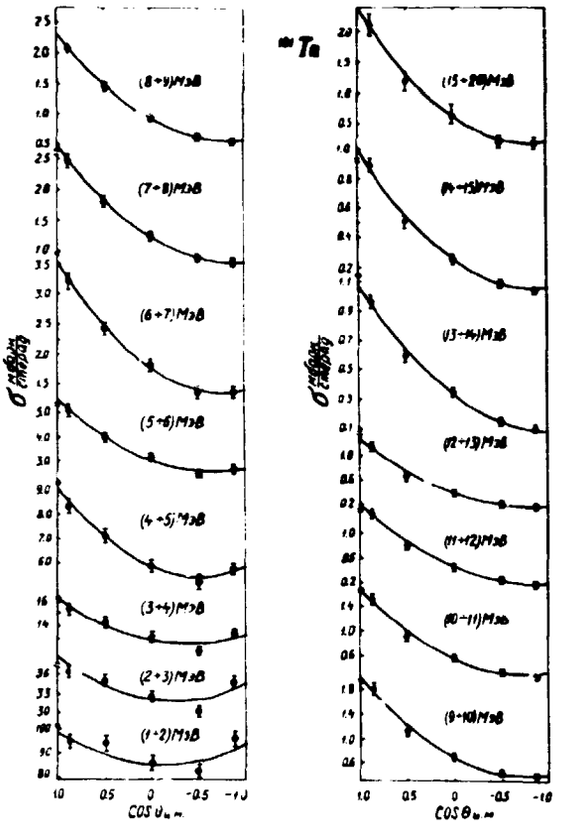

Рис.3. Угловые распределения нейтронов. Кривые – аппроксимация разложением по полиномам Лежандра.

Рис.I,2. ● – Интегральные спектры нейтронов;
о – интегральные спектры нейтронов после вычитания асимметричной компоненты;
Гистограммы – спектры нейтронов, имеющих асимметричное угловое распределение;
——— – расчет по формуле Лекутера;
– – – – расчет по МПР;
—·— – предравновесные спектры нейтронов.

Особенно хорошо это совпадение проявляется для ядер с A> 90, где энергетический диапазон, на котором вкладом от эмиссии из равновесных состояний можно пренебречь, шире вследствии более мягкой равновесной части спектров и более низких значений $Q_{p,n}$ реакций, чем для A≤ 60. Дополнительная информация о достоверности такого определения спектра нейтронов, испущенных в результате прямого взаимодействия, может быть получена из анализа спектров, остающихся после вычитания из интегральных спектров асимметричной компоненты, в рамках статистической теории равновесного распада ядер. В данной работе указанные спектры (светлые кружки на рисунках) описывались формулой Лекутера [6], полученной в модели последовательного испарения частиц.

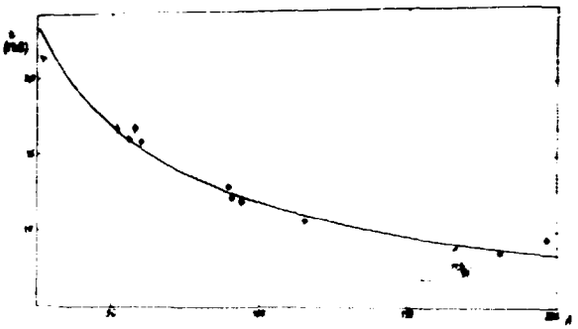

Рис.4. Зависимость термодинамической температуры от массового числа.

Таблица I.

Ядро-мишень	T (МэВ)	a ($МэВ^{-1}$)	a' ($МэВ^{-1}$)	$a_{рез.}$ [7,8] ($МэВ^{-1}$)	σ эмиссии нейтронов с энергией > I МэВ (Мбарн)	α асим (%)
^{27}Al	2,43±0,03	3,I4±0,I3	3,95±0,I6	$3,96^{+0,49}_{-0,I3}$	I94±I3	I8,5±I,3
^{52}Cr	I,85±0,02	5,50±0,I7	6,52±0,22	$^{*}6,89^{+0,49}_{-0,30}$	760±50	II,5±I,2
^{56}Fe	I,77±0,02	6,02±0,22	7,03±0,25	$^{*}7,82^{+0,24}_{-0,I9}$	667±43	7,8±I,3
^{58}Ni	I,62±0,02	5,50±0,22	6,70±0,27	$^{*}7,I9^{+0,3I}_{-0,22}$	I70±II	I6,2±I,6
^{60}Ni	I,66±0,02	6,25±0,24	7,40±0,28	$^{*}8,35^{+0,22}_{-0,I9}$	70I±45	7,6±I,6
^{90}Zr	I,34±0,0I	9,25±0,22	I0,50±0,25	$^{*}I0,I7^{+0,33}_{-0,26}$	I25I±8I	7,8±0,5
^{9I}Zr	I,43±0,0I	I0,20±0,22	II,40±0,25	$^{*}I0,34\pm0,60$ $I2,22^{+0,38}_{-0,29}$	I5I6±98	7,3±0,5
^{94}Zr	I,42±0,0I	I0,90±0,24	I2,I0±0,27	$I2,8I\pm0,25$ $I3,I5^{+0,I8}_{-0,25}$	I824±II8	6,9±I,5
^{II5}In	I,3I±0,0I	I2,70±0,30	I4,00±0,33	$I5,78^{+0,50}_{-0,37}$	I656±I07	9,3±I,4
^{I8I}Ta	I,03±0,0I	20,0I±0,63	2I,60±0,68	$^{*}2I,I8^{+I,2I}_{-I,I7}$	I948±I27	II,0±2,4
$^{I97}Au^{(+)}$	I,II±0,02	I6,40±0,68	20,03±0,74	$^{*}2I,I9^{+0,36}_{-0,30}$	I77±I3	

Примечание. α асим. – доля нейтронов в интервале энергий (I,0 ÷ E_{max}) МэВ, имеющих асимметричное угловое распределение. (*) – значения $a_{рез.}$ приведены для ближайшего атомного числа. (+) – измерения проведены только для угла 90° и анализ спектра проведен в диапазоне энергий нейтронов (I,0÷ 4,0) МэВ, где неравновесной эмиссией можно пренебречь

Результаты анализа, представленные на рисунках I,2,4 и в таблице I, показывают:

1) Спектры нейтронов в пределах экспериментальных ошибок описываются формулой Левутера;
2) Зависимость термодинамической температуры, значения которой приведены к одинаковой средней энергии возбуждения 15,4 МэВ согласно выражению $t=\sqrt{u/a}$, от массового числа соответствует предсказанию модели Ферми-газа $t=const/\sqrt{A}$;
3) Значения параметра плотности ядерных уровней "a'", определенные в соответствии с известным выражением Вайскопфа для энергетической зависимости плотности уровней, хорошо согласуются с данными по нейтронным резонансам [7,8], являющимся наиболее прямой экспериментальной информацией.

Значения параметра "a", соответствующие энергетической зависимости предэкспоненциального множителя в выражении для плотности уровней $u^{-5/4}$, несколько ниже резонансных данных. Трудно однако отдать предпочтение тем или иным значениям параметра, так как для энергий возбуждения выше энергии связи имеются указания на некоторое уменьшение плотности уровней по сравнению с предсказанием модели Ферми-газа при условии, что абсолютная нормировка произведена на данные по нейтронным резонансам [9]. В целом же можно отметить, что параметры плотности ядерных уровней, определенные нами из анализа спектров после вычитания асимметричной компоненты, находятся в разумном согласии с данными по нейтронным резонансам и с современными представлениями об изменении плотности уровней с энергией возбуждения.

Таким образом, описанный ниже способ определения спектра нейтронов, испущенных в результате прямого взаимодействия, через асимметрию в угловом распределении приводит к согласованному разделению механизма эмиссии нейтронов в исследуемых в данной работе ядерных реакциях на равновесный и прямой.

Для сравнения с полученными результатами спектры нейтронов были проанализированы также в рамках модели предравновесного распада ядер (МПР), аналогично тому как это сделано нами в работе [I]. В среднем, МПР неплохо описывает интегральные спектры нейтронов, не отражая однако структурных особенностей, наблюдаемых на эксперименте. Для ряда ядер (^{27}Al, ^{58}Ni, ^{91}Zr, ^{94}Zr, ^{115}In, ^{181}Ta) неплохое согласие имеет место и между спектрами эмиссии нейтронов из неравновесных состояний, определяемых, как из анализа угловых распределений (асимметричная компонента), так и из расчетов в рамках МПР, хотя асимметрия в угловом распределении при таких низких энергиях не объясняется в МПР. Такое совпадение указывает, пожалуй, лишь на преимущественный вклад прямых процессов в предравновесный распад ядер, интерпретация которых в МПР является слишком упрощенной.

Так как измерения спектров и угловых распределений нейтронов из (p,n) реакций проведены для достаточно большого числа ядер, представляется возможность проследить зависимость определенного нами сечения прямого взаимодействия от массового числа. Согласно Лейну [10], сечение возбуждения изобар-аналоговых состояний в (p,n) реакциях (процесса, протекающего, в основном, вследствие прямого механизма взаимодействия [II]) пропорционально $(N-Z)/A^{2/3}$. В данной работе мы определяем сечение, проинтегрированное по большому числу состояний (E_n= I,0÷E_n^{max} МэВ), и его зависимость от массового числа может быть несколько иной. Поэтому на предмет согласования с определенными из анализа эксперимен-

тальных данных сечениями прямого взаимодействия испытывались кроме зависимости $(N-Z)/A^{2/3}$, близкие к ней $(N-Z)/A$ и $(N-Z)/A^{4/3}$, а также наиболее простые зависимости $(N-Z)$ и A, не противоречащие явно совокупности экспериментальных точек.

На 5 % уровне значимости распределения только для зависимости $(N-Z)/A$ критерий $\chi^2 < \chi^2_{5\%}$ [I2]; остальные зависимости с точки зрения их согласия с экспериментальными данными должны быть отвергнуты. Как показано на рис.5, пропорциональность $(N-Z)/A$ наблюдается и для сечений прямого взаимодействия, определенных нами из анализа экспериментальных данных при энергии протонов II,2±0,I МэВ [I,2]. В предположении, что указанная зависимость от массового числа справедлива и для промежуточных энергий протонов, можно делать оценку вклада прямых процессов и их компонент (асимметричной и изотропной), используя для этого в первом приближении линейную интерполяцию.

Основные результаты работы сводятся к следующему:

а) Спектры нейтронов из (p,n) реакций измерены при энергии протонов 22,2±0,2 МэВ для ядер ^{27}Al, ^{52}Cr, ^{56}Fe, ^{58}Ni, ^{60}Ni, ^{90}Zr, ^{91}Zr, ^{94}Zr, ^{115}In, ^{181}Ta под углами 30°, 60°, 90°, I20°, I50° и для ^{197}Au под углом 90° в широком диапазоне энергий испускаемых нейтронов – $[I,0 + (E_p+Q_{p,n})]$ Мэв.

б) Анализ экспериментальных данных показал, что определение спектра нейтронов, испущенных в результате прямого взаимодействия, через асимметрию в угловом распределении приводит к согласованному разделению механизма эмиссии нейтронов в исследуемых ядерных реакциях на равновесный и прямой.

в) Показано, что изменение определенного таким образом сечения прямого взаимодействия от массового числа пропорционально $(N-Z)/A$.

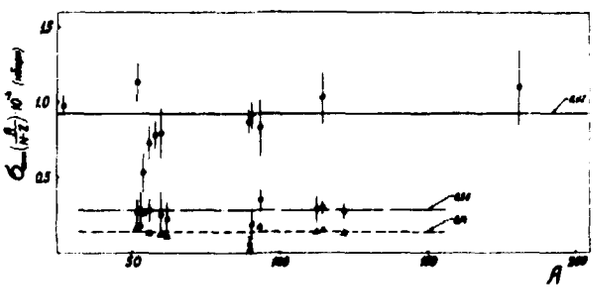

Рис.5. Зависимость сечения прямого взаимодействия от массового числа.
● – E_p=22,2 МэВ;
○ – E_p=II,2 МэВ;
▲ – E_p=II,2 МэВ, асимметричная компонента.

Литература

I. Н.С.Бирюков, Б.В.Журавлёв и др. Я.Ф., т.29, вып.6, (I970)
2.Н.С.Бирюков, Б.В.Журавлёв и др. Препринт ФЭИ-9I0, (I978)
3. Н.С.Бирюков, Б.В.Журавлёв и др. Я.Ф., т.25,767, (I977)
4. А.В.Игнатюк, В.П.Лунёв, В.Г.Проняев, Препринт ФЭИ-682, (I976)
5. Н.С.Бирюков, Б.В.Журавлёв и др. Предпринт ФЭИ-94I, (I979)
6. K.J. Le Couter and D.W. Lang. Nucl. Phys. 13,32,(1959).
7. A.Gilbert and A.G.W. Cameron. Can. J. Phys. 43, 1446, (1965).
8. H.Baba. Nucl. Phys. A159, 625, (1970).
9. А.В.Игнатюк, Материалы 3-ей школы по нейтронной физике, Алушта, (I978), Дубна, (I978г.), стр.50
I0. A.M.Lane. Nucl. Phys. 35, 676, (1962).
II. J.D.Carlson et al. Nucl. Phys. A249, 29, (1975).
I2. Д.Худсон. Статистика для физиков. Изд. "Мир", Москва,I967г.

ON THE CHARGE DEPENDENCE OF NUCLEAR FORCES

I. Rotter
Zentralinstitut für Kernforschung Rossendorf, DDR-8051 Dresden

In recent years considerable attention has been devoted to the interpretation of energy differences between mirror pairs of light nuclei, displacement energies of isobaric analog states in heavier nuclei as well as to the investigation of isospin forbidden transitions and isospin mixing in nuclei. The hope was to extract information regarding the nuclear wavefunctions since Coulomb effects in nuclei are believed to offer the possibility of separating the known Coulomb interaction from the ambiguities of the nuclear wavefunctions. The results obtained are not encouraging. Coulomb energy differences are much more complicated than originally anticipated [1]. The predictions of the Hartree-Fock theories for the neutron radii do not explain the Coulomb energy anomaly. It is not clear which radii agree with the experimental data (e.q.[2]). The situation in isospin forbidden transitions is similar (e.g.[3]). Therefore, charge dependence of nuclear forces needs discussing.

Some charge dependence of nuclear forces arises from meson exchange forces. In heavier nuclei, an additional source of charge dependence exists which is a typical nuclear many-body effect. Nir [4] showed that a correlation exists between the Coulomb displacement energies and the binding energies. Some regularities have been found also in isospin forbidden decays [5]. These facts suggest that the isospin impurities are not dominated by accidental near-degeneracies of the states with different isospin but instead arise from a mechanism which reflects general properties of the nuclear structure.

Theoretically, an effective charge dependence of nuclear forces in the subspace of a traditional nuclear structure calculation arises from the coupling of the discrete states to the continuum [6]. The effective Hamiltonian appearing in a traditional nuclear structure calculation due to the truncation of the total function space contains the coupling between the space of continuous states (P-space) and the space of discrete states (Q-space = function space of the traditional nuclear structure calculation) [7]:

$$H_{QQ}^{eff} = H_{QQ} + H_{QP} G_P^{(+)} H_{PQ} \tag{1}$$

Here, $H_{QQ} \equiv QHQ$ and $H_{QP} \equiv QHP$ where Q and P are the projection operators onto the wavefunctions in the Q- and P-space, respectively. The operator $G_P^{(+)}$ is the Green operator in the P-space.
The matrix elements of the second term of the operator (1) are given in the following manner

$$\langle \Phi_R | H_{QP} G_P^{(+)} H_{PQ} | \Phi_{R'} \rangle = \sum_c \int_{\varepsilon_c}^{\infty} dE' \langle \Phi_R | H | \xi_{E'}^c \rangle (E^+ - E')^{-1} \langle \xi_{E'}^c | H | \Phi_{R'} \rangle \tag{2}$$

Here, the functions Φ_R are eigenfunctions of the operator H_{QQ} (traditional nuclear structure wavefunctions) while the functions ξ_E^c are eigenfunctions of

H_{PP}. The eigenvalues of H_{PP} are denoted by E' whereas c and ε_c stand for the channel and its threshold energy, respectively.

A charge-dependent residual interaction has not been introduced explicitely in the term (2).
Nevertheless, it is charge dependent due to the central Coulomb field acting on the discrete (Φ_R) as well as on the scattering (ξ_E^c) wavefunctions.

The matrix elements (2) and their charge dependence are non-vanishing not only for decaying states but also for bound states. They lead to an energy shift ΔE_R of the states

$$\begin{aligned}\Delta E_R &= E_R - E_R^{SM} \\ &= \mathcal{R}e \sum_c \int_{\varepsilon_c}^{\infty} dE' \langle \Phi_R | H | \xi_{E'}^c \rangle (E^+ - E')^{-1} \langle \xi_{E'}^c | H | \Phi_R \rangle \end{aligned} \tag{3}$$

Here, E_R is the energy of the state in the continuum shell model (real part of the eigenvalue of H_{QQ}^{eff}) while E_R^{SM} is the energy of the state in the conventional shell model (eigenvalue of H_{QQ}). For bound states, the sum in eq. (3) runs over closed channels only. The width Γ_R of a decaying state is given by the imaginary part of the eigenvalue of H_{QQ}^{eff} at the energy E_R:

$$\begin{aligned}\Gamma_R &= \sum_c |\Gamma_{R,c}| \\ &= 2\pi \sum_c \langle \Phi_R | H | \xi_E^c \rangle \langle \xi_E^c | H | \Phi_R \rangle \end{aligned} \tag{4}$$

The sum in eq. (4) runs over open as well as closed channels.

The charge dependence of the effective Hamiltonian (1) is characterized by the relative energy shift between analogue states as well as by the difference between proton and neutron widths of analogue states of mirror nuclei. Both values are expected therefore to show a similar dependence on the nuclear structure properties.

The numerical calculations on the basis of the continuum shell model have shown [6] that the charge-dependent effects in nuclei depend very sensitively on the channels and the position of their thresholds. Some general trends of the charge dependence can be observed: Shell effects in the charge dependence appear in a natural manner via the distinguished parentage structure of the ground state of the nuclei just beyond the shell closures relative to the energetical lowest channel. The odd-even effect in the Coulomb displacement energy as well as the fact that the neutron decays of the lowest T = 3/2 levels of A = 4n + 1 light nuclei are always greater than the analogous proton decays are shown to be connected with regularities in the binding energy which are going with $\Delta A = 4$

That means, charge dependence of the Hamiltonian (1) explains both trends observed experimentally although they are physically very different.

References

[1] J.W. Negele, Proc. Int. Conf. Nucl. Structure and Spectroscopy, Amsterdam, vol. 2 (1974) 618

[2] A. Chaumeaux, V. Layly, and R. Schaeffer, Annals of Physics 116 (1978) 247; S. Shlomo and R. Schaeffer, Phys. Letters B38 (1979) 5

[3] A.B. McDonald and E.G. Adelberger, Phys. Rev. Letters 40 (1978) 1692

[4] D. Mir, Canadian Journ. of Phys. 52 (1974) 2132

[5] P.G. Ikossi, K.A. Snover, J.L. Osborne, and E.G. Adelberger, Nucl. Phys. 319 (1979) 109

[6] I. Rotter, J. Phys. G5 (1979) 75; B. Käpfer and I. Rotter, J. Phys. G5 (1979) 747; I. Rotter, J. Phys. G6 (1980)

[7] H.W. Barz, J. Rotter, and J. Höhn, Nucl. Phys. A275 (1977) 111

SELF-CONSISTENT DESCRIPTION OF THE GIANT DIPOLE RESONANCE INCLUDING THE PARTICLE CONTINUUM

F.A.Gareev, S.N.Ershov, N.I.Pyatov, D.I.Salamov

Joint Institute for Nuclear Research, Dubna, USSR

The description of giant resonances involves the following three important theoretical aspects:

First, the problem should be formulated self-consistently, e.g. the Hamiltonian used must be invariant under certain symmetry transformations and the connection between self-consistent field and the effective forces should be taken into account.

Second, the nuclear excitations of interest are usually located in the continuous spectrum, hence the latter should correctly be included in calculations. This allows one, in particular, to obtain that part of the resonance width which is associated with the particle decay to open channels.

And finally, the calculation of the total resonance width requires the inclusion of the damping mechanism for particle and hole states.

In the present work we have used a simple self-consistent model[1] with separable forces in which the form factors and the strength parameters are derived from the shell-model potential. Equations of the model are formulated in the coordinate representation[2,3], which allows one to take correctly into account the particle continuum in calculations of the spectra of collective excitations. Below we present some results of calculations in which the damping of particle and hole states was not included.

Figure 1 shows the strength functions for E1-excitation of nuclei ^{16}O and ^{58}Ni calculated with the Woods-Saxon potential. For ^{58}Ni also given are the results of calculations[1] in which the continuum was approximated by the discrete single-particle resonances with a relatively small width (dashed lines). It turns out that in the low-energy part of E1-resonance the particle continuum gives rise to a relatively small width only. With increasing the excitation energy the discrete states[1] are shifted and their width becomes much larger. It should be noted that the calculated widths are sums of all partial widths for the particle decay of the resonance. For ^{16}O the calculated width and the structure of the resonance are close to the observed ones. For heavier nuclei the calculated pictures are much more different from experiment.

The contributions of different parts of the excitation spectrum to the total photoabsorption cross section $\Delta\sigma_0$ (sum rule) are listed in the table. The calculated values of the center-of-gravity of the resonance $E_L = (\sigma_L/\sigma_0)^{1/2}$ and the width of the distribution of E1-transitions $W = [\sigma_L/\sigma_1 - (\sigma_1/\sigma_0)^{1/2}]$ are compared in the table with the results of ref.[1]. It is seen that the proper inclusion of the continuum leads to a certain increase of the strength of E1-transitions in the low-energy part of the resonance. This results in the increase of the magnitude of W. The center-of-gravity of the resonance is somewhat lowered.

The calculated sum rules are below the classical limit owing to the

inaccuracy of integration over the energy in the region of narrow resonances and to the neglected contribution of the high-energy part of the spectrum.

1. N.I.Pyatov, M.I.Baznat. Journ. of Nucl. Phys. (USSR), 30, no.5, 1979.
2. S.Shlomo, G.Bertsch. Nucl.Phys., A243, 507, 1975.
3. E.E.Saperstein, S.A.Fajans, V.A.Khodel. Preprint IAE-2580, Moscow, 1976.

Nucleus	Mev	E_2, Mev				W, Mev	
		present work	ref.(1)	present work	ref.(1)	present work	ref. (1)
^{48}Ca	0-14	16.2	10.7				
	14-19	67.3	74.5				
	19-32	8.9	12.4				
	0-32	92.4	97.6	15.5	16.3	2.6	1.4
^{58}Ni	0-14	13.3	11.3				
	14-25	79.6	86.9				
	25-31	0.9	0.9				
	0-31	93.8	97.6	16.7	17.1	2.5	2.3
^{90}Zr	0-13	28.9	20.4				
	13-17	57.4	75.5				
	17-35	5.2	1.2				
	0-35	91.6	97.1	13.9	14.4	2.7	2.4

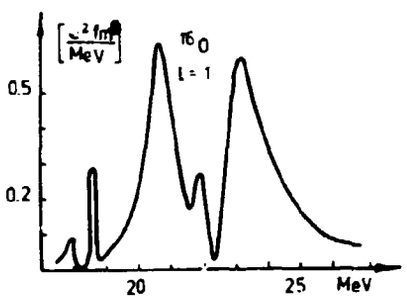

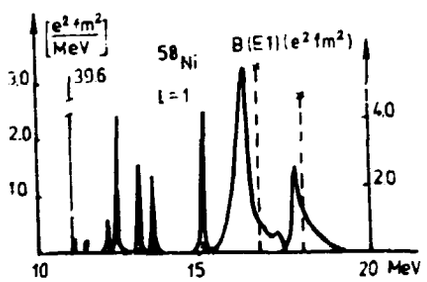

SEMI-CLASSICAL DESCRIPTION OF SLOW NEUTRON RESONANCES

M.Kaczmarczyk and M.Przytuła,
Institute of Physics, University of Łódź,
ul.Narutowicza 68, 90-136 Łódź, Poland

A b s t r a c t: An exciton model method of calculation of reduced neutron resonance widths is presented. The results of calculation are compared with experimental data.

The serious difficulties in theoretical predictions of the neutron resonance parameters, in particular the total and partial widths, call for the search of some simple approach, which could offer an easy method for the estimation of above mentioned characteristics. Such an approach was proposed in [1]. It is the semi-classical description of the structure of neutron resonances, based on the exciton model [2]. The basic feature of this approach is the possibility to find the mean time θ_i, which the excited nucleus spends in the configuration with i-particles above Fermi level, as a function of the intranuclear transition rates $\lambda_r^{\pm}$, and emission rates λ_r. As it was pointed out in [1], and in [3] or [4], the integration of the set of coupled master equations at given boundary conditions leads to the system of linear algebraic equations with θ_i. Taking into account the proper conditions for considered case, namely

$$P_i(t) = \delta_{1i} \quad \text{at} \quad t = 0 \quad \text{and} \quad P_i(t) = 0 \quad \text{for} \quad t = \infty ,$$

one obtains the solutions

$$\theta_i = \int_0^{\infty} P_i(t)dt = (-1)^i \frac{D_{1i}}{D}$$

where D is the determinant of the coefficients of master equations, i.e. $a_{r,r} = -(\lambda_r^+ + \lambda_r^- + \lambda_r)$; $a_{r,r-1} = \lambda_{r-1}^+$; $a_{r,r+1} = \lambda_{r+1}^-$, and $a_{r,s} = 0$ for $|r - s| > 1$. The D_{1i} is the minor of the element a_{1i} with "i" taking the values 1,2 ... k, where k is the maximum number of excited nucleons at given excitation energy $U = S_n$. This limitation for "i" comes from Pauli exclusion and energy conservation principles.

The mean lifetime and total width of the excited resonance level are

$$\tau = \sum_{i=1}^{k} \theta_i \quad \text{and} \quad \Gamma = \frac{\hbar}{\tau}$$

and the structure of the excited nucleus is given by average contributions of various i-particle configurations

$$p_i = \frac{\theta_i}{\tau}$$

The time θ_i, lifetime τ, width Γ and structure depend on the $\lambda_r^{\pm}$, λ_r and k;

these values are determined by the nuclear model and some proper assumptions [1].

The calculations were performed assuming the equidistant spacing model with single-particle level density $g = A/13\ (\mathrm{MeV}^{-1})$. For evaluations of intranuclear transition rates the Golden Rule was used: $\lambda_i^{\pm} = 2\pi\hbar^{-1}\cdot\overline{M^2}\cdot\varrho_f^{\pm}(i)$, where the average squared two-body transition matrix element was: $\overline{M^2} = KU^{-1}A^{-3}$ [5] and the level density of accessible final states $\varrho_f^{\pm}(i)$ was taken from [6]. Emission rates λ_r were calculated from single particle width (for neutron emission) and from Weisskopf's estimation for photon emission at quite simplified assumptions.

The average neutron reduced widths were calculated from the relation $\Gamma_n^o = p_1\Gamma_{sp}^o$, where $\Gamma_{sp}^o = 1.48\cdot 10^4\cdot A^{-\frac{2}{3}}\ (\mathrm{eV})$. In order to explain the shell effects in the dependence of Γ_n^o on the neutron number (reported in [7] and [8]) the shell model energy gaps in calculations of "k" were taken into account. The obtained results are shown in Fig.1. and Fig.2. The points in Fig.2 are the experimental data. In spite of very simple assumptions the general tendency, shown in Fig.2, can be reasonably described. The calculated absolute values of τ (and Γ) are much overestimated ($\sim$100 times) although the shape of dependence on neutron number is rather correct.

References

1. M.Przytuła, M.Kaczmarczyk; 2nd International Symposium on Neutron Induced Reactions, Smolenice, June 25-29, (1979) in press
2. M.Blann; Ann. Rev. Nucl. Sci., 25 (1975) 123, and references contained therein
3. E.Běták and J.Dobeš; Proc. of the VIIth Int. Symp. on the Interaction of Fast Neutrons with Nuclei, Gaussig, November 21-25, 1977 (ZfK-376) p.5
4. J.Dobeš, E.Běták; Z.Physik A288 (1978) 175
5. P.Obložinský, I.Ribanský and E.Běták; Nucl. Phys., A226 (1974) 347
6. F.C.Williams, Jr., Phys. Lett., 31B (1970) 184
7. L.Aldea, M.Constantinescu, V.Mateiciuc and T.Stadnicov; Rev. Roum. Phys., 21 (1976) 619
8. M.Przytuła; Proc. Int. Conf. on Nuclear Reaction Mechanisms, Varenna, June 13-17, 1977, p. 179.

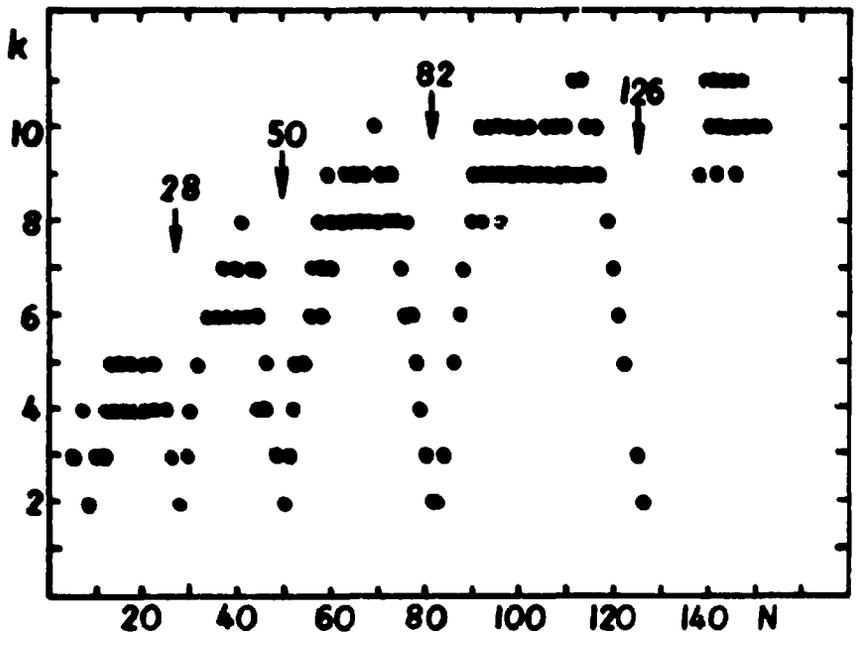

Fig.1. The maximum number of excited nucleons as a function of the target neutron number at excitation energy equal to the neutron binding energy of the composite nucleus.

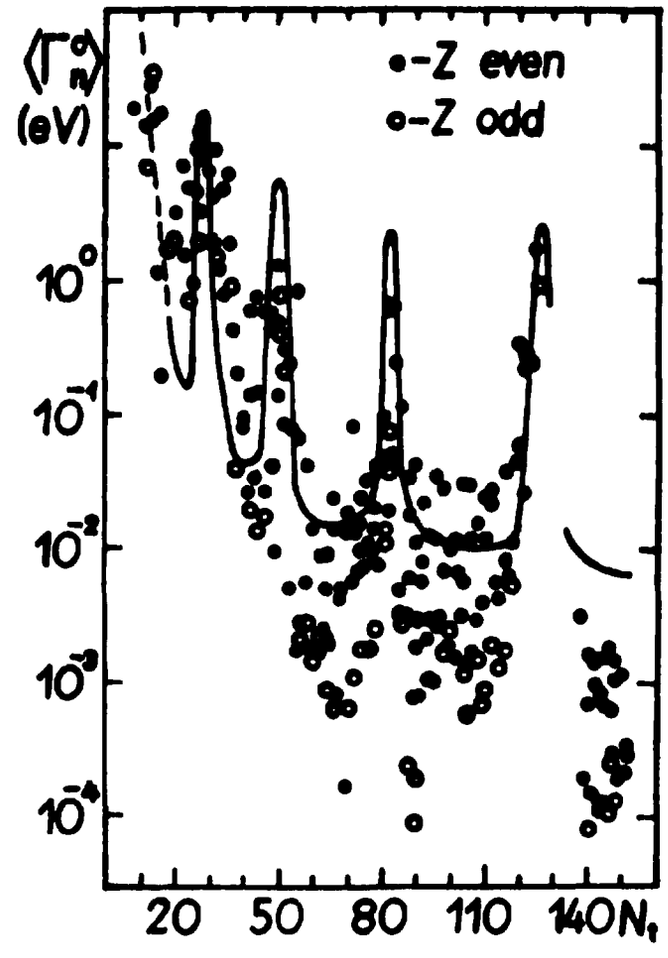

Fig.2. The comparison of experimental reduced neutron widths (points) and calculated ones (line) for K = 1000 MeV^2.

QUASIPARTICLE-PHONON COUPLING IN INELASTIC PROTON SCATTERING

B. Weißbach, TU Dresden, Sektion Physik, WB Theoretische Physik,
DDR 8027 Dresden, Mommsenstraße 13

A b s t r a c t: Multistep-processes in inelastic proton scattering from ^{89}Y are analyzed by using CCBA and DWBA based on a quasiparticle phonon nuclear structure model. Indirect excitations caused by quasiparticle phonon coupling effects are found to be very important for the transition strengths and the shape of angular distributions. Core excitations are dominant for the higher order steps of the reaction.

1. Introduction

The analysis of inelastic proton scattering from odd-even nuclei in the mass region of A 90 with a closed single neutron shell (N=50) shows, that it is necessary for a better understanding of the experimental data to overcome the weak-coupling assumptions (see for example refs. 1), 2), 3)). It seems, that such reactions are characterized by an interplay between phonon and quasiparticle (qp) modes of excitation and cannot be understand by consideration of only one of both different types of degrees of freedom. The more complicated structure of target states in the theoretical description then should be connected with a more complex excitation mechanism similar to the case of transfer reactions leading to final states which don't couple to the ground state of the target nucleus.

2. Quasiparticle-phonon coupling in $^{89}Y(p,p')$

For studying the qp-phonon coupling effects we have analyzed the experimental results of $^{89}Y(p,p')$ with E_p=20.2 MeV obtained by Hulstman et al. 1). This nucleus can be understood as an even-even ^{88}Sr core to which a $2p_{1/2}$ proton quasiparticle couples to the $1/2^-$ ground state. The qp-phonon coupling for the excited states is described by the semimicroscopic treatment of odd-even nuclei developed by Soloviev 4).

2.1. The model

Within the qp-phonon model the wave function for a target state with spin I and its projection M becomes:

$$\Psi^{\nu}_{IM} = c^{\nu}_{I}\left\{\alpha^{+}_{IM} + \sum_{ji\lambda} D^{\lambda i}_{j}(I\nu)\left[\alpha^{+}_{jm}\, Q^{+}_{\lambda i\mu}\right]_{IM}\right\} \qquad (1)$$

where α^{+}_{jm} is a quasiparticle creation operator, $Q^{+}_{\lambda i\mu}$ is a phonon creation operator for a phonon with spin λ, projection μ and root number i of the RPA calculation. ν is the number of the target state $|IM\rangle$ according the secular equation for the energy 4). In (1) two and more phonon contributions are neglected and the Pauli principle is not taken fully into account. Such an approach successfully was used for predictions of level densities and electromagnetic transition rates as well as for calculations of neutron strength functions and for analysis of the structure of giant resonances 4). Generally it gives a good description of average properties of nuclei at high excitation energies.
Based on this model we have analyzed ^{89}Y states of spin and parity $3/2^-$, $5/2^-$,

$7/2^-$, $9/2^-$, $5/2^+$, $7/2^+$, $9/2^+$ below 5 MeV excitation energy. In order to build up the wave functions of ^{89}Y, the even-even core ^{88}Sr with phonon excitations of multipolarity and parity 2^+, 3^-, 4^+, 5^- serves as a starting point. The phonons have been calculated within RPA including all single particle states from $1s_{1/2}$ up to $1i_{13/2}$ for protons and neutrons. The strengths of the multipole-multipole forces have been choosen to reproduce the experimental energies for the first (collective) 2^+ and 3^- phonons. The single particle wave functions are calculated for a Wood-Saxon potentials with parameters taken from 5). For the qp-phonon coupling in ^{89}Y we considered the odd quasiparticle to be in the following states: $2p_{1/2}$, $2p_{3/2}$, $1f_{5/2}$, $1f_{7/2}$, $2d_{5/2}$, $1g_{7/2}$, $1g_{9/2}$. Three main types of states are given by the calculations:

i) Nearly pure qp states, for which the first term of (1) dominates.

ii) Weak-coupling multiplets, where the second term of (1) dominates.

iii) States with strong qp-phonon coupling. For these cases multiple scattering should become meaningful for the excitation process. The following example of a $5/2^+$ state calculated at 3.5 MeV excitation energy shows this clearly:

$$|5/2^+\rangle = 0.17\left\{|2d_{5/2}\rangle + 5.5\left[1g_{9/2}+2^+_1\right]_{5/2^+} - 1.8\left[2p_{1/2}+3^-_1\right]_{5/2^+}\right\} \qquad (2)$$

Because the $1/2^-$ ground state of ^{89}Y is in good approximation a pure one-qp-state, it is clear from (2), that the first component can be excited by a $2p_{1/2}$-$2d_{5/2}$ qp-transition directly from the ground state and the third also can be excited directly by an octupole excitation of the ^{88}Sr core. The excitation of the second component of (2) is only possible by two or more steps. So at first a qp-transition $2p_{1/2}$-$1g_{9/2}$ (excitation of a $9/2^+$ one qp-state) followed by a 2^+ quadrupole excitation is a possible way as well as the opposite one. It should be remarked, that in (2) all components which give contributions less than 1% have been neglected.

2.2 To the calculations

The differential cross sections for the isolated levels were calculated within DWBA and CCBA by using the computer code CHUCK 6). For the calculation of the distorted waves in the incoming and exit channels the same optical potential was used as for the DWBA analyze in 1). To avoid readjusting of the optical potential parameters we ommitted the recoupling of inelastic channels to the elastic channel in the CCBA-calculations.

The non-diagonal coupling matrix elements were calculated based on (1) and used as input data for the program CHUCK. For the calculation of the single particle transition matrix elements to which the coupling matrix is decomposed we used a Yukawa interaction with the strength V_0=100 MeV and the Yukawa parameter b=1 fm. The parameters for the Wood-Saxon potential to calculate the single particle wave functions were the same as for the structure calculations.

2.3. Results

The results of the analysis of excitations of states of the first and second type discussed above may be characterized as follows:

i) The differential cross section for the excitation of the $9/2^+$ (0.908 MeV) one-qp-state is well reproduced by the DWBA-calculations. For the $3/2^-$ (1.507 MeV) and $5/2^-$ (1.74 MeV) states a pure qp-excitation gives transition strengths

which represent only 2.5% resp. 1% of the observed strengths. This fact reflects a stronger qp-phonon coupling than it is included in the model.

ii) The stronger spreading than expected in the weak-coupling theory of the collective octupole is well reproduced. Transition strengths and angular distributions for the observed $5/2^+$ (2.22 MeV), $7/2^+$ (2.53 MeV) and $5/2^+$ (2.86 MeV) are in good agreement with the experiment.

iii) The observed L=4 transitions between 4 MeV and 5 MeV excitation energy are understandable as excitations of noncollective 4^+ phonons which couple to the $2p_{1/2}$ odd quasiparticle. The transition strengths of the resulting $7/2^-$ states is slightly overestimated compared to $^{88}Sr(p,p')$ results while for the two $9/2^-$ states both agree.

iv) Also some L=3 transitions detected at excitation energies greater than 4 MeV and L=5 transitions below 4 MeV are well described by noncollective 3^- and 5^- excitations of the core.

v) The multiplets given by the coupling of 2^+ phonons to the odd $2p_{1/2}$ quasiparticle give transition strengths much larger than observed in the experiment. The observed so called experimental L=2 transitions 1) for higher lying states can be explained by the excitation of the $2d_{5/2}$-$1g_{9/2}$ neutron particle - hole configuration.

For excitation of states of the third type discussed above it was found, that interference effects between qp and phonon contribution to the coupling matrix (for example the contributions which follow from the first and third term of (2)) have essential influence to both the transition strengths and the shape of angular distributions.

In the following some typical effects caused by multistep-processes due to wave function components which do not couple to the ground state will be discussed. The structure calculation gives a $5/2^-$ state with the following important components:

$$|5/2^-\rangle = 0.25\left\{|1f_{5/2}\rangle + 3.9\left[1f_{5/2}+2_1^+\right]_{5/2^-} - 0.69\left[2p_{3/2}+2_1^+\right]_{5/2^-}\right\} \qquad (3)$$

Only the one-qp component can be excited from the ground state. The excitation of the other components generally is possible by the intermediate excitation of $5/2^-$ and $3/2^-$ one-qp states and weak-coupling similar states connected with the 2_1^+ phonon. Including these one can see from fig. 1, that the transition strength is enhanced significantly as well as the shape of the angular distribution is influenced. As the calculations show, the main effect arises from coupling due to the 2^+ excitation in the higher order step of the reaction. As one can see from fig. 1, the differential cross section of the CCBA-calculation gives a reasonable explanation of the observed angular distribution for the 3.513 MeV (L=2) transition.

A similar example of indirect excitation mechanism one has for the case

$$|3/2^-\rangle = 0.19\left\{|2p_{3/2}\rangle + 4.4\left[1f_{5/2}+2_1^+\right]_{3/2^-} + 2.7\left[2p_{3/2}+2_1^+\right]_{3/2^-}\right\} \qquad (4)$$

The results of DWBA- and CCBA-calculations for this state are shown in fig. 1 too. In opposite to the state (3) here the ratio between cross sections of the first and second maximum increases, though the coupling mechanisms are the same. The reason for this may be seen in that fact, that the phase relations between direct and indirect contributions in both cases are different. As in fig. 1 is shown, we have identified this state with the observed 3.068 MeV

(L=2) transition. The slight discrepancies of experimental and theoretical angular distributions can be explained with the too small $2p_{3/2}$ one-qp-strength in (4). The strong influence of channel couplings due to 2^+ phonons is also demonstrated in fig. 2 for the case of a $9/2^+$ state with the following structure

$$|9/2^+\rangle = 0.27\Big\{|1g_{9/2}\rangle + 0.43\left[2p_{1/2}+5^-_2\right]_{9/2^+} - 3.5\left[1g_{9/2}+2^+_1\right]_{9/2^+} - 0.48\left[2p_{1/2}+5^-_1\right]_{9/2^+}\Big\} \qquad (5)$$

As it can be seen, a state of this structure gives an appropriate description of the experimental observed angular distribution and transition strength of the L=5 transition detected at 2.565 MeV excitation energy. It is remarkable, that the channel coupling effect is here the same as one gets by inclusion of core polarization into DWBA-calculations 2).

Further fig. 2 demonstrates the influence of multistep-processes due to non-collective phonon excitations for the example of the following $5/2^+$ state:

$$|5/2^+\rangle = 0.45\Big\{|2d_{5/2}\rangle + 1.7\left[1g_{9/2}+2^+_5\right]_{5/2^+} + 0.57\left[2p_{1/2}+3^-_3\right]_{5/2^+} + 0.51\left[1g_{9/2}+4^+_1\right]_{5/2^+} - 0.39\left[1g_{9/2}+2^+_1\right]_{5/2^+} - 0.29\left[2p_{1/2}+3^-_1\right]_{5/2^+}\Big\} \qquad (6)$$

How it can be seen from fig. 2, the contribution of indirect excitation to the transition strength is important, but no influence to the shape of the angular distribution can be seen. Here direct and indirect contributions have the same phases. In such cases, where the phases are opposite, the influence of channel coupling is much smaller (see f.e. the third example in fig. 2).

3. Conclusions

The analysis show, that the qp-phonon coupling gives some progress in the theoretical interpretation of the inelastic proton scattering experiments from odd-even nuclei. Multistep-processes caused by qp-phonon coupling become meaningful for the reproduction of measured transition strengths as well as for the explanation of the shape of angular distributions, in particular for weakly excited states. Higher order excitations are mainly caused by phonon excitations of the core after excitation of one-qp components. The phase relations between direct and indirect contributions to the transitions have important influence to the results. Especially in the case of qp-quadrupole coupling the model failes in the prediction of one-qp strengths and the distribution of the quadrupole strengths. Here some effort can be expected by inclusion of two phonon components and taking into account the Pauli principle exactly.
More detailed the results will be published elsewhere.

References

1) L. Hulstman et al. Nucl. Phys. A251 (1975) 269
2) W. Benenson et al. Phys. Rev. 176 (1968) 1268
3) H.L. Blok et al. Nucl. Phys. A273 (1976) 142
4) V.G. Soloviev Theory of Complex Nuclei, Oxford, Pergamon Press 1976
5) J. Bang et al. Nucl. Phys. A261 (1976) 59
6) P.D. Kunz Univers. of Colorado (1972) unpublished

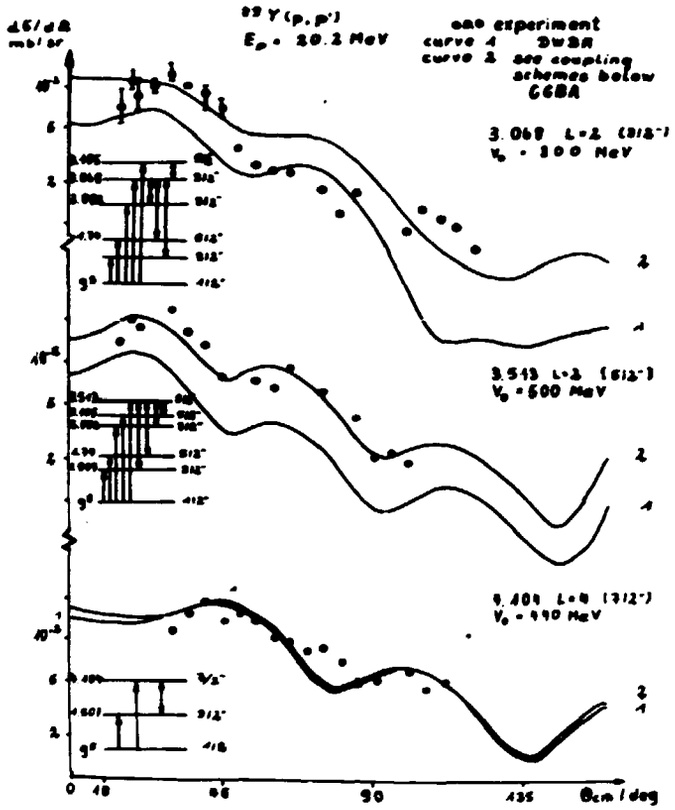

Fig. 1: Comparison between experimental and calculated cross sections for Y(p,p'), Ep=20.2 MeV, 3.513 MeV (b), L=2, and 4.104 MeV, L=4 states

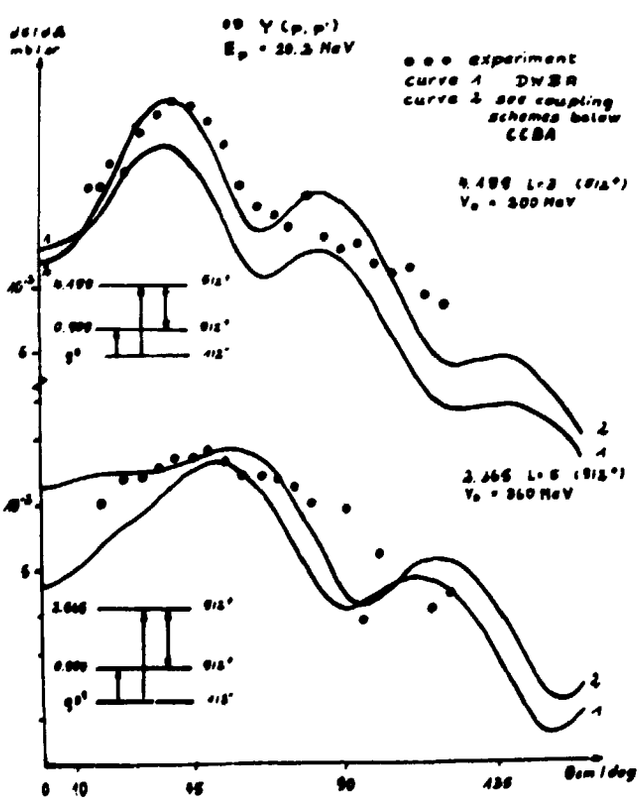

Fig. 2: The same as in Fig.1 for the 4.188 MeV, L=3 (a) and the 2.565 MeV, L=5 states

DIRECT PROCESSES IN (N,2N) - REACTIONS

R. Reif, R. Wolf

Technische Universität Dresden, Sektion Physik
3027 Dresden, DDR

A b s t r a c t: The reaction $^{29}Si(p,p'n)$ has been treated in DWBA neglecting pn-correlations in the outgoing channel. After integrating the reaction angle of the ejected neutron, numerical results have been obtained for the emission spectrum and the angular distribution of outgoing protons.

1. Introduction

A review about recent works in (ppn) reactions /1-3/ allows us to make the following conclusions /1-3/:

1. At incident energies near 40 MeV the direkt knockout mecanism dominates the (ppn) reactions /1-3/ on light nuclei and, although distortion effects are remarkable, the PWIA calculations give a reasonable agreement with experimental results /1/.
2. In the lower incident energy region, near 10 MeV are the inelastic scattering (pp') or the exchange (pn) mecanism lead to an excited nucleus (target) which then decais by a neutron or, respektively, proton boiloff the most favoured process /3/.
3. In the medium energy region both processes are in competition. There is a strong distortion from the final state interaction of the nucleons with the nucleus /2,3/.
4. The (pd) reaction is also in competition with the processes discussed above. But the (pd) reaction emphasizes the high momentum components of the wave function of the target nucleus /4/ and is not relevant here.

Our aim is to look for the yield of the direct knockout mecanism in the region of strong distortion . Our approach is based on the following simple picture:

A DWBA calculation allows for a reasonable description of precompound effects in the differential cross section of inelastic nucleon - nucleus scattering processes at medium incident energies /5/, in particular, if one includes second order effects /6/. In such an approach the total strength for a one-step transition with given energy loss and angular momentum transfer is composed incoherently out of single particle excitations with the excited nucleon occupying bound single particle states in the shell model potential of

the target. On the same basis, the contribution of direct processes to the angular correlation, angular distribution and emission spectra of (N,2N)-reactions can be calculated by assuming that a single interaction between the incoming nucleon and an active nucleon of the target is promoting the latter to a final state in the continuous part of the single particle spectrum.

2. Transition amplitude

In order to simplify the calculations the targets ground state is assumed to consist of a single neutron in a s-state $\varphi_s(r_n)$ bound to an inert core. The incoming proton with momentum interacts with the neutron via a central Yukawa interaction

$$V_{np} = V_0 \frac{e^{-\mu r_{np}}}{\mu r_{np}} \tag{1}$$

creating a final state, which is taken as a product of two continuum wave functions $\chi_{\vec{k}_{p'}}$ and $\chi_{\vec{k}_n}$ for the outgoing proton and the ejected neutron, respectively ($E_p = E_{p'} + E_n + B_n$; B_n: binding energy of the neutron). Here, it has been assumed, that the np interaction in the final channel is small compared to the mean potential , so that the formation of deuteron as an intermadiate state can be neglected. The transition matrix element in DWBA is given by

$$T(\vec{k}_p \to \vec{k}_{p'}, \vec{k}_n) = \langle \chi^{(-)}_{\vec{k}_{p'}} | C\, \chi^{(-)}_{\vec{k}_n} | V_{np} | \varphi_s(n) \rangle | \chi^{(+)}_{\vec{k}_p} \rangle \tag{2}$$

After a multipole expansion of the effective interaction

$$V_{np} = \sum_{\lambda,\mu} g_\lambda(r_{np})\, Y_\lambda^{\mu}(\hat{r}_p)\, Y_\lambda^{\mu *}(r_n) \tag{3}$$

and a partial wave decomposition of the scattering state the inner matrix element can be expressed by radial integrals

$$I_{\ell'}(r_p) = \int dr_n\, W_{\ell'}(r_n)\, g_{\ell'}(r_{np})\, u_0(r_n) \tag{4}$$

where $W_{\ell'}$ denotes the radial part of the continuum wave function of the neutron. The angular momentum transferred in the two-body interaction coincides with the angular momentum ℓ' trans- of the ejected neutron. In eq. (4), no problems with convergence appear becaus e of the exponential decay of the bound state wave function u_0 for $r \to \infty$. If the neutron is not observed in

the experiment, the differential cross section proportional to $|T|^2$ can be integrated over the direction of the emitted neutron. Consequently, the interferrence terms between the different transferred angular momenta disappear, and the total transition strength for a given inelasticity of the proton is a sum of partial cross section for transitions , in which the excited neutron occupies different partial waves in the continuum.

5. Numerical results

The emission spectrum and the angular distribution of protons have been calculated according to eq. (2) for the reaction $^{29}Si(p,pn)^{28}Si$ at an incident energy E_p = 30 MeV. The distorted waves $\chi_{\vec{k}_p}, \chi_{\vec{k}_{p'}}$ have been calculated in optical potentials with parameters taken from ref. /7/. The neutron radial wave functions u_ℓ, w_ℓ, were computed in the same real Woods saxon potential given in ref. /8/. Standard parameters V_0=100 MeV, μ = 1 fm^{-1} have been used in the effective interactions v_{np}, eq. (1). Partial waves up to ℓ' = 6 have been taken into account.

Because of the node in the $2s_{1/2}$ wave function u_0 , the reaction is not completely localized in the surface region. For a given value of ℓ' , the magnituce of the main peak in the transition formfactor varies strongly with the energy because of the single particle resonance structure of the continuum. So, the partial cross sections exhibit a rather pronounced resonance behaviour with e.g. a width of several MeV and a distance of about 10 MeV for the s- and p-waves (see fig. 1).

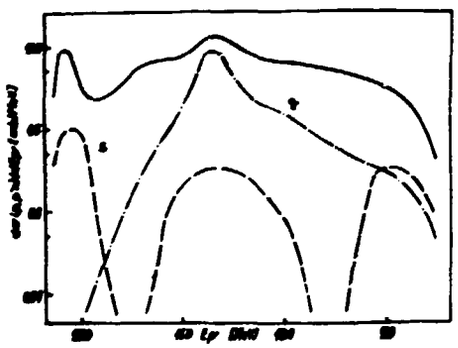

Fig. 1. Cross section of $^{29}Si(p,pn)$ E_p=30 MeV

The partial cross section decreases by several orders of magnitude if the neutron emission energy takes a value in between single particle resonances. This result supports the projection method proposed in ref. /9/. The spectrum summed over ℓ' showes a structure for $E_{p'}$ $\approx$ 20 MeV and $E_{p'}$ $\approx$ 14 MeV, which reflects the

appearance of s- and p-resonances and s- and g-resonances, respectively. The cross section of about 10mb/MeV is in good agreement with the results obtained by Yezhov and Plyuyko /10/ in similar calculation for the reaction $^{59}Co(n,2n)$, E_n = 16 MeV.

4. Conclusions

One can conclude, that an appreciable amount ($\approx$ 15%) of the cross section of (N, 2N) reactions at a medium level of incident energies result from a first-order knock-out mechanism. The DWBA can be used to estimate the influence of the (N, 2N) channel on the angular distribution of precompound processes above the threshold.

References

1. C.N. Waddell et al., Nucl. Phys. A 281 (1977) 418
2. H. Jeremie et al., Nucl. Phys. A 312 (1978) 43
3. L. Shabuson et al., . Phys. Rev. C 15 (1977) 260
4. C. A. Miller, Ph. D. Thesis, Univ. of Monitoba (1974) unpublished
5. R. Reif, Acta Phys. slov. 25 (1975) 208
. E. Arndt and R. Reif, TU-Information 05-32-76
6. T. Tamura et.al., Phys. Lett. 66 B (1977) 109
7. F. D. Becchetti and G. W. Greenless, Phys. Rev. 182 (1969) 1190
8. A. Bohr and B. R. Mottelson, Nuclear structure, N.Y. (1969)
9. H. V. Geraab and O. Nordland, Proc. Int. Conf. Nucl. Reaction Mechenisms, Varenna (1977) 299
10. S.N. Yezhov and V. A. Plyuyko, Jad. Fiz. 28 (1978) 83

КИНЕТИЧЕСКИЕ ЭНЕРГИИ ОСКОЛКОВ ДЕЛЕНИЯ ЯДЕР БЫСТРЫМИ НЕЙТРОНАМИ

Н.П. Дьяченко, Б.Д. Кузьминов, В.Ф. Митрофанов, А.И. Сергачев
Физико-энергетический институт, Обнинск, СССР

Аннотация

Выполнены измерения кинетической энергии осколков при делении ядер ^{232}Th и ^{236}U нейтронами в области энергий от порога до 5,5 Мэв. На основе полученных результатов и с привлечением экспериментальных данных для других ядер обсуждается природа локальных вариаций средних кинетических энергий осколков ($\bar{E}_K$) вблизи барьера деления. Построена систематика $\bar{E}_K$ в координатах Z и A делящихся ядер. Рассмотрена возможность извлечения сведений о диссипативных свойствах коллективного движения ядра к точке разрыва из экспериментальных данных о кинетических энергиях осколков деления.

Введение

Осколки, как конечный продукт сложного коллективного движения ядра, несут информацию о свойствах этого движения. В частности, кинетическая энергия осколков складывается из нескольких компонент, характеризующих коллективные движения ядра на разных этапах процесса деления. По величине вклада этих компонент можно судить, в какой степени энергия коллективных движений делящегося ядра диссипирует в энергию возбуждения. В связи с этим возникает задача по определению величин отдельных компонент, составляющих кинетическую энергию осколков деления ядер.

К сожалению, в прямом опыте измерить отдельные компоненты не представляется возможным. Однако, используя модельные представления о зависимости их величин от энергии возбуждения, массового числа и заряда делящихся ядер, от способа разделения нуклонов между осколками, можно надеяться оценить величину отдельных компонент. Например, существование локальных вариаций средних кинетических энергий осколков при делении ядер вблизи барьера принято связывать с влиянием коллективных переходных состояний, а изменения $\bar{E}_K$ в широком диапазоне энергий возбуждения - с проявлением диссипации при спуске ядра с барьера.

В настоящей работе отмеченные выше проблемы обсуждаются на основе новых экспериментальных данных о делении ядер ^{232}Th и ^{236}U нейтронами с привлечением результатов измерений кинетических энергий осколков для других ядер.

Метод измерений

Метод измерений кинетических энергий парных осколков при делении ядер быстрыми нейтронами был достаточно подробно изложен в работе [I]. Отметим лишь некоторые специфические моменты.

Калибровка энергетической шкалы осуществлялась с использованием констант, предложенных в работе [2] для случая деления ядер ^{235}U тепловыми нейтронами. Различие потерь энергии осколками в слоях и подложках ^{235}U и ^{232}Th определялось при делении ядер ^{232}Th нейтронами с энергией I,9 Мэв и ядер ^{235}U тепловыми нейтронами. При этом для осколков деления ядер тория принималось значение $\bar{E}_K$ = 162,79 Мэв [3]. Для использованной геометрии измерений (диаметр слоя 2 см,

рабочий диаметр детекторов - 2 см, расстояние между детекторами - 2 см) и при средней потере энергии парными осколками в подложке, делящемся слое и нечувствительном поверхностом слое полупроводникового детектора - 5 Мэв, поправка на различие угловых распределений осколков деления ядер ^{232}Th не превышала 150 кэв во всём исследованном диапазоне энергий нейтронов (1,4 - 5,6 Мэв). Поскольку в литературе появились новые данные об угловых распределениях осколков при делении ядер ^{232}Th нейтронами [4], были пересмотрены соответствующие поправки, внесённые в результаты измерений работы [5]. Исправленные значения $\bar{E}_K$ приведены в таблице I совместно с результатами, полученными в настоящей работе. В тех случаях, когда энергия нейтронов совпадала, приведены средние значения результатов измерений настоящей работы и работы [5].

Таблица I

Средние кинетические энергии осколков при делении ядер ^{232}Th нейтронами

E_n (Мэв)	$\bar{E}_K$ (Мэв)	E_n (Мэв)	$\bar{E}_K$ (Мэв)
1,32	162,10 ± 0,10	1,96	162,92 ± 0,10
1,37	161,95 ± 0,13	2,04	162,54 ± 0,10
1,42	162,52 ± 0,10	2,14	162,39 ± 0,10
1,47	162,46 ± 0,10	2,18	162,50 ± 0,13
1,52	162,50 ± 0,10	2,24	162,96 ± 0,10
1,58	162,53 ± 0,10	2,45	163,45 ± 0,10
1,60	162,70 ± 0,10	2,59	163,75 ± 0,13
1,65	162,90 ± 0,10	2,74	163,47 ± 0,15
1,70	162,93 ± 0,10	3,14	163,77 ± 0,15
1,76	162,90 ± 0,10	3,54	164,19 ± 0,14
1,86	162,78 ± 0,10	5,76	164,49 ± 0,18
1,90	162,79 ± 0,10		

Абсолютное значение средней кинетической энергии осколков при делении ядер ^{236}U нейтронами определялось для E_n = 1,14 Мэв относительно средней кинетической энергии осколков при делении ядер ^{235}U тепловыми нейтронами. Чтобы избежать неопределенностей, связанных с различием толщин слоев и подложек, измерения проводились на одной и той же мишени урана, содержащей примерно, 90 % изотопа ^{236}U и 10 % изотопа ^{235}U. Толщина слоя составляла 50 мкг.см^{2}. В результате измерений получено $\bar{E}_K$ = 172,5 ± 0,1 Мэв при E_n = 1,14 Мэв с учетом поправки на испускание мгновенных нейтронов деления. Все другие измерения на быстрых нейтронах проводились с моноизотопным ^{236}U. Поправки на различие потерь энергии осколками, обусловленное различием их угловых распределений, не превышали 200 кэв во всем изученном диапазоне энергий нейтронов (0,5 - 5,6 Мэв). Эти расчёты подтвердились экспериментальным сравнением потерь энергии осколками в подложке слоя для случаев деления ^{236}U нейтронами с энергиями 0,94 Мэв (угловое распределение осколков вытянуто по 90^{0}) и 1,14 Мэв (угловое распределение вытянуто вперёд). Разница потерь энергии в подложке не превышала ошибок измерений (100 кэв) при полной потере 2 Мэв. Результаты измерений средней кинетической энергии осколков при делении ядер ^{236}U нейтронами приведены в таблице II.

Таблица II

Средние кинетические энергии осколков при делении ядер ^{236}U нейтронами

E_n (Мэв)	$\bar{E}_K$ (Мэв)	E_n (Мэв)	$\bar{E}_K$ (Мэв)
0,61	1,7234 ± 0,20	2,54	172,20 ± 0,10
0,02	172,63 ± 0,10	2,75	172,04 ± 0,10
0,07	172,09 ± 0,12	2,96	172,06 ± 0,10
0,11	172,00 ± 0,10	3,16	172,14 ± 0,10
0,02	172,18 ± 0,10	3,34	172,20 ± 0,10
1,14	172,53 ± 0,10	3,54	171,95 ± 0,10
1,35	172,58 ± 0,10	3,60	172,00 ± 0,10
1,55	172,44 ± 0,10	3,98	172,02 ± 0,10
1,75	172,38 ± 0,10	4,46	171,84 ± 0,10
1,95	172,44 ± 0,10	4,80	171,79 ± 0,10
2,16	172,18 ± 0,10	5,12	171,90 ± 0,10
2,36	172,21 ± 0,10		

Обсуждение результатов измерений

На рисунках 1 и 2 показаны зависимости кинетических энергий осколков ($\bar{E}_K$) от энергии нейтронов, вызывающих деления ядер ^{232}Th и ядер изотопов урана. Вблизи барьера деления величины $\bar{E}_K$ претерпевают небольшие изменения, близкие по порядку величины к энергиям коллективных переходных состояний. Тот факт, что эти изменения $\bar{E}_K$ локализуются в той же области энергий возбуждения где происходят изменения угловых распределений осколков, стимулирует поиски общих причин, вызывающих эти изменения. В работах [6 - 9] в разных вариантах предлагалось величину изменения кинетической энергии осколков связать с энергией коллективных переходных состояний. Однако, недостаток сведений о структуре переходных состояний для исследовавшихся делящихся ядер ^{233}Th и ^{237}U затрудняет оценку справедливости этих концепций.

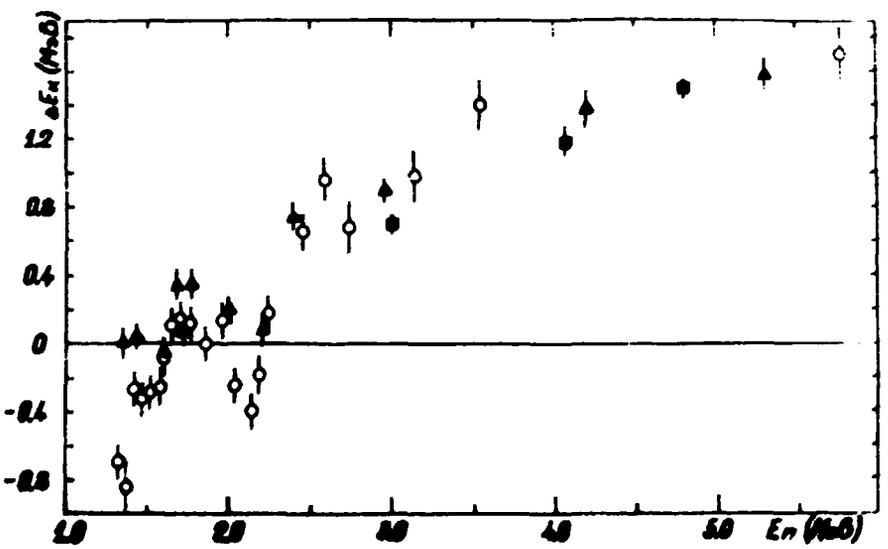

Рис. I Зависимость средней кинетической энергии осколков от энергии нейтронов, вызывающих деления ядер тория-232. В качестве опорного принято значение $\bar{E}_K$ при E_n = 1,9 Мэв. (▲ - 9, ■ - 13, ○ - настоящая работа).

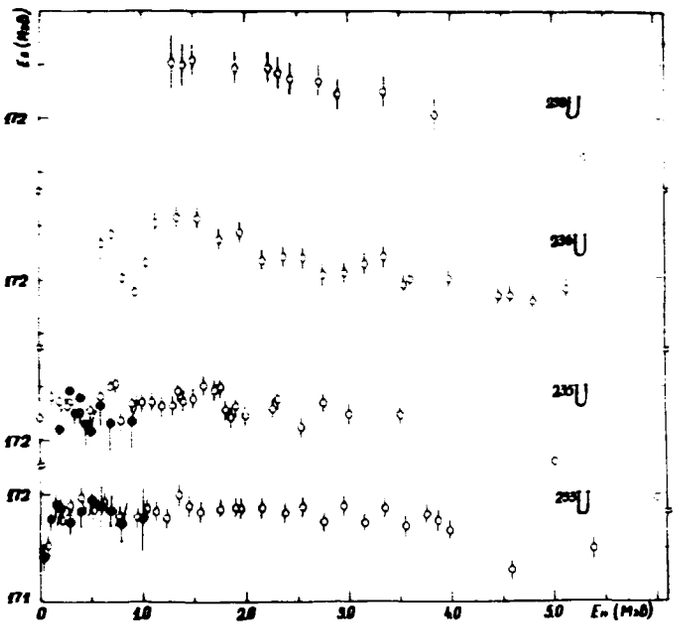

Рис. 2 Зависимость средней кинетической энергии осколков от энергии нейтронов при делении ядер изотопов урана [3]. Данные для урана-236 - результаты настоящей работы.

Существуют и другие аргументы, заставляющие проявлять осторожность по отношению к модельным концепциям [6 - 9]. В частности из них вытекает, что изменения средних кинетических энергий осколков по мере роста энергии нейтронов отражают изменения вклада в сечение деления различных коллективных состояний. Так как индивидуальным каналам деления соответствуют разные угловые распределения осколков, то следует ожидать и угловой зависимости $\bar{E}_K$. В работах [10 - 12] выполнены измерения средних кинетических энергий осколков, разлетающихся под углами 0^0 и 90^0 к направлению движения нейтронов, вызывающих деления ядер ^{232}Th, ^{235}U, ^{238}U. Результаты измерений приведены в таблице 3.

Таблица III

Угловая зависимость средней кинетической энергии осколков

Ядро-мишень	E_n (Мэв)	$\bar{E}_K$ (Мэв)		Работа
		0^0	90^0	
^{232}Th	1,55	160,6 ± 0,15	160,6 ± 0,15	[12]
	1,70	161,0 ± 0,2	161,2 ± 0,2	[12]
	3,0	161,45 ± 0,1	161,55 ± 0,1	[12]
^{235}U	0,12	170,0 ± 0,4	170,5 ± 0,4	[10]
	0,5	169,9 ± 0,4	170,3 ± 0,4	[10]
	3,0	170,08 ± 0,10	170,16 ± 0,10	[11]
^{238}U	1,5	170,2 ± 1,0	170,8 ± 1,0	[10]
	1,6	170,47 ± 0,15	170,64 ± 0,15	[11]

Различия средних кинетических энергий осколков, превышающие ошибки измерений не наблюдались. Возможно, что в работах [10 - 12] неудачно выбрана энергия нейтронов или недостаточна точность измерений или деление протекает только по одному каналу, но по-крайней мере, необходимы дополнительные исследование зависимости $\bar{E}_K$ от Θ, чтобы роль переходных состояний в изменениях $\bar{E}_K$ стала более ясной. Уменьшение кинетической энергии осколков при делении ядер ^{232}Th нейтронами с энергией 2,14 Мэв следует рассматривать как переход к делению через низко

лежащий коллективный канал или как появление при этой энергии одночастичного состояния. По мере роста энергии возбуждения роль одночастичных переходных состояний должна возрастать, а добавка к средней кинетической энергии осколков, обусловленная делением через коллективные состояния, должна уменьшаться. В случае деления ядер ^{232}Th нейтронами рост кинетической энергии осколков продолжается по-крайней мере до E_n = 5,6 Мэв.

Предположение о сохранении энергии коллективных движений, установившихся в седловой точке, вплоть до момента разрыва ядра может не выполняться, поскольку при движении ядра от седловой точки к точке разрыва меняются как деформация ядра, как и его структурные свойства, и энергия коллективных движений может диссипировать в тепло.

Другая составляющая кинетической энергии осколков деления, которая обусловлена спуском ядра с седловой точки - трансляционная кинетическая энергия - также зависит от диссипативных свойств ядерной системы при спуске с барьера. При малой энергии возбуждения делящихся ядер энергия коллективного движения к точке разрыва не диссипирует в энергию возбуждения. Поскольку расстояние между одночастичными уровнями велики. По мере увеличения энергии возбуждения диссипация будет расти, а предразрывная кинетическая энергия - уменьшаться. Такое явление наблюдается при делении изотопов плутония (рис. 3). В меньшей степени это проявляется для изотопов урана и несправедливо при делении ядер ^{232}Th нейтронами. Однако при делении плутониния в рассматриваемой области энергий нейтронов имеет место отчётливая зависимость изменений кинетической энергии парных осколков от массы тяжёлого осколка [I], причем для наиболее асимметричных способов деления с ростом энергии возбуждения происходит увеличение $\bar{E}_K$, что трудно объяснить с точки зрения диссипации.

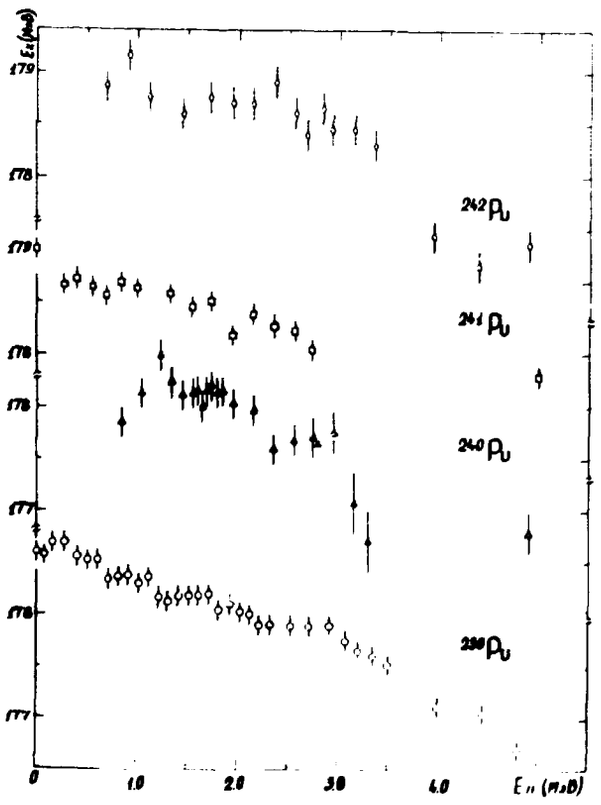

Рис. 3 Зависимость средней кинетической энергии осколков от энергии нейтронов при делении ядер изотопов плутония [3].

В настоящей работе был выполнен анализ зависимостей средних кинетических энергий осколков от порядкового номера (Z) и массового числа (A) делящихся ядер. Относительная точность измерений $\bar{E}_K$ при делении нейтронами ядер в области тория-плутония составляет

около 0,5 Мэв [3], что позволяет достаточно жёстко судить о степени соответствия модельных представлений экспериментальным данным. Спонтанное деление ядер не включено в рассмотрение, так как разница средних кинетических энергий при спонтанном и вынужденном делениях одного и того же ядра может достигать 2 - 3 Мэв [3], а физическая причина такого различия не ясна. Чтобы избежать неопределенностей, связанных с влиянием энергии возбуждения делящихся ядер на кинетические энергии осколков, значения $\bar{E}_к$ выбирались для таких энергий нейтронов, при которых энергия возбуждения достаточно удалена от барьера деления, но не достигла области, где начинается систематическое уменьшение $\bar{E}_к$. Наиболее простая модель предполагает, что подавляющая часть кинетической энергии осколков обусловлена их взаимным кулоновским отталкиванием. Если принять, что заряд ядра делится между осколками пропорционально их массам, то можно написать следующее соотношение:

$$\bar{E}_к = C \frac{Z^2 \bar{M}_н (A - \bar{M}_н)}{A^2 A^{1/3}}$$

где $\bar{M}_н$ - среднее массовое числа тяжёлого осколка, а C - включает формфактор и постоянные коэффициенты. Для определения величины C было принято, что при делении ^{235}U тепловыми нейтронами $\bar{E}_к$ = 172,2 Мэв. На рисунке 4 сравниваются расчетные и экспериментальные значения $\bar{E}_к$. Расчетная зависимость $\bar{E}_к$ от A и Z хорошо совпадает с экспериментальной. В использованную модель фактически заложено предположение о сильном демпинге при спуске с барьера. Однако хорошее совпадение расчётных и экспериментальных результатов вряд ли может быть использовано для обоснования такого принципиального вывода, так как экспериментальный материал характеризует слишком узкую область ядер, для которых изменения Z и A не превышают 5 %. Возможность включения в анализ вынужденного деления более тяжёлых ядер ограничивается отсутствием систематических экспериментальных данных и необходимостью применения более строгих моделей, учитывающих, в частности, изменения форм-фактора C.

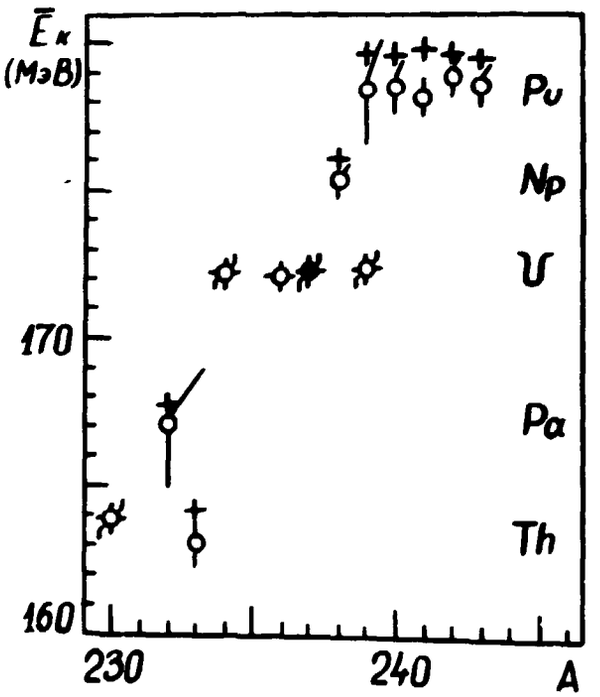

Рис. 4 Систематика средних кинетических энергий в зависимости от Z и A делящегося ядра. (+ - результаты расчета, • - результат измерений настоящей работы, остальные значения взяты из работы [3]).

В заключении следует отметить, что проблема движения ядра к точке разрыва требует дальнейших теоретического и экспериментального исследований. Для ее решения полезны изучение дифференциальных характеристик кинетических энергий осколков деления и распространение исследований на более широкую область ядер.

Литература

[1] Акимов Н.И., Воробьева В.Г., Кабенин В.Н. и др., Я.Ф., 16 (1972) 475.

[2] Schmitt H.W., Kiker W.E., Williams C.W. Phys.Rev., 137 (1965), B 837.

[3] Vorob'eva V.G., Kuzminov B.D., Manokhin V.N., Average Kinetic Energies of Fission Fragments, IAEA, INDC-128/C + Sp, Vienna, 1979.

[4] Caruna J., Boldeman J.W., Walsch R.L., Nucl. Phys., A 285 (1977) 209.

[5] Дьченко Н.П., Кузьминов Б.Д., Митрофонов В.Ф., Сергачев А.И., Я.Ф., 26 (1977) 691.

[6] Андреев В.Н., Тезисы докладов на конференции по физике деления ядер, М., издательство АН СССР, 1961.

[7] Blumkina Yu., Bondarenko I.I., Kuznetsov V. et al. Nucl. Phys., 52 (1964) 648.

[8] Струтинский В.М., Павлинчук В.А., Phys. and Chem. Fission, Vienna 1 (1965) 127.

[9] Caruana J., Boldeman J.W., Walsh R.L., Nucl.Phys., A 285 (1977) 217.

[10] Meadows J.W., Phys.Rev., 177 (1969) 1817.

[11] Воробьёва В.Г., Гентов А.Н., Кузьминов Б.Д., Сергачев А.И., Я.Ф., 10 (1969) 491.

[12] Воробьёва В.Г., Дьяченко Н.П., Кузьминов Б.Д. и др., Я.Ф., 26 (1977) 962.

[13] Holumbarsch W., Preiffer B., Gonnenwein F., Nucl.Phys., A 171 (1971) 631.

ИЗУЧЕНИЕ ЭНЕРГЕТИЧЕСКОГО СПЕКТРА НЕЙТРОНОВ СПОНТАННОГО ДЕЛЕНИЯ ^{252}Cf В ОБЛАСТИ НИЗКИХ ЭНЕРГИЙ +

М.В. Блинов, В.А. Витенко, В.И. Юревич
Радиевый институт им. В.Г. Хлопина, Ленинград, СССР

Аннотация

Методом времени пролета с использованием кристалла $^{6}LiJ(Eu)$ в качестве нейтронного детектора изучалась форма спектра нейтронов спонтанного деления ^{252}Cf в области энергий I кэВ - I МэВ. Особое внимание обращалось на энергетический диапазон ниже 200 кэВ. Полученные данные измерений указывают на возможность описания спектра во всем изучаемом диапазоне энергий однопараметровым Максвелловским распределением с T = I,42 МэВ.
(спектр нейтронов деления, нейтронный стандарт, калифорний-252).

Определение точной формы энергетического спектра нейтронов спотанного деления ^{252}Cf необходимо в связи с тем, что он рекомендо[illegible] МАГАТЭ для использования в качестве стандартного спектра нейтронов деления. Это энергетическое распределение может широко использоваться в различных нейтронно-спектрометрических исследованиях для проведения относительных измерений. Ценность данного стандартного спектра определяется точностью, с которой он известен, однако задача прецизионного его измерения является довольно сложной. Частично это связано с тем, что изучаемый спектр занимает очень широкий энергетический интервал. В настоящее время в области энергий от 0,5 до 8 МэВ результаты нескольких работ удовлетворительно согласуются между собой, хотя требуется дальнейшее существенное уточнение данных [I, 2]. В области энергий ниже 0,5 МэВ положение остается неудовлетворительным, так как разброс данных различных работ превышает 30 - 50 %, [3 - 6], что совершенно неприемлемо для стандарта. Измерения в области низких энергий представляет особые трудности, которые прежде всего связаны с влиянием рассеяния нейтронов более высоких энергий и ухудшением фоновых условий эксперимента.

В настоящей работе представлены результаты измерений спектра нейтронов спонтанного деления ^{252}Cf в области энергий от I кэВ до I МэВ. Наиболее детально изучалась область энергий ниже 200 кэВ. Для повышения точности измерений влияние нейтронов, рассеянных детекторами спектрометра и окружающей средой, определялось, как экспериментальным, так и расчетным путем. В работе был существенно уменьшен фон случайных совпадений.

Энергия нейтронов измерялась методом времени пролета. Нейтроны регистрировались кристаллом $^{6}LiJ(Eu)$ диаметром I7 мм, толщиной 2 или 4 мм. Детектором осколков служил газовой сцинтилляционный счетчик, приклеенный непосредственно к миниатюрному фотоумножителю ФЭУ-7I. Слой калифорния наносился вакуумным распылением на дно газового счетчика. Использовались два слоя калифорния ($I \cdot IO^5$ дел/с и $2 \cdot IO^4$ дел/с). Электр[illegible] часть спектрометра подверглась существенным изменениям по сравнению с п[illegible]дущей работой [5]. Так, например, был использован время-амплитудный анализ импульсов нейтронного детектора, который привел к сущест-

+ Работа проводится при поддержке Международного Агентства по атомной энергии (исследовательский контракт № 2048/RB).

венному уменьшению фона случайных совпадений. Путем амплитудной селекции в быстром канале регистрации осколков деления исключалась фон, связанный с появлением двух актов деления в измеряемом интервале времени. Эти усовершенствования позволили проводить измерения с интенсивными источниками калифорния на малых базах в области низких энергий. Поскольку для уменьшения влияния рассеяния от фотоумножителя мы вынуждены использовать детекторы нейтронов с кристаллами малых размеров, эффективность регистрации нейтронов низка. Это приводило к существенному увеличению необходимого времени измерений и, следовательно, к высоким требованиям к стабильности работы спектрометра. Одна серия измерений с соответствующими контрольными опытами занимала от одного до двух месяцев круглосуточной работы установки.

Измерения производились на нескольких пролетных расстояниях (62,5, I25, 250 и 500 мм) для сравнения результатов, полученных в различных условиях и повышения статистической точности измерений.

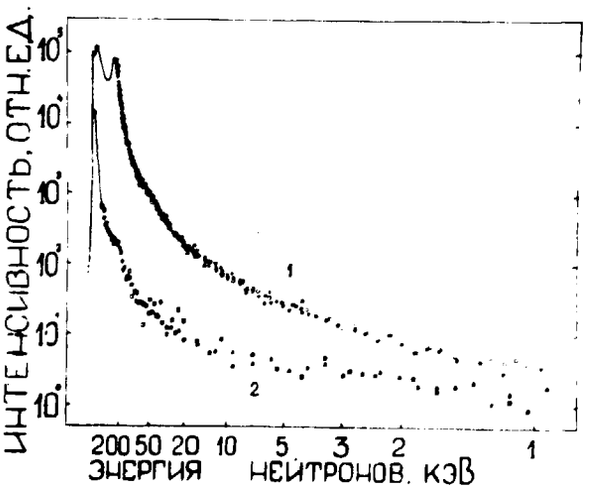

Рис. I Аппаратурные нейтронные спектры (показана область низких энергий), полученные с помощью кристаллов,
I - кристалл $^6LiJ(Eu)$ (Δ,∇ - данные различных серий измерений для пролетной базы I25 мм, ●,○,+ - данные для базы 62,5 мм),
2 - кристалл $^7LiJ(Eu)$ (□ - данные для пролетной базы I25 мм, ■,▲ - данные для базы 62,5 мм).

На рис. I показаны экспериментальные спектры по времени пролета. Для иллюстрации вклада от реакций на ядрах иода здесь же приведены спектры, полученные с помощью кристалла $^7LiJ(Eu)$ аналогичного по своим характеристикам рабочему кристаллу. Временное разрешение, оцененное по ширине гамма-пика на полувысоте, равно I,5 нс. Фон случайных совпадений составлял при энергии I0 кэВ I0 % от эффекта. Для сравнения можно привести данные о фоне из работы [3], который был равен 300 % для этой же энергии.

В наших предыдущих работах [5, 7] мы стремились к уменьшению массы детекторов и создали весьма миниатюрные счетчики по сравнению с обычно используемыми аналогичными детекторами в других работах [3, 4]. В данной работе детекторы нейтронов и осколков остались теми же. Однако, мы считали необходимым определить влияние рассеяния от них более точно и в более широком диапазоне энергий, чем делали ранее. Экспериментальная оценка влияния рассеяния на газовом счетчике производилась путем удвоения его массы с примерным сохранением геометрического расположения. Оценить вклад рассеяния от нейтронного детектора было труднее, так как сохранить геометрию при удвоенной массе весьма сложно из-за непосредственной близости кристалла к фотоумножителю. Поэтому были выполнены как измере-

ния, так и расчеты для оценки вклада нейтронов, рассеянных от фотоумножителя. Полученные таким образом поправки хорошо коррелировали между собой. Многократное рассеяние в кристалле и его упаковке приводит как к изменению эффективности регистрации нейтронов данной энергии, так и временному сдвигу момента регистрации. Для коррекции этих искажений В.Н. Душиным была составлена программа, которая решает уравнение переноса нейтронов в геометрических условиях детектора методом Монте-Карло [10]. Использовалось 40 групповое приближение. Для нейтронов каждой группы вычислялся временной отклик сцинтиллятора, который затем использовался для вычисления поправочной функции. При анализе возможных источников рассеяния нейтронов, мы пришли к выводу, что воздух также может вносить заметный вклад. Расчеты показали, что этот эффект существенно зависит от измеряемого интервала энергии и пролетной базы (например, для базы 6,25 см поправка равна 7 % при энергии 10 кэВ).

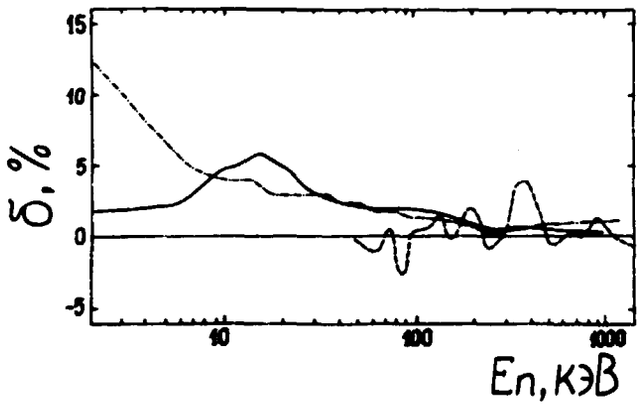

Рис. 2 Энергетическая зависимость поправок на многократное рассеяние нейтронов, в кристалле для базы 250 мм, расчет (- - -), в фотоумножителе нейтронного детектора для базы 62,5 мм, расчет (———) и на взаимодействие нейтронов с ядрами иода в кристалле для базы 62,5 мм, эксперимент (- - -).

На рис. 2 показаны энергетические зависимости некоторых поправок на рассеяние и на взаимодействие нейтронов с ядрами иода. Величина суммарной поправки в области энергий I - 10 кэВ достигает десятых долей от эффекта. Естественно, что неучет этого явления приводит к существенному завышению интенсивности в этой области.

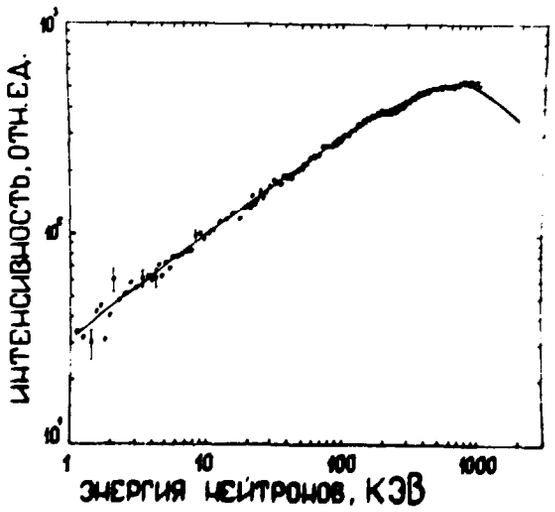

Рис. 3 Спектр нейтронов спонтанного деления ^{252}Cf, полученный в данной работе (•). Сплошная линия - Максвелловское распределение (T = I,42 МэВ). Данные нормированы в области энергий 0,4 - 0,8 МэВ. Указанные ошибки - статистические.

На рис. 3 представлен спектр нейтронов спонтанного деления ^{252}Cf в области энергий I кэВ - I МэВ, полученный в данной работе с учетом всех поправок, При вычислении эффективности использовались значения сечения реакции $^{6}Li(n,\alpha)$ из файла $ENDF/B\text{-}V$ которые хорошо согласуются с последними экспериментальными данными [8, 9]. На рис. 3 сплошной линией показано Максвелловское распределение с T = I,42 МэВ. Экспериментальные точки располагаются достаточно близко от этой кривой во всем измеряемом диапазоне. Разброс точек в основном находится в пределах указанных статистических ошибок. Небольшое (~5 %) систематическое отклонение точек вблизи энергии 250 кэВ по-видимому обусловлено погрешностью использованных значений сечения реакции $^{6}Li(n,\alpha)$. Таким образом, спектр нейтронов деления ^{252}Cf в области энергий I кэВ - I МэВ может быть аппроксимирован однопараметровым Максвелловским распределением.

Литература

[I] Smith, A.B., Prompt Fission Neutron Spectra (Proc. Cons. Meeting) IAEA, Vienna (1972), 3.

[2] Stewart, L., Eisenhauer, C., Neutron Standards and Applications (Proc. Symposium) NBS Special Publication 493 (1977), 198.

[3] Meadows, J.W., Phys. Rev. 157 (1967) 1076.

[4] Jeki, L., Kluge, Gy., Lajtai, A., Djachenko, P.P., Kusminov, V.D., Prompt Fission Neutron Spectra (Proc. Meeting) IAEA, Vienna (1972), 81.

[5] Blinov, M.V., Vitenko, V.A., Touse, V.T., Neutron Standards and Applications (Proc. Symposium) NBS Special Publication 493 (1977), 194.

[6] Нефедов В.Н., Старостов Б.И., Семенов А.Ф., Нейтронная Физика (Материалы 4-й Всесоюзной конференции по нейтронной физике), М., (I977), 205,

[7] Блинов М.В., Витенко В.А., Крисюк И.Т., О временных характеристиках эмиссии низкоэнергетических нейтронов при спонтанном делении ^{252}Cf, Препринт РИ-30, Ленинград (I974),

[8] Gayther, D.B., Annals of Nuclear Energy, vol. 4, N 11/12, 515 (1977)

[9] Lamaze, G.P., Schrack, R.A., Wasson, O.A., Nucl. Sci. and Eng., vol. 62, N 2, 183 (1978).

[I0] Дунин В.Н., Proc. of the VIII Inter. Symposium on the Interaction of Fast Neutrons with Nuclei-Nuclear Reaction Mechanism - Gaussig (DDR) (1978), 153.

АБСОЛЮТНОЕ ИЗМЕРЕНИЕ СЕЧЕНИЯ ДЕЛЕНИЯ 235 ПРИ Е = 2,6 МЭВ ПО МЕТОДУ КОРРЕЛИРОВАННЫХ ПО ВРЕМЕНИ СОПУТСТВУЮЩИХ ЧАСТИЦ

Р. Арльт, В. Вагнер, М.Ём, Г. Музиоль, Х.-Г. Ортлепп, Г. Пауш, У. Рихтер, Р. Тейхнер.
Технический Университет г. Дрездена, ГДР.

Л.В. Драпчинский, В.Н. Дунин, В.И. Шпаков
Радиевый Институт им.Хлопина, Ленинград, СССР.

I.Введение

Оптимальная конструкция и экономическая эксплуатация реакторов на быстрых нейтронах требует по возможности точное знание сечения деления важнейших изотопов горючего /I /. Требования к точности данных особенно высокие в области около 2.5 Мэв,так как в этом районе энергии находится еще много делительных нейтронов. Кроме того, сечения деления 235U является важным стандартом,для которого требуется однопроцентная точность /2-4/. На рис. I сопоставлены данные из некоторых важных оценок. Представленная в работе /5/ программа измерений должна помочь в преодолении существующих разногласий. Как часть реализации этой программы настоящая работа представляет предварительные результаты абсолютного измерения сечения деления 235U нейтронами энергии 2,6 МэВ

2. Метод измерения

В экспериментах на I50 киловольтном каскадном генераторе Технического Университета г. Дрездена впервые был применен метод коррелированных по времени сопутствующих частиц для абсолютного измерения сечения деления /6,7/ при энергии налетающих нейтронов - 2,6 МэВ /рис.2/.

Чтобы достичь требуемую точность I - 2% нужно добыть меньше одного процента статистической погрешности в счёте событий деления. Для этого необходимое время измерения составляет несколько недель. Для сбора и предварительной

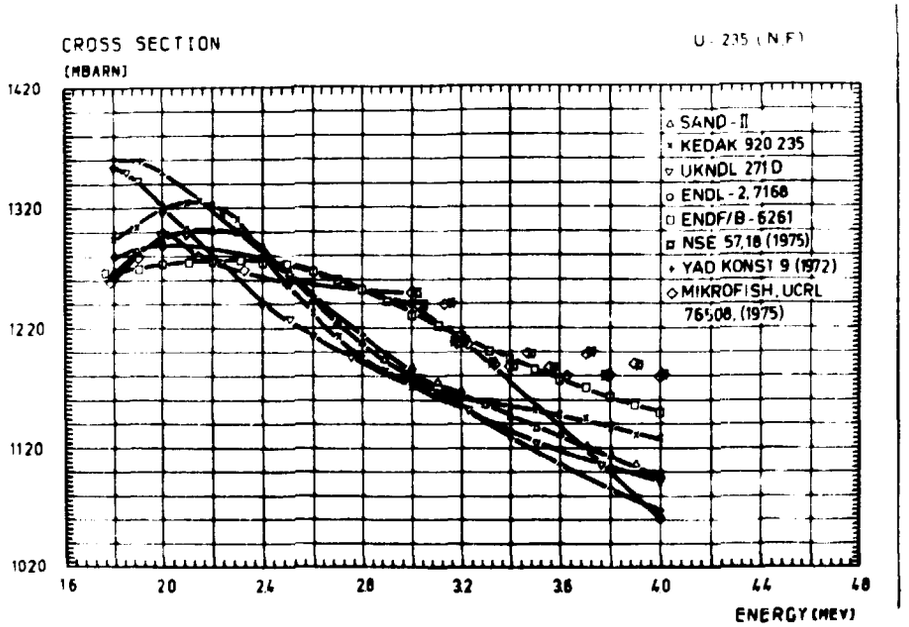

Рис.I

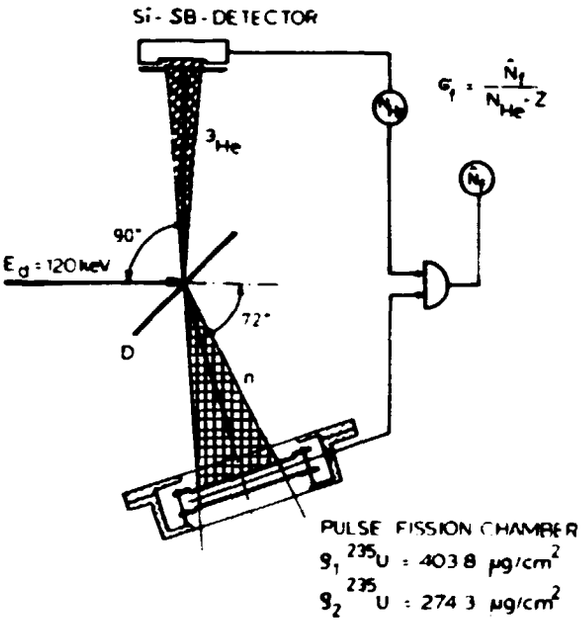

Рис. 2

обработки множества в это время появляющихся данных служит связь эксперимента с малой ЭВМ типа KRS 4200 через КАМАК / 8/. Моноэнергетические нейтроны энергии 2,6 МэВ производятся реакцией $D(d,n)^3He$ . . Коллиматором исключался сдвиг фокуса по дейтериевой мишени, так как стабильные условия являются неотъемлемым предусловием для метода сопутствующих частиц.

Для отделения геолинов от большого числа рассеяных дейтонов введена тонкая алюминиевая фольга, толщину которой необходимо точно подобрать, так как энергия геолинов лишь 800 кэВ. Для точного определения фона тритонов под пиком геолинов было проведено измерение спектра с толстой фольгой /рис.3/. Толщину подобрали таким образом, чтобы гелионы были поглощены при минимальной потере энергии тритонов. Эта проверка и показала, что на число гелионов в окошке не влияют электронные шумы. Необходимым предположением безошибочного применения метода сопутствующих частиц является точное знание пространственного распределения нейтронов, связанных с детектируемыми геолинами. Для проверки топографии нейтронного конуса был применен спичкообразный пластический сцинтиллятор, с помощью которого было определено

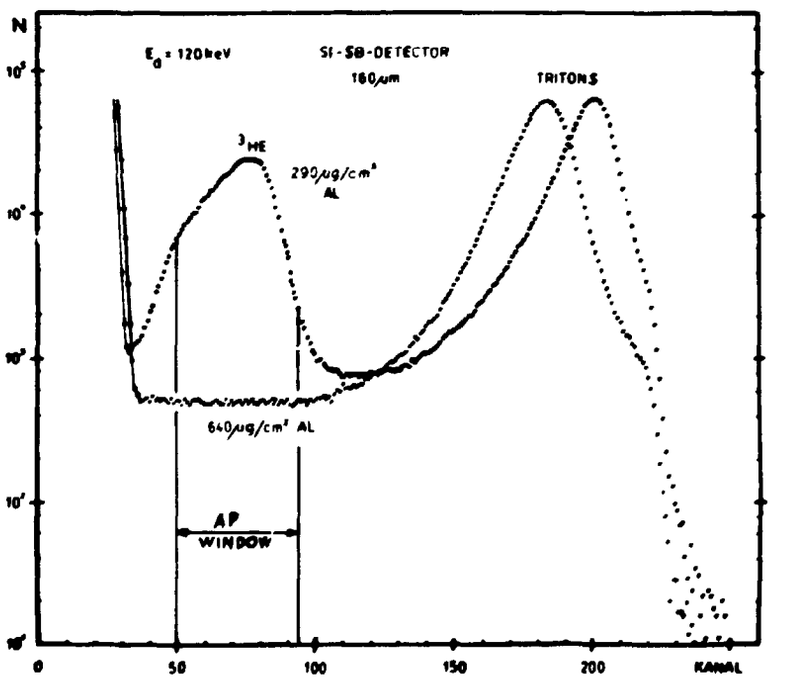

Рис. 3.

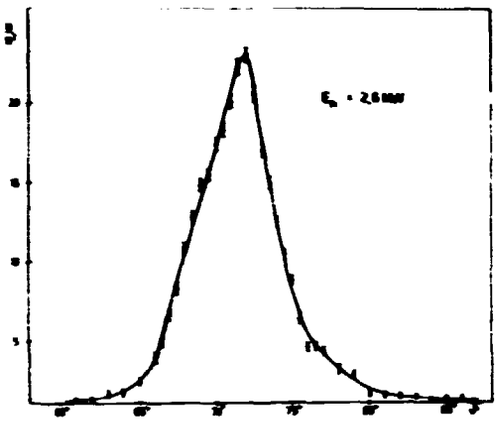

Рис. 4.

число совпадений $n-^3He$ как функция угла относительно направления налетающих дейтонов /рис.4/. Детектором осколков деления служила быстрая импульсная ионизационная камера наполненная метаном /9/. Для улучения статистики она выполнена двухплатной /10/. Достигнутое временное разрешение в районе 3-4 ns /рис. 5а,в/ позволяло в достаточной мере подавлять случайные совпадения. Кроме временного спектра совпадений набирался амплитудный спектр событий деления /рис. 5с,d /. Из этого рассчитано число потерянных из-за порога системы временной привязки импульсов методом экстраполяции плато. Кроме того проведена коррекция на поглощение в мишени осколков деления /11/. Методом монте-карло рассчитан вклад рассеяных нейтронов попадающих вне мишени /12/. Кроме того при этом и учитывалась коррекция толщины мишени для нейтронов налетающих не-перпендикулярно. Число ядер в мишенях определялось измерением их - активности в малой геометрии. При расчете числа ядер использовался период полураспада /7.0381 ± 0.0048/ $\cdot 10^8$ лет полученный в работе /13/. В октябре 1979 года проведенный эксперимент дал предварительный результат для сечения деления 235U при энергии 2,6 МэВ:

$$\sigma_f = (1,154 \pm 0,020) \cdot 10^{-24}\ см^2$$

Величины поправок и их погрешности составлены в таблице I.

На рис. 6 показаны наши предварительные результаты /23 и эта работа/ вместе результатами других авторов / 14 - 22 /.

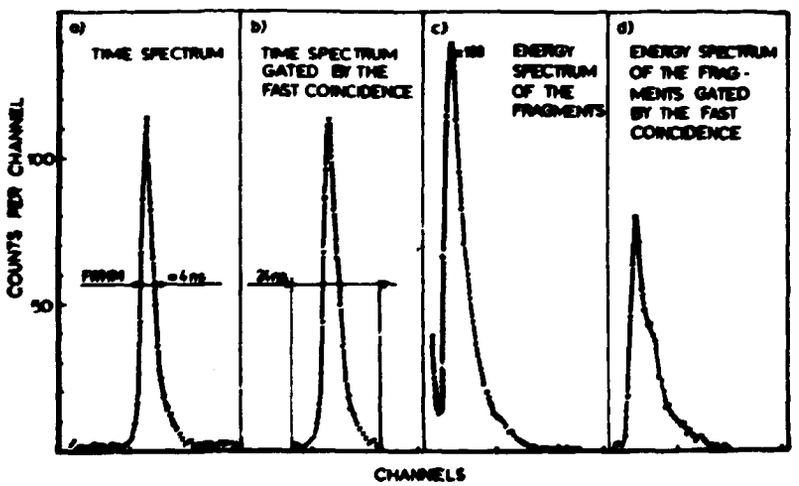

Рис.5.

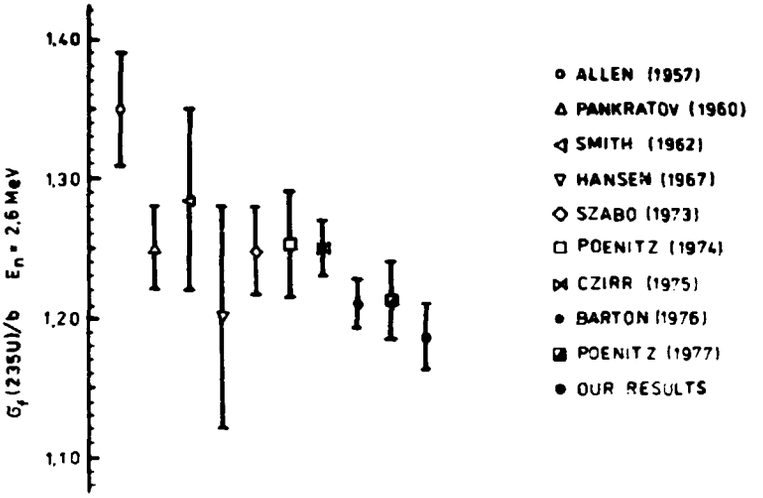

Рис. 6.

Таблица I

Величины поправок, их погрешности и их вклад в суммарную ошибку σ_f.

	K	ΔK/K	Δσ/σ
Статистическая погрешность	-	-	I.07%
Случайные совпадения	- 9.I4%	7%	0.66%
Экстраполяция к нулевой энергии осколков	+ 0,68%	30%	0.20%
поглощение в мишени осколков деления	+ 2.II%	I5%	0.30%
Фон тритонов	+ 3.28%	20%	0.66%
рассеяние нейтронов	+		0.30%
Число ядер в мишени	-	-	0.90%
нейтроны налетающие неперпендикулярно	+ 0.28%	30%	0.I%

Литература

/1/ ANL-76-90, Proc. of the NEANDC/NEACRP Spec. Meeting on Fast Fission Cross Sections, Argonne 1976

/2/ Usachev,L.N. et.al., Proc. of the Symp. on Appl. of Nucl. Data in Science and Technol., Paris 1973, IAEA-SM-170/91 Vienna, Vol.1, 129

/3/ WRENDA 1979/80, INDC(SEC)-73/URSF

/4/ Soverby,M.G., ANL/ND-77-1, 23

/5/ Arlt,R. et.al., ZfK-315(1976)172

/6/ Alchasov,I.D. et.al.,Mat. 2-nd Conf. on Neutron Physics, Kiev 1973, p.4,13

/7/ Arlt,R. et.al., Proc. of the VIII. Internat. Symp. on the Interact. of Fast Neutrons with Nuclei, Gaussig 1978, ZfK-382(1979)172

/8/ Arlt,R. et.al., Nucl. Instrum. and Meth.(will be publ.) Preprint TU Dresden 05-23-79

/9/ Arlt,R. et.al., Preprint TU Dresden 05-37-78

/10/ Adolph,L., Diplomarbeit TU Dresden 1979

/11/ Arlt,R. et.al., Preprint TU Dresden 05-05-79

/12/ Dushin,V.N., Proc. of the VIII. Internat. Symp. on the Interact. of Fast Neutrons with Nuclei, Gaussig 1978, ZfK-382(1979)153

/13/ Jaffey,A.H. et.al., Phys. Rev. C4(1971)1889

/14/ Allen,W.D. et.al., Proc. Phys. Soc. 70A(1957)573

/15/ Pankratov,W.M., At. Energija 9(1960)395

/16/ Smith,H.L. et.al., Phys. Rev. 125(1962)1329

/17/ Hansen,G. et.al., WASH-1074(1967)75

/18/ Szabo,I. et.al., Nat. 2-nd Conf. on Neutron Physics, Kiev 1973,part 3,27

/19/ Poenitz,W.P., Nucl. Sc. and Eng. 53(1974)370

/20/ Czirr,J.B. et.al., Nucl. Sc. and Eng. 58(1975)371

/21/ Barton,D.M. et.al., Nucl. Sc. and Eng. 60(1976)369

/22/ Poenitz,W.P., Nucl. Sc. and Eng. 64(1977)894

/23/ Arlt,R. et.al., Proc. of the VIII. Internat. Symp. on the Interact. of Fast Neutrons with Nuclei, Gaussig 1978, ZfK-382(1979)180

ИЗМЕРЕНИЕ ОТНОШЕНИЯ СЕЧЕНИЙ ДЕЛЕНИЯ ^{233}U И ^{235}U В ОБЛАСТИ ЭНЕРГИЙ 0,01 - 2 МэВ

С.А. Бирюков, Т.А. Мостовая, В.Н. Мостовой
Институт Атомной Энергии им. Курчатова, Москва, СССР

аннотация

На 60 МэВ линейном ускорителе электронов с помощью ионизационной камеры с газовым усилением измерено отношение сечений деления ^{233}U и ^{235}U. Номинальное разрешение в измерениях составляло 3 нсек/м. Полученная энергетическая зависимость удовлетворительно согласуется с данными других авторов, полученными в последнее время.

Привлекательность реакторов на ^{233}U - ^{232}Th цикла, как реакторов экономичных, индицирует работы по получению нейтронных сечений, необходимых для их расчетов и, в частности, сечений деления. После работы Беренса и др. [1], в последние годы в различных лабораториях выполнены измерения сечений деления ^{233}U и его отношения к сечению деления ^{235}U в области энергий нейтронов, представляющей интерес для быстрых реакторов. Здесь можно упомянуть работы, выполненные в СССР Фурсовым и др. [2], в Аргонской национальной лаборатории Поеницом и др. [3] и в Харуэлле Джеймсом и др. [4].

На 60 МэВ линейном электронном ускорителе "Факел" ИАЭ им. И.В. Курчатова, используемом в качестве источника нейтронов, были проведены измерения сечений деления ^{233}U и ^{235}U в области энергий от 1 эв до 10 КэВ, а их отношение в области до 2 МэВ. В докладе представлены результаты в области энергий 10 КэВ - 2 МэВ, отвечающей интересом данного семинара.

Высокая удельная α-активность ^{233}U, а также жесткое γ-излучение продуктов распада ^{232}U, присутствующего всегда в образцах или мишенях, вызывает значительные трудности в экспериментах. Для достижения высокой точности и хорошего разрешения, при доступных интенсивностях источников нейтронов, необходимо использовать образцы или мишени ^{233}U весом ~1 грамм и более. Поэтому при измерениях сечения деления путем прямой регистрации осколков необходимы детекторы с высоким временным расрешением (~10 нсек). При использовании же методики измерений сечений деления по вторичным нейтронам с помощью сцинтилляционных детекторов, чтобы избавиться от фона γ-излучения продуктов распада ^{232}U, необходимо иметь образцы, в которых примесь этого изотопа была бы $\lesssim 10^{-6}$. Мы не располагали таким чистым изотопом. Поэтому в данной работе для регистрации делений была использована ионизационная камера с сетками. Она работала в режиме газового усиления (коэффициент усиления 20), и имела временное разрешение 20 нсек. ^{233}U в виде окиси-закиси был нанесен на обе стороны плоского алюминиевого электрода размером 10 x 20 см^2.

Общее количество ^{233}U, с обогащением лучше чем 96 %, нанесенного на поверхности 400 см^2, составляло 0,180 г. $^{235}U_3O_8$ с обогощением лучше чем 99 % в количестве 0,8 г был нанесен на идентичный электрод. В ионизационной камере слои находились на расстоянии 3,5 см.

Измерения проводились при следующем режиме работы ускорителя:

1. Энергия ускоренных электронов - 60 МэВ,
2. Длительность импульса ускоренных электронов - 50 нсек,
3. Ток электронов в импульсе на урановой мишени - 1,2 А,
4. Частота посылок - 460 герц.

Пролетное расстояние до ионизационной камеры составляло 26 м. Для устранения эффекта рециклических нейтронов пучок перекрывался фильтром из ^{10}B, толщиной 0,15 г/см^2. Перегрузка камеры за счет γ-вспышки ускорителя полностью устранялась теневой защитой из свинца, толщиной 60 см.

Эффекты делений от слоя ^{233}U и ^{235}U регистрировались на отдельных анализаторах АИ-4096 одновременно с шириной каналов τ = 50 нсек. Старт задавался электронным импульсом, возникающим от ускоренных электронов на мишени.

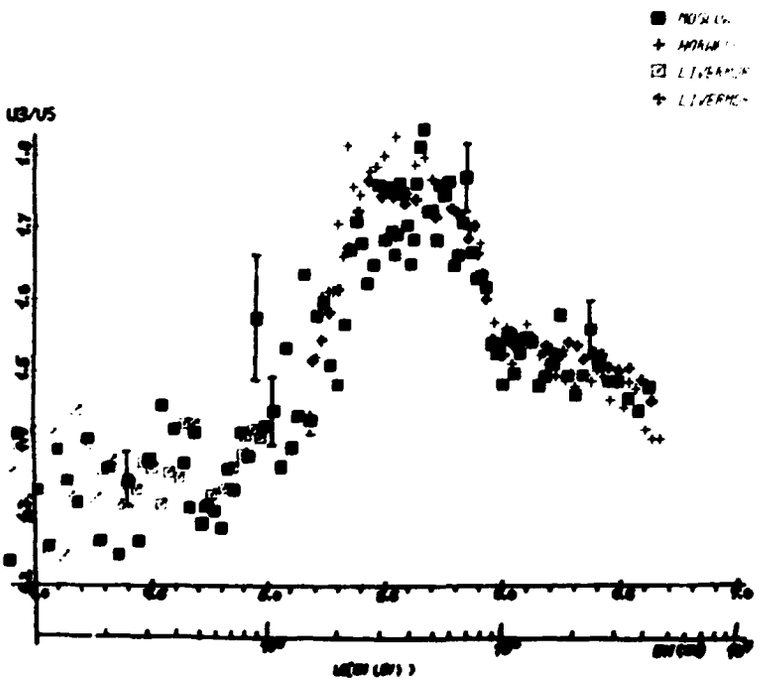

Фон нетаймированных нейтронов оценивался по счету в каналах анализатора до начала регистрации γ-лучей от вспышки ускорителя, а также в области, отвечающей энергиям нейтронов выше 16 МэВ. Этот фон был мал и для области энергий выше 10 КэВ не превышал 1,5 %.

Результаты измерений энергетической зависимости $\sigma_f(^{233}U)/\sigma_f(^{235}U)$, нормированные в области (1 - 2) МэВ энергий к значению 1,523 (5), представлены на графике. Там же нанесены данные работ [1, 4, 5].

Видно, что измеренное отношение в среднем удовлетворительно согласуется с данными работ [1, 4, 5], хотя имеются и отдельные отклонения точек, превышающие величину ошибок (~2 ÷ 3 %). Эти выбросы точек частично могут быть связаны с нерегулярной структурой спектра нейтронов в пучке. Эта структура обусловлена конструкционными материалами, находящимися на пути пучка нейтронов и ее эффект,

по видимому, полностью не устраняется при приведении скоростей счета делений на слое ^{233}U к пролетному расстоянию слоя ^{235}U.

Литература

[I] J.W. Behrens, G.W. Carlson and R.W. Bauer, Proceedings of a conference Washington, D.C. March 3-7, 1975, p.591.

[2] Б.И. Фурсов, В.М. Куприянов, Г.Н. Смиренкин, Атомная Энергия том. 44, вып. 3, 1978, стр. 236,

[3] Poenitz W.P. Argonne National Laboratory Report ANL/NDM-36 (1978).

[4] James G.D., Syme D.B., Cooke M.C. and Gadd A.D. AERE Harwell Progress Report AERE PR/NP25 (1978).

[5] G.W. Carlson and J.W. Behrens, Report UCRL-79577.

SEARCH FOR HIGH-ENERGETIC NEUTRONS IN THE 14,6 MEV NEUTRON INDUCED FISSION OF ^{238}U

H. Märten and D. Seeliger

Technical University Dresden, GDR

Using the method of n/μ-pulse-shape discrimination to suppress the cosmic background counts of the scintillation detector and measuring simultaneously the time of flight and the proton recoil energy of the neutron events to determine exactly the expected effect field and the optimum analysis threshold of the proton recoil energy for each time of flight channel an attempt was made to detect neutrons with abnormally high energies in the 14,6 MeV neutron induced fission of 238-U. These neutrons could be a result of an excessive energy release in the fission process due to the formation of superdense fragments with a possibly higher binding energy per nucleon compared to normal nuclei. The upper limit of the yield of neutrons with energies over 38 MeV amounts to about $5 \cdot 10^{-8}$ per MeV and per fission event.

INTRODUCTION

One conclusion of some theoretical works, which were published since 1971, was the possible existence of superdense nuclei /1-3/. Many attempts to search for such abnormal nuclei in the nature or to produce them in the laboratory have been carried out without success /4-14/.

Migdal et al. proposed to search for superdense fragments in the fission of normal nuclei /2/. Hitherto such experiments were centred on the detection of positrons and the search for electrons, γ-rays and neutrons with abnormal high energies in the spontaneous fission of ^{252}Cf or in the neutron induced nuclear fission at relatively low incident energies /11-14/.

It is conceivable that there is a higher possibility of the formation of superdense nuclei in the non-stationary phase of the fission process compared to spontaneous transitions. For the theoretically possible case, that the binding energy per nucleon in the superdense state is higher than in the normal one, one may expect a higher energy release in an abnormal fission event with the simultaneous formation of superdense fragments, i.e. an energy release of 10^3 to 10^4 appears instead of about 200 MeV in the normal case. Higher energies of the prompt fission neutrons and a higher average number of fission neutrons because of the changed ratio between the proton number and the mass number in superdense nuclei /2/ would be a consequence.

In distinction to the works /12,13/, this experiment was aimed at the search for neutrons with energies over (30...40) MeV in the neutron induced fission at the higher incident neutron energy of 14,6 MeV.

EXPERIMENTAL ARRANGEMENTS

The aim of the experiment was to detect a very small effect. Hence, it was necessary to realize a high rate of fission events, to suppress the background, to apply a high-efficient neutron detector and so on. The measurement was carried out at a 150 kV deuteron accelerator using the fast neutron time of flight technique. A pulsed deuteron beam of (30...35) μA ion current, 1 ns pulse width and 5 MHz repetition rate was focused on the neutron producing tritium target.

The sample of natural uranium (99,3 % ^{238}U) of 2137 g mass was located beside the tritium target between this target and the detector. In this way, a primary fission event rate $dN_{f0}/dt = 4,0 \cdot 10^7\ s^{-1}$ (average) was reached. The rate of fission events induced by primary fission neutrons and by scattered neutrons dN_{f1}/dt amounted to about $1,0 \cdot 10^7\ s^{-1}$.

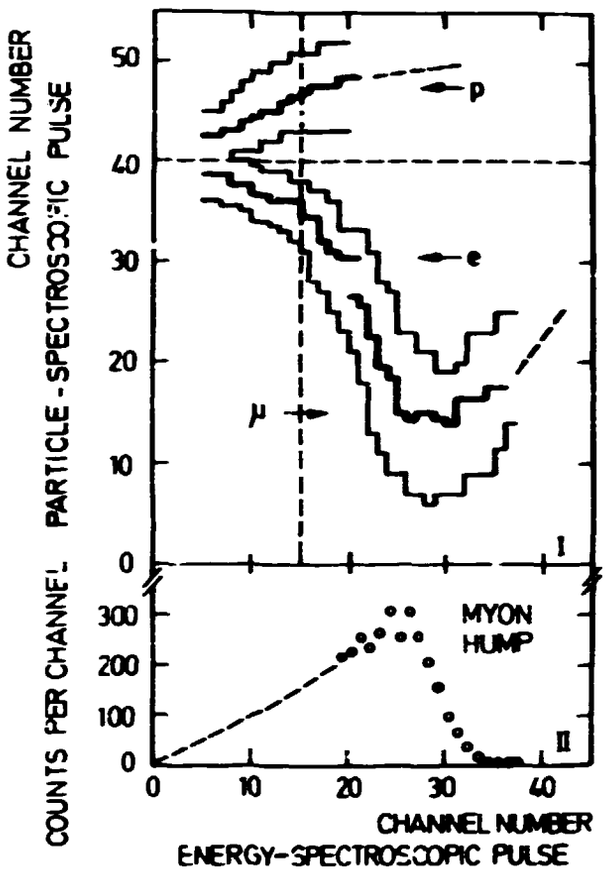

Fig. 1/I

Particle branches in a two-dimensional representation illustrate the performance of the n/μ-discrimination. The radiation is from a Po-Be-neutron-source.

p - branch of neutron events (recoil protons);
e - branch of γ-events (electrons);
μ - branch of cosmic myon events.

External limits of the branches (weak lines) indicate the 5 % level of the peak height for a given energy-spectroscopic pulse channel number.

Fig. 1/II

Background pulse height spectrum of the detector used in the experiment (calculated from the results of the two-dimensional measurement represented in Fig. 1/I).

The neutron detector consisted of a liquid scintillator with pulse shape discrimination properties (Nuclear Enterprises, NE 213, 12,5 cm in diameter and 12,5 cm thick) viewed by a fast photomultiplier (EP 2040).

The detector arrangement was located in a heavy shielding of paraffin, lithium paraffin, iron, lead and graphite. The distance between the uranium sample and the scintillator was 500 cm.

The detector was completely shielded against the weak component of the cosmic rays. An electronic system for n/μ-pulse-shape discrimination by the charge comparison method (comparison of the fast component of the detector anode signal with the whole signal) was used to suppress the remaining cosmic background counts of the detector, which are mainly caused by myons /16/ (Fig. 1). The separability of neutron and myon events is possible because of the different specific energy loss of protons with energies up to 100 MeV and cosmic myons with energies between 0,1 and 2,0 GeV. The stated myon energy range is the main one of this penetrating cosmic ray component in the near of the sea-level. Because of the approximately constant energy loss of myons per path length unit in matter for the stated energy interval the scintillator geometry determines mainly the form of the background pulse

height spectrum of the detector (Fig. 1/II). For the scintillation detector used in the experiment this spectrum shows a hump at about 20 MeV with reference to the proton recoil energy. The used n/μ-discrimination method makes it possible to suppress the background to 0,5 % in the region of the myon hump. The upper limit of the effective range of this discrimination method amounts to about 40 MeV with reference to the proton recoil energy (Fig. 3, compare with Fig. 1).

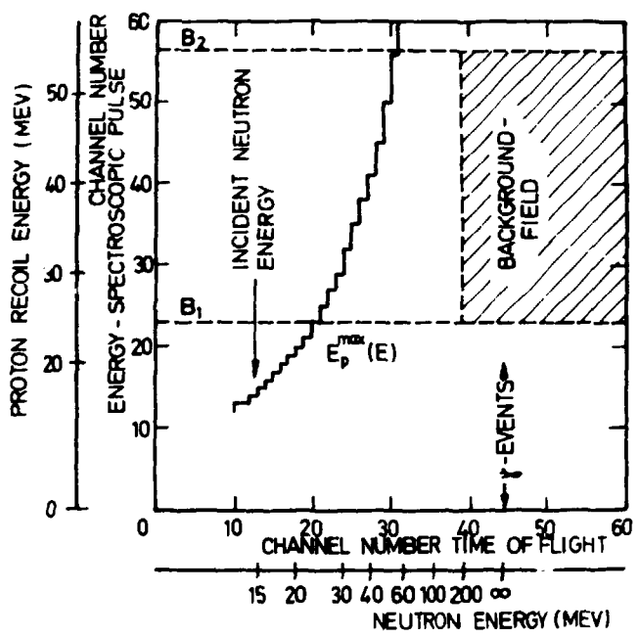

Fig. 2

Illustration of the two-dimensional measurement of the time of flight and the proton recoil energy of the neutron events; E_p^{max} is the maximum proton recoil energy for a given time of flight channel corresponding to the neutron energy; B_1 is the analysis threshold of the proton recoil energy, which can be determined as an optimum for each time of flight channel (see text); B_2 is the upper measured value of the proton recoil energy-spectroscopic signal.

To reduce the load of the spectrometer by γ-events a lead filter of 2 cm thickness was located in front of the detector.

The fast output of the detector was used as the start signal for the time-to-pulse height converter. The stop signal was extracted from the pulsing system of the accelerator. The total time resolution of the neutron time of flight spectrometer, including the ion pulse width of the accelerator, was about 2,5 ns. Moreover, the output signal of the detector was used to get a proton recoil energy-spectroscopic signal by integration. In this way, the time of flight and the proton recoil energy of the neutron events were measured. The adequate signals were two-dimensionally stored in a 4096 channel analyser (64 channels x 64 channels) in coincidence with the neutron identifying output signal of the electronic pulse shape discrimination system. This arrangement permited the precise definition of the storage field, in which the searched effect was to be expected. On the other hand, one is able to determine the optimum of the threshold B_1 of the proton recoil energy, which is used in the analysis. The following criterion for the determining of the B_1 optimum is applicable for a given time of flight channel: The quotient between the statistical error of the determined sum of counts in the allowable channel range of the proton recoil energy above the threshold B_1 and the detector efficiency as a function of B_1 is minimum. It is obvious that the quantity of the threshold B_1 is higher than the value of the incident neutron energy.

Using the described method it was possible to measure simultaneously the effect and the background (Fig. 2).

The measuring range of the proton recoil energy was limited. The upper measurable value was signed as B_2 (Fig. 2).

ANALYSIS OF THE EXPERIMENT. RESULTS

Neglecting the differential non-linearity of the time measuring equipment the following equation is valid for the calculation of the neutron energy spectrum:

$$N(E) = \frac{\frac{X(k)}{\Delta t}\cdot f\cdot\frac{dt}{dE}}{k_T(E)\cdot\frac{\Omega}{4\pi}\cdot\varepsilon(E,B_1,B_2)\cdot\frac{dN_f}{dt}\cdot T} = \frac{X(k)}{\Delta t}\cdot f\cdot F(E); \qquad (1)$$

$X(k)$ - sum of effect counts in the time of flight channel k calculated for the allowable proton energy range (Fig. 2):

$B_1 < E_p < E_p^{max}$, if $E < B_2$;
$B_1 < E_p < B_2$, if $E > B_2$;

E_p^{max} is the maximum proton recoil energy for a given time of flight channel corresponding to the neutron energy;

Δt - time of flight channel width, $\Delta t = 2{,}44$ ns;

f - dead time correction factor;

$k_T(E)$ - transmission coefficient for neutrons with the energy E determined by the neutron absorption in the lead filter and in the sample itself;

Ω - detector solid angle;

$\varepsilon(E,B_1,B_2)$ - detector efficiency;

$$\frac{dt}{dE} = \frac{36{,}2\cdot L/m/}{(E/MeV/)^{3/2}}; \qquad (2)$$

L - path of flight.

The search experiment consisted of 31 single measurements. The whole measuring time was 73 h. With about the same duration supplementary cosmic background measurments without neutron beam have been carried out. The whole number of the induced fission events was calculated starting from the measuring geometry and considering roughly multiple effects caused by the reactions (n,n), (n,n'), (n,2n), (n,3n) and secondarily induced fission events by primary fission neutrons. This quantity $N_f = N_{f0} + N_{f1}$ amounts to $(1{,}3 \pm 0{,}4)\cdot 10^{13}$.

Some further simplifications of the analysis were possible because of the specific features of the experiment. The transmission coefficient $k_T(E)$ is nearly constant for the interesting neutron energy range:

$k_T(E) \approx$ constant $= 0{,}60$.

The detector efficiency was calculated considering only the single neutron scattering at protons. Because of the high threshold B_1 other processes

practically don't influence the detector efficiency.

The function F(E) (see Fig. 5, equ. 1) characterizes the sensibility of the measurement. Its dependence on the neutron energy is weak. It follows

$$F(E) \approx \text{constant} = (4{,}5 \ldots 5{,}0) \cdot 10^{-8}\ \text{MeV}^{-1} \qquad (3)$$

for the interesting neutron energy interval (B_1 = 24 MeV, B_2 = 56 MeV, L = 5m, $\Omega = 4{,}52 \cdot 10^{-4}$ sr).

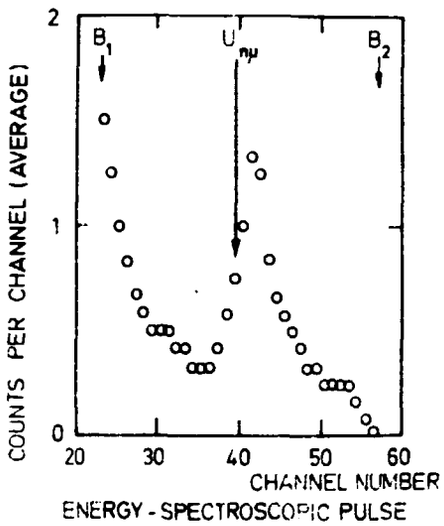

Fig. 3

Background pulse height spectrum per time of flight channel for the whole experiment; $U_{n\mu}$ is the upper limit of the effective range of the n/μ-discrimination.

Fig. 4 shows the time of flight spectrum of the whole measurement at the optimum proton recoil energy threshold B_1 = 24 MeV both for the whole and for the allowed proton recoil energy range. The background line was calculated applying the number of counts in the background field (Fig. 2); it is plotted for the allowed proton recoil energy in Fig. 4 too.

In the neutron energy range above 33 MeV no significant enhancement of the measured spectrum over the background line appears. Equs. (1) and (3) were used to estimate the upper limit of the yield of neutrons in some energy ranges.

The sum of the "effect"-counts in the time of flight channel range $28 \leq k \leq 39$ (38 MeV $\leq E \leq$ 180 MeV) amounts to (5 ± 29). It follows

$$N(E) \lesssim 5 \cdot 10^{-8}\ \text{MeV}^{-1}.$$

Using the average statistical deviation of the effect spectrum from the zero level (2,8 counts per time of flight channel) one gets the same result.

A similar calculation was done for the time of flight channel range $25 \leq k \leq 27$ (30 MeV $\leq E \leq$ 38 MeV) at the threshold B_1 = 22,2 MeV. In this case the sum of effect counts amounts to (6,5 ± 6,5).

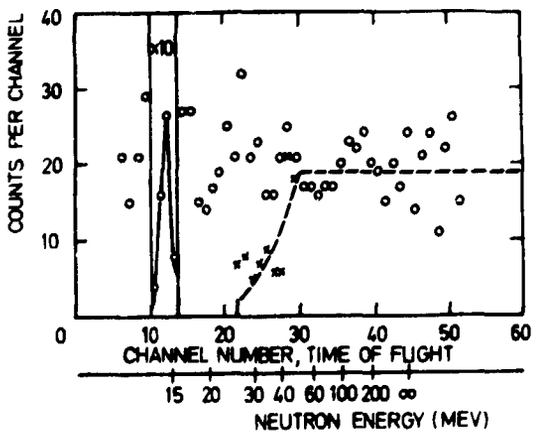

Fig. 4

Time of flight spectrum of the whole measurement;

- o - counts per time of flight channel over the threshold B_1;
- x - counts per time of flight channel for the allowable proton recoil energy range ($B_1 < E_p < E_p^{max}$);
- --- - background line (see text).

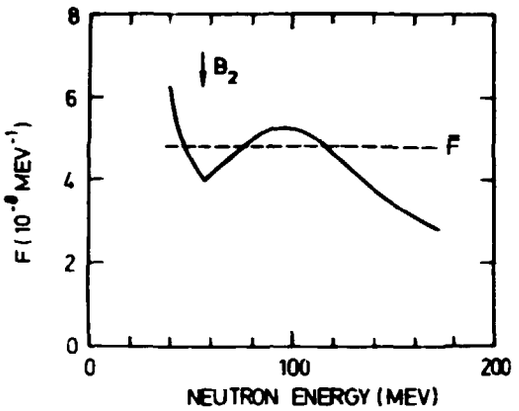

Fig. 5
Sensibility function F(E) via neutron energy (see text)

The adequate neutron yield amounts to $(6 \pm 9)\cdot 10^{-7}$ for the stated neutron energy range. However, this small effect is probably caused by the evidence of highest-energetically normal fission neutrons.

DISCUSSION

In the presented experiment no neutrons with abnormal high energies, which could allow the conclusion of the real existence of a fission process with an excessive energy release, were detected. The main restraints to the sensibility of the experiment are caused by the residuel background (Fig. 3) and the limitation of the fission event rate, i.e. the intensity.

The used experimental arrangement is especially suitable for the spectroscopy of neutrons in the high-energetic range at low intensities.

The authors whish to thank S. Sassonov, T. Schweitzer and S. Unholzer for their assistance during the experiment and helpful discussions.

REFERENCE

/ 1/ Migdal, A.B., J.E.T.P. 61(1971)2209
/ 2/ Migdal, A.B. et al., Phys. Lett. 65B(1976)423
/ 3/ Lee, T.D. and G.C. Wick, Phys. Rev. D9(1974)891
/ 4/ Price, P. and J. Stevenson, Phys. Rev. Lett. 34(1975)409
/ 5/ Fraenkel, K. and J. Stevenson, Phys. Rev. C14(1976)1455
/ 6/ Holt, R. et al., Phys. Rev. Lett. 36(1976)183
/ 7/ Fraenkel, S. et al., Phys. Rev. C13(1976)737
/ 8/ Bugorski, A.P. et al., JINR 13-10216, Dubna, 1976
/ 9/ Kulikov, A. and B. Pontecorvo, JINR P 1-10202, Dubna, 1976
/10/ Aleshin, W.I. et al., Lett. in J.E.T.P. 24(1976)114
/11/ Aleshin, W.I. et al., Yad. Fiz. 26(1977)916
/12/ Nikolenko, W.G., A.B. Popov, G.S. Samosvat, Lett. in J.E.T.P. 27(1978)65
/13/ Popov, A.B. and G.S. Samosvat, Yad. Fiz. 30(1979)315
/14/ Aleshin, W.I. et al., Yad. Fiz. 30(1979)318
/15/ Seeliger, D. and K. Trützschler, Nucl. Instr. Meth. 66(1968)157
/16/ Märten, H. and S. Sassonov, ZfK-385(1979)219, Gemeinsamer Jahresbericht 1978

A METHOD FOR THE ABSOLUTE MEASUREMENT OF FISSION CROSS SECTIONS AT NEUTRON ENERGIES OF ABOUT 8.5 MeV

R. Arlt, M. Josch, G. Musiol, H.-G. Ortlepp, R. Teichner, W. Wagner

Technical University Dresden, Section of Physics, DDR - 8027 Dresden

I.D. Alkhazov, L.V. Dzerzhinsky, O.I. Kostochkin, S.S. Kovalenko, V.I. Shpakov

Khlopin - Radiuminstitute Leningrad, USSR

The precise knowledge of nuclear constants is of particular importance in reactor calculations. In the present situation of nuclear energetics accuracies of about 1 - 2 % are required for the fission cross-sections (f. c.-s.) of most of the fuel isotopes in a wide energy range/1/. Especially at higher energies effectual in fast breeders the necessary accuracies yet are not obtained /2/.

In addition to relative measurements of the f. c.-s. by use of "white neutron souces" /3/ absolute measurements with high precision give the possibility of accurate normalization of the fission cross-section shape to the absolute value. Alternatively to measurements performed with a "black neutron detector"/4/ for an absolute monitoring of the neutron flux the time correlated associated particle method (TCAPM) has been employed for the measurement of absolute f. c.-s. at spot-point energies favorably choosen on the high energy plateaus of the f. c.-s. /5,6,7/.

Recently at the TU Dresden the TCAPM was applied in f. c.-s. measurements on the nuclides ^{235}U, ^{238}U, ^{237}Np and ^{239}Pu at a neutron energy of (14.70±0.15)MeV, where this method at present time is well established /8/. In Tab. 1 our results are compared with the data of other groups also using the TCAPM. The values of the f. c.-s. agree within the given standard deviations, exept for ^{239}Pu where a discrepancy of ± 4.5 % can be observed.

Tab. 1 : Absolute fission cross-sections at a neutron energy of 14.7 MeV

Nuclide	Technical University Dresden /7,8/	Radiuminstitute Leningrad /9/	Centre d'Etudes de Bruyères-le-Chatel 14.6 MeV /10/
^{235}U	(2.085 ± 0.023) barn	(2.096 ± 0.034) barn	(2.063 ± 0.039) barn
^{238}U	(1.166 ± 0.027) barn	(1.178 ± 0.024) barn	(1.149 ± 0.025) barn
^{237}Np	(2.226 ± 0.024) barn	(2.292 ± 0.044) barn	
^{239}Pu	(2.394 ± 0.024) barn	(2.505 ± 0.045) barn	(2.290 ± 0.052) barn

The TCAPM at other neutron energies

The extention of the TCAPM to other neutron energies is conected with the following principal problems :

i) establishment of an appropriate intense source of monoenergetic neutrons using e.g. the well known reactions $T(d,n)^4He$ or $D(d,n)^3He$.

ii) arrangement of such geometrical and experimental conditions, that the associated charged particles (a. p.) are detectable. According to the de-

fined kinematics of the source reactions the neutron energy and its spread than is given.

iii) development of a detecting system for the a. p. which allowes timing and accurate counting of the a. p. in the presence of an intense background of nonassociated charged particles and gamma-rays.

Special measuring systems were developed at the TU Dresden applying the TCAPM at neutron energies of 2.6 MeV /11/ and 8.2 MeV. Accuracies of the measured f. c.-s. of about 2 % have been obtained or could be expected /7/.

The TCAPM at a neutron energy of 8.2 MeV

To produce an 8.2 MeV neutron beam a similar system to that of Schuster /12/ and Bartle et al. /13/ has been built up at the 5-MV-Tandem-generator of the CINR Rossendorf (G.D.R.).

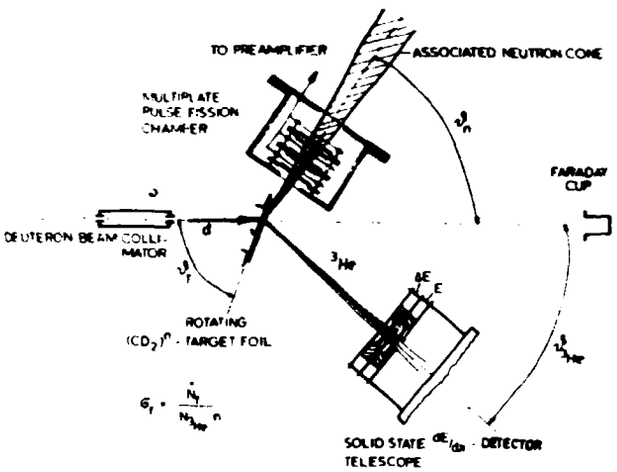

Fig. 1: Principle of the f. c.-s. measurement at a neutron energy of 8.2 MeV

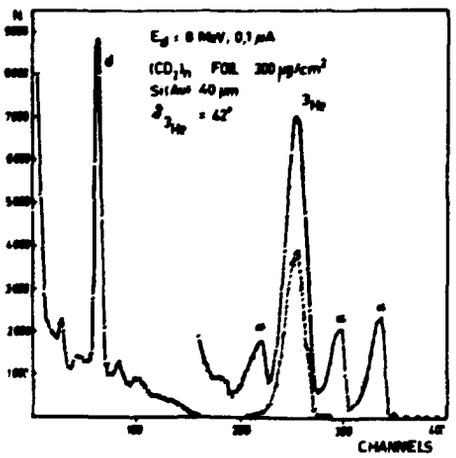

Fig. 2: Spectrum of charged particles at the a. p. angle $\vartheta_{^3He} = 42\ ^{o}$.

A scheme of the experimental set-up is shown in fig. 1. The 9 MeV deuteron beam hits a rotating target foil of deuterated polyethylen. The associated ^{3}He-particles from the reaction $D(d,n)^3He$ were detected at an angle $\vartheta_{^3He} = 42\ ^{o}$. The a. p. diaphragma defines an associated neutron cone. Fission events from fife ^{235}U-target layers were registrated in a multiplate pulse fission chamber.

As it is illustrated in fig. 2 the a. p. ^{3}He are covered by alpha-groups from the competitive reaction $^{12}C(d,\alpha)^{10}B$. A rather high peak of scattered deuterons is located at about 800 keV. Therefore the discrimination of the ^{3}He was realized by use of a telescope of two Si-surface-barrier detectors/14/. The single spectra of the telescope detectors are shown in fig. 3. The amount of alpha-background is shown in the single spectra of fig. 4, which have been measured replacing the deuterated foil by a usual polyethylen foil of comparable thickness.

The dE/dx-E_r-particle identification is illustrated in the two-dimensional map of fig. 5. A good separation of the ^{3}He was obtained by optimizing the parameters of the telescope. The marked thresholds for ^{3}He-counting

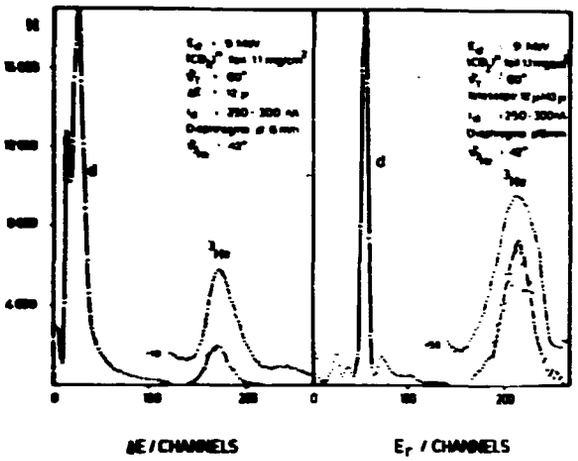

Fig. 3: Single spectra of the telescope detectors using a $(CD_2)^n$-foil

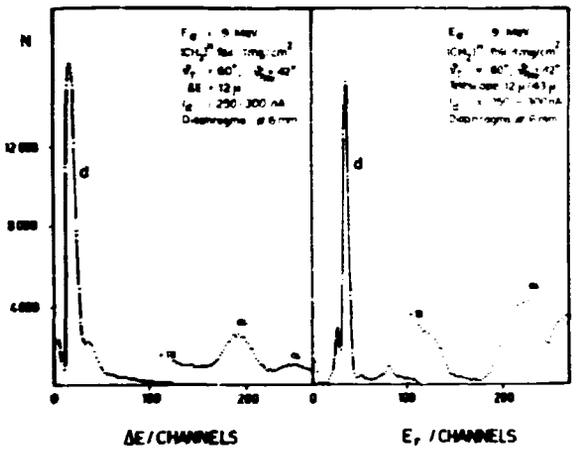

Fig. 4: Single spectra of the telescope detectors using a $(CH_2)^n$-foil

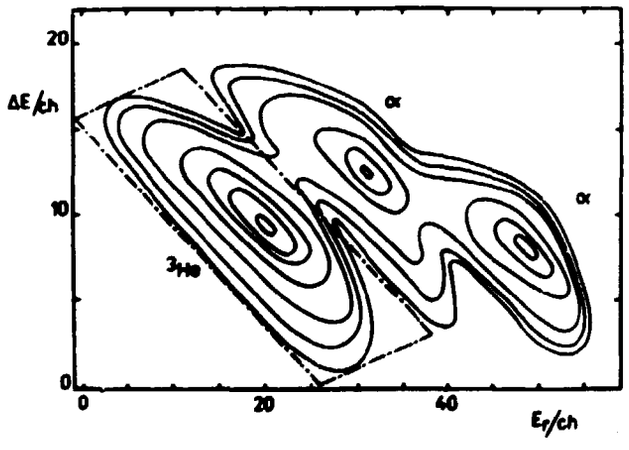

Fig. 5: Twodimensional picture of the particle identification

were set by a discriminating circuit/14/. The amount of alpha-events within this ^{3}He-window runs typically to 1 - 3 %.
The real distribution of neutron intensity inside the cone defines the geometrical conditions for the fission chamber/15/. Therefore a precise scanning of the topography of the neutron cone was carried out to fulfil the main condition of the TCAPM, that all neutrons of the cone must be able to hit the fission targets.
The distribution, shown in fig. 6, has been measured by use of a small Stilben-scintillation counter applying n-γ-discrimination.
The coincidence spectra between the ^{3}He and the neutrons were corrected for the time uncorrelated background, which limited the accuracy at a level of 1 : 1000.
In a first measurement the small solid angle of the telescope of 0.2 msrad allowed at 0.5 μA beam current and foil thicknesses of about 1 mg/cm^2 ^{3}He-rates of 250-450 per second.
The experiment was coupled on-line on a KRS 4200 minicomputer via a CAMAC-branch /16/.
The experimental value of the fission cross-section has been corrected for random coincidences, the efficiency of the fission chamber, alpha-background within the ^{3}He-window and neutron scattering in wall materials and target backing. The corrections were listed in Tab. 2. They are relatively small, so that it seems to be possible to measure f.c.-s. with an accuracy of about 2 % applying the TCAPM in this energy region.
In a first run the fission cross-section of ^{235}U could be measured with a statistical error of 5.6 %. A preliminary value of

(1.74 ± 0.11) barn has been obtained/7/. Further improvements of the system to reach a higher neutron flux are in progress.

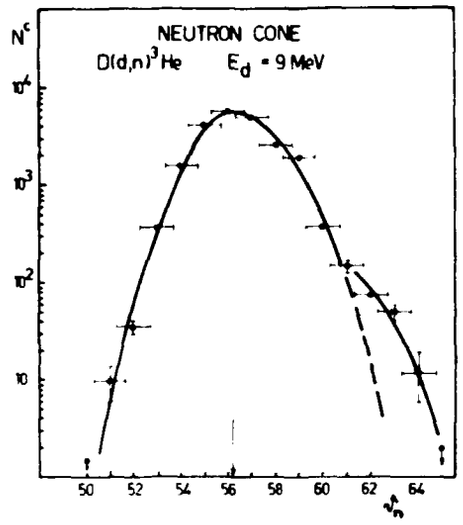

Fig. 6: Neutron intensity distribution in the cone

Tab. 2: Corrections and uncertainties of the measured fission cross-section

	corr./%	uncert./%
weighing of the fission layers		0.9
effective inhomogenity		1.14
efficiency of the fission chamber	+5.5	1.41
neutron scattering	+0.23	0.4
geometrical certainty		0.5
alpha-background	+2.1	0.5
uncertainty connected with TCAPM		2.1 %
statistical error		5.6
random coincidences	-7	2

Literature

/1/ WRENDA 76/77, INDC (SEC) - 55/ URSF, part II, p. 56, IAEA Vienna

/2/ Proc. of the Spec. Meet. on Fission Cross Sect.,Argonne 1976, ANL-76-90

/3/ J.B. Czirr et al., Nucl. Sci. Eng. 57 (1975) 18

/4/ W.P. Poenitz, Nucl. Sci. Eng. 53 (1974) 370

/5/ I.D. Alkhazov et al., Mat. d. II. Konf. über Neutronenphys.,Kiew 1973,IV,13

/6/ M. Cance et al., Transact. Am. Nucl. Soc. 22 (1975) 664

/7/ R. Arlt et al., Proc. of the Int. Conf. on Nucl. Cross Sect. for Technology, Knoxville 1979 , to be published

/8/ R. Arlt et al., Preprint TU Dresden 05-36-79 (1979), subm. to Kernenergie

/9/ V.M. Adamov et al., ibid. /7/

/10/M. Cance et al., Nucl. Sci. Eng. 68 (1978) 197

/11/R. Arlt et al., Proc. of the VIII. Internat. Symp. on the Interact. of Fast Neutrons with Nuclei, Gaussig 1978, ZfK - 382 (1979) 180

/12/D.G. Schuster, Nucl. Instr. and Meth. 76 (1969) 35

/13/C.M. Bartle et al., Nucl. Instr. and Meth. 144 (1977) 437

/14/R. Arlt et al., Jahresbericht 1977, ZfK - 350 (1978) 209

/15/R. Arlt, ibid. /11/, 172

/16/R. Arlt et al., Preprint TU Dresden 05-23-79 (1979), subm. to Nucl. Instr. and Meth.

COMPUTERISATION OF THE γ-SPECTROMETRIC METHOD FOR FISSION YIELD MEASUREMENT BASED ON GAMANAL PROGRAM*

S. Nagy, P. Raics and S. Daróczy
Institute of Experimental Physics, Kossuth University, Debrecen, Hungary
K. Erdei and I. Rápolti
Computer Center, Kossuth University, Debrecen, Hungary

The principles and applicability of a system of programs capable for the routine evaluation of experimental data in the direct γ-spectrometric measurement of fission product yields is described. The main programs in the system are modified versions of GAMANAL (for automatic evaluation of γ-spectra) and CLSQ (for the flexible analysis of decay curves), supported by additional programs for the efficient data handling.

Introduction

The measurement of the fission product yields means practically the quantitative analysis of a very complex radioactive source which is produced by the irradiation of a fissioning sample. The excellent resolution of the Ge(Li) detectors made it possible to do this nondestructively, using the gross γ-spectra of the unseparated sample. If absolute yields (or partial fission cross sections) are determined directly by γ-spectrometric investigation of the given fissioning sample itself (avoiding any comparisons to the spectra of other fissioning samples), the procedure is referred as direct γ-spectrometric method[1]. In this procedure the γ-lines of fission products are identified by their half-lives in addition to their energies, as well as the unresolved multiple peaks are resolved by the investigation of decay curves of the peaks in the spectra. In order to have enough experimental points at any time region to the analysis of the mostly complex decay curves (according to the various half-lives of the fission products to be measured) the evaluation of numerous (30-60) γ-spectra is needed following a single irradiation[2]. The complete exploitation of the simplicity of this method demands the computerisation of the γ-spectrum evaluation procedure including the analysis of the decay curves.

One of the authors, participating in a program for the measurement of the ^{238}U fission yields at different neutron energies by both the radiochemical and γ-spectrometric method in the Argonne National Laboratory[3], had the opportunity to use existing computer programs to the above described purposes. Later these programs were adapted to the ES 1030 computer and significantly modified, to get a chain of compatible programs suitable for routine application in γ-spectrometric fission yield measurements. The principles and the applicability of this system in its present status is described below, while for details of the method itself the review of Daróczy et al.[1] at the previous symposium in Gaussig is referred.

General organisation of the system

According to the two major functions in the evaluation procedure, the system is organized around two main programs: the GAMANAL, which automatically evaluates the complex γ-spectra supplying the energies and activities of the γ-peaks; and the CLSQ, which fits the (complex) decay curves supplying the activities of the single resolved γ-lines with given half-lives at the time of the end of irradiation. The scheme of the system and the flow of data is shown in the figure.

The run of GAMANAL is preceded by a few "preparatory" programs. They convert the spectra, originating from various spectrometer systems and thus existing on different media and in different formats, into standard format on magnetic tape while adding a parameter set to them which characterizes the spectrum (indentification of the sample, irradiation, spectrum, geometry of the counting, time of the end of

irradiation and start of counting, real- and live-time of counting, random pile-up correction - if they are known before the evaluation of the spectrum - etc.) and is taken from input data cards. In addition to this main function, these programs can do corrections on spectra, e.g. for overflow automatically and for dropped channels according to input data cards as well as some rearrangement of the spectra using two input and one output magnetic tape.

The program GAMANAL runs under the control of "control cards" and, according to them, takes some input parameters (e.g. efficiency, shape and energy calibration function, identification of peaks for shape - or energy - calibration, etc.) from cards and the γ-spectra from magnetic tape in the above mentioned standard format. It evaluates even the very complex spectra automatically (without any preceding information on the peaks in it). The output "peak lists" are supplied both on magnetic tape (accompanied by the characteristic time parameters) and in a little more detailed format on lineprinter. More details on GAMANAL see below.

A program named ISOTOPE is inserted between the GAMANAL and CLSQ to prepare input data sets to the latter on magnetic tape, from the magnetic tape outputs of the former, selecting a γ-line of a given energy from successive spectra following an irradiation (separate program is available to merge "peak list" tapes of independent GAMANAL runs). The cooling times are calculated from characterisic time data, while the corrected (for the dead time and random pile-up losses) peak areas from the corrected activities supplied by the GAMANAL and the real time of counting (its role see below at the description of CLSQ). The energies for the selection accompanied by the half-lives of components to be fitted by CLSQ are taken from card input. The preparation of this information is not automatised yet and needs good catalogues of γ-ray energies and intensities (of fission products)[4] as well as lots of informations on the γ-line interferences, accumulated through the years devoted to the evaluation of fission product spectra.

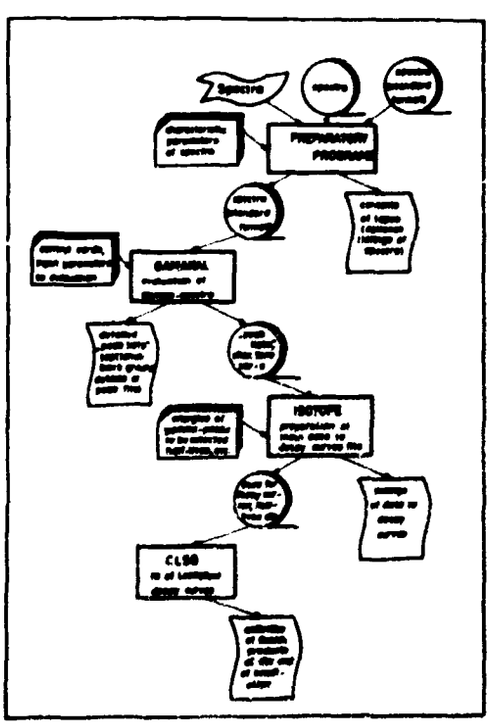

The GAMANAL program

The computer program for the automatic evaluation of very complex γ-spectra, named GAMANAL, was developed in the Lawrence Livermore Lab. by R.Gunnink and J.B.Niday[5]. A reduced (without graphical output and isotope identification options) and modified version was adapted to the IBM 370/195 computer by S.B.Kaufman at the Argonne Nat. Lab. This version was adapted to the ES 1030 in Debrecen by slight modifications mainly in the input and output routines.

The most important feature of this program is the way how the continuous background of the γ-spectra is handled. In most γ-spectrum fitting programs the background in a peak grouping, which is fitted at the same time, is described by the quite arbitrary function of polinomial (usually linear or quadratic) and is fitted together with the peaks. The result of this treatment is that the fitted background under a wide, complex

peak group can deviate from the realistic shape quite strongly, disturbing heavily the peak areas. In contrast with the procedure above, in the GAMANAL program a less arbitrary curve is used for the background, based on the regions between peaks (nonpeak regions) and interpolated beneath a peak with a smoothed step function taking into account both the hight and the slope of the background outside the peak region. The peak regions are distinguished from the nonpeak regions by a successive multiple smoothing, comparison, substitution procedure proposed in Ref[6]. This background is substracted from the entire spectrum resulting a net spectrum differing significantly from zero in the peak regions only.

The peak regions are fitted by an iterative procedure with the following "tailing Gaussian" function to each peak in the region:

$$y_i = y_o e^{\alpha(x_i-x_o)^2} + A y_o e^{B(x_i-x_o)} [1-e^{C(x_i-x_o)^2}]\delta$$

where $\delta=1$ for $(x_i-x_o)<0$ and $\delta=0$ for $(x_i-x_o)>0$; y_i: the net counts in channel x_i; x_o and y_o: the position and hight of the peak; while the remaining ones are the "shape parameters" of the peaks, namely $\alpha=-1/2\sigma^2$: the width of the peak; A, B and C: parameters describing the tailing function. It was found that the shape parameters B and C are constant for each peak in a spectrum while the energy dependence of the others can be described as follows:

$$[(FWHM)^2-0.46]\cdot(GAIN)^2=S1+S2\cdot E \quad \text{and} \quad \ln A=S3+S4\cdot E$$

where $FWHM=2.355\sigma$; 0.46:the Sheppard's correction; E:the peak energy. The six shape parameters (S1-S4, B,C) are characteristic to a spectrometer system at least at a given counting rate region and can be determined from single peaks of good statistics. Later they are used as input parameters at the fit of complex peak regions.

The program has options for outer and inner energy calibration by polynomial function, input of efficiency data for activity calculations and the determination of the product of dead-time and random pile-up corrections from a pulser peak in the spectrum. At the fit of shape parameters the printout contains the values of parameters in every step of iteration and a channel by channel list of the peak and the residuals, while at the evaluation of spectra this is an option only, as it is the list of the background and the "net spectrum", and the standard printout is a detailed peak list. Some special options of changing different criteria at the background determination and the fit procedures allow some control on the program (forcing to find very small peaks, resolving very close multipletts, etc.).

The CLSQ program

The program for the flexible analysis of complex decay curves, named CLSQ, was developed by J.B. Cumming in the Brookhaven Nat. Lab. and was used by S.B. Kaufman in the ANL. These versions of the program were to handle the experimental information on decay curve as points using the average activity at the midpoint time of the measurement. This leads to distortions if the time of a single counting is not short enough compared to the decay half-lives, which frequently occurs in the case of fission product spectra, since many products having very different half-lives should measure simultaneously. This problem was eliminated by the method applied in Debrecen long time ago using the integral number of emitted γ-quanta during the counting period instead of activity, describing them by the following formula[7]:

$$N_i = \sum_{k=1}^{K} \frac{A_k}{\lambda_k} [e^{-\lambda_k t_i} - e^{-\lambda_k (t_i + \Delta t_i)}]$$

where N_i: the number of γ-quanta in the i-th point of decay curve calculated from the corrected (dead-time and pile-up) activity supplied by the GAMANAL, multiplied

by the real time of the counting (Δt_i); t_i: its cooling time; K: the number of components in the decay curve; λ_k and A_k: the decay constant and the activity at zero cooling time (at the and of irradiation) of the k-th component. In our modification the program prints out, in addition to the parameters determined and their errors as well as the list of fitted points and residuals, the correlation coefficients of parameters, which are needed at error calculation of independent yields.

In the case of fission yield determinations the fits are done by fixed half-lives resulting more accurate determination of the initial activities while the program can fit the half-life of any component too by an iterative procedure. Further options of the program allow the substraction of constant or point by point changing background, known decaying components (decaying background), automatic rejection of points with too high residuals, dead-time correction, etc.

Application, acknowledgments

Currently this system is in use for fission yield determinations from the measurements made to determine the $^{238}U(n,2n)$ excitation function[8]. It seems to be flexible enough to be applicable in the case of the very complex spectra at the direct γ-spectrometric fission yield measurement, but can be operated efficiently enough to make possible the routine evaluation of the enormous amount of experimental information received at the application of this method for systematical investigations, like the one mentioned above. The most time consuming part of the system, the GAMANAL needs 5-10 minutes of computer time on the ES 1030 for a 4096 channel spectrum.

The system could be useful at any experiment concerned with the analysis of complex radioactive sources, e.g. the activation analysis of complex samples or the measurement of the product yields from heavy-ion-induced nuclear reactions[9].

The authors, especially the one who got acquainted with the computer programs in his possession at ANL, are very much obliged to Sheldon B. Kaufman for the programs supplied and for his expert advices in their use. We are also indebted to P. Jékel who paid special attention to our work in the Computer Center, to L. Sipos and B. Biró for their effort to handle incompatible magnetic tapes and for the entire staff of the center for their reliable work. The cooperation of I. Juhász and K. Sailer in the early part of adaptation work is acknowledged.

References

1. S.Daróczy et al., ZfK-376 (1978) p. 147
2. S.Daróczy, S.Nagy, P.Raics, Laboratory Manual, IAEA Training Course on Utilization of Neutron Generators, Debrecen, 1978
3. S.Nagy, et al., Phys. Rev. 17C (1978) 163
4. For example Ref's 9-12. in Ref. 2.
5. R.Gunnink, J.B.Niday, UCRL-51061, Vol. I-IV (1971-1972)
6. H.R.Ralston, G.E.Wilcox, Modern Trends in Activation Analysis (Ed.J.R.De Voe), National Bureau of Standards, Washington, D.C. (1969) Vol.II. p. 1238
7. S.Nagy, Flux Measurements Associated with Neutron Generator (Thesis), Inst. of Exp. Phys., Kossuth Univ., Debrecen, Hungary, 1970 (in Hungarian)
8. N.V.Kornilov, B.V.Zhuravlev, O.A.Salnikov, P.Raics, S.Nagy, S.Daróczy, K.Sailer, J.Csikai, Measurement of Cross Sections for the $^{238}U(n,2n)$ Reaction from 6.5 to 10.5 MeV, contribution to the present Symposium.
9. D.J.Morrisey, et al., Nucl. Instr. Meth. 158 (1979) 499

* Supported in part by the Hungarian Ministry of Education and the Acad. of Sci.

NUCLEAR DATA NEEDS AND RELATED ACTIVITIES OF THE IAEA NUCLEAR DATA SECTION

J.J. Schmidt

Nuclear Data Section, International Atomic Energy Agency, Vienna

Abstract

This paper gives an overview of part of the requests contained in the most recent edition of the World Request List for Nuclear Data (WRENDA 79/80) for charged particle, γ-ray and neutron nuclear data needed in selected areas such as the nuclear fission fuel cycle, nuclear fusion, nuclear materials safeguards, radiation damage and radiotherapy. Some of the activities of the IAEA Nuclear Data Section related to these requirements are briefly discussed.

1. Introduction

This report is not meant to give a complete overview of current nuclear data needs, but to present and discuss a few of the more recent nuclear data requirements for purposes other than fission reactor core design and to mention some of the activities of the IAEA Nuclear Data Section related to these requirements. Since the next speaker in this meeting will cover the area of nuclear data needs for fission reactors, I have chosen to speak about selected current nuclear data requirements for areas such as the nuclear fission fuel cycle, nuclear fusion, nuclear materials safeguards, radiation damage and radiotherapy. Under nuclear data we will, as usually, understand the numerical results of any scientific investigation of the nuclear properties of matter, with a subdivision in the three categories of nuclear structure, decay and reaction data. The energy range, over which nuclear reaction data are needed, extends today from thermal (for neutrons) to about 50 MeV (for neutrons and charged particles), covering the typical spectra of existing thermal and fast reactors and of planned fusion reactors, and higher energy spectra used for purposes such as radiation damage investigations for fusion reactors or cancer therapy. As basis for our discussion we choose the 1979/80 edition of the World Request List for Nuclear Data, WRENDA 79/80.

2. WRENDA 79/80

WRENDA 79/80, which has just been published [1], is the sixth edition of the World Request List for nuclear data measurements and evaluations. It is being published by the IAEA Nuclear Data Section on behalf of the National Nuclear Data Center (NNDC) of the Brookhaven National Laboratory in the USA, the Nuclear Energy Agency Data Bank (NEA-DB) at Saclay in France, the Centr po Yadernym Dannym (CJD = Nuclear Data Centre) at Obninsk in the USSR and the Nuclear Data Section (NDS) of the IAEA in Vienna. The WRENDA publication is produced from a computer file of nuclear data requests which is maintained by IAEA/NDS. The input to this file is provided predominantly by national nuclear data committees through these four nuclear data centres. 15 different IAEA Member States and one international organisation have contributed requests to WRENDA 79/80.

WRENDA is being used as a guide to experimentalists, applied nuclear theoreticians, evaluators and administrators for the planning of nuclear data programmes. The major WRENDA request areas are fission and fusion reactors and associated fuel cycles, and nuclear materials safeguards. In the 1979/80 issue, deviating from previous issues, in which requests for these three areas were listed separately, requests have been combined into a single unified list in order to allow the user, particularly the potential generator of the requested data, an easier identification of all requests for the same material and quantity. The status of requested standard reference and other data of crucial importance are under continuous review by the International Nuclear Data Committee (INDC) and the Nuclear Energy Agency Nuclear Data Committee (NEANDC).

A typical request is the following (request no. 35 in WRENDA 79/80):

Requested quantity:	3 LITHIUM 6 (N,TRITON) ALPHA
Energy:	1 KeV - 3 MeV
Accuracy:	1 %
Priority:	1
Country:	USA
Requester:	C.E. Till, Argonne National Laboratory P.R. Hemmig, US Department of Energy
Comments:	Accuracy of 3 % useful; energy resolution must reproduce true shape.
Justification:	For use as a standard.

WRENDA 79/80 contains altogether 1780 of such requests. The following table gives a breakdown of the WRENDA 79/80 requests into the major application areas in comparison to the previous edition WRENDA 76/77.

Application area	WRENDA 76/77	WRENDA 79/80
Fission	1194	1210
Fusion	328	449
Safeguards	150	121
Total	1672	1780

The only real change in the number of requests is seen to be in the field of nuclear fusion, i.e. an increase by more than 100 requests, reflecting the increasing interest in fusion as the nuclear energy source alternative to fission. The request turnover from the previous edition, however, is rather considerable: from WRENDA 76/77 465 requests were withdrawn and 487 requests modified; 573 requests, i.e. roughly one third, are new.

In the published list the requests for the same element/isotope and quantity (isoquant) are compressed in blocks which contain from one up to a maximum number of 18 different requests (neutron capture cross section of ^{241}Am). WRENDA 79/80 contains 900 request blocks corresponding to 900 different isoquants. On the average there are about two requests per individual isoquant. The following table gives a statistical breakdown of the isoquants into major data types (R = fission reactors, F = fusion, S = safeguards, E = energy deposition calculations for radiotherapy)

Data type	no. of isoquants	%	Major application area
Neutron reactions	814	90.4	R, F, E
Charged particle nuclear reactions	26	2.9	R, F, S
γ-ray yields	22	2.4	S
γ-reaction data	15	1.7	S
spontaneous fission data	5	0.6	S, R
half lives	12	1.3	S, R
decay heat	6	0.7	S
Total	900	100.0	

Most of the requests apparently still pertain to neutron data with fission and fusion reactors as major application areas. In the following we will briefly review the requests for "non-neutron" data, and for neutron data pertinent to fusion. In a few examples it will also be shown that,

- in spite of the large number of isoquants requested, neither all important application areas are as yet covered by WRENDA nor do all isoquants appear, which could have been expected to be entered into WRENDA for R, F and S applications,
- in spite of the fairly careful review of the previous WRENDA requests, a number of requests should not have appeared in WRENDA, because they are actually fulfilled and the requested data are available from the nuclear data centres.

3. "Non-neutron" data requests

3.1. Charged particle nuclear reaction data

Charged particle nuclear reaction data are requested for a variety of purposes, such as fission reactor fuel cycles, fusion and safeguards. There are important biomedical applications, which are not covered in WRENDA 79/80.

(i) Fission reactor fuel cycle

(α,n)-reactions initiated by α-particles emitted in α-decay of actinide nuclei present an actual (or potential) neutron source during all stages of the fission reactor fuel cycle from those elements or isotopes which have an (α,n)-threshold below the highest emitted α-energies. Requests appear in WRENDA 79/80 for

elements/isotopes: ^{6}Li, B, ^{13}C, ^{14}N, O, ^{17,18}O, ^{19}F, Mg, Si;
($A \cong 40$ is about the upper limit, since the (α,n)-threshold becomes too high);

α-energies: ~100 KeV – 7 MeV (or 10 MeV);

requested accuracy: 20–30 %

priority: mostly 2

purposes: fuel reprocessing;
neutron shielding during fuel transport and evaluation of neutron source strengths;
estimation of neutron output of solidified nuclear waste containing actinides.

(ii) "Conventional"-fuel fusion devices

The basic reaction for the present "conventional" magnetic confinement fusion devices such as tokamaks is the T(d,n)α-reaction. This reaction is well known at all practically important energies except below 10 KeV. Since these lower energies are important in the fusion ignition phase, measurements are requested there with high priority and 10 % relative accuracy.

In a plasma containing deuterons and tritons, also (T,T) and (D,D) reactions will occur, though less frequently as (T,D) reactions. The cross sections for these reactions are less well known than those for the (T,D)-reaction, nevertheless there is only one request for the T(t,2n)-reaction for energies below 10 KeV, with high priority and 10 % accuracy, for the purpose of analyzing background neutrons and estimating tritium ion temperatures.

The α-particles resulting from the $T(d,n)\alpha$ reaction can undergo elastic scattering on the plasma deuterons and tritons and thus contribute to plasma heating: the cross sections for these reactions are requested for energies up to 2 MeV, with high priority and 10 % accuracy, to calculate the associated plasma fuel heating.

One special lower priority 10 % accuracy request, illustrating the extent to which nuclear data are needed in nuclear energy design, is concerned with the $^{16}O(\tau,n)^{18}F$ reaction for triton energies below 12 MeV. This reaction needs to be known for a precise estimation of Li_2O burnup in fusion reactor blankets and the evaluation of the build-up of ^{18}O atoms from the β^+ decay of ^{18}F produced in the above reaction.

(iii) "Advanced"-fuel fusion devices

These devices are based on fusion reactions between light nuclei with no (or much less than in "conventional"-fuel devices) neutron production. The advantage of such fuel is less induced radioactivity, the disadvantage the need for much higher temperatures, at which the reactions become significant, than in (D,T) fusion reactors.

Only for illustration purposes we quote below an example of a fusion chain reaction which involves only charged particles:

$$p + {}^6Li \longrightarrow {}^3He + \alpha + 4.0\ MeV$$
$$\underline{{}^3He + d \longrightarrow p + \alpha + 18.4\ MeV}$$

Net reaction: $\underbrace{d + {}^6Li}_{\text{fuel}} \longrightarrow \underbrace{2\alpha}_{\text{ash}} + \underbrace{22.4\ MeV}_{\text{energy gain}}$

p and ^3He act as chain carriers.

In WRENDA 79/80 priority 1, 10 % accuracy requests are found for different reactions such as:

$^6Li\ (^3He,p)$
$^6Li\ (^6Li;\ n,\ p,\ d,\ \tau,\ ^3He,\ \alpha,\ n\alpha,\ p\alpha)$
$^{11}B\ (p,n);\ ^{11}B\ (\alpha,n)$ and $^{11}B\ (\alpha,p)$

always for incident particle energies of 500 KeV - 2 MeV.

(iv) Safeguards

For non-destructive nuclear materials safeguards thick target neutron yields from (α,n)-reactions with the following elements or isotopes are requested:

^6Li, ^9Be, C, O, ^{19}F, Mg, ^{27}Al, Ca
energy: 100 KeV - 6.5 MeV
accuracy: 3 % (relative); 6 % (absolute)
α-energy resolution: 100 KeV
priority: 2

(v) Biomedical application

As an example of charged particle and also neutron nuclear data requirements not contained in WRENDA we quote a typical biomedical application, i.e. cancer therapy by neutron irradiation of the afflicted tissue. As one common cyclotron neutron source the reaction ^{9}Be (d,n) is used. For this reaction the deuteron energy dependence of its cross section and the angular and energy distribution of the emitted neutrons need to be known for deuteron energies up to about 50 MeV. Then, as a function of neutron energy, cross sections for all reactions occurring in the energy range 15–50 MeV are needed as well as secondary angular and energy distributions for the neutron-producing reactions for the major constituents of the human body H, C, N, O, P and Ca. Particularly the neutron data are still largely lacking.

3.2. Gamma-ray data

(i) γ-ray yields

All requests for γ-ray yields contained in WRENDA 79/80 pertain to non-destructive safeguards measurement techniques. Requested are

- γ-ray yields per α-disintegration for well-defined γ-rays for the assay of Pu-isotopes by γ-spectrometry for
  - isotopes: $^{238,239,240,241}Pu$
  - γ-energies: ~ 45 KeV to ~ 650 Kev
  - accuracy: 1 % (!) (for ^{241}Pu: 5 %)
  - priority: 1;
- γ-ray yields per disintegration of individual fission products for well-defined γ-rays for burnup calculations from non-destructive measurements for
  - fission products: ^{103}Ru, ^{106}Rh, ^{125}Sb, ^{134}Cs, ^{140}La, ^{144}Ce, ^{144}Pr, ^{155}Eu
  - γ-energies: ~ 100 KeV to ~ 2.2 MeV
  - accuracy: 1 % (!)
  - priority: 2 (1 for ^{144}Pr);
- γ-ray yields per disintegration of individual fission products for detection of fuel failure for well-defined major γ-rays for
  - fission products: $^{87,88}Br$, ^{90}Kr, 135, 137, 138, 139$_{I}$, ^{139}Xe
  - γ-energies: ~ 100 KeV to ~ 1 MeV
  - accuracy: 10 %
  - priority: 3.

Obviously the first two groups of high accuracy γ-ray yield requests are not yet fulfilled.

(ii) γ-ray nuclear reaction data

All WRENDA 79/80 requests for γ-ray nuclear reaction data pertain to photonuclear assay of Pu and other fissionable isotopes. Two groups of requests can be discerned:

- In the first group, for the photonuclear assay of Pu, cross sections for the (γ, total neutron yield) and (γ-fission) reactions and the associated fission product mass yield spectra are requested for $^{238,241}Pu$ and ^{241}Am for γ-energies up to 10 MeV, 10 % accuracy and priority 2.

- In the other group, for Bremsstrahlung - photonuclear assay of nuclear materials the total fission yields produced by the Bremsstrahlung and the cumulative yields of high-fission-yield isotopes are requested for $^{235,238}U$ and $^{238,239,240,241}Pu$, the spectra covering γ-energies between 4 and 14 MeV, with 5-10 % accuracy and priority 3.

3.3. Spontaneous fission data

(i) For spontaneous fission (SF) measurements of plutonium in non-destructive safeguards $\bar{\nu}_{sf}$ is requested for $^{238,\ 240,\ 242}Pu$ to an accuracy of 1% and priority 2.

(ii) For the ^{252}Cf - $\bar{\nu}_{sf}$ standard NSEDNA 79/80 contains four priority 1 requests with accuracies between 0.25 and 0.3 %. The present situation as discussed by Smith [2] and Spencer [3] at the recent International Conference for Nuclear Cross Sections for Technology at Knoxville, USA, is summarised in the table below; this table is taken from the above references and contains the available measured $\bar{\nu}_{sf}$ data in the current state of correction.

Liquid scintillator measurements		
Spencer et al. [3,4]	3.792 ± 0.011	Weighted Average: 3.780 ± 0.009
Boldeman [5]	3.755 ± 0.016	
Asplund-Nilsson et al. [6]	3.792 ± 0.040	
Hopkins and Diven [7]	3.777 ± 0.031	
Manganese bath measurements		
Axton et al. [8]	3.743 ± 0.019	Weighted Average: 3.750 ± 0.011
de Volpi and Porges [9]	3.747 ± 0.019	
Bosorgnanesh [10]	3.744 ± 0.023	
Alekseandrov et al. [11]	3.747 ± 0.036	
White and Axton [12]	3.815 ± 0.040	
Boron pile measurement		
D.W. Colvin et al. [13]	3.739 ± 0.006	

The difference between the weighted average values resulting from the liquid scintillator and manganese bath measurements respectively is 0.8 %, and it should be noted, that, with the exception of the White-Axton value, the manganese bath results are in excellent agreement.

J.R. Smith discussed at the recent Knoxville Conference [2] a possible systematic error associated with all manganese bath measurements. In determining the source strength in these measurements the thermal absorption cross section of sulfur may have been assumed too low, in accordance with the old measurements by Pomerance [14]. A re-analysis of the Pomerance data and of the available total cross section data of sulfur in the thermal energy range led Smith to the conclusion, that the thermal absorption cross section of sulfur may be higher by 5 % or more, which could account for as much as 0.5 % of the 0.8 % difference between Mn bath and liquid scintillator measurements. In order to confirm this conclusion, Smith recommends a remeasurement of the thermal surlfur absorption cross section to an accuracy close to 1 %.

(iii) Spontaneous fission neutron spectrum of ^{252}Cf

Five requests in WRENDA 79/80 pertain to this quantity. Spectral data are requested with 5–10 % accuracy at the low (< 0.25 MeV) and high (>5 MeV) energy tails of the spectrum, and the average energy to 1–2 % accuracy. This subject will be extensively discussed at the forthcoming IAEA/NDS Consultants Meeting on Neutron Source Properties to be held at Debrecen, Hungary, 17–21 March 1980. First results from IAEA/NDS contract work performed at Leningrad for energies between 10 KeV and 2 MeV reported in another paper to this Symposium [16] can be well described by a smooth Maxwellian spectrum shape with a nuclear temperature T = 1.42 MeV and reveal definitely no structure in the low-energy tail of the spectrum.

3.4. Half life data

The following table summarizes the half life requests contained in WRENDA 79/80 and compares the requested accuracies to those presently reached, in accordance with recent recommendations by the members of the IAEA/NDS Coordinated Research Programme on the Measurement and Evaluation of Transactinium Isotope Decay Data [17].

Isotope	Decay type	Accuracy (%)		Priority	Purpose
		requested	reached [17]		
^{232}U	α	0.5	1.4	1	(a)
^{233}U	α	0.5	0.13	1	(a)
^{234}U	α	0.3	0.29	1	(a)
^{235}U	α	0.3	0.10	1	(a)
^{238}U	α	0.3	0.10	1	(a)
^{237}Np	α	1.0	0.47	1	(a)
^{238}Pu	SF	1.0	2.7	2	(b)
^{239}Pu	SF	1.0	9.0	2	(b)
^{240}Pu	α	1.0	0.30	1	(a)
^{240}Pu	SF	1.0	4.0	2	(b)
^{242}Pu	SF	1.0	1.1	2	(b)

(a) Verification of α-half lives required for the mass determination of fissionable deposits;

(b) Detection of plutonium by spontaneous fission measurements in non-destructive safeguards.

The table shows that most of the α-decay half lives are known to better accuracies than the ones requested, except for ^{232}U. For spontaneous fission half lives the situation is just the inverse: the accuracies reached are much lower than those requested, with the exception of ^{242}Pu where the requirement seems to be met. IAEA/NDS has communicated these facts to the requestors concerned.

On the other side it is astonishing and illustrates the incompleteness of WRENDA to see that one of the most urgently needed actinide half-lives, i.e. that of ^{241}Pu, whose measured values differ by several percent, does not show up in WRENDA.

3.5. Decay heat data

For the first time WRENDA contains requests for decay heat measurements for the calorimetric assay of plutonium for safeguards purposes, for the Pu isotopes ($238 \leq A \leq 242$) and ^{241}Am, with an accuracy of 0.3 - 0.5 % and priority 1.

4. Neutron cross section requests for fusion

We restrict our discussion to selected neutron data requests for fusion applications contained in WRENDA 79/80. The requirements and status of nuclear data for fusion were comprehensively reviewed at the recent IAEA Advisory Group Meeting on Nuclear Data for Fusion Reactor Technology held in Vienna in December 1978 [18].

(i) Blanket tritium breeding

^{6}Li(n,α)T and ^{7}Li(n,n'α)T are the well-known nuclear reactions to be used for tritium breeding in fusion reactor blankets. For tritium breeding calculations one has not only to know the cross sections for these two reactions, but also those for all competing reactions with ^{6}Li and ^{7}Li over the energy range of fusion reactor neutrons. As a consequence, in addition to the cross sections for the above two breeding reactions, cross sections for no less than 27 competing neutron reactions with ^{6}Li and ^{7}Li are requested, e.g. (with Θ and E' meaning angle and energy of the emitted particles):

(n,n), (n,n)(Θ), (n,n'), (n,n')(Θ), (n,n')(E'),
(n,2n), (n,2n)(Θ), (n,2n)(E'), (n, neutron emission)(Θ,E'),
(n,p), (n,np), (n,nd), (n,γ),
(n, total photon production), (n, total proton production) and
(n, total α-production),

for neutron energies up to 15–20 MeV, with accuracies of 10–20 % and priority 1–2. In the table below we give a brief summary of a few more prominent requests.

Isotope	Quantity	Energy	Accuracy %	Priority
^{6}Li	(n,nd)	up to 15–20 MeV	10–20	1–2
	(n,α)	100 KeV - 15 MeV	3–10	~ 1
^{7}Li	(n,n)(Θ)	1–20 MeV	~ 10	~ 1
	(n,n'), (n,n')(Θ)	0.5–20 MeV	10–20	~ 1
	(n, neutron emission)(E',Θ)	9–14 MeV	10	~ 1
	(n,n'α)	3–20 MeV	5–20	1

The current discrepancy of 25 % between the recent Harwell measurements [19] and previous measurements on ^{7}Li (n,n'α) has not yet been resolved.

In addition to the above, for the calculation of helium accumulation in Li-oxide blankets ^{16}O(n,α) and ^{16}O(n,nα) cross sections are requested with 15 % accuracy, for neutron energies up to 15 MeV, and with priority 2.

(ii) Coolant

^{19}F is considered as a potential constituent of FLiBe coolant. This explains requests for (n,n)(Θ), (n,n'), (n,2n), (n,d), (n,p) and (n,α) cross sections for neutron energies up to 15 MeV, 10–20 % accuracy and priority 2–3.

(iii) First wall and structural materials

For the most important materials considered, i.e. Cr, Fe, Ni (as the most important "classical" steel constituents), but also Ti, V, Mo and W, (n,n'), (n,2n), (n,p), (n,α), (n,γ) and (n, total γ-production) cross sections are requested for neutron energies up to 15 MeV, mostly with 10–15 % accuracy and priority 2–3.

(iv) Radiation damage calculation

The following table excerpted from table IB of reference [18] illustrates the wide variety of materials and material compounds for which radiation damage is to be calculated; more common structural materials are not included in this table.

Material use	Materials									
	Be	B	C	N	O	F	Al	Cu	Sn	Pb
Internal first wall protection	X		X		X		X			
Neutron multipliers	X									X
Structural materials			X				X			
Magnet conducting materials	X						X	X	X	
Reflectors and moderators	X	X	X		X					
Shielding materials		X	X		X					X
Coolants	X			X	X	X				X

For the purpose of radiation damage calculations, for the structural materials appearing under (iii) and for ^{9}Be, $^{10,11}B$, C, ^{14}N, O, ^{19}F, ^{27}Al, Si, Cu, ^{93}Nb, Sn and Pb data for the following quantities are requested:

(n, p-production)(E_p, Θ_p), (n, α-production)(E_α, Θ_α),
(n, total p-production), (n, total α-production),

for neutron energies between 9 and 14 MeV with accuracies of 10 % and priority 2.

In response to the many WRENDA requests for fusion, but also fission reactor and other purposes, entailing in particular the requirement for better 14 MeV cross section and secondary particle distribution data, and in view of the potential of several developing countries to contribute to a co-operative effort, IAEA/NDS is planning a coordinated research programme for the determination, i.e. measurement and calculation, of those 14 MeV data which need improvement, particularly for the purposes of fusion. In this context the conclusions and recommendations of the IAEA/NDS Fusion Nuclear Data Advisory Group Meeting [18] will also be taken into account.

(v) Requirements for the Fusion Materials Irradiation Test Facility

I would like to finish with a brief discussion of a group of completely new data requests contained in WRENDA 79/80. The US Department of Energy has submitted a number of new neutron data requests related to the Fusion Materials Irradiation Test Facility (FMIT) planned to be built at the Hanford Engineering Development Laboratory for the main purpose

of investigating radiation damage through neutron reactions with fusion reactor materials. The Li (d,n) reaction used to simulate the radiation damage expected in fusion reactors produces neutrons with energies up to 50 MeV. This requires an extension of the knowledge of neutron nuclear data to equally high energies. In the following we group the WRENDA requests concerning FMIT in tabular form according to different purpose.

<u>Material damage calculations</u>

Materials: Ti, V, Cr, Fe, Ni, Cu, ^{93}Nb, Sn

Quantities: (n,n)(Θ), (n, neutron emission)(E',Θ)
(n, total p-production), (n, total α-production)

Energies: 15–35 MeV

Accuracy: 10 %

Priority: 1

<u>FMIT Shield design</u>

Materials: C, O, Si, Ca, Fe

Quantities: (n,total), (n,n)(Θ), (n,X)

Energies: 20–50 MeV

Accuracy: 10 %

Priority: 1

<u>FMIT neutron dosimetry</u>

Quantities: ^{54}Fe(n,α), ^{59}Co(n; 2n; 3n; 4n), ^{59}Co(n,p),
^{58}Ni(n; 2n; 3n), ^{58}Ni(n,p), ^{60}Ni(n,p),
^{197}Au(n, 2n; 3n; 4n; 5n)

Energies: threshold (or 1 MeV) – 40 MeV

Accuracy: 20 %

Priority: 1

These higher energy neutron data requests, together with biomedical nuclear data requirements, present a new challenge to the community of nuclear data measurers and theoreticians.

References

1. WRENDA 79/80, "World Request List for Nuclear Data", D.W. Muir, IAEA/NDS, editor; INDC(SEC)-73/URSF, October 1979.

2. J.R. Smith, "The ^{252}Cf $\bar{\nu}$ discrepancy and the sulfur discrepancy", International Conference on Nuclear Cross Sections for Technology, Knoxville, USA, October 1979, paper GA 4.

3. R.R. Spencer, "Absolute measurement of $\bar{\nu}_p$ for ^{252}Cf by the large liquid scintillator tank technique", International Conference on Nuclear Cross Sections for Technology, Knoxville, USA, October 1979, paper GA 2.

4. R.R. Spencer, R. Gwin, R. Ingle, and H. Weaver, ORNL/TM-6805, 1979.

5. J.W. Boldeman, Nucl. Sci. Eng. 55, 188, 1974.

6. I. Asplund-Nilsson, H. Condé and N. Starfelt, Nucl. Sci. Eng. 16, 124, 1963.

7. J.C. Hopkins and B.C. Diven, Nucl. Phys. 48, 433, 1963.

8. E.J. Axton, A.G. Bardell and B.N. Andric, EANDC(UK)-110, p. 70, National Physical Laboratory, 1969; E.J. Axton in "Neutron Standard Reference Data", p. 261, 1974.

9. A. de Volpi and K.G. Porges, Phys. Rev. C1, 683, 1970.

10. H. Bozorgmanesh, PhD dissertation, University of Michigan, 1977.

11. B.M. Aleksandrov et al., Proceedings of the 1975 Kiev Conference on Neutron Physics, Vol. 5, p. 166.

12. P.H. White and E.J. Axton, J. Nucl. En. 22, 73, 1968.

13. D.W. Colvin, M.G. Sowerby and R.I. MacDonald, Proceedings of the IAEA Conference on Nuclear Data for Reactors, Vienna, Vol. I, p. 307, 1967.

15. H. Pomerance, Phys. Rev. 83, 64, 1951.

16. V.A. Vitenko, M.B. Blinov et al.. "Spectral shape of fission neutrons from the spontaneous fission of ^{252}Cf in the low-energy range", paper reported at this Symposium.

17. Proposed recommended list of transactinium isotope decay data, Part I. Half lives (September 1979 edition); A. Lorenz, editor; INDC(NDS)-108/N, September 1979.

18. IAEA Advisory Group Meeting on Nuclear Data for Fusion Reactor Technology, Vienna, 11-15 December 1978; Summary Report INDC(NDS)-101/LF, edited by A. Lorenz and D.W. Muir, IAEA/NDS, May 1979.

19. M. Swinhoe and C.A. Uttley, "Tritium breeding in fusion", International Conference on Nuclear Cross Sections for Technology, Knoxville, USA, October 1979, paper CA 3.

THE INFLUENCE OF DIFFERENT LEVEL DENSITY REPRESENTATIONS ON ACTINIDE NEUTRON CROSS SECTION CALCULATIONS

G.V.Antsipov, V.A.Zenevich, A.B.Klepatskii, V.A.Konshin, E.Sh.Sukhovitsky

Heat and Mass Transfer Institute,BSSR Academy of Sciences,Minsk,USSR

At present the Fermi-gas level density model is widely used in statistical theory calculations. Recently, there have appeared a number of works showing that the Fermi-gas level density model is not consistent with the microscopic theory and some experimental data [1]. Alongside the rigorous and very tedious microscopic level density models [2,3], the statistical averaging methods [4,5] are also developed. The latter are rather simple, convenient for practical calculations and incorporate the basic results of the microscopic theory. These models allow for the existing shell inhomogeneities in the single-particle level spectrum and both for the superconducting correlation and coherent collective effects. In statistical calculations, the radiative capture cross section, $\sigma_{n\gamma}$, proves to be most sensitive to the level density model adopted. Moreover, the calculation of the $\sigma_{n\gamma}$ cross section of heavy fissile nuclei should take into account the fission competition and deformation of these nuclei. The latter fact involves a substantial change in the level density due to a contribution of the rotational bands and a change in neutron transmission coefficients caused by the direct excitation of the lower collective states.

Based on the simultaneous calculation of all neutron ^{238}U cross sections, an attempt is made in the present work to study the influence of different level-density models on the energy dependence of the $\sigma_{n\gamma}$ cross section, to analyze the effect of the uncertainties in $\langle D \rangle$ and $\langle \Gamma_\gamma \rangle_{obs}$ on $\sigma_{n\gamma}$ and to substanciate a choice of the spectral factor.

The neutron transmission coefficients required for statistical calculations were predicted using the coupled channel method [6] with the parameters of the non-spherical potential carefully optimized using the experimental data:

$$V = (45.37-0.4\ E\ )\ \text{MeV}, \quad r = 1.258\ f, \quad a = 0.626\ f$$

$$W_D = (2.95 + 0.4\ E\ )\ \text{MeV}, \quad r_D = 1.260\ f, \quad a_D = 0.530\ f \qquad (1)$$

$$V_{SO} = 7.5\ \text{MeV}$$

$$\beta_2 = 0.216, \quad \beta_4 = 0.078.$$

This potential allows us to calculate, within experimental errors, the strength functions S_0 and S_1; σ_t, σ_{el}, and elastic and inelastic angular neutron distributions up to E = 5 MeV. Thus, we can consider that the neutron transmission coefficients are calculated rather reliably.

1. Level density models used for calculations and radiative capture transmission coefficients

The traditional Fermi-gas model gives the following expression for $\rho(U,J)$:

$$\rho_{F.-G.}(U,J) = \frac{2J+1}{24\sqrt{2}\sigma^3 a^{1/4}(U-\delta)^{5/4}} \exp\{2\sqrt{a(U-\delta)} - \frac{(J+0.5)^2}{2\sigma^2}\},$$

$$\sigma^2 = \frac{6}{\pi^2}\bar{m}^2/\tilde{a}(U-\delta) \qquad (2)$$

where a is the main level density parameter proportional to the single-particle state density on the Fermi surface and determined from the neutron resonance density. The quantity $\bar{m}^2$ is usually chosen based on the quasi-classical estimation of $(0.22 \div 0.25\ A^{2/3})$, and the value of δ is identical with the similar one in the mass formula.

The shell effects in the Fermi-gas model are allowed for, by introducing into the mass formula [7], the excitation energy-dependent parameter a and the shell correction δW:

$$a = \tilde{a}[1 + f(U).\delta W/(U-\delta)],$$
$$f(U) = 1 - \exp[-\gamma(U-\delta)] \qquad (3)$$

where $\tilde{a}$ and γ are the parameters determined in terms of systematics.

With the collective effects taken into account, formula (2) assumes the form:

$$\rho(U,J) = K_{rot} \cdot K_{vib} \cdot \rho_{F.-g.}(U,J) \qquad (4)$$

The level density increase coefficients K_{rot} and K_{vib} due to the rotational and vibrational modes and the factor σ^2, following the adiabatic estimation, are expressed as in [5,8]:

$$K_{rot} = F_{\perp} \cdot t \quad , \qquad (5)$$

$$K_{vib} = \exp(0.25\ a^{2/3}t^{4/3}), \qquad (6)$$

$$\sigma^2 = F_{\perp}^{2/3} \cdot F_{\parallel}^{1/3} \cdot t \qquad (7)$$

where $F_{\perp}$ and $F_{\parallel}$ are the perpendicular and parallel inertia moment, respectively; t the excited nucleus temperature.

The relations for the level density of the superfluid nucleus model were taken from [5]. Unlike [5], we used K_{vib} in the form of (6) and did not allow for the energy dependence of the parameter a which can be ignored at small δW.

The radiative capture transmission coefficients were calculated by the cascade γ-quantum emission theory [9], with the competition reactions $(n,\gamma n')$ and $(n\gamma f)$ being taken into account as in [10]. The expression for the radiative capture transmission coefficients is of the form:

$$T_{\gamma J^{\pi}}(E) = 2\pi \int_{\frac{A}{A+1}E}^{\frac{A}{A+1}E_{\gamma S}} \sum_{J_k=|J-1|}^{J+1} \rho(E+S_n-\varepsilon_{\gamma}, J_k^{\pi}k) f(E,\varepsilon_{\gamma}) d\varepsilon_{\gamma} \qquad (8)$$

$\sigma_{n\gamma}$ cross sections are usually calculated using the spectral factor $f(E,\varepsilon_{\gamma})$ either in the Weisskopf form $(f(E,\varepsilon_{\gamma}) \sim \varepsilon_{\gamma}^3)$ or in the Lorentz form that follows from the experimental data on photoabsorption cross sections:

$$f(E,\varepsilon_{\gamma}) = \frac{8}{3}\frac{NZ}{A}\frac{e^2}{\hbar c}\frac{1.4}{m_e c^2}\sum_{i=1}^{2}\left(\frac{i}{3}\right)\frac{\Gamma_{iG}\ \varepsilon_{\gamma}^4}{(\varepsilon_{\gamma}^2-E_{iG}^2)^2+(\Gamma_{iG}\varepsilon_{\gamma})^2} \qquad (9)$$

The Weisskopf factor in many cases gives satisfactory results for $\sigma_{n\gamma}$ but does not ensure the agreement with the experimental data for the energy dependences of the

radiative strength functions [11]. The use of the Lorentzian spectral factor is more physically grounded, but in this case, as has been mentioned, for example, in [12], the agreement between the experimental and calculated $\sigma_{n\gamma}$ becomes worse and the calculated values of $\sigma_{n\gamma}$ prove to be substantially higher against the experimental ones.

Since the radiative capture transmission coefficients depend on the level density of a compound nucleus, it may be assumed that this disagreement between theory and experiment is caused by the incorrectness of the Fermi-gas model. This conclusion was made in [1] where ^{238}U $\sigma_{n\gamma}$ calculations were performed up to 1 MeV (when fission competition was not allowed for) using the spherical optical neutron transmission coefficients.

2. Discussion

The ^{238}U neutron cross sections were calculated by Hauser-Feshbach's statistical model. The modified Hauser-Feshbach's model was used up to 1.3 MeV and allowed for the fluctuation effects of neutron widths and the correlation effects of the elastic inlet and outlet channels [14]. Above 1.3 MeV, the calculations were made using Tepel's formalism [15]. The scheme of the ^{238}U nucleus levels was taken from [16]. The fission competition was allowed for in terms of the fission transmission coefficients in the form that takes into account their spin dependence

$$T_{FJ^{\pi}} = (2J+1)\exp\left[-\frac{(J+\frac{1}{2})^2}{2\sigma^2}\right]T_f \qquad (10)$$

where T_f was determined by fitting the calculated fission cross section to the experimental one.

The calculated cross sections for discrete level excitation in the energy range up to 2.0 MeV agree well with the experimental ones (Fig. 1).

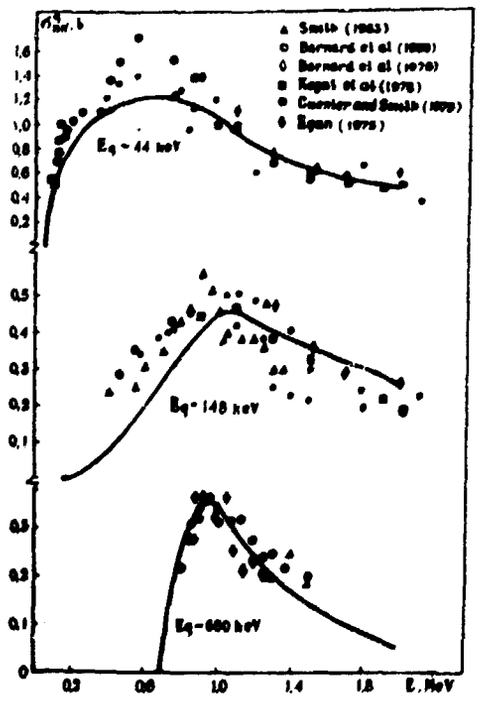

Fig. 1. Comparison of the calculated 44, 148 and 680 keV excitation level ^{238}U cross sections with the experimental ones

Thus, the chosen parameters of the statistical model govern all neutron cross sections, except $\sigma_{n\gamma}$. The calculated radiative capture cross section depends strongly on the adopted level density model. This fact permits us to choose such a level density model that ensures the best agreement between the calculated and experimental cross sections over a wide energy range.

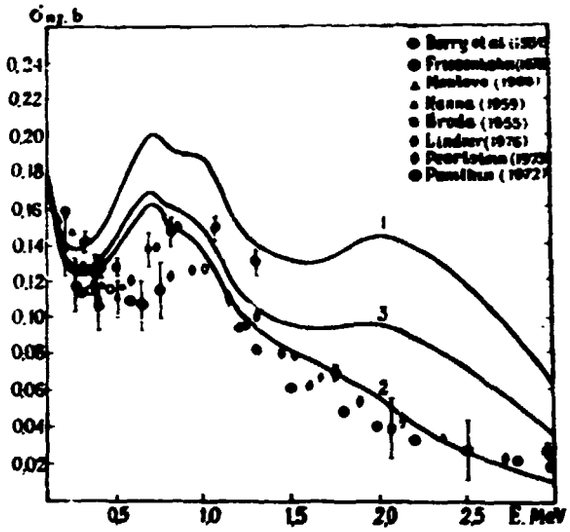

Fig. 2. Comparison of the ^{238}U $\sigma_{n\gamma}$ cross sections calculated by different level density models and the Lorentzian spectral factor with the experimental ones: 1, Fermi-gas model; 2, Fermi-gas model involving the collective modes; 3, superfluid model involving the collective modes ($\langle D\rangle_{obs}$=24.8 eV [17], $\langle\Gamma_\gamma\rangle_{obs}$=23.5 meV (ENDF/B-IV))

Figure 2 gives the comparison between the radiative capture ^{238}U cross section, predicted using the Lorentzian spectral factor and different level density models, and experimental $\sigma_{n\gamma}$ in the energy range from 0.1 to 3 MeV where the non-compound mechanism of the radiative capture can be neglected. This comparison illustrates that the better agreement between theory and experiment in the whole energy range is achieved when the Fermi-gas model involving the collective modes is used. The use of the superfluid nucleus level density model leads to the discrepancy between theory and experiment in the 1.2 - 3.0 MeV range, while in the range up to 1.2 MeV the agreement is just the same as in the case of the Fermi-gas model involving the collective modes. The greatest discrepancy between theory and experiment is observed when the traditional Fermi-gas model is employed. The introduction of the energy dependence of the parameter a into the Fermi-gas model does not substantially change the calculated $\sigma_{n\gamma}$ cross section. This can be attributed to a relatively small value of the shell corrections, δW, for ^{238}U and ^{239}U.

The use of the Weisskopf spectral factor does not lead to a better agreement between the calculated and experimental $\sigma_{n\gamma}$ cross sections than the one achieved using the Lorentzian spectral factor and the Fermi-gas model involving the collective modes. Therefore, bearing in mind the greater physical significance of the Lorentzian spectral factor that follows from the photoabsorption experiments and the better agreement between the calculated and experimental data for the (n,γf)-reaction, it becomes advisable to use it in statistical theory calculations.

It should be noted that the unique choice of a better level density model used for $\sigma_{n\gamma}$ calculations may be substantially affected by the uncertainties of such quantities as $\langle D\rangle_{obs}$ and $\langle\Gamma_\gamma\rangle_{obs}$ and by the values of the neutron transmission coefficients (Fig. 3), although these uncertainties unable to explain this considerable difference between the experimental and calculated data obtained using

the traditional Fermi-gas model. Note that our calculated ^{238}U $\sigma_{n\gamma}$ data give evidence for a high value of $\langle D \rangle_{obs}$=24.8 eV [17].

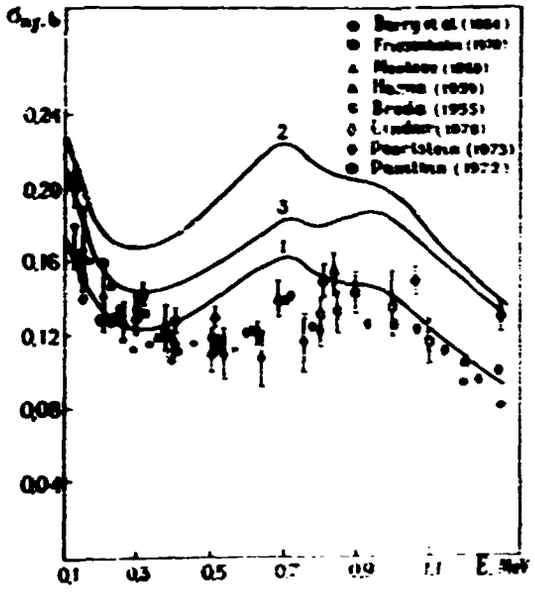

Fig. 3. The calculated ^{238}U $\sigma_{n\gamma}$ cross section versus $\langle D \rangle_{obs}$ and neutron transmission coefficients (Fermi-gas model involving the collective modes, the Lorentzian spectral factor, $\langle \Gamma_{\gamma} \rangle_{obs}$=23.5 meV (ENDF/B-IV): 1, $\langle D \rangle_{obs}$ = 24.8 eV [17], potential (1); 2, $\langle D \rangle_{obs}$= =17.7 eV [18], potential (1); 3, $\langle D \rangle_{obs}$= 17.7 eV [18], spherical potential [16]).

We assume that the conclusions of the present work may be employed to predict neutron cross sections of heavy nuclei that are insufficiently studied experimentally. As an example, Figure 4 gives the comparison of the ^{242}Pu $\sigma_{n\gamma}$ cross sections evaluated by different authors and our $\sigma_{n\gamma}$ predicted using potential (1), the Lorentzian spectral factor and the Fermi-gas model involving the collective modes.

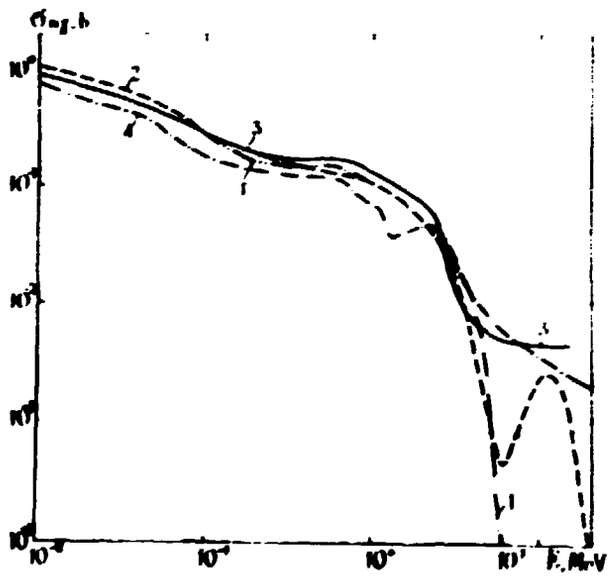

Fig. 4. Comparison of the calculated ^{242}Pu $\sigma_{n\gamma}$ cross section with the evaluated data of other authors : 1, [19]; 2, [20]; 3, present work; 4, ENDF/B-IV)

3. Conclusion

1. The use of the non-spherical optical potential, the Lorentzian spectral factor and the Fermi-gas level density model involving the collective modes permits the self-consistent calculation of all ^{238}U cross sections, including $\sigma_{n\gamma}$,

over a wide energy range.

2. The application of the traditional Fermi-gas model gives a considerable disagreement between the calculated and experimental $\sigma_{n\gamma}$ cross sections for both forms of the spectral factor which cannot be explained by the uncertainties of the parameters used.

3. It is necessary to adopt the non-spherical potential for calculations of the neutron transmission coefficients used in the statistical model.

4. When calculating the radiative capture cross section, special attention should be paid to a proper choice of $< D >_{obs}$ and $< \Gamma_\gamma >_{obs}$ which must be based on the experimental data evaluation.

5. As compared to the Lorentzian factor, the use of the Weisskopf spectral factor does not ensure better ^{238}U $\sigma_{n\gamma}$ cross section calculations.

References

1. Blokhin A.I., Ignatyuk A.V., Platonov V.P., Tolstikov V.A., Yadernye Konstanty (Nuclear Constants), issue 21 , 1976, p. 3.
2. Soloviev V.G.,Stoyanov Ch.,Vdovin A.I.,Nucl.Phys.,1974, A224,p.411.
3. Voronov V.V.,Komov A.L.,Malov L.A.,Soloviev V.G., Yadern.Fiz.,1976,v.24,p.504.
4. Ignatyuk A.V.,Shubin Yu.N.,Izv.AN SSSR,Ser. Fiz., 1975, v. 37, p. 1947.
5. Ignatyuk A.V.,Istekov K.K.,Smirenkin G.N., Yadern.Fiz., 1979, v.29, p.875.
6. Tamura T., Rev. Modern Phys., 1965, v. 37, p. 679.
7. Ignatyuk A.V., Smirenkin G.N., Tyapin A.S., Yadern.Fiz., 1975, v. 23, p.485.
8. Ignatyuk A.V.,Istekov K.K.,Smirenkin G.N., Proc. 4th All-Union Conference on Neutron Physics,Kiev, 1977, pt. 1, p. 60.
9. Blatt J.M., Weisskopf V.F.,Theoretical Nuclear Physics,Wiley,New York,1952
10. Sukhovitsky E.Sh., Klepatskii A.B., Konshin V.A., Antsipov G.V., Proc. 4th All-Union Conference on Neutron Physics, Kiev, 1977, pt. 4, p. 68.
11. Bartholomew G.A. et al.,Advanced Nuclear Physics, 1974, v. 7, p. 232.
12. Friche M.P. et al., Proc. IAEA Conference on Nuclear Data for Reactors,Vienna, 1970, v. 2, p. 265.
13. Hauser W., Feshbach H., Phys. Rev., 1952, v. 87, p. 366.
14. Moldauer P.A., Phys. Rev., 1961, v. 123, p. 968.
15. Tepel J.W., Hofmann H.M., Weidemüller H.A., Phys. Lett., 1974, v.49B, p.1.
16. Lambropoulos P., Nucl.Sci.Eng., 1971, v.46, p. 355.
17. De Saussure G.,Olsen D.K.,Perez R.B.,Difilippo F.C., ORNL/TM-6152/ENDF-257/, 1978.
18. Mughabghab S.F., Garber D.I., BNL-325, 1973, 3rd ed., v.1.
19. Lagrange Ch.,Jary J., NEANC(E) 198 "L", INDC(FR)30/L, 1978.
20. Baxman C.I., Young P.G., LA-7432-PB, 1978.

FIRST RESULTS IN EVALUATION OF NEUTRON NUCLEAR DATA FOR Si

D. Hermsdorf, L. Neumann
Technische Universität Dresden, Sektion Physik, DDR - 8027 Dresden

1. Introduction

At present the main activity of the nuclear data evaluation group of the TU Dresden is focused on the evaluation of a complete file for Si including all neutron induced reaction cross sections, angular distributions and emission spectra for particles and γ- quanta up to 20 MeV neutron incidence energy. A complete file has been envisaged regarding to the eminent practical importance of Si for reactor design, both in fusion and fission reactors, in radiation shielding and solid state physics.

Such a comprehensive work has to be divided into subsequent steps in order to retain the survey. Therefore only the first results can be reported on.

The contribution is aimed at

i comments on the reliability of recommended data files for Si;
ii problems in application of reaction models for cross sections calculations;
iii interpretation of experimental data in the frame of different reaction models.

2. Analysis of available nuclear data files for Si

In order to substantiate the decision of creating a new evaluated data file and to motivate the extensive and labourious work related to it, all available data files have been investigated intensively. Up to now, in free international exchange the compiled in table 1 files exist.

Abstracting from all details of an intercomparison of recommended data four arguments for a new evaluation can be given

i there is no really independent evaluation later then 1973;
ii recommended data strongly deviate in nearly all quantities given in the files (figs. 1 to 5 are examples choosen for demonstration);
iii recently most reliable experiments have been carried out and are available via the EXFOR library which can be managed by the DAPROC computer code developped at the TU [7]. Also those measurements performed by the nuclear physics group of the TU should be involved [8,9];
iv in the author's opinion, a data file should not be a complete file only but also as flexible as possible against different purposes. So the most convenient representation type for every quantity has to be loocked for and should be preferred.

3. Models used for evaluation

In table 2 all models applied for nuclear data evaluation for Si have been compiled along with their ranges of validity and the reaction types which are

calculable in the frame of them.

First of all, in the whole energy range considered here the optical model has been applied to yield the optical potential well fitting all elastic scattering data. Basing on these parameters (or the related transmission coefficients respectively) the treatment of the compound - elastic scattering and the excitation of discrete levels in ^{28}Si and the corresponding residual nuclei ^{28}Al and ^{25}Mg by the Hauser - Feshbach - formalism has been performed by use of the code ELISA [10] which is a modified version of the well - known Japanese code ELIESE-2. The ELISA code is limited to the handling of the discrete level structure only. So the calculations has to cut off at 9 MeV because spin and parity assignments are ambigous above this energy [11].

The continuation of the calculations including the excitation of states within the level continuum has been done by the code STAPRE [12]. Besides the inclusion of continuously distributed levels the main advantage of this code is the extension of the Hauser - Feshbach - formalism to deal with γ- deexcitation of all populated levels as a competitive decay mode, the successive multi - particle emission as well as the treatment of first chance particle emission in terms of the Exciton model.

The low - lying level spectrum of ^{28}Si shows features of vibrational as well as rotational motions. The interpretation of the excitation of these states via the $^{28}Si(n,n')$ reaction has been carried out by Streil [13] in the frame of collectiv reaction models using both DWBA and coupled - channels - mode of the computer code CHUCK-2. In the context of the present contribution only the analysis in terms of the Optical model and different statistical models will be reported on.

According to the main constituents of natural Si the model calculations have been performed for ^{28}Si with only three exceptions concerning the threshold reactions $^{29}Si(n,p)$, $^{29}Si(n,\alpha)$ and $^{29}Si(n,2n)$.

4. Problems and results of the application of nuclear models for the evaluation of cross sections, angular distributions and particle spectra

4.1. Consistency of parameters

In all models applied, a point has made of the use of the same parameters, i.e. optical potentials, deformations, level densities, binding energies and other ones. Some problems of finding such a parameter set arise from the failure of experimental data or from their uncertainties and disagreement.

4.2. Neutron elastic scattering

Different optical potential parameter sets given by Bhat [3], Holmqvist [14], Obst [15] and others summarized in table 3 have been studied intensively to find out the best one which fits all experimental data in the range from 1 to 26 MeV neutron incidence energy [23 ... 45]. A slightly modified version of Obst's potential well yields an optimum interpretation of all available data [13,17]. Contributions from compound - elastic scattering have been taken into account

in terms of the Hauser - Feshbach - formalism.

Figure 6 demonstrates the experimental and theoretical situation for integrated elastic scattering cross sections. The remarkable spread of experimental values below 10 MeV are due to the intermediate structure also visible in the total cross section.

The potential well found in the described manner has been used in the DWBA and Coupled - Channel - analysis after a proper reduction of the imaginary potential depth [13].

4.3. Neutron inelastic scattering

Neutron inelastic scattering exciting the low - lying levels can be understood well from the threshold up to about 5 MeV in terms of the Hauser - Feshbach - formalism including width - fluctuation corrections. Comparable results have been obtained by the codes ELISA and STAPRE. Above 5 MeV deviations appear indicating the contributions resulting from reaction modes other than statistical one. Usually the excitation by collective nuclear reactions is held to be responsible [13] for this.

Here also the population of low - lying states via pre - equilibrium neutron emission has been investigated. A substantial improvement of the calculated values in comparison to the experimental ones could be achieved in the whole energy range. Above 15 MeV there are no experimental data to supply or refuse these results. In fig. 7 the excitation function for the $^{28}Si(n,n_1)^{28}Si$ reaction demonstrates the situation mentioned above. The more flat energy dependence of the calculations obtained by ELISA above 9 MeV results from the level cut - off.

The understanding of the angular distributions of inelastically scattered neutrons is excellent using an incoherent superposition of statistical and direct reaction modes [13].

Excitation functions of highly excited states or the inelastic scattering to the continuum can be reasonable described by statistical methods because contributions from collective motions are small. The pre - equilibrium reaction mode strongly enhances the emission of high - energy neutrons from the level continuum visible in both neutron sprctra and the total inelastic scattering cross section (fig. 8).

Using the code STAPRE neutron emission spectra can be calculated in reasonable agreement with measurements available.

Commonly, angular distributions of neutron inelastic scattering to high excited levels or the continuum are assumed to be isotropic.

4.4. Neutron - induced reactions

In the energy region considered here only the $^{28}Si(n,p)^{28}Al$ and $^{28}Si(n,\alpha)^{25}Mg$ reactions contribute to the non - elastic cross section. Both channels have been examined in terms of statistical models using the codes ELISA and STAPRE.

In agreement with the experiencies got in dealing with neutron inelastic scattering the code ELISA yields good results up to about 6 MeV. Above this neutron incidence energy a continuous level distribution must be introduced in the corresponding residual nuclei. The consideration of nuclear level densities causes some problems in preparation of calculations performed by STAPRE. A serious one is the correct matching between the discrete level counting and a continuously distributed density. Using different published level density parameters (see table 4) for all nuclei under investigation (isotopes of Si, Al and Mg) such a consistent set of parameters has to be found which fit all available experimental data in all open reaction channels. Figs. 9 and 10 present a good and a bad example for calculated excitation functions. The deviations in the (n,α) reaction are due to an inadequate adjustment of parameters used in STAPRE calculations.

By this method the particle spectra can be calculated with reasonable accuracy. Such spectra are of interest for different purposes in solid state physics.

Finally, first results have been obtained to describe the angular distribution of particle transitions populating the low - lying levels in the residual nuclei by direct processes using the code CHUCK-2.

5. Outlook for works being in progress

In order to create a complete file some tasks will be prepared to start in 1980. Mainly following problems are waiting for treatment

i evaluation of the cross sections in the thermal and epithermal energy range;
ii evaluation of resonance parameters;
iii evaluation of γ- production cross sections and γ- ray spectra induced by neutrons.

Concerning the last item, valuable experiences have been collected in the use of statistical methods for the description of the γ- deexcitation of highly excited nuclei [22].

Finally, all numerical results have to be compressed and checked against inconsistencies in partial and total cross sections. After that the data set will be coded in the format of the ENDF/B - library (for convenience of an international exchange) and added to the SOKRATOR - library representing the file 2015.

References

[1] Barrington, AEEW-R-351, 1964
[2] R. Howerton, UCRL-50400, Vol. 15, Part A, 1975
[3] M. R. Bhat et al., BNL-50379, 1973
[4] S. Igarasi et al., JAERI-1261, 1979
[5] N. O. Bazazyanc et al., Yad. Konst. 8 (1972) 61
[6] R. L. Simsons, W. A. McElroy, BNWL-1312, 1970
[7] D. Hermsdorf, TU Preprint 05-36-78, 1979

[8] Th. Schweitzer et al., ZfK-382, 1979, 125 and INDC (GDR) in preparation
[9] Adel-Fawzy et al., ZfK-382, 1979, 129
[10] G. Kießig, Thesis, TU Dresden, 1975
[11] ENSDF-File, Version August 1978
[12] M. Uhl, B. Strohmaier, IRK-01/76, 1976
[13] Th. Streil et al., Proc. 2nd Symposium on Neutron - induced Reactions, Smolenice, Acta Phys. Slov., in press
[14] B. Holmqvist, T. Wiedling, Jour. Nucl. Energy 27 (1973) 543
[15] A. W. Obst, J. L. Weil, Phys. Rev. C7 (1973) 1076
[16] S. Kliczewski, J. Lewandowski, Nucl. Phys. A304 (1978) 269
[17] L. Neumann, Diploma work, TU Dresden, 1979
[18] A. Gilbert et al., Can. Jour. Phys. 43 (1965) 1466
[19] H. Vonach, M. Hille, Nucl. Phys. A127 (1969) 289
[20] W. Dilg, W. Schantl, Nucl. Phys. A217 (1973) 269
[21] E. Gadioli, L. Zetta, Phys. Rev. 167 (1968) 1016
[22] B. Basarragtscha, D. Hermsdorf, ZfK-382, 132, 1979 and Proc. 2nd Symposium on Neutron - induced Reactions, Smolenice, Acta Phys. Slov., in press
[23] W.E. Kinney et al., ORNL-4517, 1970
[24] G. A. Petitt et al., Nucl. Phys. 79 (1960) 231
[25] D. Brandenberger et al., Nucl. Phys. A196 (1972) 65
[26] D. E. Velkley et al., Phys. Rev. C9 (1974) 2181
[27] R. O. Lane et al., Ann. Phys. 12 (1961) 135
[28] W. E. Kinney et al., Proc. Conf. Lowell, 1976
[29] J. Rapaport et al., Nucl. Phys. A286 (1977) 232
[30] R. L. Clarke et al., Nucl. Phys. 53 (1964) 177
[31] D. J. Bredin et al., Phys. Rev. B135 (1964) 412
[32] S. A. Cox, EXFOR entry 11519
[33] P. H. Stelson et al., Nucl. Phys. 68 (1965) 97
[34] K. Tsukada et al., Proc. Conf. Vienna, 1961
[35] S. Tanaka et al., Proc. Conf. Helsinki, 1970
[36] H. H. Knitter et al., Z. Physik 207 (1967) 56
[37] Mittler et al., EXFOR entry 50301
[38] D. M. Drake et al., EXFOR entry 51828
[39] anon., EXFOR entry 52213
[40] F. G. Perey et al., EXFOR entry 52216
[41] W. M. Currie et al., AERE-PR/NP-9, 1966
[42] J. Roturier et al., EXFOR entry 60762
[43] I. O. Korzh et al., EXFOR entry 80197
[44] V. I. Popov et al., EXFOR entry 80327
[45] M. Joppich, Thesis, Univ. Erlangen, 1974
[46] J. Hoehn et al., Nucl. Phys. A134 (1969) 289
[47] V. Fasoli et al., EANDC (E) 66, 1966
[48] D. Hermsdorf et al., Kernenergie 18 (1975) 83
[49] J. B. Marion et al., Phys. Rev. 101 (1956) 247
[50] B. Mainsbridge et al., Nucl. Phys. 48 (1963) 83
[51] M. Birk et al., Nucl. Instr. a. Methods 21 (1963) 197
[52] J. M. F. Jeronymo et al., Nucl. Phys. 47 (1963) 157
[53] R. Bass et al., EANDC (F) 66, 1966
[54] A. V. Cohen et al., Nucl. Phys. 1 (1956) 73

[55] B. D. Kern et al., Nucl. Phys. 10 (1959) 226
[56] M. Bormann, Handbook on Nuclear Activation Cross Sections, Vienna, 1974
[57] N. Ranakumar et al., Nucl. Phys. A122 (1968) 679
[58] E. B. Paul et al., Can. Journ. Phys. 31 (1953) 267
[59] J. E. Strain et al., ORNL-3672, 1965
[60] J. J. Singh et al., EXFOR entry 10217
[61] G. Andersson-Lindström et al., Soc. Roy. Science 10 (1964) 265

Table 1: Compilation of files of recommended data for Si

library	designation	reference	year of publication	remarks
UKNDL	DFN 25E	[1]	1964	very old file, neutron data only
UKNDL-2	MAT 7120	[2]	1972	complete file
UKNDL-76	MAT 7120		1975	no changes
UKNDL-78	MAT 7820		1978	no changes
ENDF/B-III	MAT 1151	[3]	1973	graphs only
ENDF/B-IV	MAT 1194		1975	complete file, available since 1979
JENDL-1	MAT 1140	[4]	1979	neutron data only, includes ENDF/B-IV totally
BACAZYANC		[5]	1972	only elastic neutron scattering
CAND-IV		[6]	1970	only (n,p) and (n,α)

Table 2: Applied models and their range of validity to calculate cross sections

Model	energy range	quantities	data typ	computer code
Optical model	1 to 20 MeV	(n,n)	ang. distr.	LIISA
Hauser - Feshbach - formal.	1 to 9 MeV	(n,n), (n,n$_i$') (n,p), (n,α)	excitation function, ang. distr.	ELISA
			excit. funct.	STAPRE
H. - F. - formalism + multi - step - formalism + Exciton-model	9 to 20 MeV	(n,n), (n,n$_i$') (n,n'), (n,p) (n,α) ... (n,2n), (n,np) (n,nα) ...	excitation function, particle spectra	STAPRE
DWBA + CCBA	5 to 20 MeV	(n,n)(n,n$_i$'), (n,α$_i$)	ang. distr.	CHUCK-II

Table 3: Optical potential well parameters for ^{28}Si

	Bhat [3]	Holmqvist [14]	Kliczewski [16]	Obst [15]	Streil [13]
V_r/MeV	56.3-0.32E	48.5	43.13	52.0	52.0
R_r/fm	1.17	1.191	1.27	1.15	1.15
a_r/fm	0.75	0.66	0.68	0.78	0.78
W_d/MeV	13.0-0.25E	7.89	9.63	12.1	12.1
R_d/fm	1.26	1.201	1.23	1.25	1.25
a_d/fm	0.58	0.48	0.45	0.47	0.47
V_{so}/MeV	6.2	8.0	8.91	4.9	9.0

Table 4: *Parameters for description of nuclear level continuum for* ^{28}Si

Parameter	Gilbert [18]	Vonach [19]	Dilg [20]	Gadioli [21]	present work [17]
a/MeV^{-1}	3.2	3.1	4.3	4.5	3.0
Δ/MeV	3.9	0.2	0.2	1.4	1.0
I_{eff}/I_{rigid}	1.0	1.0	1.0	0.7	1.0

Figure captions

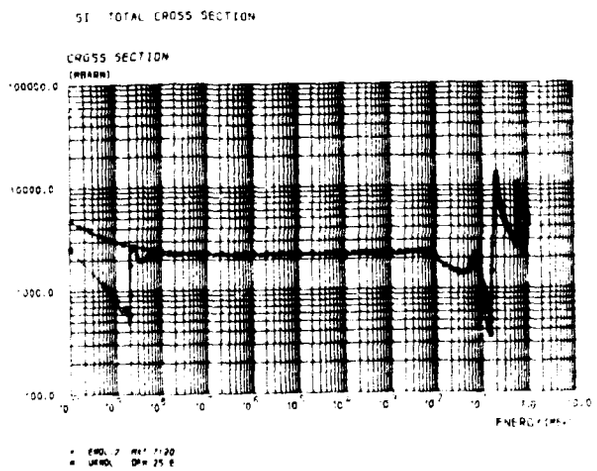

Fig. 1
Total cross section in the energy range from 0.000 1 eV up to 1 MeV recommended by the libraries UKNDL and ENDL-2

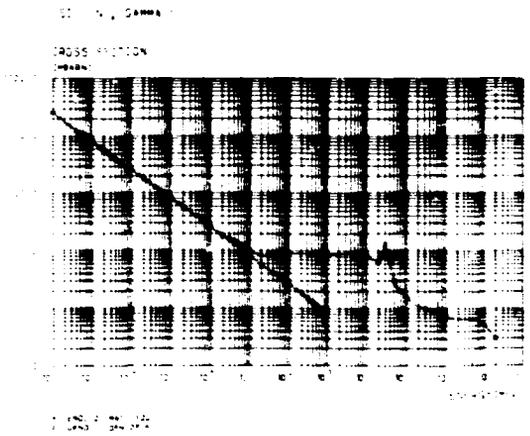

Fig. 2
Neutron capture cross section in the energy range from 0.000 1 eV up to 20 MeV recommended by the libraries UKNDL and ENDL-2

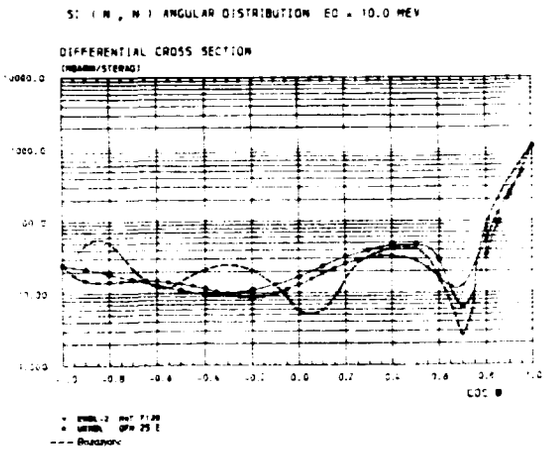

Fig. 3
Angular distribution of elastically scattered 7 - MeV - neutrons recommended by the libraries UKNDL, ENDL-2 and BAZAZYANC

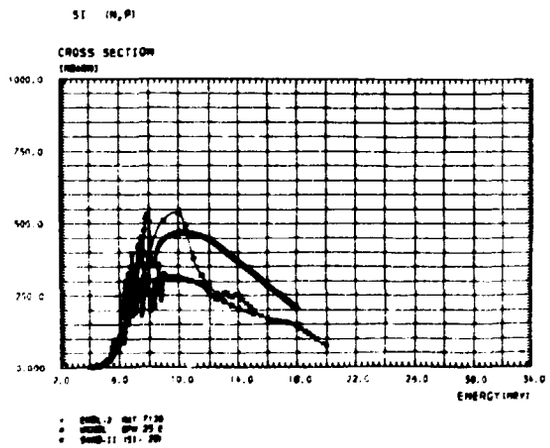

Fig. 4
Excitation function for Si (n,p) recommended by the libraries UKNDL, ENDL-2 and SAND-II

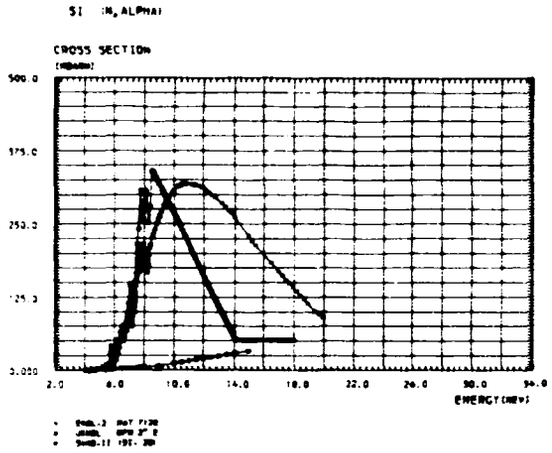

Fig. 5
Excitation function for Si (n,α) recommended by the libraries UKNDL, ENDL-2 and SAND-II

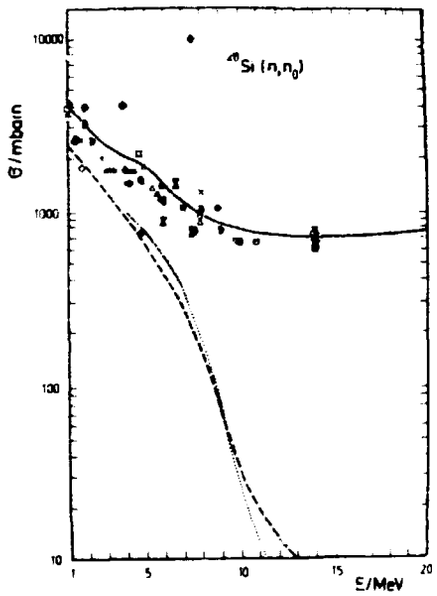

Fig. 6
Angular integrated elastic scattering cross section calculated by use of ELISA (full line) and STAPRE (compound - elastic scattering only) without (dotted line) and with pre - equilibrium particle emission (dashed line) in comparison with experimental data measured by [23] ✱ , [24] + , [25] ◗ , [15] ◒ , [26] ● , [27] □ , [28] ○ , [29] ◡ , [30] ■ , [31] ◆ , [32] Δ , [33] ▽ , [34] ● , [35] ✱ , [36] ▲ , [16] ◬ , [37] ⧗ , [38] ⧗ , [39] ◗ , [40] ◆ , [41] ◖ , [42] ▲ , [43] ✗ , [44] ◓ , [8] ▲ , [45] ▽

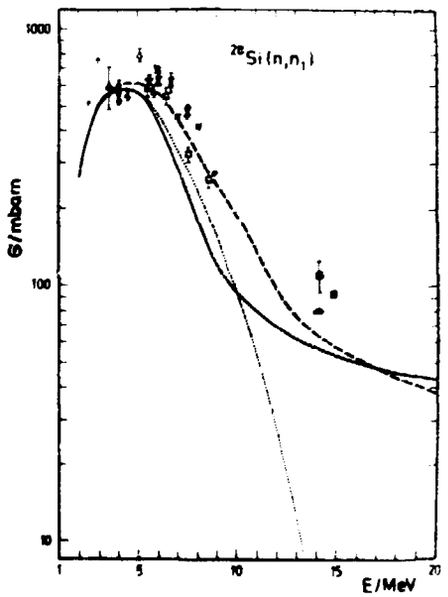

Fig. 7
Neutron inelastic scattering to the first excited level of ^{28}Si calculated by use of ELISA (full line) and STAPRE without (dotted line) and with pre - equilibrium particle emission (dashed line) in comparison with experimental data measured by [24] + , [8] ◆ , [36] Δ , [38] ⧗ , [23] ✱ , [35] ✱ , [26] ● , [16] ◬ , [30] ■ , [46] ■

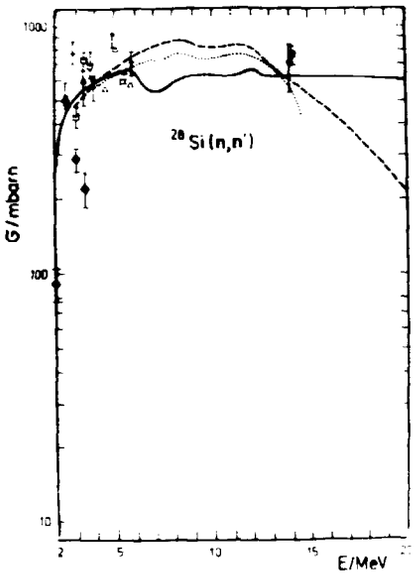

Fig. 8
Neutron inelastic scattering cross section calculated by use of ELISA (full line) and STAPRE without (dotted line) and with pre - equilibrium particle (dashed line) in comparison with experimental data measured by [40] ◆, [24] +, [47] ⊠, [48] ▼, [8] ▲, [32] Δ, [23] ✕, [30] ■

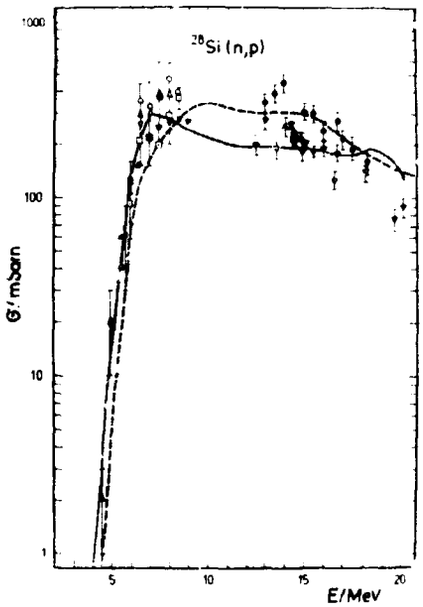

Fig. 9
Excitation function for Si (n,p) calculated by use of ELISA (full line) and STAPRE without (dotted line) and with pre - equilibrium particle emission (dashed line) in comparison with experimental data measured by [49] Δ, [50] ○, [51] △, [52] ▽, [53] □, [54] ▼, [55] ●, [56] ▲, [57] ⧗, [58] ◇, [59] ◬, [60] ■

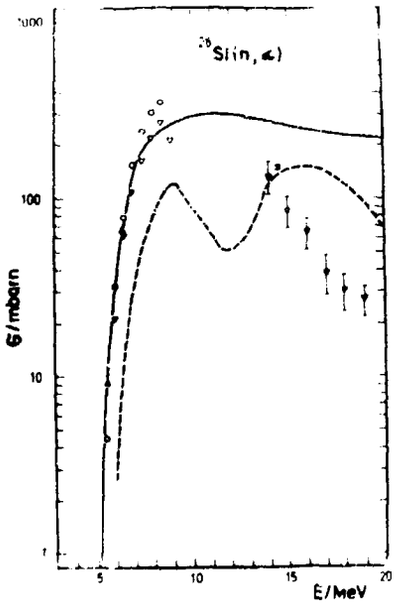

Fig. 10
Excitation function for Si (n,α) calculated by use of ELISA (full line) and STAPRE with pre - equilibrium particle emission (dashed line) in comparison with experimental data measured by [50] ○, [51] △, [61] ▽, [3] ✱

CONFIGURATION OF DATA PROCESSING SYSTEM AT SECTION OF PHYSICS
- PRESENT STATE AND DEVELOPMENTS -

W. Meiling

Technische Universität Dresden, Sektion Physik, DDR-8027 Dresden

1. Introduction

Development of nuclear physics experiments during the last twenty years is characterized by a remarkable increasing complexity of experimental apparatus due to more severe demands from higher data rate and from more accurate and more reliable measurements. This requires the application of electronic digital techniques to acquisite and process experimental data and to control the experimental devices [1].

In this way, in 1960 and later in nuclear physics laboratories many projects of data processing centres basing on a central computer, which is on-line coupled to experimental devices over small or longer distances, were worked out and proved (fig. 1a). The advantage of such systems is the acquisition and processing of great data massives by means of the computer and its peripheral units. If real-time processing is realized, this mode provides a good physicist's monitoring on the running experiment. Despite of this advantage, coupling the experimental device to a central computer installed in the computing centre of the institute or outside exhibits some serious problems, e.g.:

- Access of the physicist to the centralized computer, to its peripheral units, to the software system and the working regime is limited - this gives difficulties especially in real-time processing.
- An electronic data processing system is not well interfaced to couple experimental devices like counters or analog-digital converters in nuclear physics devices; reaction time for identification and processing of interrupt demands is considerably long.
- Data acquisition and real-time processing of physical experiments, which can run many hours or days, require long operation times or a more complicate time-sharing regime of the computer and result in high costs.

An essential step towards the better application of computer techniques was the development of the so-called minicomputers about 1965, permitting direct coupling (on-line coupling) to the measuring system without troubles arising from any multi-user regime (fig. 1b). Wellknown types of these comparatively cheap and powerful minicomputers are PDP-8, the Hungarian equivalents TPA-1001, the GDR-type KSR 4100, and later especially the PDP-11 family which has successors produced in many countries. Furthermore, the GDR-computer Robotron KRS 4200 has to be mentioned.

In our institute the development of computer-aided experimental devices began in the years 1971/72. The application of the KRS 4200 was the only alternative in order to realize direct assigning a computer to the experimental arrange-

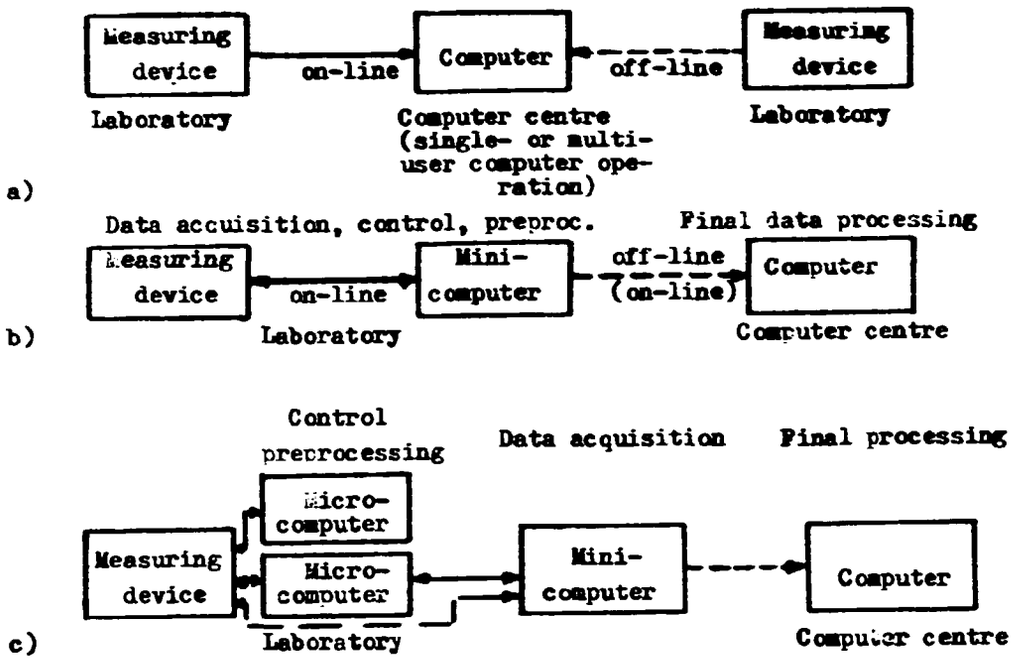

Fig.1: Structure of computer-coupled measuring devices
a: Centralized computer
b: On-line coupled minicomputer immediately placed at the measuring device
c: Hierarchical system including mini- and microcomputers

ment (comp. Fig.1). Due to the distance of about 15 miles to the university computing centre in Dresden a coupling to its machines would lead to high effort and many troubles to agree physicist's requirements and preconditions in the computer centre. Therefore, we did not plan the on-line coupling to computer centre for the aim of data acquisition and control of experiments. Apart from this, on the other hand such a coupling using any telephone cable from our institute in Pirna to the computer centre would improve the working conditions of physicists, because many theoretical calculations and work on nuclear data evaluation could be carried out immediately from the institute. Unfortunately, powerful terminals to do this coupling with some intelligence, with punched card reader and alphanumeric display are not available. Therefore, installing a terminal in Pirna has to be delayed until the technical preconditions for installing, for data transfer and for connection to the computer centre are given.

About 1972, derived from the described situation the conception of data processing and control of nuclear physics experiments in our institute was clear:

- Application of a KRS 4200 minicomputer.
- Providing a suitable interface to couple computer and nuclear electronis.
- Working out software to acquisite and process data and to control the experimental arrangement.

- Later addition of further minicomputers and connecting them separately to the independently running experiments; these ideas came out of date, at least in some aspects, by development of microcomputers allowing powerful hierarchical systems (fig. 1c).

Recently, realizing a structure like fig. 1c is the main topics of our work. Nevertheless the installation of a second KRS 4200 or 4201 minicomputer would increase the performance of the data processing capabilities and is planned for next future.[2]

In the following some remarks on the KRS 4200 minicomputer and on the modular instrumentation system CAMAC will be made before some comments on the conception of distributed processing using KRS 4200 and microcomputers are given.

2. Minicomputer KRS 4200

The main parameters of the Robotron KRS 4200 computer are summarized in table 1. The availability of various standard interfaces to couple external units to the computer is very important. The producer worked out program-controlled input/output channels which correspond to following standards [1,4,5]:

- AS 1: Sif 1000, interface to couple typical computer input/output devices like typewriter, paper-tape reader and paper-tape puncher.
- AS 3: SI 2.2, interface standard developed in GDR [6] for process-control modules like input and output of analogous and digital signals, slow counters, multiplexers based on relays and others [7]. Commercially produced modules suitable for nuclear physics experiments are not available.
- AS 5: SI 1.2, standard interface to chain devices [8], e.g. units of the data acquisition and output systems made by Funkwerk Erfurt [9]. Mainly developed for coupling of numeric controlled machine tools, AS 5 allows connection only of about 4 units. Several nuclear electronics devices made from Central Institute of Nuclear Research in Rossendorf are adapted to SI 1.2 [10].
- AS 10: CAMAC-interface [11], this connection to KRS 4200 based on developments in our institute [12] is an important precondition to use the international wellknown instrumentation system CAMAC.

In spite of the flexible input/output channels of KRS 4200, and especially of KRS 4201, which contains more input/output channels compared to KRS 4200, these computers show some insufficient parameters:

- The memory contains 16 K words in maximum (the 4201 is to be said to include up to 32 K words) - that is not sufficient to store great data blocks which are given in semiconductor detector aided nuclear spectroscopy or in multiparameter coincidence experiments.
- External magnetic memory with high capacity and random access like magnetic disks are not available; the only possibility is to use magnetic drum memories with 96 K words capacity. Magnetic disks will be expected.

Installation of the powerful alphanumeric and graphic display developed in the Rossendorf institute is in preparation. A digital plotter for accurate plotting

Table 1: Some parameters of the KRS 4200 minicomputer (Robotron Dresden) [3]

Central processing unit:

- word length: 16 bit
- number of instructions: 53
- execution time
  fixed point addition: 2,6 µs
  floating point addition: 650 µs (subroutine)
- addressing modes: direct (2 sectors, each 512 words), indirect, indexing

Memory:

- technology: ferrite core
- capacity: 8 or 16 K
  (4201: up to 32 K)
- cycle time: 1,3 µs

Input/output channels:

- program-controlled channels: AS 1: Sif 1000 interface
  (4200: up to 4 possible, AS 3: SI 2.2 interface
  4201: up to 16 possible) AS 4: ESER-computer coupling
  AS 5: SI 1.2 interface
  AS 8: V24 interface
  AS 10: CAMAC interface (According to EUR 4600)
  and others
- direct memory access: for 1 device
- interrupt inputs: 16 external, 2 using real-time clock

Peripheral units:

- standard equipment: typewriter SM 4000; paper-tape reader CT 2001; paper-tape puncher C8025, daro 1215; serial plotter daro 1156
- extended equipment: magnetic drum store PBB 204-2; magnetic tape store; magnetic disk ISOT 1370 (announced); alphanumeric display PBT 4000

Software:

- assembly language: SYPS 4200
- dialogue programming system: DIWA 4200
- high-level language: FOR 4200 (FORTRAN)
- real-time system program: ESKO 4200
- loader, debugging program, editor, mathematical standard routines and oth.
- problem-oriented software to do economic and data processing tasks, not suitable to control physical or other measuring devices

of the measured and processed spectra is missing in our configuration

Great problems are derived from the disproportion of available and required software, that means high-level software to control CAMAC-devices and to execute dialogue between computer and its peripheral units.

Altogether the parameters of the KRS 4200 computer and its deficiences in memory capacity, input/output channels, software and other topics defined essentially the configuration of our measuring system and required great effort to develop special hard- and software.

3. Modular instrumentation system CAMAC at KRS 4200

Among the various interface standards like SI 1.2, SI 2.2 and CAMAC we decided to use CAMAC [11]. The reasons for this choice are clear:

- CAMAC is a well defined instrumentation system, adapted primarily to nuclear physics measurements.
- CAMAC has global spread, thus facilitating international cooperation; in our case this cooperation is referring to the Joint Institute of Nuclear Research in Dubna.
- CAMAC electrical and logical conditions permit data transfer rates, which are higher than processing rates in minicomputers; therefore, CAMAC can be successful also in future using considerably faster minicomputers.

On the other hand due to orientation to CAMAC we are forced to extend the input/output channels of the KRS 4200 computer (AS 10 [12]) and to develop some system software to program CAMAC devices on a moderate or high programming level [13,14].

The function of CAMAC data transfers and the structure and code of CAMAC commands are wellknown, therefore, a detailed description can be omitted. The various possibilities of coupling between CAMAC modules and the computer are represented in fig.2 [5]. With KRS 4200 computer we selected the structure with branch driver working as input/output channel and, consequently, the "vertical" CAMAC dataway according to EUR 4600 and the crate controller type A1 [15,16]. This solution guarantees the coupling of up to 7 CAMAC crates to one driver without serious restrictions for transmission length and without blocking of a great number of computer input/output addresses - last object was in correspondence with the requirement of the computer producer.

With the selected CAMAC-dataway a structure of the measuring system as depicted in fig. 3 was realized. In table 2 some of CAMAC modules, developed in our institute during last years, are listed [17,18,19].

At present, our programming of CAMAC is based on the assembly language SYPS 4200 of the KRS 4200 and on the language CAMAC-4200 [1], which contains CAMAC adapted elements in the kind of a problem-oriented higher language. In both cases the conversion of the CAMAC-programs into the machine code is effected in a compiling manner, that means, all modifications of the running program due to exchange of separate modules or to variations of measuring strategy require all precompiling and assembling passes. This makes programming inconvenient and time-consuming. It is to be emphasized that improvements in pro-

Table 2: CAMAC modules, developed at the Technical University of Dresden, Section of Physics (selection):

CAMAC crate controller type A1 (EUR4600)
Manual and external programmable crate controller 3312
Serial link module
CAMAC branch driver AS 10 for KRS 4200 computer (EUR 4600)
Parameter input module 1240
Dataway display 3111
Pulse counter 1111 (2 x 24 bit)
Presettable up/down counter 1170
SI 1.2 adapted input register 1221
SI 1.2 adapted output register 1421
Timer
Switch register input module 1240
Control and level converter module 1520

gramming strategy are necessary in order to support the application of CAMAC. Furthermore, dialogue possibilities are essential if program is to be modified or if test operations during program debugging and adjustment of the devices have to be performed. In this direction, at KRS 4200 work to extend the programming language BASIC with CAMAC commands requires attention [14, 20]. Another alternative can be seen using FORTRAN-CAMAC subroutines [21] and at the KRS 4200 the magnetic drum memory saving unreliable paper-tape work during the compiling phases.

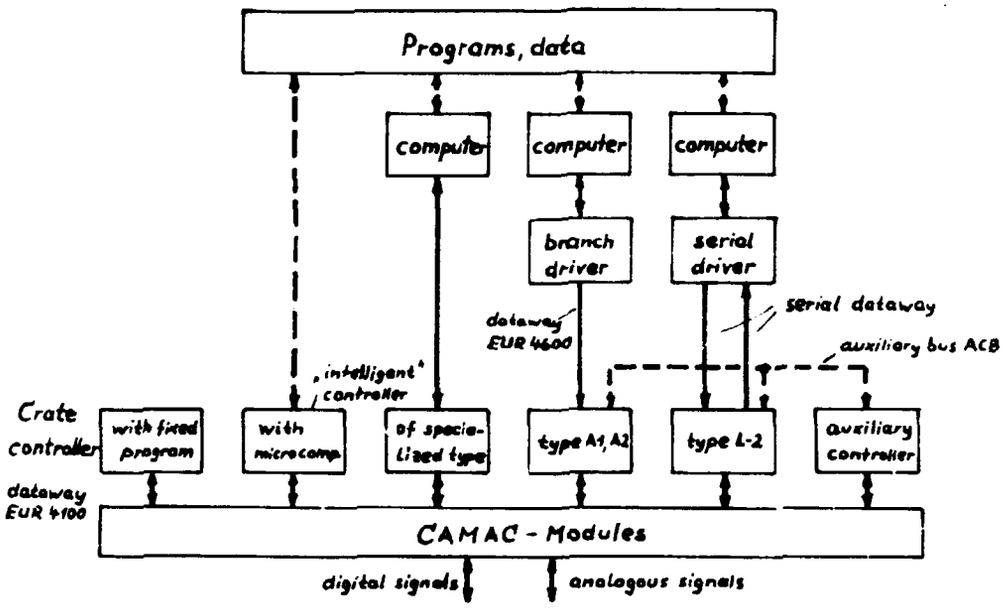

Fig.2: CAMAC configurations

4. New developments basing on microcomputers

The development of small-size and low-cost microcomputers with high computing power, which is similar to the performance of first minicomputers, opened new ways in automation and data processing by digital techniques [22]. According to fig. 2 there are three essential variants to include microcomputers in CAMAC:

V1. Coupling of an external microcomputer to CAMAC by use of

- V1.1 a branch driver for one or more CAMAC crates,
- V1.2 a specialized CAMAC crate controller adapted to microcomputer input-output channel,
- V1.3 another standard interface like SI 1.2, which is realized in GDR microcomputers and which supposes a CAMAC crate controller fitted to

this standard interface.

V2. Expanding the CAMAC crate controller by an in-built microcomputer resulting in an "intelligent" crate controller (ICC), which saves an external computer to control CAMAC [23].

V3. Addition of further CAMAC-modules placed on normal station numbers, which include microcomputer elements to organize work of a connected peripheral unit without loading of the computer. Presence of several controllers in a crate requires, however, an auxiliary controller bus ACB to share access to the CAMAC-dataway according to selected controller priorities [24].

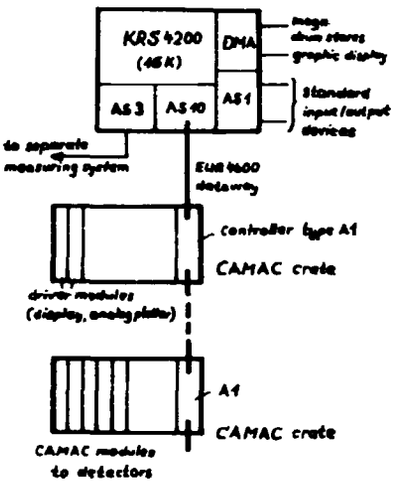

Fig.3 : KRS 4200 minicomputer coupled to CAMAC

Consequent installation of microcomputers in a system like fig. 1c suggested a hierarchical structure which is shown in fig. 4. The KRS 4200 is the central computer having suitable peripheral units and via the AS 10 access to 7 CAMAC crates in maximum. Furthermore CAMAC crates can be controlled by microcomputers of the type SDK-80 [25] or MPS 4944 [26] using 8080 microprocessors. That means systems with moderate data processing requirements can be controlled independently of the KRS 4200 by separate microcomputers. This principle of distributed dataprocessing simplifies essentially software problems compared to a multi-user regime on a more powerful central computer.

If access to the central computer would be necessary, then coupling of the microcomputer controlled CAMAC crate by use of datalinks as CAMAC modules can be recommended [27,28]. This represents a two-level hierarchical structure, which opens many possibilities to find out an optimum system solving special tasks. More precisely, from the variants mentioned above we selected such variants which are compatible with demands from experiments and from limited technological suppositions:

V1.1 Development of a simple branch-driver adapted to the 8255 programmable peripheral interface chips of the SDK-80 microcomputer [25,29]. A standard crate controller type A1 is usable.

V1.3 Application of the SI 1.2 interface card of the MPS 4944 microcomputer, which does not include programmable interfaces like 8255 or Z80-PIO. This required the development of a SI 1.2 adapted crate controller [30].

V3. Additional controllers in a crate like the "intelligent" controller ALCA-80 [31], need the auxiliary controller bus [24]. This suggested the development of a controller which is adapted to SI 1.2 and includes the ACB connection; manual and external programmable controller 3312 [30].

Worth mentioning that the controller 3312 can work independently of a computer. It allows programming of two commands NAF using front paneel switch register. In this regime tests of CAMAC modules, especially as long-term reliability mea-

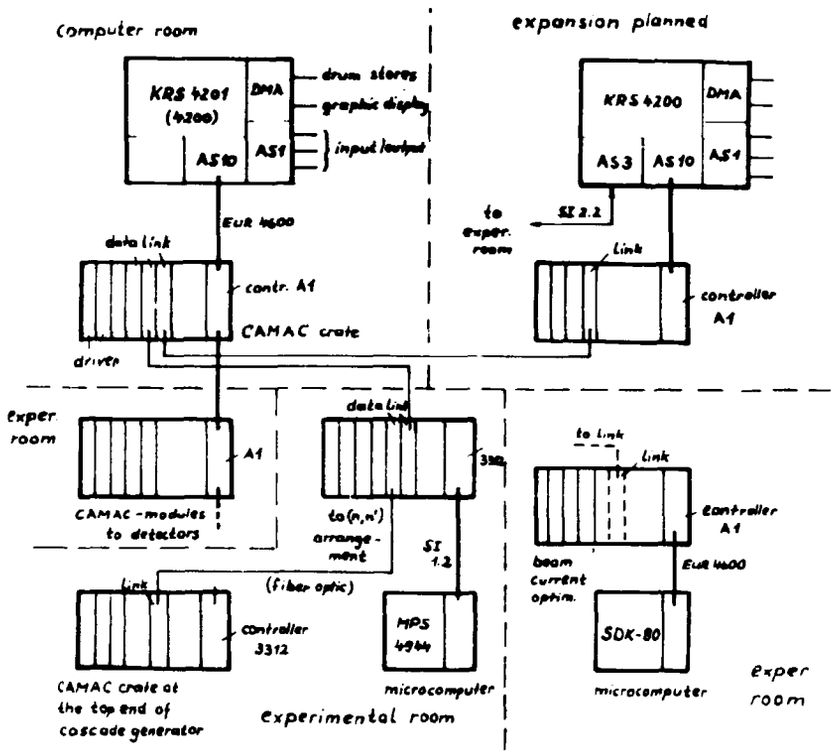

Fig.4: Data processing based on system shown in fig. 3 and expanded by microcomputers

surements, can be performed without blocking of a controlling computer.

To simplify CAMAC programming when using microcomputers SDK-80 and MPS 4944 the standard monitor program was extended by CAMAC commands [32, 33]. These commands call subroutines to compose the command NAF (or in SDK-80 applications CNAF) from separate bytes, to test signals X and Q depending on declaration by the user and to supervise the time of CAMAC dataway operations. This programming does not correspond to the application of a high-level programming language, because the user must know a lot of CAMAC hardware and microcomputer details. Nevertheless a programming language like BASIC with CAMAC expansion would be very desirable when to use microcomputers.

Because of the general application of CAMAC the coupling of crates controlled by computer or by the controller 3312 using data link modules is suggested. The data link modules developed in our institute exhibit several data transfer modes and, therefore, good adaption to special transfer lines.

Satisfaction of higher data processing requirements let the installation of a second KRS 4200 or 4201 computer to be an important task for next future. As

indicated in fig.4 this is independent of additional application of microcomputers.

Experience was obtained by application of KRS 4200 controlled CAMAC-system to measure the (n,f) cross-sections with very high accuracy [34]. The SDK-80 microcomputer is used to control the current of a quadrupole lens for highest ion current at the neutron producing target [32,35]. Applying a fiber-optic transmission line is in preparation to transfer data from MPS 4944 via data link modules to a CAMAC crate with 3312 controller having the 500 kV potential of the top end of a cascade generator. Furthermore, the automation of (n,n') scattering experiments by means of a MPS 4944 microcomputer and data block transfer to KRS 4200 is planned [36].

References

[1] W. Meiling: Digitalrechner in der elektronischen Meßtechnik, I, II, WTB-Reihe 236, 237, Akademie-Verlag Berlin, 1978

[2] W. Meiling, W. Grimm, P. Jugelt: Konzeption zur weiteren Entwicklung des on-line-Datenverarbeitungssystems, TU Dresden, Sektion Physik, 1978 (interner Bericht)

[3] Rechnersysteme ROBOTRON 4000 4200 4201 - Anwendung und Weiterentwicklung, Rechentechnik/Datenverarbeitung 12 (1975), 3. Beiheft

[4] W. Baumann, P. Kurtze, G. Naumann: Standard-Interfaces der elektronischen Meßtechnik, Reihe Automatisierungstechnik 165, Verlag Technik Berlin, 1974

[5] G. Naumann, W. Meiling, P. Stscherbina: Interfaces der Elektronik, Verlag Technik Berlin, 1980 (im Druck)

[6] DDR-Standard TGL 29711: Standard-Interface für Linienverkehr auf Basis Transistor-Transistor-Logik SI 2.2, Okt. 1974

[7] Impuls, Zeitschrift des Industriezweigs Automatisierungsgeräte, Dresden

[8] DDR-Standard TGL 29248: Standard-Interface für Kettenverkehr auf Basis Transistor-Transistor-Logik SI 1.2, Okt. 1974

[9] B. Schmidt, K. Eckert et al.: 3. Generation des Erzeugnissystems "Digitale Messung und Meßwertausgabe - Grundgeräte", radio fernsehen elektronik 23 (1974) 113

[10] Datenblätter Elektronische Geräte, Zentralinstitut für Kernforschung Rossendorf (ZfK Rossendorf), Bereich Technik

[11] CAMAC: A modular instrumentation system for data handling, description and specification, Report EUR 4100, 1969, rev.1972, CEC Luxembourg

[12] W. Hirsch, W. Reiss, W. Meiling: Entwicklung einer CAMAC-Anschlußsteuerung für den Rechner KRS 4200 sowie einer Handsteuereinheit, Jahresbericht ZfK Rossendorf ZfK-283, 1974, 158

[13] K.-W. Leege, D. Werner: CAMAC 4200 - eine algorithmische Echtzeitprogrammiersprache für das Kleinrechnersystem KRS 4200 mit CAMAC-Peripherie, Rechentechnik/Datenverarbeitung 14 (1977) 3, 17-20

[14] W. Grimm, W. Meiling: CAMAC-software for the KRS 4200 minicomputer, this report, p. 183

[15] CAMAC: Organisation of multi-crate systems. Specification of the branch highway and CAMAC crate controller type A, Report EUR 4600, 1972, CEC Luxembourg

[16] W. Hirsch, S. Gläser et al.: Entwicklung eines CAMAC Crate Controllers Typ A und eines Datenweg-Testmoduls, Jahresbericht ZfK Rossendorf, ZfK-283, 1974, 156

[17] W. Hirsch, W. Meiling et al.: CAMAC-Module für Impulszählung und Datentausch mit externen Geräten, Jahresbericht ZfK Rossendorf, ZfK-283, 1974, 159

[18] R. Krause, W. Meiling: CAMAC-Modul "Zweikanal-Zeitsteuerung 1311", Jahresbericht ZfK Rossendorf, ZfK-295, 1975, 141

[19] F. Weidhase, P. Gerlach et al.: CAMAC-Geräteentwicklungen an der Technischen Universität Dresden, Jahresbericht ZfK Rossendorf, ZfK-350, 1977,224

[20] W. Grimm, P. Hoffmann: Real-time BASIC for CAMAC - principles and implementation for KRS 4200 minicomputer, this report, p. 186

[21] R. F. Thomas: Specifications for standard CAMAC subroutines, CAMAC Bulletin No.6, 1973, 23

[22] W. Meiling: Mikroprozessor - Mikrorechner, Funktion und Anwendung, Beiträge zur Forschungstechnologie, Band 5, Akademie-Verlag Berlin, 2.Aufl.1979

[23] Microprocessors for CAMAC, CAMAC Bulletin No. 14, 1975, 3-21

[24] Distributed Intelligence in CAMAC: Multiple crate controllers in a single crate, Report EUR 6500, ESONE Committee, 1978

[25] Intel MCS-80, System design kit (SDK-80), User's guide, Intel Corp., 1976

[26] Mikroprozessorsystem MPS 4944, Informationsschrift ZfK Rossendorf 1978

[27] M. Borkenhagen, K. Faulstich et al.: Test und Erprobung des seriellen Link-Moduls 1470, Jahresbericht ZfK Rossendorf, ZfK-385, 1978, 213

[28] F. Weidhase, J. Pöthig, this report, p. 172

[29] W. Meiling, F. Gleisberg, W. Enghardt: Steuerung eines CAMAC-Meßsystems durch einen Mikrorechner, Nachrichtentechnik Elektronik 29 (1979) H.1, 9

[30] J. Pöthig, F. Weidhase: The manual and external programmable crate controller 3312, this report, p. 180

[31] AMCA-80, Informationsschrift Zentralinstitut für Elektronenphysik Berlin, 1978

[32] W. Enghardt: Diplomarbeit Technische Universität Dresden, Sektion Physik, 1979

[33] W. Enghardt, W. Meiling: CAMAC-Monitor für den Mikrorechner SDK-80, Jahresbericht ZfK Rossendorf, ZfK-385, 1978, 207

[34] W. Meiling, R. Arlt et al.: CAMAC bei neutronenphysikalischen Untersuchungen, Kernenergie 21 (1978) H.9, 292

[35] F. Gleisberg, W. Enghardt, W. Meiling: Contribution to automation of a cascade generator using microcomputers, this report, p. 168

[36] G. Kloß, this report, p. 176

CONTRIBUTION TO AUTOMATION OF A CASCADE GENERATOR USING A MICROCOMPUTER

P. Gleisberg, W. Enghardt[1] and W. Meiling
Technische Universität Dresden, Sektion Physik, DDR - 8027 Dresden

Demand for higher precision of nuclear physics experiments increases permanently. With regard to experiments at 150 kV and 500 kV cascade generator to produce neutrons this demand implies:

- maximum value of the beam current
- long-term stability
- stabilisation of beam bunching.

Additionally, starting the generator requires long experience and good dexterity from the operator. Hence, it follows, that the generator should be automatically controlled so relieving the operator and giving better stability of important parameters of the cascade generator.

First work for automation of the cascade generator was carried out step by step:

- construction of a CAMAC-connection to the microcomputer, to use the existing CAMAC-interface consequently
- defining a CAMAC-monitor for the microcomputer
- stabilization of an essential parameter of the cascade generator and testing the performance of the microcomputer used.

In additional steps more parameters of the cascade generator should be controlled till the complete automation is realized.

For work at the cascade generator the microcomputer SDK - 80 was available. This is a single-board microcomputer kit, including the 8080 CPU, 4 k bytes ROM and 1.75 k bytes RAM. Coupling to peripheral devices is performed by two 8255 programmble peripheral interface and one 8251 programmable communication interface. A system monitor is included in mask-programmed ROM, for general software utilities and system diagnostics.

The CAMAC-connection is realized by using a branch driver [1] , according to the CAMAC-Branch Highway by EUR 4600. During each branch operation the branch driver can communicate with a maximum of three crate controllers.
The CAMAC-commands CNAF are directly generated on the microcomputer address

[1] now Zentralinstitut für Kernforschung, Rossendorf

and data bus

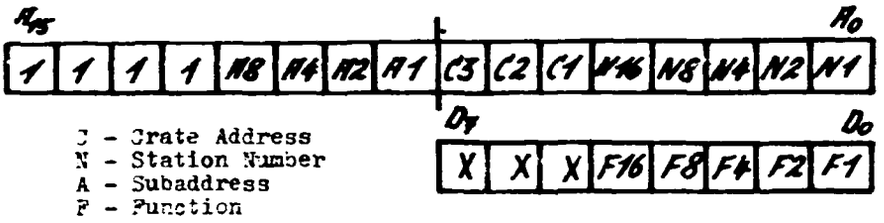

Fig. 1: Format of the address and data bits representing the CAMAC command

The CAMAC-commands are written into the branch driver command register. The CAMAC-write and read data are buffered in the two 8255 interfaces. Moreover, one 8255 stores an 8-bit status word in every CAMAC-cycle. This includes the X- and Q-response and the status of the interrupt sources. The control unit of the branch driver organizes the timing, supervises the branch operation and releases if required demand signals.

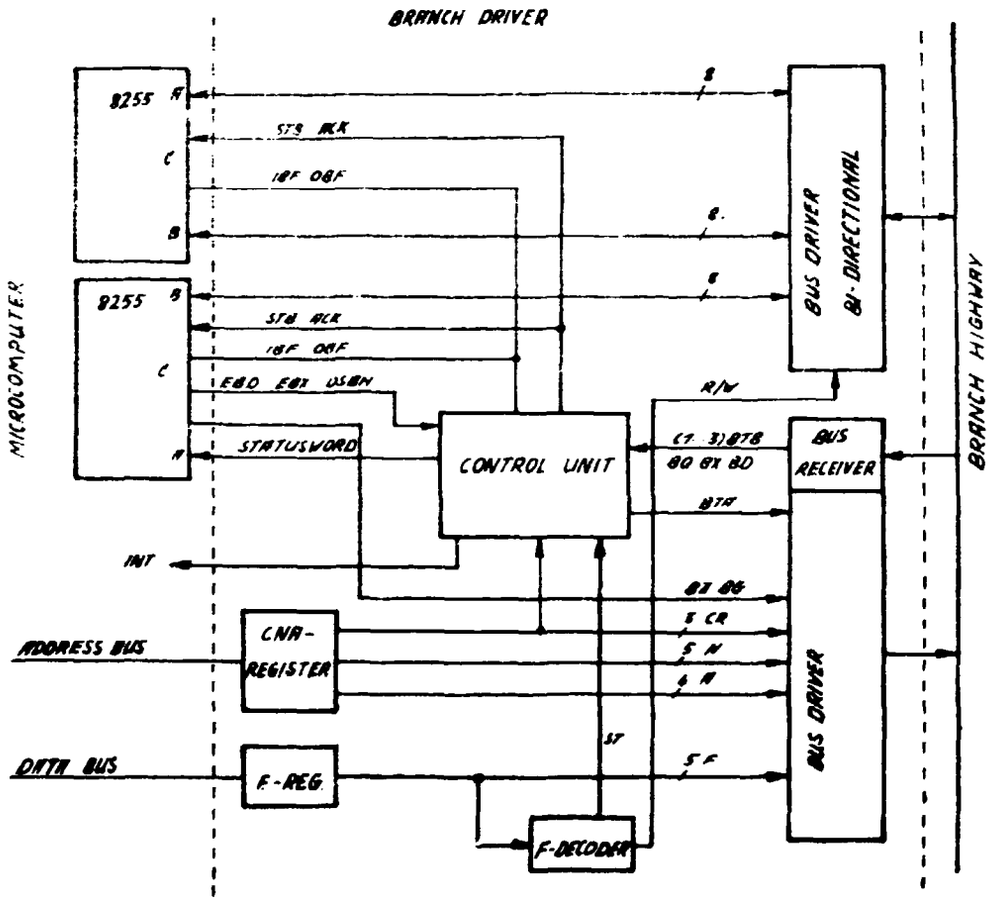

Fig. 2: Block diagramm of branch driver

The microcomputer with branch driver needs for generating one CAMAC-read or write command about 75 microseconds and for one CAMAC-control command about 30 microseconds.
In expansion of the SDK 80 microcomputer standard monitor a CAMAC-monitor was defined facilitating the attendance of the CAMAC-configuration [2] .

First application on the cascade generator

By control of the current through a quadrupole lens doublett the beam current, measured on the target, is hold permanently in the maximum.
This is a problem to find the optimum of a function which depends on two parameters. This requires to look for a optimization method suitable for the microcomputer with regard to the permissible computer execution time and the available storage capacity. Using the SDK - 80 microcomputer which is coupled to CAMAC a suitable optimization method was selected and programmed.

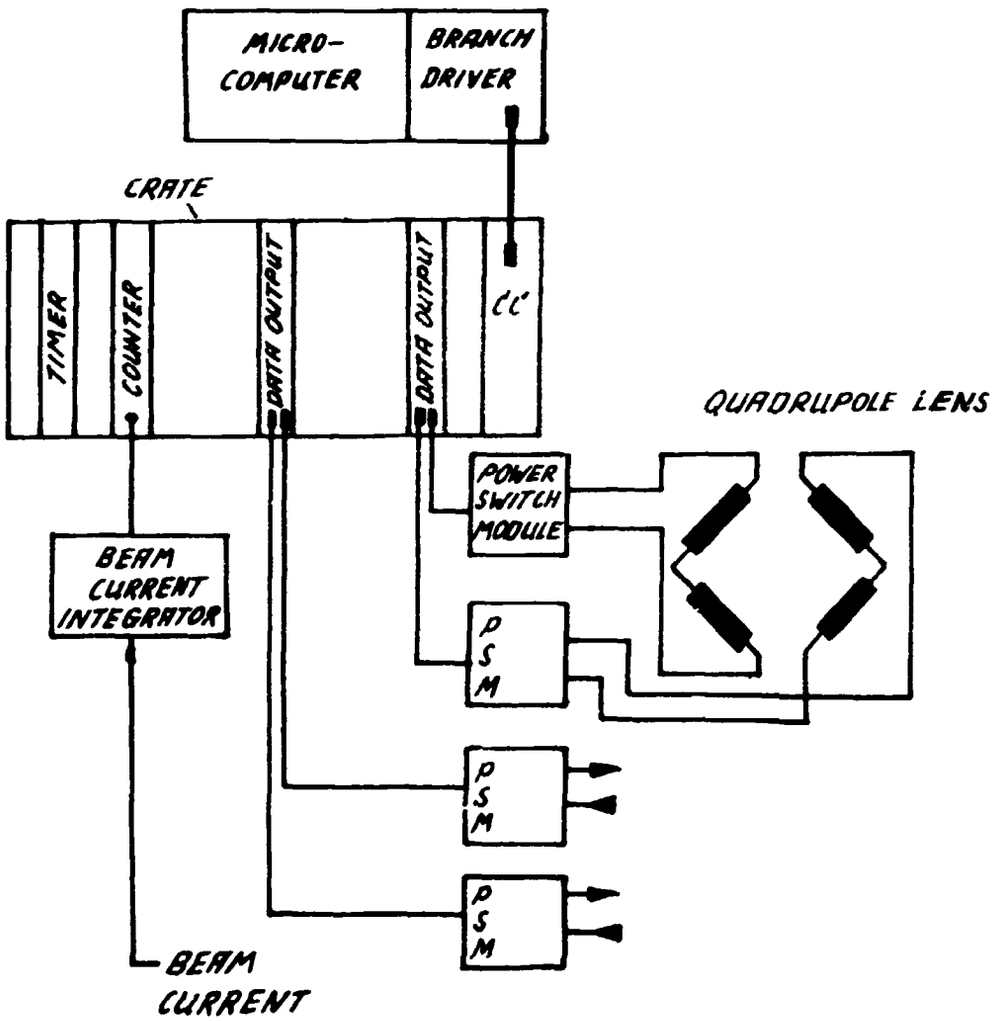

Fig. 3: The experimental configuration

A digitaly controlled power-switch module provides, after the input of a data word, transfered via a data output module, the current of one branch of the quadrupole lens. The beam current integrator provides a frequency proportional to the target current. A counter module counts these pulses during a time fixed by the timer module. Therefore, the data word of the counter includes information of the actual beam current value.
Further, the timer module determines the time interval between two succeeding optimization runs. During this interval, the microcomputer can curry out other tasks.
One optimization process takes about 5 seconds; this time results from the long integration time of the beam current integrator.

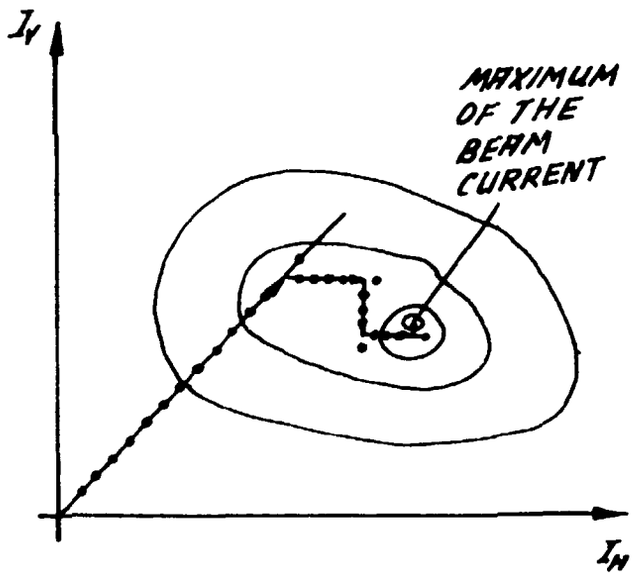

Fig. 4: The succession to find out the maximum of the beam current at the target
I_H - current of the horicontal focus lens
I_V - current of the vertical focus lens

At the beginning,the quest is done along the line, where the currents of the horicontal focus lens and the vertical focus lens are the same. Where the relative maximum is reached, the quest courses along the lines parallel to the axises, this means, the current of one lens is holded constantly.
After this, where the maximum is founded too the asymmetry of the coil currents is to be varied to obtain the absolute maximum.

References:

[1] F. Gleisberg, Diplomarbeit, TU Dresden, Sektion Physik 1978
[2] W. Enghardt, Diplomarbeit, TU Dresden, Sektion Physik 1979

ПЕРЕДАЧА ЦИФРОВЫХ ДАННЫХ ПРИ ЭКСПЕРИМЕНТАХ В ЯДЕРНОЙ ФИЗИКЕ

Ф. Вайдхазе, А. Пэтиг
Технический Университет Дрезден, Секция физики, Дрезден, ГДР

I. Задачи передачи цифровых данных

В ближайшем будущем физики чаще будут пользоваться микропроцессорами. Их назначение состоит в "он лайн"-управлении экспериментами и в редукции данных. Для вычислений на спектрах лучше всего применять электронновычислительные машины (ЭВМ). Связь между этими и более маленькими ЭВМ происходит при помощи так называемых "Линк модулей" [I]. При этом можно использовать скорости передачи данных, согласно рисунку I.

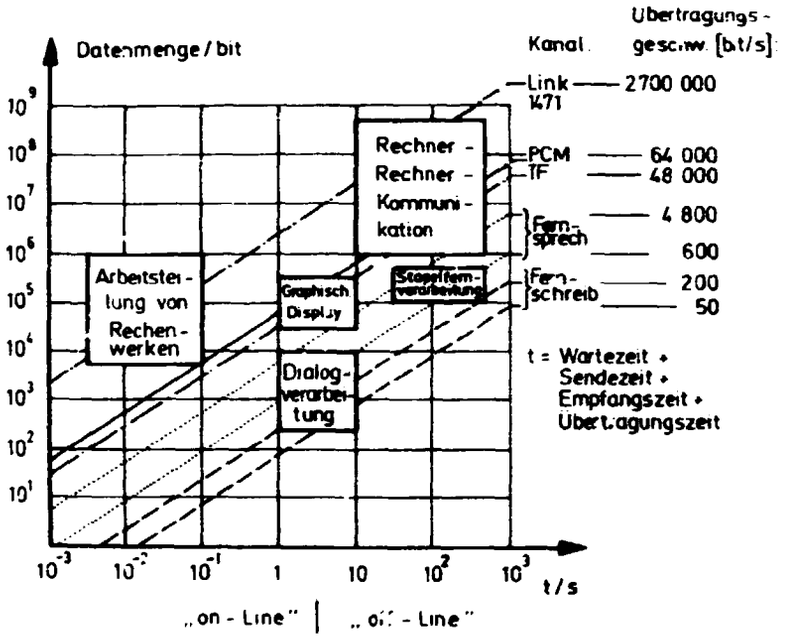

Рис. I Типичные скорости при передаче данных

Другое назначение состоит в установке, управлении и контроле ускорителя с помощью микропроцессоров [2]. При этом требования на скорости низкие, а на безошибочную передачу данных высокие.

Все вышеперечисленные аспекты находят отражение в проекте отдела ядерной физики Технического Университета Дрездена [3]. Рисунок 2 показывает одну Микро-ЭВМ типа МПС 4944 (Центральный институт ядерных исследований, ГДР), лежащую на потенциале земли. С помощью пластоволокнистого кабеля происходит передача на высоковольтную аппаратуру ускорителя. Мы применяем для модуляции и демодуляции Линк-модульи, типа I47I [3, 4]. В ближайшем будущем цифровые измерительные звенья и блоки питания с цифровым управлением будут находиться на высоковольтной аппаратуре в одном телеуправляемом КАМАК каркасе (крейт).

Нам хочется подчеркнуть, что связи к маленькой ЭВМ типа КРС 4200 (Роботрон, ГДР) также идут по Линк модулю, типа I47I.

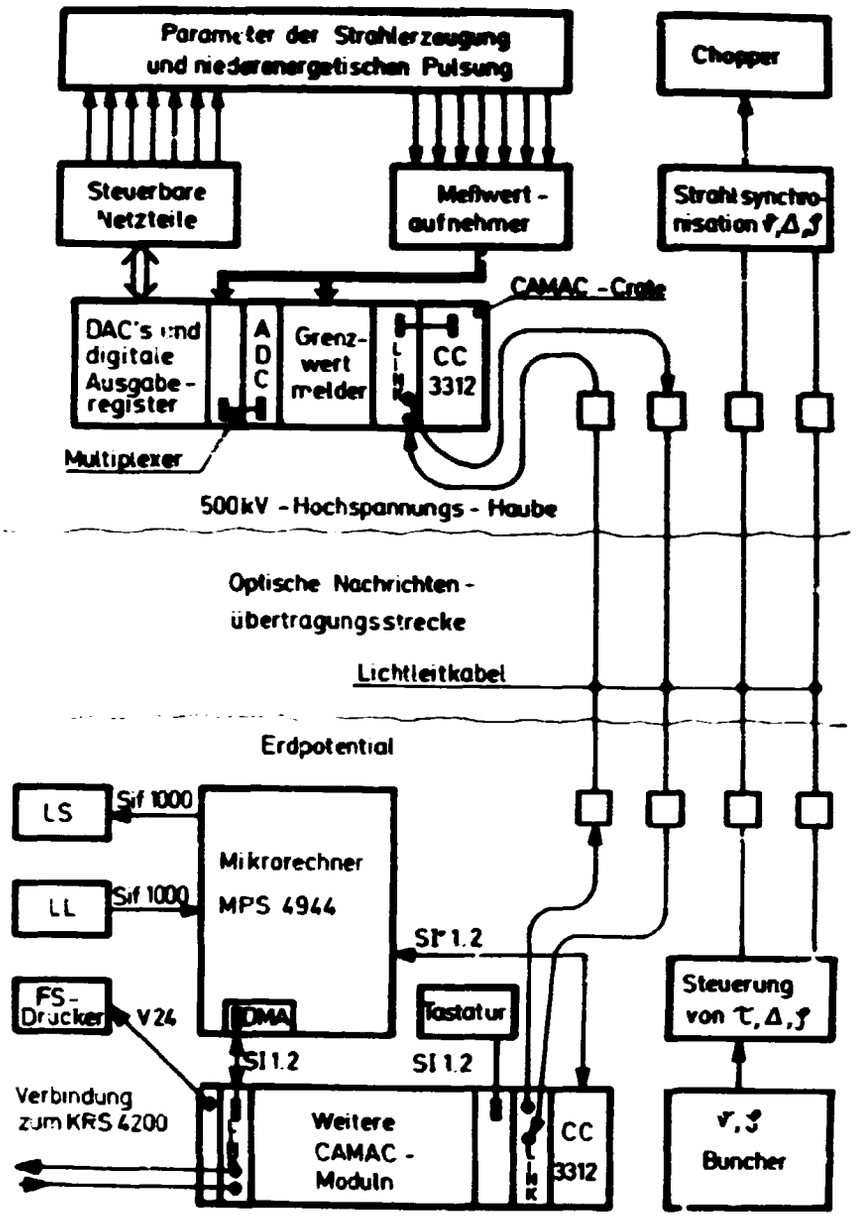

Рис. 2 Проект Технического Университета Дрездена для телеуправления одного КАМАК каркаса при установке, управлении и контроле ускорителя с помощью микропроцессоров

2. Некоторые параметры Линк модуля I47I

Линк модуль построен для быстрой передачи данных [4, 5]. Поэтому в нем находятся два пути: соответственно для входа и выхода, то есть через КАМАК магистраль или передной панель. Модуль работает последовательно на кабеле. С помощью параллельного передного входа или выхода возможно быстрое осуществление ДМА связей. Кроме того, они нужны для телеуправления одного раккаса.

Обычно скорость передачи данных составляет 2 мега бит в секунду, причем защита от ошибок очень хорошая. Например, без затруднений можно дать импульсы в 600 В при передаче на четырёхсотметровый кабель. Восходящее время импульсов составляет 30 нс. В основном, защита против ошибок достигается при помощи ферритокольцевых трансформаторов. В модуле однократной ширины находится 79 интегральных микросхем.

3.Некоторые параметры участка для световой передачи

Мы построили чувствительный светоприёмник. Он работает очень надежно при входной мощности света 10^{-7} ватт. Приёмник пригоден для диапазона с частотой до 5 Мгц. У нас применяется длина только в 5 метров, поэтому мы смогли использовать дешёвый кабель типа Grinifil LIK (Кварц., ГДР). Этот кабель имеет минимум затухания (демпфирования), для красного света. Мы смогли применить обычные люминисцентные диоды, типа VQA 12. Его световая мощность составляет $3 \cdot 10^{-4}$ ватт.

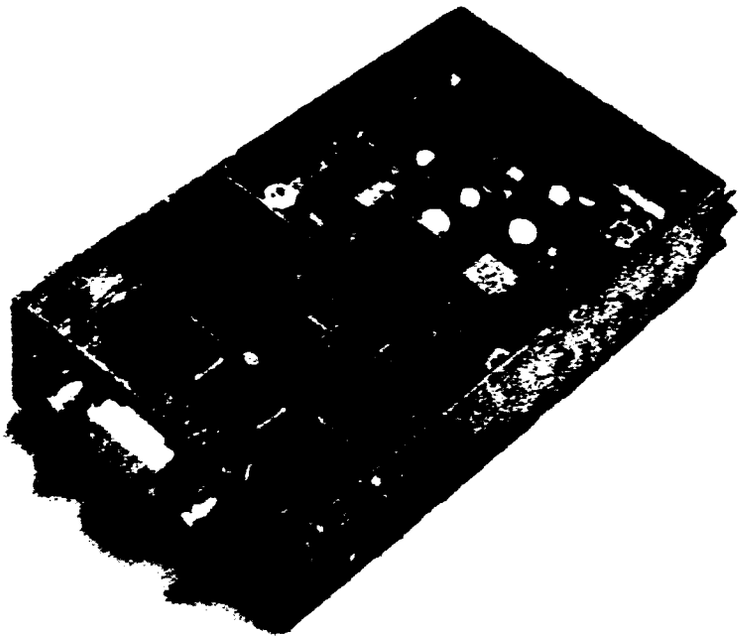

Рис. 3 Блок для световой передачи. Он содержает два светоприёмника, два светопередачика и два стабильных трансвертера (+ 5В вход, а -5В и +30В выход)

4. Уровень реализации

Мы стараемся производить Линк модули и светоприёмники. Все проведённые испытания образца прошли успешно. Пластоволокнистый кабель уже один год находится в ускорителе. За это время мы не смогли установить каких-либо изменений в кабеле.

5. Литература

[1] Zacharov, V.: Distributed Computing for the Support of Experiments of Experiments in a Multi-Discipline Laboratory.
Preprint VIK Dubna, D 13-11182, Dubna, 1978.

[2] Axelrad, C.: Microprocessor and Evolution of the Control on the Instrumentation.
Preprint VIK Dubna, D 13-11182, Dubna, 1978.

[3] Pöthig, J.; Weidhase, F.: Manuell und extern steuerbarer CAMAC-Crate Controller Typ 3312.
Preprint TU Dresden, 05-14-79, Dresden, 1979.

[4] Weidhase, F. and other ones: Anwendungsmöglichkeiten und Konzeption des seriellen Link-Moduls 1471.
Preprint TU Dresden, 05-28-78, Dresden, 1978.

[5] Вайдхазе, Ф. и др.: К проблеме безошибочной передачи данных в распределенных системах.
Препринт ОИЯИ, Д13-III82, Дубна, 1978, стр. 379.

ИСПОЛЬЗОВАНИЕ МИКРО-ЭВМ В ЭКСПЕРИМЕНТЕ НА КАСКАДНОМ ГЕНЕРАТОРЕ

Г. Хайнрих, Г. Клосс
Технический университет Дрезден, Секция физики, Дрезден, ГДР

Описываются задачи микро-ЭВМ типа "МПС-4944" при автоматизации экспериментов на нейтронном генераторе, в частности подключение многоканалного анализатора типа ИЦА-70.

I. Введение, задачи микро-ЭВМ

При автоматизации спектрометра быстрых нейтронов по методу времени пролета с помощью микро-ЭВМ можно установить автономные системы и проводить простые проверки эксперимента и управляющие функции.

С помощью микро-ЭВМ и на базе данной техники возможно выполнить физические задачи более эффективно и точнее, например

- определение сечений рассеяния нейтронов в широком диапазоне углов,
- использование более длинных баз пролета,
- определение параметров аппаратуры, например напряжение для отклонения пучка, ток через квадруполные линзы.

Кроме того преимужество микро-ЭВМ по сравнению с постоянно поянными системами состоит в модулярном характере электронных блоков и в возможности свободного программирования эксперимента. Это означает, что система с микро-ЭВМ соответствует наилучшим образом различным режимам измерений.

Началась у нас автоматизация нейтронного генератора на базе микро-ЭВМ типа МПС-4944 ЦИЯИ Россендорф (стандарт Академии Наук, ГДР) [I]. Уровень развития этой микро-ЭВМ соответствует техническим возможностям 1977/78 годов.

При этом МПС должна выполнить следующие задачи:

- проводение механ эских функций управления при помощи специальных дачиков,
- обслуживание специального интерфейса многоканального анализатора для измерения спектров,
- установление связи к стандарту КАМАК при помощи управляющего ручного контроллера и к мини-ЭВМ КРС-4200 при помощи КАМАК-КАМАК-линк,
- протоколлирование эксперимента на телетайпе или на дисплее в иде обычного телевизора и обслуживание периферных установок,
- управление режимом старт-стоп мониторных счетчиков в КАМАКе,
- предварительная обработка спектров на простом уровне.

2. Конкретная конфигурация эксперимента и электроники

Данная конфигурация микро-ЭВМ МПС-4944 вместе с подключением периферии показано на рис. I.

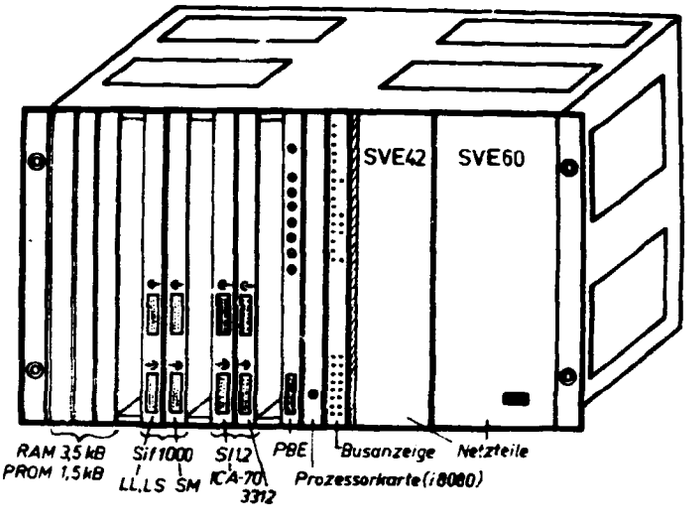

Рис. I Данная конфигурация микро-ЭВМ МПС-4944

Процессорная плата работает с микропроцессором ИНТЕЛ 8080. Блок "PBE" например позволяет обрабатывать сигналы прерывания из процесса. С помощью пульт управления возможно прекращать программу на любом адресе.

Исходя из физических требований и выше названных задач получилось следующие степени реализации всей системой:

I) Управление венгерским многоканалным анализатором для измерения ядерно-физических величин и предварительная обработка данных при помощи микро-ЭВМ,

2) Подключение электроники в стандарте КАМАК к микро-ЭВМ,

3) Установление канала связи для передачи данных от микро-ЭВМ МПС 4944 до мини-ЭВМ КРС 4200 на базе КАМАК-линк,

Этие факты определяют один вариант (n,n')-эксперимента, как указанно на рис. 2. К пунктам 2) и 3) посмотрите другие статьи этого выпуска.

С учитыванием следующих аспектов мы связывали многоканалный анализатор ИЦА-70 и МПС-4944 [2]:

- использование 8 кбайт ферритной памяти ИЦА-70 постоянным запоминающим устройством для МПС,
- применение мощной аналогой части анализатора,
- приготовленная подходящий к ЭВМ конфигурация интерфейсной электроники ИЦА-70 например для подключения мини-ЭВМ ТПАи или ТПА-70 и
- существование hand-shake - интерфейса СИ I.2 у микро-ЭВМ МПС-4944.

С этим предположением развивали интерфейсную плату, которую в анализаторе прямо работает без дополнительных изменений.

Плата выполняет следующие функции:

- управление анализатором на основе стандарта СИ I.2,
- изменение режима работы (амплитудно-импульсный анализ, время-амплитудный ана-

лиз или вывод на печать и.т.д.),

- выбор зоны внутренней памяти,
- установка стартового адреса в выбранной зоне памяти и
- чтение и запись данных [3].

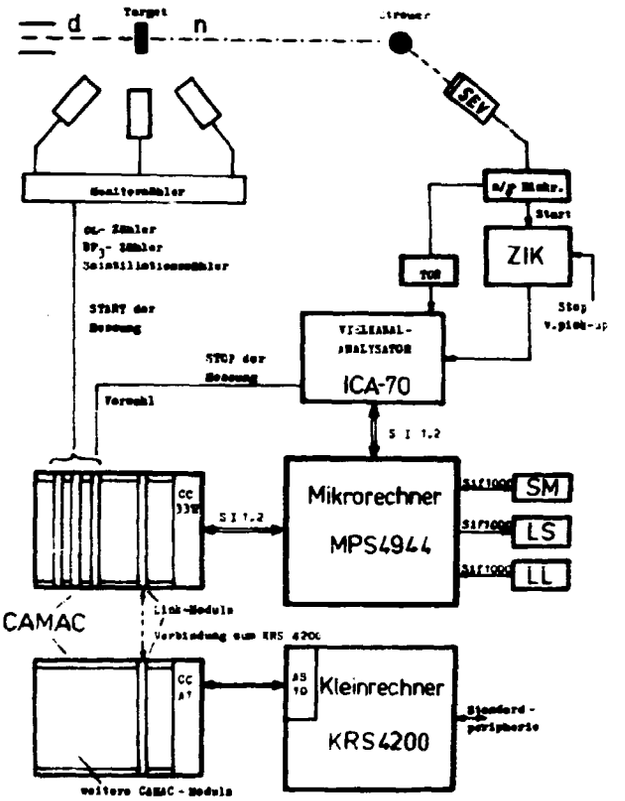

Рис. 2 Блок-схема варианта (n,n')-эксперимента с микрокомпютером МПС 4944

Вся система работает на осн е программ-монитор "МИМО-80" (минимальный монитор) а будущее на базе "СМ-80" (стандартный монитор) [4]. Монитор реализирует

- изменение и манипулация содержания регистров,
- коммуникация, это означет обслуживание перфоратора, перфочитателя или телетайпа,
- арифметические и другие операции.

На основе монитора главный программ эксперимента выполняет например такие функции, как

- суммирование
- умножение
- деление
- сдвиг в диапазсие 256 каналов

} спектров.

Таким обрасом имеется возможность управления анализатором и предварительной обработки данных на простом уровне физического эксперимента с помощью микро-ЭВМ.

3. Литература

[1] Modulares Mikrorechnersystem MPS-4944, Firmenschrift ZfK Rossendorf, 1978;

[2] ICA-70 user manual, KFKI Budapest;

[3] Heinrich, G.: Kopplung eines Vielkanalanalysators ICA-70 an den Mikrorechner MPS-4944 sowie Schaffung von Rahmen-Applikationaprogrammen für (n,n')-Flugzeitexperimenten,
Technische Universität Dresden, Sektion Physik, Diplomarbeit, Aug. 1979;

[4] Werner, D.: Steuerprogramm MIMO. Minimalmonitor für das Mikroprozessorsystem MPS-4944, Informationsschrift, TU Dresden, Sektion Informationsverarbeitung, 1978.

Manual and External Programmable Crate Controller Type 3312

J. Pöthig, F. Weidhase
Technische Universität Dresden, Sektion Physik, DDR-8027 Dresden

The development of the crate controller type 3312 was started from the following aspects /1/:

- The remarkable international progress of microelectronics gave the possibility to automate more and more processes. For work with CAMAC systems this implies to apply computers in measurement, for service and testing purposes. Such computers have a various size, they can be placed into or out of the CAMAC crate. Therefore in future crate controllers are needed, which are able to be controlled by external computers, by crate-internal computers or/and for using in service to be controlled by hand.
- Crate controller, indicator of dataway signals and parameter input switch register are essential components of any CAMAC system using in measurements. The concentration of these functions into one module offers lower hardware expense (e.g. only one AF-decoder necessary) and saving plug-in station numbers.
- Combined modules like the crate controller type 3312 can be used without any modification in CAMAC configurations of different size.

Therefore, the manual and external programmable crate controller type 3312 performs following functions, generally realized as separate modules:

1. Single-crate controller as connection between CAMAC crate dataway and the control unit using a parallel datatransfer controlled by handshake signals.
2. Manual controller to do service and development tests without additional computer, with several possibilities for triggering and indicating.
3. Minimal controller in a CAMAC crate, which contains more than one controller using the Auxiliary Controller Bus /2/. This minimal controller has the task to supply the dataway N-lines and to lead the L-lines signals to a LAM-grader and to the auxiliary controller.
4. Display of dataway signals to support test programs and to monitor dataway operations. Separate storing and indicating data of the dataway lines is available.
5. Parameter input switch register, which is coupled to the input-W-register due to the function of a controller. Data can be transfered from this register to the dataway W-lines and to an external computer using the parallel interface.

In the following, some possibilities to use the crate controller type 3312 are summarized showing the flexible application.

1. The CAMAC configuration consists of one crate, the crate controller (CC) type 3312 and the modules (M) needed for the measurements (see lower part of fig. 1). The crate controller type 3312 is used as a manual controller.
2. The configuration built into the crate is far away controlled by a computer (KRS 4200). The connection between computer and crate is realized by CAMAC link modules (L) type 1470 or type 1471 /2/ (fig. 1).

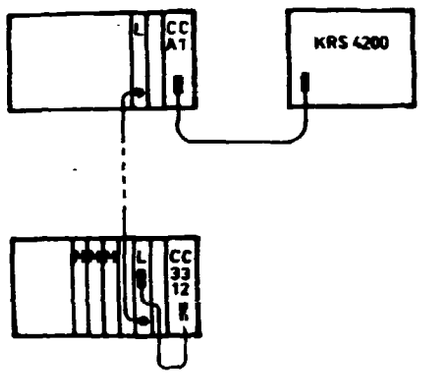

Fig. 1: Far-away controlled CAMAC configuration

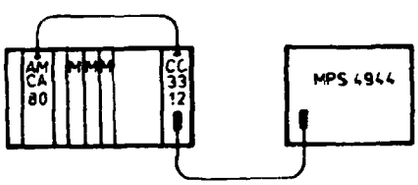

Fig. 2: CAMAC configuration controlled by a microcomputer

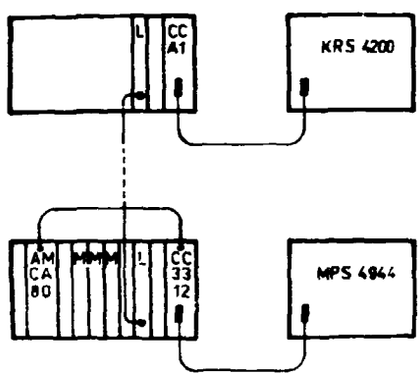

Fig. 3: Computer system using CAMAC as interface for connection and measurement

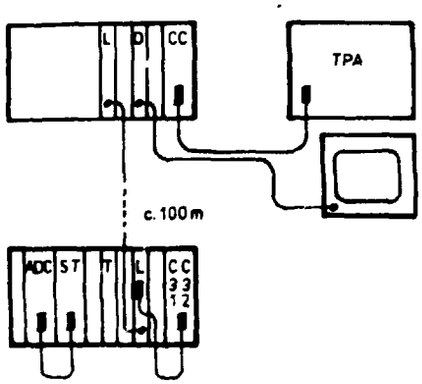

Fig. 4: Far-away controlled CAMAC using Multichannel Analyzer

3. The crate is cotrolled by a computer (MPS 4944) placed near the crate using the SI 1.2 interface. Software problems of such configuration are spoken about in /4/ (fig. 2).

4. The crate is controlled by the external computer (MPS 4944), but there is a difference to print 3, a far-away standing computer (KRS 4200), which is connected to the system by CAMAC link modules (L); this represents a hierarchical computer system.

5. No external computer controls the crate, but an internal one, e.g. using an intelligent auxiliary controller, for instance the AMCA 80, developed in the Central Institute of Electron Physics /5/.

6. The last application, which is to be mentioned, represents the combination of all these described possibilities (fig. 3). This means, that a computer system consisting of three computers would be realized.

At last, a special application of the crate controller type 3312 is mentioned, where a far-away controlled multichannel analyzer based on CAMAC instrumentation was built (fig. 4). The configuration consists of a minicomputer TPA, which is connected to CAMAC by a special controller (CC), a display driver (D) with a display and a link module on the one side. On the other side it consists of the CAMAC multichannel analyzer, that means a analogue-digital-converter, a memory and a timer-scaler. At measurement, there was a cable length of about 100 m between the two parts of the system.

The aim of testing this configuration was to get experience with a far-away controlled CAMAC system; the results confirmed the function of the controller.

/1/ Pöthig,J; Weidhase,F: Manuell und extern steuerbarer Crate Controller 3312
Preprint, TU Dresden, 1979

/2/ Multiple Controllers in a CAMAC-crate
Report, EURATOM EUR 6500, 1978

/3/ Weidhase,F; Borkenhagen,M; Faulstich,K; Miekmann,S: Anwendungsmöglichkeiten und Konzeption des seriellen Link-Moduls 1471
Preprint, TU Dresden, 1979

/4/ Enghardt,W: CAMAC-Monitor für den Mikrorechner MPS 4944
in: Diplomarbeit, TU Dresden, 1979

/5/ Beuchel,T; Lingertat,J; Messing,G; Starepravo,A: Basic Design Consideration to a Multicontroller Configuration in a CAMAC-crate
Preprint, ZIE Berlin, 1977

CAMAC - SOFTWARE FOR THE KRS 4200 MINICOMPUTER

W. Grimm and W. Meiling
Technische Universität Dresden, Sektion Physik, DDR - 8027 Dresden

Some work has been carried out to develope CAMAC instrumentation adapted to a KRS 4200 minicomputer and to provide software for the CAMAC control in nuclear physics experiments [1] . The main purpose of this work is the improvement of the efficiency and accuracy of the measurements. For this, the following features have to be considered:

1. Computer aided control of the whole measurement including periods to adjust and test the devices.
2. On-line data processing and evaluation.
3. Increasing quantity of data, which are to be checked and stored, and requirements on data processing.
4. High reliability of data processing and controlling the arrangements including the long-term stability by the use of specific programming techniques.
5. Facilitation to realize the communication and dialogue between the operator and the measuring equipment.

Table 1: Comparison of some programming languages referring t the KRS 4200

	SYPS 4200	CAMAC 4200
notation of application programs and processing	-assembly language SYPS 4200; application for CAMAC control, data processing and numerical analysis with very high effort by programmer -application programs with optimum execution times and memory efficiency programmable	-high-level programming language CAMAC 4200; comfortable description for CAMAC control and CAMAC data processing operations, some facilities to define numerical analysis -high execution speed of CAMAC control and CAMAC data processing -compiling, editing, and debugging with high effort by operator
real-time conditions	-reaction time for CAMAC-look-at-me (programmable) down to 10 microsecond	-reaction time for CAMAC-look-at-me less then 300 microsecond
recommendations for use	-use only for special application programs	-use for application programs with some CAMAC processing instructions and a small part for numerical analysis

What are the requirements to the software for measuring programs running on an on-line coupled minicomputer like KRS 4200 type equipped with CAMAC process periphery?

- The development of CAMAC-application programs must be based on a high-level programming language. In this way, the operator ist able to define his specific measuring problem as a computer program. Not only comfortable expressing possibilities, a well defined syntax structure, statements for real-time processing and interrupt handling, but also extensive compatibility with well-known programming languages such as FORTRAN, ALGOL, PL1, BASIC or PEARL are important. On the other hand, this would be helpful to support understanding and documentation of tested programs and to enable program exchange.
- The defined measuring algorithm has to be transferred in a machine-running program for the KRS 4200 minicomputer by use of programming aids which can be handled easily. Of course, it is desirable that the user must not know minicomputer hardware details or details of program work referred to the interface units.
- To realize an effective application of any computer aided measuring arrangement it is necessary to include debugging facilities and

minicomputer

FORTRAN 4200	FORTRAN (FOBS) 4200	BASIC 4200
-high-level programming language FORTRAN (subset of Basic FORTRAN); efficient and comfortable description of numerical analysis, subroutines and functions for CAMAC control and CAMAC data processing -compiling, editing, and debugging with a moderate effort	-comfortable compiling and editing data processing with extern memories (magnetic tape stores and magnetic drum memories)	-high-level programming language BASIC; unification of all the system functions including editing, running, debugging, filemanagement in the coherent language, extended by the introduction of statements for CAMAC control and CAMAC data processing, interrupt-handling and real-time operations -interactive programming -debugging facilities
-no facilities for processing of CAMAC-look-at-me		-reaction time for CAMAC-look-at-me about 1 millisecond, real-time operations
-use for application programs requiring considerable amount of numerical data processing		-is qualified for most applications

a comfortable detection system to find out erroneous function of the process periphery.

- The execution time of commands must satisfy the requirements on real-time data processing, especially, if high data rate is to be stored.

Table 1 shows a summary of recently realized or projected software systems of the KRS 4200 minicomputer, pointing out their advantages and disadvantages. The programming systems listed in table 1 are described in references [2,3,4]. The programming system BASIC 4200 is under developements.

References

[1] Meiling, W.: Configuration of Processing System at Section of Physics - Present State and Developments, this report p. .

[2] Loeper, H., u.a.: FORTRAN - Programmierung der Rechnerfamilie R 4000, Schriftenreihe Informationsverarbeitung, BSB B.G. Teubner Verlagsgesellschaft, Leipzig, 1978.

[3] Leege, K.-W., Werner, D.: CAMAC 4200 - eine algorithmische Echtzeitprogrammiersprache für das Kleinrechnersystem KRS 4200 mit CAMAC- Peripherie, Rechentechnik/Datenverarbeitung 14 (1977) 3, S. 17 - 20.

[4] Grimm, W., Hoffmann, P.: Real-time BASIC for CAMAC - Principles and Implementation for KRS 4200 Minicomputer, this report p. .

REAL-TIME BASIC - PRINCIPLES AND IMPLEMENTATION FOR KRS 4200 MINICOMPUTERS

W. Grimm
Technische Universität Dresden, Sektion Physik, DDR - 8027 Dresden

P. Hoffmann
Ingenieurhochschule Dresden, DDR - 8019 Dresden

Abstract

A special programming system for the KRS 4200 minicomputer with CAMAC periphery is described. The programming language BASIC has been extended by some types of variables, special statements for CAMAC control commands, CAMAC read/write statements, interrupt handling and bit manipulation. Comfortable programming aids for editing running, debugging, file management allow to work out application programs for nuclear physics experiments.

1. The programming language BASIC

The Basic language [1] is composed of easily understood statements and commands, it is one of the simplest programming language to learn. It is developed for the dialogue between user and computer during production and test of the programs. Advantages are:

1. Each statement line has a line number. You can type the lines in any order. The BASIC system stores them in numeric order by line number. It is easily possible to delete, to insert and to change statement lines.
2. Most of the syntax errors are notified by the system directly after the input of the statement line.
3. You can use commands to test parts of the program.
4. The dialogue system can give good support for the test by test commands.

The BASIC statements are analogous to the statements of the programming languages ALGOL and FORTRAN. The first both elements of the statement line are the line number and a keyword specifying the type of operation to be performed. Additional elements of the language set are: constants, variables operators and functions. For example:

```
100 LET A(I,J)=B*SIN(X)                          assignment-statement
 :
200 FOR I=1 TO 2*N+1 STEP 2                      loop-statements
210     B(I)=K*C(I)
220 NEXT I
 :
300 IF X=0 THEN 400                              alternative-statement
 :
400 PRINT "THE VALUES OF A(I,J) AND K2 ARE: ";   input/output-statements
410 INPUT A(I,J),K2
```

2. The extension of BASIC for CAMAC applications

1. Names and types

The original BASIC know only variables of numerical type represented by floating point values. A CAMAC-BASIC language must include also variables of other types. In CAMAC-BASIC each name begins with two letters which characterize the type. There are the following types:

Variable name	meaning	length
BSname	binary short	8 bits
BNname	binary normal	16 bits
BLname	binary long	32 bits
FLname	floating point	48 bits
CHname	character	8 bits
CMname	CAMAC adress	16 bits

name ::= letter $\left\{\begin{matrix}\text{letter}\\ \text{digit}\end{matrix}\right\}$

Other names are:

FIname	file
FNname	one-line function
PCname	procedure

A variable name which with less then three letters characterizes a type of binary normal (if the first letter is I...N) or a type of floating point.

2. Assigment statement for CAMAC addresses

LET CMname = c-adress

c-address ::= $\left\{\begin{matrix}\text{C(c)}\\ \text{CMname}\end{matrix}\right\}$ [N(n)] [A(a)]

c: Crate number n: station a: subaddress

3. Control statement

CON (CMname) cc-function

cc-function: F8... F15, F24... F31, mnemonics for crate and branch commands

4. Read/write statements

READ (CMname, cr-function) sn-variable
WRITE (CMname, cw-function) sn-variable
BREAD (CMname,cr-function)vn-variable [(from-index-variable [..to-index-exp])]
BWRITE(CMname,cw-function)vn-variable [(from-index-variable [..to-index-exp])]

with: READ/WRITE for simple CAMAC transfer
BREAD/BWRITE for block transfer

sn-variable: simple variable with a numerical value
vn-variable: vector variable with numerical values
cr-function: F0... F7 cw-function: F16... F23

The from-index-variable indicates before transfer the first vector element and after transfer the last transferred element + 1.

5. Interrupt handling

You can define the link to a subroutine or a procedure which will be activated by a CAMAC interrupt.

LINK (c_address) { label / PCname } (label is a line-number)

The interrupt routine is left by

EXIT (return from interrupt subroutine)
PCEXIT (return from interrupt procedure)

6. Functions for bit manipulations

NOT(exp)	SHL(shift-exp,exp)	with: STC: set bit and test its change
AND(exp,exp)	SHR(shift-exp,exp)	
OR (exp,exp)	BIT(position,exp)	
XOR(exp,exp)	STC(position,exp)	RTC: reset bit and test its change
	RTC(position,exp)	

exp: expression

7. Global system variables

QCM: Q-semaphore, XCM: X-semaphore and SCM: state of the AS10 branch driver of the KRS 4200 mini-computer

8. Example

This simple measuring program controls a CAMAC equipment consisting of five binary decimal counters which are started and readed out after five minutes simultinously. The counted results are printed out by teletype.

```
10 REM MEASUREMENT WITH FIVE COUNTERS
20 AND OUTPUT OF THE VALUES OF THE BINARY CUNTING REGISTERS
30 DIM CMC (5)
40 LET CMC (1) = C(1) N(1) A(0)  #DEFINE THE CAMAC ADDRESSES
50 LET CMC (2) = C(1) N(2) A(0)
60 LET CMC (3) = C(1) N(3) A(0)
70 LET CMC (4) = C(1) N(4) A(0)
80 LET CMC (5) = C(1) N(5) A(0)
90 DIM M(5)
100 PRINT "NUMBER OF MEASUREMENTS ?"
110 INPUT  NM
120 FOR  I=1  TO  NM
130   PRINT "MEASUREMENT";I;":";
140   CON  (CMC) CZ              #ACTIVATE CRATE Z'BUS
150   CON  (CMC) ENB             #ENABLE THE COUNTERS
160   CON  (CMC) CC              #CLEAR THE COUNTING REGISTERS
```

```
180   REM START THE MEASUREMENT
190   CON  (CMC) CLRCI              #CLEAR CRATE INHIBIT
200   WAIT (0:5:0)                  #WAIT 5 MINUTES
210   CON  (CMC) SETCI              #SET CRATE INHIBIT
220   FOR J=1 TO 5
230     READ (CMC(J), F0) IX        #READ COUNTING REGISTER
240     REM CONVERT THE COUNTED BINARY DECIMAL VALUES
250     REM INTO VALUES OF THE BINARY TYPE
260     LET IY = AND('17,IX) + 10 * AND('17,SHR(4,IX)
270     LET IY =    IY       + 100*AND('17,SHR(8,IX)
280     OUTPUT (IY, F(6))
290   NEXT J
300   PRINT
310 NEXT I
320 END
```

Reference:

[1] Specification for Standard BASIC - Bull, Freeman and Garland published by: NCC Publications 1973.

CAMAC-MONITOR FOR MPS 4944 AND SDK-80 MICROCOMPUTERS

W. ENGHARDT, ZENTRALINSTITUT FÜR KERNFORSCHUNG ROSSENDORF

The CAMAC-software described in the present article simplifies the development of user-programs for two microcomputer systems with CAMAC-interface, which exist at the Section of Physics of the Dresden Technical University.

The first microcomputer is a kit system (SDK-80), which bases on the 8080-CPU, with 1.75k byte RAM and 4k byte ROM (PROM). The CAMAC-interface is a special branch driver 1) for maximum three crates including a crate controller A1. The second microcomputer is the modular system MPS 4944 from the Central Institute for Nuclear Research Rossendorf, also with a 8080-CPU, which memory-size depends on the system configuration. The interface between microcomputer and one crate controller 3312 Ref. 2) is a handshake system according to the G.D.R. standard interface SI 1.2. The user communicates with the microcomputers by using a teletype for SDK-80 and a typewriter or an alphanumerical display for MPS 4944. Each microcomputer is supported by a system-monitor of about 1k byte length 3,4).

The CAMAC-monitor had to fulfil the following demands:

- Development of assembler programs for CAMAC-applications should be the same for both microcomputers, that means, a program tested on one system should, without changes, also work on the other one.
- Subroutines of system-monitors should, as far as possible, be used by the CAMAC-monitors.

The length of the CAMAC-monitor is 1k byte for SDK-80, and 1.25k byte for MPS 4944.

Functions of the CAMAC-monitor:

1. Input of CAMAC-instructions in their computation sequence in a dialogic mode and arranging them in a memory table controlled by a pointer. The same is done for the sources of interrupts (LAM). Additionally the user has to provide tables (also controlled by pointers) for reading and writing data.
2. Initalization of the CAMAC-crate and the interface unit.
3. Execution of CAMAC-instructions by a subroutine, which determines the status of the interface unit, organizes data transfer, and tests the signals Q, X, and special handshaking signals. The execution time of one CAMAC-instruction is 200 µs ... 350 µs for SDK-80, and 540 µs ... 680 µs for MPS 4944.
4. LAM-handling:
   The LAM-pattern is divided in eight bits for Express-LAM (bit 24 ... bit 17), i.e., each bit is biuniquely connected with one LAM-source. The bits 16...1 of the LAM-pattern are dedicated to ored LAM. In this case any number of LAM-sources can be ored on each bit, and the program identifies the interrupt source by using the F(8)-instruction.
   The minimum time between the arrival of the LAM from the CAMAC-crate and the execution of the first instruction of the interrupt-subroutine amounts to 44 µs for SDK-80, and 345 µs for MPS 4944.
5. Error handling:
   The events X=0 or missing the excepted handshake signals after execution of the CAMAC-dataway cycle are followed by an error message, including the type

of error, the incorrect CAMAC-instruction, and its address in the instruction table. After that the computer waits for new user-commands.

The following example illustrates the usage of the CAMAC-monitor:
We assume, that a counter is located at the station N(3) of the crate. The program has to solve the following tasks: set counter status word, start counting, stop counting after a certain time, and transfer the content of the register into the memory of the microcomputer.

1. Preparing the system by dialogue with the computer. Note: The underlined characters are to be written by the user.

```
G0500
INADC: 1100
ADDR: 1100, N: 03, A: 11, F: 17, Q: -, X: T, NL
ADDR: 1102, N: 03, A: 00, F: 26, Q: -, X: T, NL
ADDR: 1104, N: 03, A: 00, F: 24, Q: -, X: T, NL
ADDR: 1106, N: 03, A: 00, F: 02, Q: -, X: T, NL
 .
 .
 .
```

The first line is the command, which starts the program, in the second line the computer demands the first address of the instruction table, in order to set the pointer. In the following lines firstly the current content of the pointer is printed, then the user has to write the C (for SDK-80 only), N, A, and F of a CAMAC-instruction. By the characters "T" and "-" respectively the user can invoke the program to test or not to test the signals Q and X. The input of the instruction list is terminated by writing a space.

2. The execution of described CAMAC-instructions is performed by the following sequence of assembler instructions:

```
INAD : DW        ; CAMAC-instruction table.
       .
       .
       .
INAR : DW        ; (NAF = 3, 11, 17), set counter status.
       DW        ; (NAF = 3, 0, 26), start counting.
       DW        ; (NAF = 3, 0, 24), stop counting.
       DW        ; (NAF = 3, 0, 2), read and clear register.
       .
       .         ; further instructions.
       .
RDAT : DW        ; table for data to be read.
       .
       .
       .
RDAR : DW        ; 24 bit data to be
       DB        ; read from the counter.
       .
       .
       .
WDAT : DW        ; table for data to be written.
       .
       .
       .
WDAR : DW        ; 24 bit counter
       DB        ; status word.
```

```
        .
        .
        .
BEGPR:  CALL INI    ; initialize crate and interface unit.
        .
        .
        .
        LXI H,INAR  ; load pointer INADC
        SHLD INADC  ; with address INAR.
        LXI H,RDAR  ; load pointer RDADC
        SHLD RDADC  ; with address RDAR.
        LXI H,WDAR  ; load pointer WDADC
        SHLD WDADC  ; with address WDAR.
        CALL NAF    ; execute (NAF = 3, 11, 17)
        CALL NAF    ; execute (NAF = 3, 0, 26)
        CALL WAIT   ; wait for a certain time.
        CALL NAF    ; execute (NAF = 3, 0, 24)
        CALL NAF    ; execute (NAF = 3, 0, 2),
        .
        .
        .
```

The described CAMAC-monitor was used to perform an optimization of the beam current of a 150 keV particle accelerator, to realize a microcomputer controlled multichannel-analyzer for (n,n'γ)-experiments, and to support the development of new CAMAC-modules 5).

References

1) GLEISBERG, F., Diplomarbeit, TU Dresden, Sektion Physik, 1978
2) PÜTHIG, J., Diplomarbeit, TU Dresden, Sektion Physik, 1979
3) INTEL 8080 System Design User's Guide, 1976
4) WERNER, D., Dialog-Steuerprogramm MIMO, TU Preprint 08-08-78
5) ENGHARDT, W., Diplomarbeit, TU Dresden, Sektion Physik, 1979

RECENT RESULTS ON 14 MeV ACTIVATION CROSS SECTION MEASUREMENTS FOR SHORT HALF-LIFE REACTION PRODUCTS

P.N.Ngoc, F.Deák, S.Gueth and Á.Kiss
Department of Atomic Physics
Roland Eötvös University
Budapest, Hungary
H-1088.Budapest, Puskin u. 5-7.

Abstract

Activation cross sections for the reactions $^{28}Si/n,p/^{28}Al$ /$T_{1/2}$=2.31 m/, $^{29}Si/n,p/^{29}Al$ /$T_{1/2}$=6.6 m/, $^{37}Cl/n,p/^{37}S$ /$T_{1/2}$=5.06 m/, $^{37}Cl/n,\alpha/^{34}P$ /$T_{1/2}$=12.4 s/, $^{23}Na/n,\alpha/^{20}F$ /$T_{1/2}$=11.41 s/, $^{34}S/n,p/^{34}P$ /$T_{1/2}$=12.4 s/ have been measured by using the mixed powder method. A fast pneumatic sample transport system /with transport time of about 1 sec/ was used. The γ-rays were detected in a low background measuring place by Ge/Li/ detector. The measured cross sections are: 234 ± 15; 104 ± 8; 34 ± 3; 26.3 ± 1.9; 111± 9; 72.4 ± 5.2 mb respectively. The results will be compared with other published data.

I. Introduction

There is a large number of 14 MeV neutron cross-section data, which were mostly measured by the activation method. However, large discrepancies can be found among the results published by different authors. This is especially true for reactions with second or minute-range half-life products[14,16]

The aim of this paper is to present some recent results on 14 MeV neutron activation cross-sections. We investigated reactions which produced activities in the minute-second range. The measurements were made by the mixed powder method[18] using fast sample transport system and Ge/Li/ γ-ray detector in a low background measuring place.

2. Experimental procedure and calculation of the cross section

The block diagram of the experimental set-up is shown in fig. 1.

The fast neutrons were produced by the usual $^{3}H/d,n/^{4}He$ reaction by a neutron generator of NA-2 type[19].

The samples were powders in cylindrical polyethylen boxes /Ø = 2 cm/, that were placed in 0°, 7 mm far from the tritium target. As the deuterons were accelerated to 125 keV, the energy of neutrons incident on the sample was 14.6 ± 0.2 MeV.

The samples were transported by a pneumatic rabbit system to a low background measuring place. The transport system used 3 at pressed air in a tube of 12 m length and of 2.5 cm diameter.

The typical transport time was about 1.2 sec. The positioning of the sample was better than 0.2 mm[22].

The gamma rays were measured by a coaxial 52 cm^3 Ge/Li/ detector with an energy resolution of about 4.5 keV /FWHM/ at 1332.5 keV. The detector was installed in a lead cube of 80 cm side length and 5 cm wall thickness.

The background was about 50 counts/sec over 50 keV.

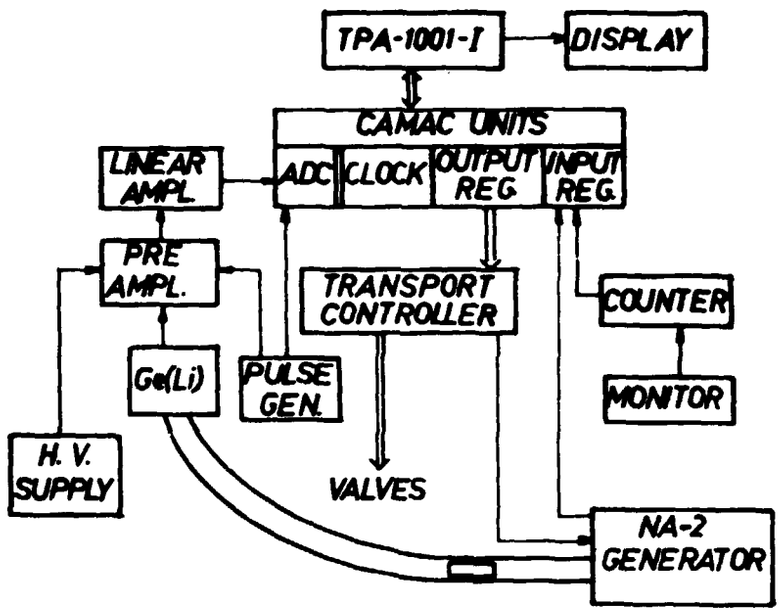

Fig.1. Block diagram of the experimental set-up.

The signals from the detector were fed through the preamplifier and spectroscopy amplifier into a CAMAC-type 4096 channel ADC. The data were collected by a 16 K computer /type: TPA 1001/I/.

The computer controlled the whole procedure: irradiation, transport of sample and data taking. The parameters of the procedure /irradiation time, measuring time. etc./ could be chosen as the input data set of the control program. In addition, there was a possibility to repeat the measurement cycle many times if the statistics made it necessary.

For the stabilization of the spectrum two high precision mercury pulse generators were used. Pulses from these generators were added to the first and the last some channels of the spectrum in the following way: the smaller pulses were fed directly to the ADC, but the larger ones were led to ADC through the two amplifiers. The computer periodically looked for these standard signals and corrected the amplification parameters to make the spectrum stable.

The evaluation of the spectra, the energy calibration, the determinations of the peak positions, background, peak areas and half-lives can be done semi-automatically by the computer.

For monitor reactions we used $^{27}Al/n,\alpha/^{24}Na$, $T_{1/2}$=15 h, σ =114.2 ± 1.3 mb[1] and $^{27}Al/n,p/^{27}Mg$, $T_{1/2}$=9.48 m, σ =73 ± 5 mb[21]

In all cases the monitor powder was carefully mixed with the powder of material under investigation. The measurements for the second-range half-life products were done by using the possibility of periodical repetition of the experimental procedure. In these cases the cross-sections were calculated by the

following formula:

$$\sigma = \sigma' \frac{\lambda C (e^{-\lambda T}-1)^2}{\lambda' C' (e^{-\lambda' T}-1)^2} \frac{(1+\alpha)}{(1+\alpha')} \frac{\varepsilon' f_s' I_\gamma' n' e^{-\lambda' t_c'}}{\varepsilon f_s I_\gamma n e^{-\lambda t_c}} \times$$

$$\times \frac{(1-e^{-\lambda t_i})(1-e^{-\lambda' t_m'})\left[e^{-(k+1)\lambda' T}-(k+1)e^{-\lambda' T}+k\right]}{(1-e^{-\lambda' t_i'})(1-e^{-\lambda t_m})\left[e^{-(k+1)\lambda T}-(k+1)e^{-\lambda T}+k\right]}$$

where C is the total counting number obtained in k cycles; T is the duration of each cycle; t_i, t_c, t_m are the intervals for irradiation, cooling and measuring respectively in each cycle; ε is the relative efficiency of the detector for the measured peak; f_s is the self-absorption correction factor for the studied gamma ray; I_γ is the intensity /or branching ratio/ of the gamma ray; n is the number of nuclei of the investigated isotope in the sample; α is the total internal conversion coefficient for the studied transition; λ is the decay constant of the reaction product; the comma refers to the parameters of the monitor reaction.

The cross-sections for the minute-range half-life products were calculated according to the formula given by Ref.20. For each investigated reaction four samples were used with different ratios of monitor and target masses. The results were obtained by averaging the cross-section values from the independent measurements. It should be mentioned that for the reactions with second-range half-life product at least hundred cycles were carried out for each sample.

3. Results and discussion

In Table I. the investigated materials, the product half-life /$T_{1/2}$/, the gamma energy /E_γ /, the branching ratio /I_γ /, the obtained cross-section are presented together with results of other authors. The data for $T_{1/2}$, E_γ, I_γ, were taken from Ref.2.

The errors quoted in Table I. for the present work contain the statistical error /less than 0.5 % in each case/, the ambiguity in the relative photo peak efficiency /~ 4 %/, in the self-absorption correction /~ 1 %/, the error of weighing, timing, homogenious mixing /~2%/ and the errors of the used monitor cross-sections.

Comparing our values with the results of other works we can see the following.

For the ^{28}Si/n,p/^{28}Al reaction there are discrepancies among the results quoted in Table I. The two measurements with the smallest errors were performed by the /β-γ/coincidence method. The present result is somewhat smaller. For ^{29}Si/n,p/^{29}Al we support the value obtained by Siobolev and Ramendik[6].

For ^{37}Cl/n,p/^{37}S our result is about the average value of the other references.

In the case of ^{37}Cl/n,α/^{34}P,a large discrepancy can be found among the quoted values. Our result is smaller than all these references. For ^{23}Na/n,α/^{20}F all references before 1970 gave the values larger than 130 mb. Only the work done by Janczystyn and Górsky /1973/ gave the value smaller than 80 mb, but with large error. The present work gives the value of 109 mb with the smallest error. For ^{34}S/n,p/^{34}P, the value of 0.15 for I_γ which was taken from Ref.17 was used

Table 1.

The measured cross-sections of the investigated nuclear reactions comparing with other data

Target	Reaction	$T_{1/2}$	E_γ /keV/	I_γ	Cross-section				
					This work /mb/	Literature			
						E_n/MeV/	σ /mb/	Method	Ref.
SiO_2	$^{28}Si/n,p/^{28}Al$	2.31 m	1778.8	1.00	234±15	14.8±0.1	265±8	β-γcoinc	8/73/
						14.7	222±12	β count	3/67/
						14.7±0.1	297±14	β count	4/68/
						14.8±0.1	269±6.3	β-γcoinc	6/77/
SiO_2	$^{29}Si/n,p/^{29}Al$	6.6 m	1273	0.91	104±8	14.8	147±18	β,γ count	7/71/
						14.8±0.1	131±14	β-γcoinc	8/73/
						14.8±0.1	98.5±23	β-γcoinc	6/77/
ClNa	$^{37}Cl/n,p/^{37}S$	5.06 m	3102.4	0.90	34±3	14.8	21.3±2.1	β,γ count	9/66/
						14.8	25.5±1.2	β count	3/67/
						14.8	42±4	β,γ count	7/71/
ClNa	$^{37}Cl/n,\alpha/^{34}P$	12.4 s	2128	0.25	26 3±1.9	14.8	28±10	β count	10/66/
						14.5±0.2	112±12	γ count	15/67/
						14-15	36±10	average	11/73/
ClNa	$^{23}Na/n,\alpha/^{20}F$	11.41 s	1633.1	1.00	111±9	14.1	136±14	γ count	12/66/
						14.89	164±22	γ count	13/65/
						14	78±30	γ count	16/73/
S	$^{34}S/n,p/^{34}P$	12.4 s	2128	0.25	72.4±52	14.8	32±8	β,γ count	7/71/
						14.9	73±7	average	5/74/
						14	72±7	average	14/71/

by other authors. In this work I_γ was taken to be 0.25 /Ref.2/ which resulted in the value of 72.4 mb for the cross-section of the reaction. Therefore in this case the average value presented by Pai and Clark /Ref.14/is supported by us.

Acknowledgements

We are indebted to K.Berényi, Cs.Pongrácz, and J.Szivák for their kind help in the experiments.

References

1. H. Vonach et al.; Z. Physik 237/1970/155
2. G. Erdmann and W. Soyka ; J. Radioanal. Chem. V26/1975/375
3. Pasquarelli A.; Nucl. Phys. A93/1967/218
4. Cuzzocrea P. et al.; Nuov. Cim. 54 B/1968/53
5. Handbook of Nuclear Activation Cross Section /Technical Reports Series N° 156/Vienna, IAEA, 1974
6. Siobolev V. T.; Ramendik Z. A.; Atomnaja Energia 43/1977/54
7. Prasad R., Sarkar D.C.; Nuov. Cim. V3A/1971/467
8. Robertson J. et al.; J. Nucl. Energy 27/1973/531
9. Mitra B. and Ghose A.M.; Nucl. Phys. A83/1966/157
10. Prasad R., Sarkar D.C.; Nucl. Phys. 85/1966/476
11. Levkovskii V.N.; Sov.J. Nucl. Phys. 18/1973/705
12. Wölfer G., Bormann M.; Z. Physik 194/1966/75
13. Picard J. and Williamson C.F.; Nucl. Phys.63/1965/673
14. Pai H.L., Clark R.L., Cross W.G.; Nucl.Phys. A164/1971/526
15. Bormann M. et al.; EANDC/E/76 "U",51/1967
16. Janczyszyn J., Górsky L.; J. Radioanal. Chem. 14/1973/201
17. Lederer C.M. et al.; Table of Isotopes 1967 6th ed.
18. Venugopala Rao P. and Fink R.W.; Phys. Rev. 154/1967/1023
19. Pásztor E., Klopfer E.; KFKI Közl. 12/1964/143 and Pribori i Tekhn. Eksperim. N°4, /1965/ 36-38
20. Wen-Deh-Lu et al.; Phys. Rev. C1,1 /1970/350
21. L. Husain et al.; Phys. Rev. C1 /1970/1233
22. Cs. Sükösd, K. Berényi, F. Deák, S. Gueth, Á. Kiss, Cs. Pongrácz; A computer-controlled system for 14 MeV neutron activation analysis. Nucleonika /accepted for publication/

АВТОМАТИЗАЦИЯ ЭКСПЕРИМЕНТОВ СО СВЕРХТОНКОЙ ВНУТРЕННЕЙ МИШЕНЬЮ НА НАКОПИТЕЛЕ

Б.Б.Войцеховский, Б.А.Лазаренко, Д.Н.Николенко, С.Г.Попов

Институт ядерной физики СО АН СССР, Новосибирск

Аннотация

Описана автоматизация эксперимента на накопителе ВЭПП-2 ИЯФ СО АН СССР на основе ЭВМ ОДРА-1325 и микро-ЭВМ "Электроника-60", включающая аппаратуру сбора информации с индукционно-дрейфовых камер магнитного спектрометра и систему контроля параметров детекторов ядерных частиц.

I. В ИЯФ СО АН СССР в течение последних лет проводятся эксперименты на электрон-позитронном накопителе ВЭПП-2 с использованием сверхтонкой внутренней мишени. Подобные эксперименты имеют ряд преимуществ по сравнению с использованием внешней мишени: равномерность возникновения событий, возможность регистрации малоэнергетичных вторичных частиц, поляризации электронного пучка и мишени, высокая направленность и монохроматичность пучка в накопителе. Для постановки экспериментов требуется разработка многоканальной аппаратуры на основе многопроволочных камер и других подобных приборов. Основные результаты в настоящее время получены в эксперименте по электровозбуждению ядер, общая структура управления и автоматизации которого показана на рис.I.

Система включает центральную ЭВМ ОДРА-1325, аппаратуру связи [1], систему контроля характеристик детекторов ядерных частиц СКАТ, электронику обработки сигналов с полупроводников. детекторов (ППД) электронику индукционно-дрейфовых камер магнитных спектрометров (МС), амплитудно-цифровой преобразователь для контроля режимов накопителя, спектрометров с точностью 10^{-5} [2].

II. При изучении уровней ядер в реакции /e,e'/ энергия рассеянных электронов определяется по радиусу их траектории в однородном магнитном поле [3], для определения которого на пути частиц помещены двухкоординатные индукционно-дрейфовые камеры (ИДК) и пара сцинтилляционных счетчиков (Рис.2). Логика работы спектрометра следующая: сигналы с ФЭУ, возникающие после пролета электрона через счетчики, проходят через дискриминаторы с плавающим порогом (ДПП) и поступают на схему совпадений СС-I, которая вырабатывает импульс "старт" для время цифровых преобразователей (ВЦП) и блока управления (БУ). БУ запирает СС-I и открывает схему совпадений СС-2 и регистр РМ. Сигналы с анодных проволочек ИДК, сформированные в блоке П-Д, подаются в СС-2 и РМ. При наличии срабатывания всех трех камер СС-2 дает сигнал в БУ, который формирует запрос L (с задержкой на время работы ВЦП). В противном случае БУ вырабатывает импульс сброса на шину P_I или С. Сигналы, снимаемые с линий задержек (катодных плоскостей) ИДК после усиления и формирования в ДПП поступают на входы "стоп" ВЦП.

По запросу L от БУ контроллер производит опрос аппаратуры и запись данных в буферную память. После заполнения памяти информация массивом пере-

дается в центральную ЭВМ для дальнейшей обработки и хранения. Быстродействие системы 2 кгц. ИДК позволяет определить место пролета электрона через плоскость камеры с точностью 0,1 мм. Для этого необходима точность измерения времени распространения сигналов по линиям задержки лучше 0,5 нс. Поскольку стабильность ВЦП существенно хуже, а также из-за необходимости учитывать изменения задержек при смене блоков, кабелей и т.п. введена автоматическая проверка трактов с помощью генераторов, управляемых от ЭВМ. Программа определяет поправочные коэффициенты по результатам проверки.

Ш. В ряде экспериментов возникла необходимость в постоянном контроле за амплитудами сигналов, поступающими с систем регистрации, за временными сдвигами между сигналами. Поскольку число этих сигналов довольно велико и внесение контролирующей схемы в каждый канал нецелесообразно, разработана СКАТ. В основе схемы СКАТ – рис.3 – логические и аналоговые коммутаторы в стандарте КАМАК, которые позволяют подключить к ВЦП и АЦП необходимый канал. Система программ обеспечивает набор спектров и сравнение с критическими параметрами указанными оператором при запуске системы, запись спектров на магнитный диск. Возможно построение любого из спектров на экране дисплея или отпечатать на DZM-180. Систему можно использовать по одному из каналов для настройки детекторов в качестве многоканального (до 16К) анализатора. В дальнейшем для увеличения скорости набора информации в эксперименте с регистрацией вторичных частиц (ПЦД) на совпаденных с электроном рассеянным в спектрометре (МС) крейты ПЦД и МС будут подключены к микро-ЭВМ "Электроника-60" (Э-60). Новые эксперименты (Д) также разгружены на Э-60.

Литература

1. М.Н.Захваткин, М.М.Карлинер, Э.А.Купер, Э.Л.Неханевич и др. "Управление ускорительно-накопительными комплексами ИЯФ СО АН СССР при помощи ЭВМ. Труды IУ Всесоюзного совещания по ускорителям заряженных частиц. /Москва 1974/ т.II, стр.203, "Наука" 1975.
2. Карлинер М.М., Купер Э.А., Леденев А.В. и др. "Многоканальная прецизионная система для измерения сигналов микроволнового диапазона". Семинар "Вопросы теории и проектирования преобразователей информации". /Киев 1975/ т.I,стр.II.
3. П.И.Бутурин, Б.А.Лазаренко, Д.М.Николенко, С.Г.Попов и др. "Аппаратура для изучения рассеяния электронов атомными ядрами на накопителе". ПТЭ, 1978, № 4, стр.38.

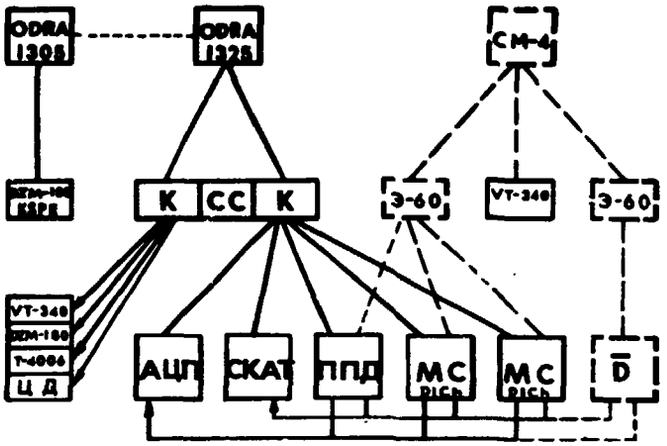

Рис.I Общая структура управления экспериментами.

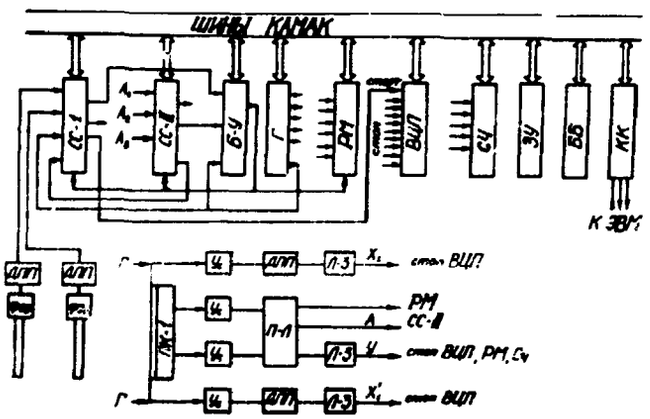

Рис.2 Электроника магнитного спектрометра.

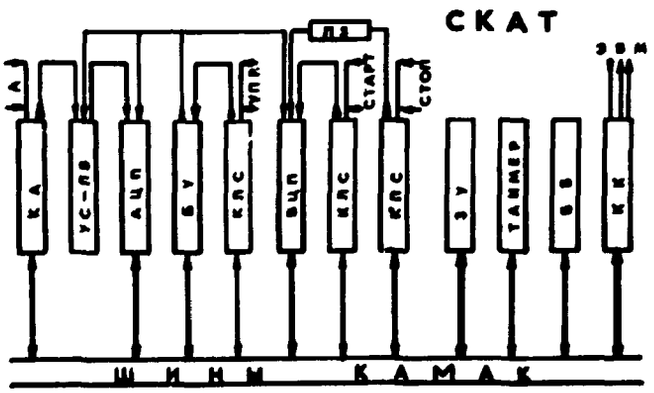

Рис.3 Функциональная схема СКАТ.